Modulation of BIN1 expression rescues different forms of centronuclear myopathies in murine models

Valentina Maria Lionello

UNIVERSITÉ DE STRASBOURG

ÉCOLE DOCTORALE DES SCIENCES DE LAVIE ET DE LA SANTÉ

IGBMC, INSERM, UNIVERSITÉ DE STRASBOURG

THÈSE

présentée par :

Valentina Maria LIONELLO

soutenue le : **11 Mars 2019**

En vue d'obtenir le grade de:

Docteur de l'université de Strasbourg

Discipline : Science du vivant

Spécialité : Biologie moléculaires et cellulaires

Modulation of BIN1 expression rescues different forms of Centronuclear myopathies in murine models

THÈSE dirigée par :

Mr. Le Docteur Jocelyn LAPORTE	Directeur de recherche INSERM, Université de Strasbourg
Mme. Le Docteur Belinda COWLING	Chargée de recherche INSERM, Université de Strasbourg

RAPPORTEURS :

Mme. Le Docteur Fanny PILOT-STORCK	Maître de conférences, Université Paris-Est
Mr. Le Docteur Aurélien Roux	Professeur, Directeur de recherche, Université de Genève

---

AUTRES MEMBRES DU JURY :

Mr. Le Docteur Olivier Dorchies	Chargée de recherche, Université de Genève
Mr. Le Docteur Fabien Alpy	Chargée de recherche INSERM, Université de Strasbourg

Acknowledgment

I would like to thank you the member of the jury for accepting to read and evaluate my work.

I would like to say a gigantic thank to my mentors Belinda and Jocelyn. Thank you for welcoming me in the lab and thank you for encouraging and helping during these four years. Thank you for your positive support which has been the key to find solutions and to continue our research. You have been always available and ready to help answering my messages and phone call! Thank you, Belinda, I have been enjoying working with you and sharing the happiness of the positive results! Thank you for being always ready to help even in the most odd situation! I would like to thank Jocelyn for animating the development of new ideas and for understanding my “volcanic” way of being!

Thanks you to all the people who have been in the lab since I join the international MAD team. During these four years of PhD I have been really like. I have met wonderful co-workers and friends who have made my PhD fantastic!

Merci beaucoup à AnneSo to be as a third supervisor! You teach me a lot in the lab and have been always ready to give me advice even 400 km far. Thank you for all your nice motivational messages.

Thanks to my bellissima Ariel! Long chat, a lot of sweets and laugh... Unforgettable! Your contagious energy welcomed me in Strasbourg! I loved running and biking with you! I am super grateful to have met you and shared with you difficulties and satisfactions! You were always ready to help me with Suzie and Cathrine in all the occasions!

Tantissimi grazie alla mia adorata Susy! You have been super sweet and kind during these years, always ready to listen and to help in all the situation! You took care of me when I was sick and when I was having my Bridget Jones moments!

Merci beaucoup à Cathrine, your suggestions and multitasking abilities have been really useful even with IKEA bed!

Un grazie speciale to Aymen! We did our PhD together and we shared a lot during these years! Thanks for the hugs and for always be ready for chatting! Thanks for sharing fashion and politics ideas! As we always said, we will work together again!

Merci beaucoup à Maxime! I think we should create a politic movement together! We had great discussion during our PhD, we shared not only scientific project but also fun moments! Your

jokes helped me to improve my French and I appreciate your amazing sense of humor! It is unique! You are a great actor and good friend!

Thank you to Ivana, your motivation and love for science helped me the first months in the lab! You spent time on teaching all the techniques useful for my PhD!

I would like to thank Pascal for all the long chat and informatics helps, you facilitate a lot of analysis during my PhD! I would like to thank all the previous lab member, in particular to Hichem, Vanessa, Raphael and Matthieu to share with me fun moments and scientific discussions.

A magic purple and shining Merci à CriCri! I am sure the team won't be the same without you! You don't manage only all the mice projects of the lab, you also help all of us to do whatever. Thanks for being my desk-mate, you shared all your materials and gossips with me! You perfectly understand my fear of the mice since the first day I enter in the animal house…and guess what, I had 4 years with mice phenotyping coming. Without you, Susy, Aymen, Vasu and Roby I was still in the 2015 to look for the nicest mouse in the cage, the one smiling!

I would like to நன்றி my little Vasu. Thank you to make me closest to India culture. You are a great friend and co-worker. Thank you for the long scientific discussion and for your constant support! Your energy and independence are a great example! I am still waiting an Indian dinner!

جَزِيلاً شُكْرًا to the two wonderful Sarah(s). I have been always impressed by your kindness and precision at work. Thank you my friends for sharing your incredible cooking skills with me and fun discussions! A special thank you to Sarah who shared a part of my project, you are a great collogue! Thanks to our little Sarah to be always ready to help everyone and be always smiling!

Gràcies mil a Xenia, thank you for exchanging scientific hypothesis. We do not miss imagination! Thank you for being co-worker and friend, we have supported each other during these years. I love your way of being so clear and direct with everyone, never change.

In the last year I have also worked a lot with the tireless Evelina. I would like to большое спасибо for investing so much energy in all the projects you are involved. Your scientific knowledge have been beneficial for all the people in the lab.

Muchas gracias a Roby and Raquel, with you is impossible to get bored, you are always motivated in helping everybody. Hard work does not scared you at all!

Merci beaucoup à Amandine and Alexia to be always so cheerfulness, we need to do a karaoke with all the old French songs! Danke schön to Johann and merci beaucoup à Xaviere for organizing meetings and social activities which make our team unique! Thank you Johann

to organize all the meeting with the patients. I have been always impressed by your amazing communication skills which you share with all of us. Than you, Xaviere, for remembering all of our birthdays. You are always motivated to plan all the important events of the lab!

I would like to thank all the new lab members: Coralie, Juliana and Quentin(s).

I would like to thank all my Milan and “Vecchie Comari” friends to share fun, songs, laughs and chat between experiments! It is always great to be loud together!

Merci beaucoup à mon chéri Adri. Tu es toujours prêt à m'encourager et à partager des idées et des suggestions avec moi. Merci beaucoup pour ta patience. Merci de partager les meilleurs moments et le plus stressant. Enfin, merci beaucoup d'avoir lu et amélioré le manuscrit de thèse, ce ne serait pas si agréable sans tes suggestions.

Le persone che devo ringraziare di piu’ al mondo sono tutta la mia famiglia: Mamma, Papa’, Marianna e Ilaria. Grazie mille per avermi incoraggiato fin da piccolina ad andare sempre avanti senza sosta, non ci sarei riuscita senza il vostro supporto. Grazie mille per essere sempre pronti ad ascoltare ogni mia ansia e problema che ai miei occhi appaiono catastrofici. Grazie per riportarmi con i piedi a terra ogni volta e ripetermi che ce la posso fare. Lo sapete quanto e’ difficile stare lontani da tutti voi e condividere sempre meno momenti insieme. Siete stati la mia energia e in parte ho lavorato cosi’ duro anche per voi. Grazie mille ai miei due magici cognati, o meglio fratelloni, Michele e Luca. Grazie per incoraggiarmi ed essere sempre pronti a darmi una mano. Non mi lasiate mai sola e mi trattate sempre come la vostra sorellina rompina. Grazie ai miei straordinari nipotini, Fabietto, Elione, Giaco, Cloti, Iolina ed Elsina. Siete tutti meravigliori e fantastici, ognuno nella sua unicita’. La vostra allegria sono sempre le miglior pillola per affrontare qualsiasi momento. Grazie a tutti voi, vi amo tutti da matti!

Table of Contents

List of abbreviations

AAV	Adeno associated virus
AD	Alzheimer's disease
ADCNM	Autosomal dominant centronuclear myopathy
ARCNM	Autosomal recessive CNM
ASO	Antisense oligonucleotide
BAR	Bin/Amphiphysin/Rvs
BIN1	Amphiphysin 2
BSE	Buddle signaling element
CLAP	Clathrin and AP2 binding
CMV	Cytomegalovirus
CNM	Centronuclear myopahy
DHPR	Dihydropyridine receptor
DNM2	Dynamin 2
EEA1	Early endosome antigen 1 (early endosome marker)
EGFR	Epidermal Growth Factor Receptor
EHD1	Eps15 homology-domain protein 1
EM	Electron microscopy
FAK	Focal adhesion kinase
GED	GTPase effector
GTP	Guanosine triphosphate
HE	Hematoxylin and eosin
KO	Knock-out
m-TORC	Mammalian target of rapamycin complex 1
MAD	Myotubularin1- Amphiphysin2- Dynamin2
MBD	Myc binding domain
MO	Morpholino
MTM1	Myotubularin 1
MTMR14	Myotubularin-related protein 14
MTMRs	Myotubularin-related proteins
NADH-TR-TR	Nicotinamide adenine dinucleotide tetrazolium reductase
N-WASP	Wiskott–Aldrich syndrome protein
PH	Pleckstrin homology
PH-GRAM	Pleckstrin Homology-Glucosyltransferase, Rab-like GTPase Activator and Myotubularin

PI	Phosphoinositide binding motif
PRD	Proline-rich sequence recognition domain
PTB	Phosphotyrosine-binding
PtdIns	Phosphatidylinositol
PtdIns (4,5)P_2	Phosphatidylinositol-4,5-bisphosphate
PtdIns(3)P	Phosphatidylinositol-3-phosphate
PtdIns(3,5)P_2	Phosphatidylinositol-3,5-bisphosphate
PtdIns(5)P	Phosphatidylinositol-5-phosphate
PTP/DSP	Dual specificity phosphatases domain
Rab5	Ras-related protein 5 (early endosome marker)
Rab7	Ras-related protein 11 (late recycling endosome marker)
Rab11	Ras-related protein 11 (late recycling endosome marker)
RID domain	Rac1-Induced Recruitment Domain
RyRs	Ryanodine Receptors
SDH	Succinate dehydrogenase
SH3	Src homology 3
SID domain	SET-protein Interaction Domain
SPEG	Striated muscle preferentially expressed protein kinase
SR	Sarcoplasmic reticulum
T- tubules	Transversal tubules
TA	Tibialis Anterior
TEM	Transmission electron microscopy
TTN	Titin
XLCNM	X-linked myotubular myopathy
WT	Wild type

List of Figures

Page

Note: Results Part1 and 2a figures are not part of the List of Figures as they are incorporated into manuscripts.

Introduction

Brief introduction to skeletal muscle biology

Skeletal muscles form the most abundant tissue comprising 40 % of total human body. Over 650 different types of skeletal muscles contribute to maintain posture and body homeostasis, to allow locomotion and to generate force (Frontera and Ochala, 2015)

Skeletal muscles have a unique architecture. They are externally wrapped in a dense connective tissue, called epimysium, which allows muscle contraction, and protects and separates the muscle from other organs (Fig. 1A). Inside, the skeletal muscle is divided in fascicles by another layer of connective tissue, the perimysium from which another thin layer of connective tissue, the endomysium is attached. The endomysium contains blood vessels and surrounds the muscle fibers which are the morphological unit of the muscle. The muscle fibers are formed during development by the fusion of myoblasts. They are multinucleated post-mitotic cylindrical cells. Their nuclei are normally distributed along the muscle fibers and localized on the periphery of the cells, closed to the plasma membrane which is called sarcolemma (Fig.1 B). Most of the internal compartment of skeletal muscle fibers is occupied by packed and aligned myofibrils which are divided in functional contraction units called sarcomeres (Fig. 1C) (Sweeney and Hammers, 2018). The main proteins of the sarcomere are actin (thin) and myosin (thick) filaments. Electron microscopy pictures shows that sarcomeres are striated in skeletal muscle. Each sarcomere is delineated by two Z-lines which appear dark by electron microscopy. The part of the sarcomere occupied by only actin (thin) filaments, located close to the Z-line is called the I-band. The zone at the center of the sarcomere which is occupied only by myosin (thick) filaments is the H-band. The entire length of one thick filament is called the A-band (Hanson and Huxley, 1953; Squire, 1997)

Muscle contraction is triggered by an excitation signal from a motor neuron to muscle fibers, transmitted at the neuromuscular junction. At the neuromuscular junction, the acetylcholine released by the motor neuron binds the nicotinic acetylcholine receptor. These events cause membrane depolarization which promotes a conformational change of the voltage dependent Ca^{2+} channel/dihydropyridine receptors (DHPRs). DHPRs are clustered on the muscle transversal invaginations of the sarcolemma called T-tubule. T-tubules are present in skeletal and cardiac muscle and allow a deep transmission of the membrane depolarization in muscle. The DHPR conformational modification impacts on the activity of another receptor, the sarcolemma voltage sensors Ryanodine Receptors (RyRs) which localizes on the sarcoplasmic reticulum (SR), a network of tubules and cisternae which store Ca^{2+}. RyR allows the Ca^{2+} release from the SR, which will drive the skeletal muscle contraction. In skeletal muscle, one T-tubule and two cisternae of the SRs form a triad (Al-Qusairi et al., 2009; Capes

et al., 2011; Flucher, 1992; Posterino and Lamb, 2003; Sweeney and Hammers, 2018)Triads are normally found between the A-I bands of the sarcomere.

Disorganisation of this tightly regulated architecture can lead to severe muscle defects. Congenital myopathies are a rare heterogeneous group of genetic neuromuscular disorders which are caused by different abnormalities in skeletal muscle architecture and function.

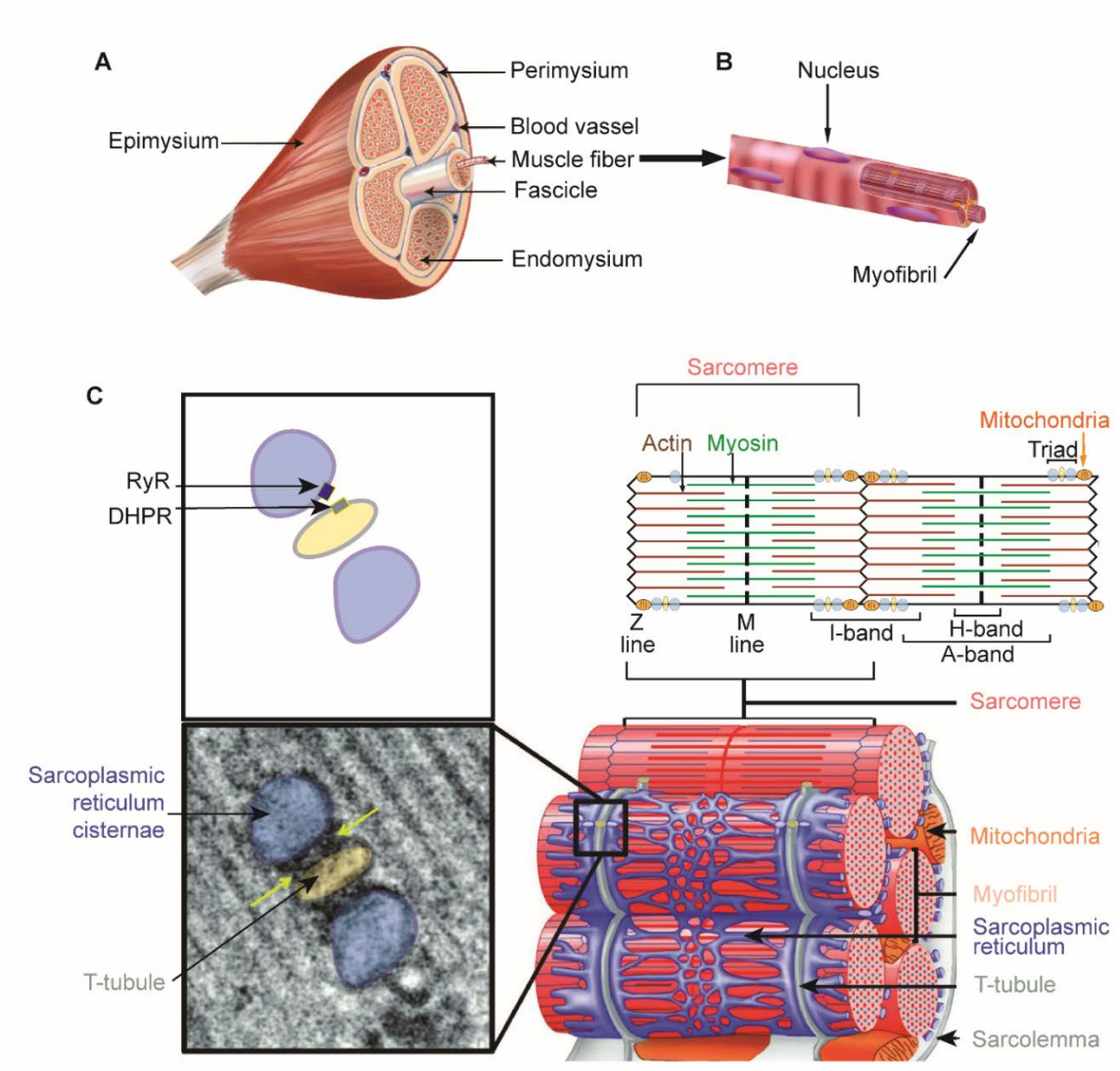

Figure 1: The complex muscle architecture.

A, Muscle are composed of three connective tissue layers: the epimysium, the perimysium and the endomysium. Figure adapted from: https://training.seer.cancer.gov/anatomy/muscular/structure.html. **B**, Structure of a normal muscle fiber. Muscle fiber are composed of several myofibrils. Nuclei are positioned at the periphery of the muscle fiber next to the sarcolemma. Figure adapted from: http://lyceum.algonquincollege.com/lts/onlineCourses/anatomy/content/module6-3.htmB.**C**, Organisation of a normal muscle fiber. The myofibrils are surrounded by the Sarcoplasmic reticulum (in blue) and by the Sarcolemma (in grey). The Sarcolemma invaginates in T-tubules to stay in close-contact with myofibrils. On the left, the electro microscopy (EM) picture illustrates the triad structures with a central T-tubule associated with two terminal cisternae of the sarcoplasmic reticulum. The yellow arrows indicate the feet of the triads where the DHPR and RYR complex is found. The functional subunits of the myofibers are called Sarcomeres, which are highly organised. Adapted from Al-Quasairi *et al*., 2011).

Congenital myopathies

Congenital myopathies have an incidence of 1 in 20,000 live births per year. Patients display various degrees of muscle weakness and severity with a slowly progressive course. The common clinical patterns are facial muscle weakness, generalize hypotonic posture, and weakness of the respiratory and bulbar muscles (Cassandrini et al., 2017; North et al., 2014).

Congenital myopathies are classified based on distinctive histopathological features observed on muscle biopsies, next generation sequencing for genetic diagnosis, and magnetic resonance imaging. There are 5 main groups of congenital myopathies: nemaline myopathy, core myopathy, centronuclear myopathy (CNM), congenital fiber-type disproportion myopathy and myosin storage myopathy (Cassandrini et al., 2017; North et al., 2014). The majority of genes implicated in congenital myopathies are involved in excitation-contraction coupling, calcium homeostasis, redox regulation, membrane trafficking and autophagy pathway (Jungbluth et al., 2017). In the last decade, the improved genetic and molecular understanding of the various forms of congenital myopathies has led to the identification of specific therapeutic targets and strategies which are now under development, some of which have reached clinical trials (Jungbluth and Voermans, 2016).

During my PhD I focused my studies and research on centronuclear myopathies.

Centronuclear myopathies

As suggested by the name, patient muscle histology often presents abnormally localized nuclei in the center of muscle fibers in the absence of regeneration (Romero, 2010). CNM patients present with varied disease onset and clinical features depending on the causative genetic mutation. This group of diseases is divided in:

- X-linked myotubular myopathy (or X-linked CNM, XLCNM) due to mutation in myotubularin (*MTM1*) (Laporte et al., 1996) and
- Autosomal recessive or dominant CNM due to mutation on amphiphysin 2 (BIN1) (Bohm et al., 2014; Nicot et al., 2007), dynamin 2 (*DNM2*) (Bitoun et al., 2005), skeletal muscle ryanodine receptor (*RYR1*) (Wilmshurst et al., 2010), myotubularin-related protein 14 (*MTMR14*) (Tosch et al., 2006), titin (*TTN*) (Ceyhan-Birsoy et al., 2013), or striated muscle preferentially expressed protein kinase (*SPEG*) (Agrawal et al., 2014).

Currently there are no therapies available for CNM patients.

X-linked Myotubular myopathy

Mutations in *MTM1* (OMIM # 300415) cause one of the most severe congenital muscle disorders, X-linked myotubular myopathy, also called X-linked centronuclear myopathy (XLCNM, OMIM # 310400). To date 300 mutations have been identified on this gene, the majority of which are loss-of-function mutations (Laporte et al., 1996) (Buj-Bello et al., 1999; de Gouyon et al., 1997; Laporte et al., 2000; Laporte et al., 1996; Laporte et al., 1997b; Tanner et al., 1998) (https://www.omim.org/entry/300415).

Incidence, clinical and histological features

The incidence of XLCNM is 1 out of 50,000 newborn males (https://www.orpha.net/consor/cgi-bin/OC_Exp.php?lng=EN&Expert=595). XLCNM male patients are characterized by severe hypotonia, muscle weakness and atrophy. Perinatal asphyxia has been documented in several cases, and tracheostomy is often needed to maintain the patient alive. Indeed, respiratory failure is the main cause of death for many XLCNM affected males in the first years of life (Amburgey et al., 2017; Jungbluth et al., 2008). Only a small percentage of boys survive into childhood and adulthood (Biancalana et al., 2003).

In addition to the centralized position of nuclei (Fig. 2A, B), histology analysis on muscle biopsy have reported small muscle fibers resembling to fetal myotubes (Fig. 2A-B) (Spiro et al., 1966) with increased interfiber space and predominance of atrophic fibers. In addition, muscle fibers display abnormal oxidative staining in their central part and at their periphery, a phenotype called “necklace fibers” often observed by Nicotinamide adenine dinucleotide tetrazolium reductase staining (NADH-TR-TR) (Fig. 2C) or succinate dehydrogenase (SDH) staining. The ultrastructural analysis often shows increased mitochondria, glycogen aggregates, T-tubules and sarcoplasm reticulum cisternae accumulation in the center of the fibers and myofibril misalignment(Fig. 2D-E) (Romero et al. 2011). The abnormalities observed by ultrastructural analysis have been confirmed by immunohistochemical studies. Muscle patient biopsies display an accumulation in the center of the fibers of the DHPR and RyR1, key proteins for excitation-contraction coupling normally localized on the T-tubule and on the sarcoplasmic reticulum respectively. In addition, fetal-specific sarcomere structural proteins such as desmin and vimentin were abnormally detected in the center of the fibers (Sarnat et al., 1981; Shichiji et al., 2013). An increased labelling with anti-laminin and anti-collagen IV was also detected around patient muscle fibers (Van der Ven et al., 1995), indicating abnormalities in extracellular matrix composition.

On the contrary to male patients, XLCNM affected female carriers, who carry two X-chromosomes, are often asymptomatic. Most are not affected during childhood but often still

considered not sportive or athletic (Biancalana et al., 2017). However, a recent detailed clinical, histological and imaging study from 43 XLCNM affected females has reported a wide range in severity of symptoms. In the most severe cases, they can display an asymmetric phenotype in limb and facial muscle weakness and in skeletal development due to distinct X-chromosome inactivation ratio which leads to the expression of the mutated gene in only some part of the body (Fig. 3A). The muscle biopsy shows abnormal nuclei position and in some cases centralized nuclei as for males with XLCNM (Fig. 3B). Only few affected carriers present necklace fibers reactive for oxidative staining (Fig.3C). The muscle ultrastructure shows misorganisation of muscle fibers (Fig. 3D) (Biancalana et al., 2017).

To date, no prenatal exams are normally performed for parents to detect the XLCNM disease during the first child pregnancy, in the absence of a family history of disease.

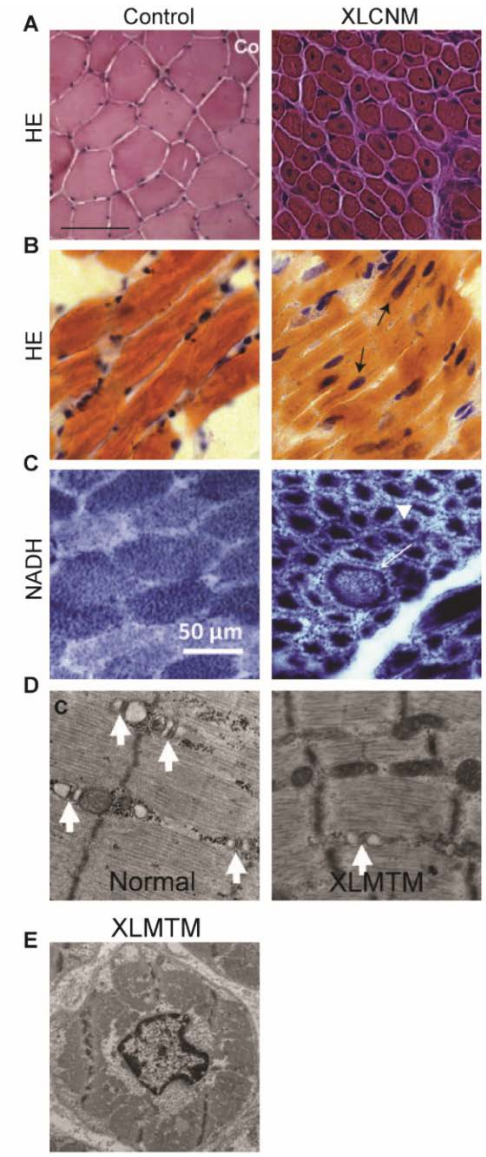

Figure 2: Histological features of XLCNM patient muscles

A, Transversal sections of control (on the left) and XLCNM muscles (on the right) stained with Hematoxylin and Eosin (H&E). The control muscle has hexagonal fibers tightly packed with nuclei in the periphery while the XLCNM muscle has round fibers and internalized nuclei. Derived from Abath Neto *et al*., 2016 and D. Biral *et al*., 2008, scale bar of control muscle: 100µm. **B**, Longitudinal sections of control (on the left) and XLCNM muscles (on the right) stained with HE. The control muscle has nuclei in the periphery while the XLCNM muscle has nuclei localized in the center of the myofibers (arrows). Adapted from M. Lawlor I., 2016. **C**, Transversal sections of control (on the left) and XLCNM muscles (on the right) stained with nicotinamide adenine dinucleotide tetrazolium reductase (NADH-TR). The XLCNM muscle patient fiber show a marked increase in the oxidative activity in the center, surrounded by a clear halo, forming “necklace” fibers (white arrow). The control muscle scare bar is 50µm and the XLCNM muscle scale bar is 100 µm. Adapted from Abath Neto *et al*., 2016 and Bohm *et al*., 2013. **D**, Ultrastructure of longitudinal muscle sections from control (right) or human X-linked myotubular myopathy (XLCTM) patients. XLCNM muscle has abnormal triad structure with misaligned Z-lines. White arrows indicate the triad structures. Adapted from M. Lawlor *et al*., 2016. **E**, Ultrastructure of transversal muscle sections from human X-linked myotubular myopathy (XLCTM) patients. The sections display nuclei in the center of the fiber, bordered by mitochondria, glycogen, and some tubular structures. Adapted from N. Romero *et al*., 2011.

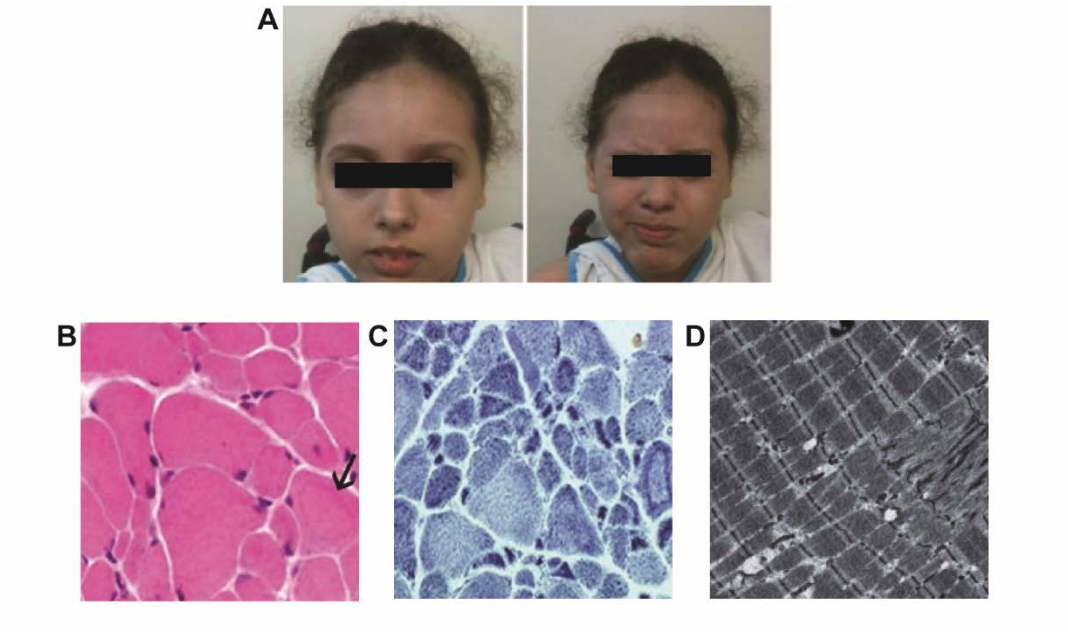

Figure 3: Facial and histological features of XLCNM females.

A, Patient section with facial asymmetry. **B**, Transversal XLCNM female muscle stained with H&E. Fibers display heterogeneous diameter and a necklace fibers display basophilic ring underneath the sarcolemma (arrow). **C,** Transversal section of a XLCNM female muscle stained with NADH-TR-TR. The section shows a high number of necklace fibers. D, Ultrastructure of a longitudinal section from XLCNM female muscle. The section shows a misorganisation of the muscle fiber. Adapted from Biancalana *et al*., 2018.

Characterization of the MTM1 gene

In 1990 Thomas *et al.* mapped the causative XLCNM region on the X-chromosome Xq28. Only 6 years after thanks to identification of new XLCNM patients with frameshift and missense mutations, Laporte *et al.* and a consortium of other 2 laboratories restricted the candidate region to 280 kb and identified the mutated gene responsible for X-linked myotubular myopathy by cloning, which they named Myotubularin 1 (*MTM1*) (Laporte et al., 1996) (https://www.omim.org/entry/300415).

MTM1 gene is 104 749 bp in length and consists of 15 exons (Laporte et al., 1998); it encodes a ubiquitous expressed transcript of 3.9 kb, and a 2.4 kb transcript only expressed in muscle and testis after birth. The 2 transcripts differentiate in the presence of polyadenylation signal on the mRNA (Laporte et al., 1997a) . Interestingly, point mutations, deletions and insertions causing XLCNM have been found along all the gene and lead to absence of protein expression or to a truncated non-functional MTM1.

Characterization of the MTM1 protein

MTM1 encodes the phosphatidylinositide phosphatase myotubularin (MTM1), a protein of 603 amino acids. It is highly conserved through evolution from yeast to mammals and is a member of a large tyrosine phosphatase subfamily with other 13 myotubularin-related proteins (MTMRs) (Laporte et al., 2003; Robinson and Dixon, 2006). Not only mutations in MTM1 are linked to a severe genetic disease but also the other MTMRs proteins are also associated with the severe genetic disorder Charcot-Marie-Tooth, demyelinating neuropathy.

Four domains have been identified in MTM1 proteins and in other MTMRs: the PH-GRAM domain (Pleckstrin Homology-Glucosyltransferase, Rab-like GTPase Activator and Myotubularin), the RID domain (Rac1-Induced Recruitment Domain), the dual specificity phosphatases domain (PTP/DSP) and the SID domain (SET-protein Interaction Domain) (Fig. 4A). The N-terminal PH-GRAM domain allows the binding to lipids, specifically to the phosphoinositide PtdIns(3,5)P_2 (Tsujita et al., 2004) that are enriched in early endosomes. This domain drives the interaction also with effector proteins. The RID domain helps the localization of MTM1 on the plasma membrane and allows the interaction with an intermediate filament protein, desmin (Hnia et al., 2011; Laporte et al., 2002). The PTP/DSP domain contains the His-Cys-X2-Gly-X2-Ar motif (HCSDGWDRT), a conserved phosphatase motif necessary for MTM1 to dephosphorylate phosphoinositide (Taylor et al., 2000). The SID domain interacts with SET domain proteins, common in protein involved in epigenetic regulation (Cui et al., 1998).

In vitro experiments showed that MTM1 increases its phosphatase activity in oligomerization state and binds the phosphoinosides as a heptamere. Interestingly, MTM1, as

the other active myotubularin-relative proteins, increases its phosphatase activity also in heterodimer state binding active or dead phosphatase such as MTMR10 (Schaletzky et al., 2003). In the heterodimer state, the dead phosphatase might regulate the localization and the activity of the active member (Lorenzo et al., 2006).

Characterization of MTM1 function

MTM1 and phosphoinositide regulation

Several studies showed the important role of MTM1 in phosphoinositide regulation. *In vitro* and in mammalian cells experiments described the ability of MTM1 to regulates the pool of PtdIns(3)P and PtdIns(3,5)P_2 levels, by dephosphorylating the position D3 (Fig. 4B) (Lorenzo et al., 2006; Tronchere et al., 2004). PtdIns(3)P are enriched in early endosomes and middle body endosomes (Fig. 4C). They are implicated in membrane trafficking recruiting proteins with a FYVE domain, such as EEA1 or PX domain that is found in endosomal sorting nexin SNX proteins (Marat and Haucke, 2016). PtdIns(3,5)P_2 is the other substrate of MTM1. They are mainly found in endosomal membrane and specifically bind VPS24, a protein involved in endosomal sorting (Whitley et al., 2003). MTM1 dephosphorylate PtdIns(3)P into PI and PtdIns(3,5)P_2 into PtdIns(5)P. PtdIns(5)P is present on late endosomes and in intermediate compartment trafficking from endosomes to plasma membrane (Fig. 4C).

MTM1 in membrane recycling and remodeling

The dephosphorization activity of MTM1 plays a crucial role in membrane recycling. Overexpression of MTM1 affects endosomal sorting through a reduction of PtIns(3)P in the cells. Co-localization studies with endosomal markers showed that endogenous MTM1 co-localizes with Ras-related protein 5 (Rab5) (marker for early endosomes) and Ras-related protein (Rab7) (marker for late endosomes) in cells (Fig. 4D). In addition, immunoprecipitation assay showed that hVPS-15/hVPS-34 lipid kinase, which is important for the formation of PtIIns(3)P on the endosomal membrane, associates with MTM1 and Rab5 or Rab7 in the endosome membrane in a mutually exclusive manner (Cao et al., 2007). In addition, MTM1 has been involved in the recycling of Epidermal Growth Factor Receptor (EGFR) and integrin (Cao et al., 2008; Tsujita et al., 2004). *mtm1* depletion in *Drosophila* caused accumulation of integrin inside the muscle fibers. The same phenotype was also observed in XLCNM patient fibroblasts (Ketel et al., 2016; Ribeiro et al., 2011).

In skeletal muscle immunogold labelling and biochemical analysis showed that MTM1 localizes on the SR (Introduction, Brief introduction to skeletal muscle biology). Modulation of MTM1 protein level in skeletal muscle allowed to visualize different shape of the SR suggesting that MTM1 and the level of PtdIns(3)P are both involved in SR membrane remodelling (Amoasii et al., 2013).

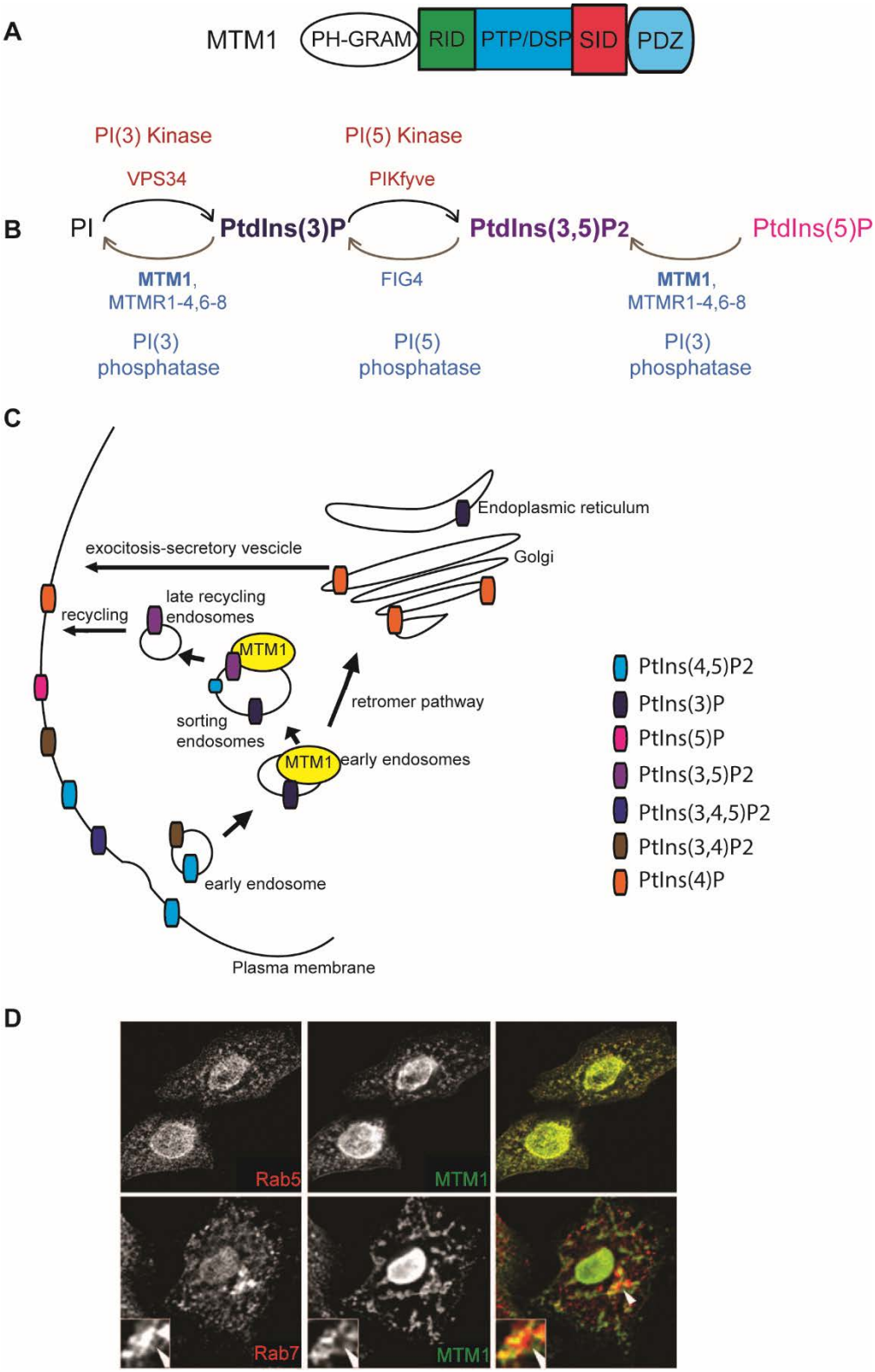

Figure 4: MTM1 PI phosphatase activity and subcellular localization

A, MTM1 protein domains. **B**, Phosphoinositide synthesis in human. Kinases are represented in red, and the phosphatases in blue. **C,** Representation of phosphoinositide localisation in selected membrane trafficking pathways. The phosphoinositide are represented with different colours. Adapted from J.O De Craene *et al*., 2017. **D,** Endogenous MTM1 (in green) colocalizes with Rab5 (red, on the top) and Rab7 (red, on the bottom) in the in A431 cells. Cao *et al*., 2007.

MTM1 and autophagy

A depletion of MTM1 leads to the increase of PtdIns(3)P which was reported to promote autophagosome biogenesis (Cebellero et al. 2012). Two parallel studies conducted in a mouse model deficient for *Mtm1* (*Mtm1-/y*) reported an accumulation of LC3 and p62, polyubiquitinated proteins and an unexpected persistent high level of mTORC1 (mammalian target of rapamycin complex 1) activation which is known to suppress autophagy and cell growth (Al-Qusairi et al., 2013; Fetalvero et al., 2013). In both studies the loss of MTM1 causes an inefficient autophagic process.

Animal models

After the discovery of the gene implicate in XLCNM, several models have been produced to better investigate the pathophysiology of XLCNM.

The first XLCNM animal model was generated by A. Buj- Bello in 2002. The Knock-out mouse model was produced by the deletion of exon 4 in the *Mtm1* gene (*Mtm1-/y*) in a B6N background (Buj-Bello et al., 2002b). *Mtm1-/y* mice displayed muscle weakness around the 3rd week of age, developed ptosis and kyphosis around 6 weeks of age (Fig. 5A) and had a severe reduction of muscle mass (Fig. 5B). They died around 7 weeks of age due to a progressive myopathy affecting breathing and eating. The histology of *Mtm1-/y* muscle showed hypotrophic fibers with almost 30% of internal nuclei (Fig. 5C). NADH-TR staining showed abnormal mitochondria localization at the sarcolemma (necklace like fiber) (Fig.5C) and ultrastructure analysis shows misalignment of the myofibrills (Fig. 5D), an increase of abnormal mitochondria shape and dimension and a decrease in the number of triad. Neuromuscular junctions were enlarged with reduced invagination (Buj-Bello et al., 2002a; Dowling et al., 2012). A similar phenotype was also observed in conditional muscle specific *Mtm1-/y* mouse (Buj-Bello et al., 2002a).

The Zebrafish XLCNM model was created by Dowling in 2009. The antisense morpholino (MO) technology was used to knockdown myotubularin (MTM MO) (Dowling et al., 2009). The MTM MO zebrafish displayed abnormal morphology at the embryonic state (Fig. 6A) followed by abnormal motor function with decreased spontaneous muscle contraction. Histological muscle analysis identified enlarged nuclei and hypotrophic fibers with an increase in the interfiber space (Fig. 6B). In addition, ultrastructure pictures illustrated aberrant T-tubule and some fibers have large membrane accumulation of unclear origin (Fig. 6C) (Dowling et al., 2009).

CNM is a natural occurring disease in dog. The first XLCNM dogs reported were Labrador Retriever pups in 2010 (Beggs et al., 2010). The XLCNM Labradors have been bred onto beagle background and have been used for preclinical studies. The myopathy phenotype

appeared around 8 weeks of age with pelvic limb weakness that progressed to an inability to walk. The muscle biopsies displayed an increase variability of fiber size and many of the small fibers have internalize nuclei (Fig. 7A). This animal model also showed abnormal NADH-TR stained fibers with stained in the center (as is reported in XLCNM patient) and closed to the sarcolemma (as is observed in the murine model) (Fig. 7A). Ultrastructure pictures displayed

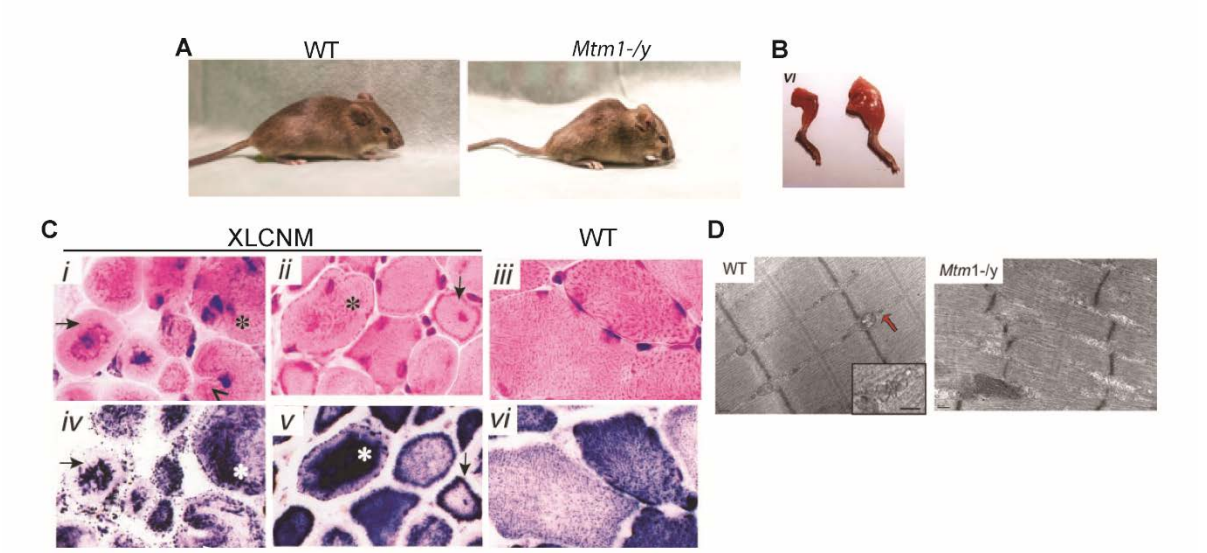

abnormal T-tubules orientation and misalignment of the Z-line (Fig. 7B) (Beggs et al., 2010).

Figure 5: Mtm1-/y (XLCNM) mouse model.

A. Difference between the XLCNM mouse model and the wild-type (WT) control. The XLCNM mouse shows signs of kyphosis, due to lesions in paravertebral muscles and hind limb paralysis. Adapted from E. Gayi *et al*., 2018. **B**, Illustration of the significant reduction in muscle mass reduction in the hind limb (Left) compared to WT (Right). **C,** Transversal muscle sections of 6-week-old mice stained with H&E (i–iii) and NADH-TR -TR (iv–vi). The WT (iii and vi) muscle, have nuclei on the periphery and homogenous NADH-TR staining. XLCNM mouse model muscle have nuclei in the center of the fiber (black arrow) (i, ii, iv, and v) and central (black arrow) or peripheral (*) accumulation of NADH-TR-TR staining. Derived from Buj-Bello *et al*., 2002. **D**, Ultrastructure of longitudinal section of skeletal muscles from control or Mtm1-/y mice. The arrow points at the normally localized triad in the control muscle. High magnification of the triad is shown in the insert. XLCNM muscles display smaller myofibrils than the control, misaligned Z line and few or no normal triads can be detected. Scale bars: 200 nm; 100 nm (high magnification). Adapted from: Cowling *et al.,* 2014.

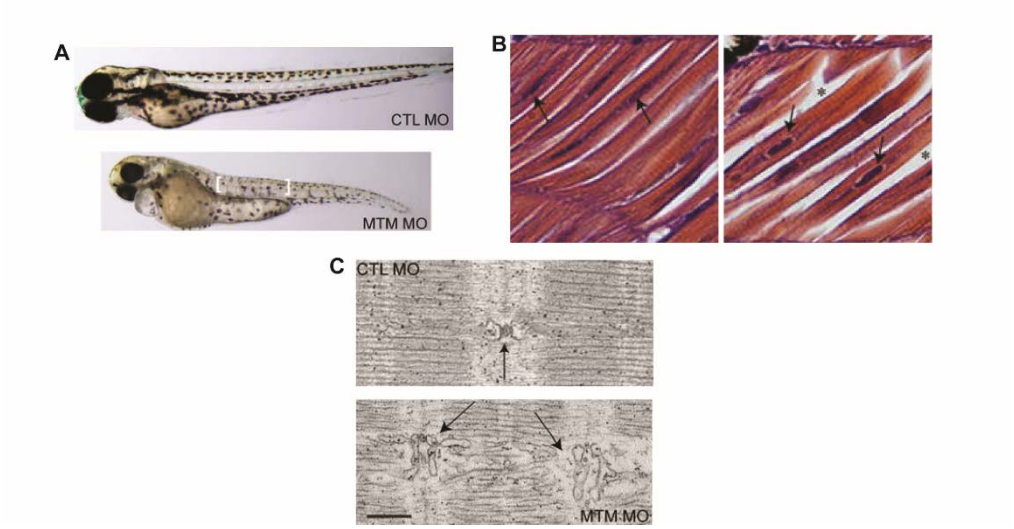

Figure 6: Myotubularin morpholino zebrafish model has abnormal morphology and muscles.

A, Live embryos 72 hour post injection with control (CTL MO) or myotubularin (MTM MO) morpholinos. MTM morphants have thinning of the muscle compartment (brackets) and shorter tails compared to the control. **B,** Longitudinal sections of myofibers from CTL MO and MTM MO morphant embryos stained with HE. The MTM KO muscle displays abnormally rounded myonuclei (arrows) and increased inter-fiber space. **C,** Ultrastructure of longitudinal muscle sections. CTL MO has normal and well-organized triads with T-tubule and SR network (arrow). Myotubularin morphants (panels 2–4): shows severely dilated SR and unrecognizable triads. Scale bar = 500 nm. Adapted from J.Dowling *et al.,* 2009

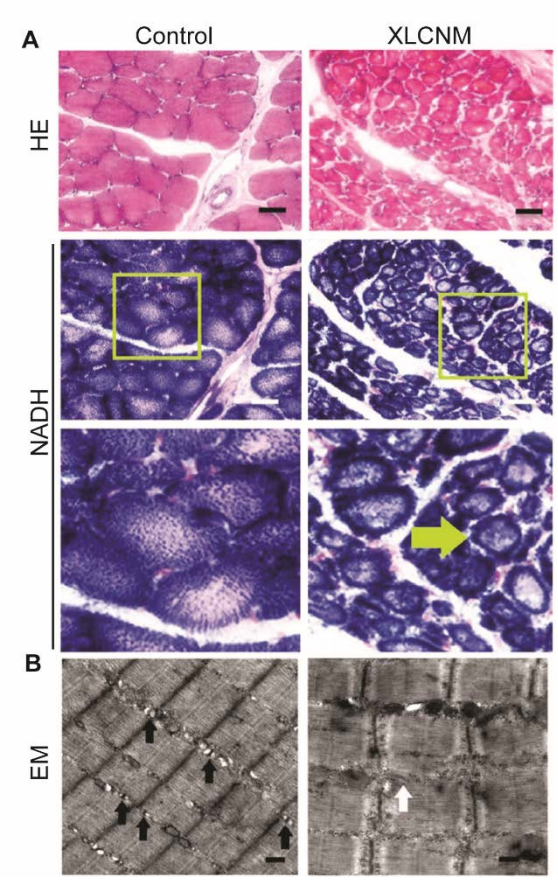

Figure 7: XLCNM canine model.

A, Transversal sections of cranial tibialis muscle stained with H&E and NADH-TR-TR. The fiber size of XLCNM dog model are smaller with accumulation of the NADH-TR-TR staining compared to the control. (Scale bars = 25 µm). **B,** Electron microscopy pictures of longitudinal muscle sections shows normal T-tubules (black arrows) in the control muscle and abnormal L-tubules (white arrow) in XLCNM dogs. Scale bars = 500 nm. Adapted from M.K.Childers *et al.,* 2014.

MTM1 function and activity was also studied in Drosophila. Total depletion of *mtm* in *Drosophila* reduced fly viability while loss of *mtm* in muscle had no effect in larvae stage but rather in later development (Ribeiro et al., 2011; Velichkova et al., 2010). Indeed, muscle depletion causes lethality or development delay. The adult *mtm Drosophilae* were flightless compared the control (Ribeiro et al., 2011). This model was mainly used for studying the ß1 integrin recycling as it was found that these animals have abnormal accumulation of ß1 integrin inside muscle fibers (Ribeiro et al., 2011).

All the other type of CNMs are divided in Autosomal dominant or recessive CNM groups. In addition to XLCNM, The following section provides an overview of these diseases, including genetic basis, implicated gene, and animal models, with a focus on *BIN1* and *DNM2*.

Autosomal Centronuclear Myopathy: *BIN1*-related

Autosomal recessive CNM (ARCNM)

Homozygous loss-of-function mutations were first identified in *BIN1* to cause autosomal recessive centronuclear myopathy (ARCNM) (OMIM #255200), which affects the proximal muscles (Romero, 2010).

Incidence, clinical and histological features

Patients have a large clinical variability from severe to moderate symptoms. There are common features: diffuse muscle weakness which appears in infancy or childhood, facial weakness, feet abnormalities and high-arched palate and some patients have respiratory problems. 30 to 70% of the patients reported difficulties in movement and in climbing stairs with generalized hypotonia (http://rarediseases.info.nih.gov).

Histology analysis of patient muscle show a prevalence of fibers with centralized nuclei in comparison to control (Fig. 8A). Fibers are smaller and rounder compared the muscle of controls. The oxidative staining shows a radial (or spoke of wheel) shape in the center of the fiber (Fig. 8A) due to abnormal accumulation and localization of mitochondria, which is also visible by electronic microscopy. Ultrastructure analysis has revealed Z line misalignment, T tubules defects and internalized nuclei surrounded by an area without myofibril and containing glycogen granules and other organelles (Fig. 8B) (Bohm et al., 2013; Nicot et al., 2007; Romero and Bitoun, 2011).

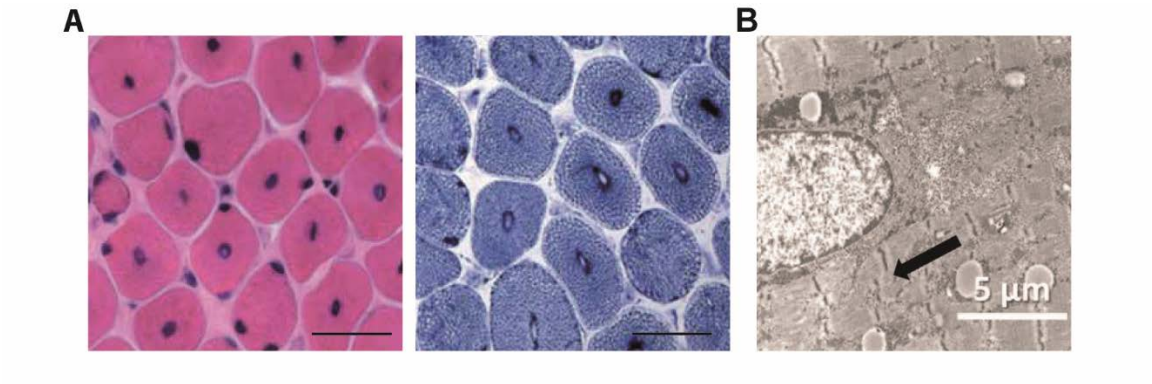

Figure 8: ARCNM skeletal muscle histology and structure.

A, Transversal section of deltoid muscle from ARCNM patient stained with HE (left) and NADH-TR (middle). The majority of nuclei are located at the center of the fibers and the NADH-TR staining reveals that the centralized nuclei are surrounded by dense staining. Scale bar 20 µm. Adapted from Nicot *et al.,* 2007. **B,** Ultrastructure of longitudinal sections of ARCNM skeletal muscle. The picture shows a centralized nucleus surrounded by organelles and misaligned Z lines. Scale bar 5µm. Adapted from Bohm *et al*., 2013

Autosomal dominant CNM (ADCNM)

Heterozygous mutations have also been identified to cause autosomal dominant CNM (Bohm et al., 2014).

Incidence, clinical and histological features

The patients display a mild phenotype with an adult-onset. The main clinical feature is progressive muscle weakness on the proximal muscle of the lower limb which lead to walking difficulties and some patients needs wheelchair (Bohm et al., 2014). Facial weakness and respiratory problems were not reported, in contrast to ARCNM.

Skeletal muscle histology pictures show fiber diameter variability and a high percentage of nuclei localized in the center of the fibers (Fig. 9A). In addition, a predominance of type 1 fibers was detected such as in the ARCNM. Another common feature with the ARCNM is the abnormal spoke of wheels staining observed with the NADH-TR staining (Fig. 9). In addition, in some fibers invaginations of the sarcolemma were observed. Ultrastructure analysis highlighted central nuclei surrounded by glycogen granules and mitochondria, enlarged vacuoles and autophagosomes (Fig. 9B) (Bohm et al., 2014).

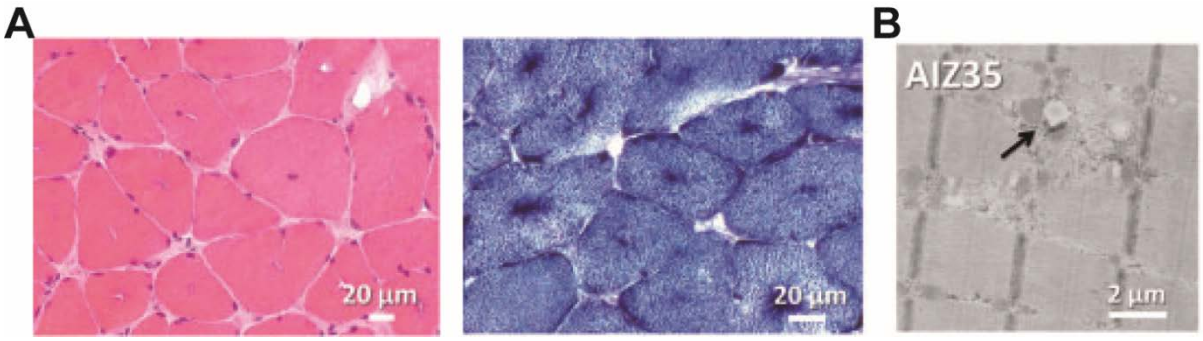

Figure 9: ADCNM skeletal muscle histology and structure.

A, Transversal section of skeletal muscle from ADCNM patient stained with HE (left) and NADH-TR (middle). The HE staining shows central nuclei. The NADH-TR staining shows a radial dense staining in the center of the fiber. **B,** Electron microscopy picture from ADCNM patient showing abnormal triads (black arrow) Scale bar 20 µm. Adapted from Bohm *et al*., 2014.

Characterization of the BIN1 gene

Amphiphysin II, Amphiphysin-like, Bridging integrator 1 and SH3P9 are the alternative name to Box-dependent MYC-interacting protein I (*BIN1*) (OMIM#601248). BIN1 was identified in 1996 thanks to a yeast two-hybrid screening for proteins interacting with Myc (Sakamuro et al., 1996). In the same year, Negorev *et al.* mapped the location of *BIN1* gene on the human chromosome region 2q14 using fluorescence *in situ* hybridization (FISH) revealing a coverage of 59,38 kb (Negorev et al., 1996). In mice the gene is located on chromosome 18q32 (Mao et al., 1999). Human and mouse *BIN1* genes share 89% homology. Mammals have two amphiphysin genes: amphiphysin I and BIN1 (amphiphysin II). Amphiphysin I is express in neuron while BIN1 is ubiquitously expressed.

The *BIN1* gene has 20 exons and alternative splicing produce tissue specific isoforms (Fig. 10A) (Nicot et al., 2007; Prokic et al., 2014). The muscle specific isoform is called isoform 8, and is the only one containing the exon 11 that codes for a muscle specific domain (Fig. 10B). It was initially called exon 10 (Lee et al., 2002; Toussaint et al., 2011; Wechsler-Reya et al., 1997). The isoform 8 does not include the exon 7, 13, 14, 15 and 16 which are neuronal specific exons (Prokic et al., 2014). In addition, the exon 17 has been identified in 42% of isoform 8 in human skeletal muscle and only in 9% of isoform 8 in mouse skeletal muscle (Toussaint et al., 2011). Inclusion of exon 7 and exclusion of exon 11 in the muscle isoform 8 lead to a myotonic dystrophy (Fugier et al., 2011). The cardiac and ubiquitous isoforms, called isoform 9 and 10, do not contain the exons 7, 13, 14, 15, 16 (as isoform 8) and exon 11 (Fig. 10B) (Prokic et al., 2014).

Characterization of the BIN1 protein

The mouse and human BIN1 proteins share 95% of homology. BIN1 is ubiquitously expressed, however it is highly present in brain and skeletal muscle where its expression dramatically increases during muscle cell growth and proliferation (Butler et al., 1997; Wechsler-Reya et al., 1998). Immunogold and immunofluorescence staining showed that BIN1 co-localizes with T-tubules in skeletal muscle fibers and its localization changes during muscle development corresponding to T-tubule reorganization (Butler et al., 1997). In neonatal muscle fibers BIN1 has longitudinal striation and switches to transversal orientation around 3 months of age (Toussaint et al., 2011).

BIN1 has various protein domains that are differently present in the different isoforms: Bin/Amphiphysin/Rvs (N-BAR) and phosphoinositide binding motif (PI) domain; clathrin and AP2 binding (CLAP) domain, important for endocytosis; Myc binding domain (MBD) and Src homology 3 (SH3) domain, implicated in protein interaction (Fig. 10C).

The exons from 1 to 10 encode for the N-BAR domain. In 1996 when BIN1 was discovered, extensive similarities were identified with the terminal regions of amphiphysin I and RVS167 for this reason the name: Bin/Amphiphysin/Rvs (BAR) (Sakamuro et al., 1996). This domain is ubiquitously expressed between all the BIN1 isoforms and it is involved in membrane and proteins binding (Fig. 10A-C, yellow) (Prokic et al., 2014; Royer et al., 2013).The brain specific isoforms domain is encoded by exons 13 to 16 and it is called CLAP. It is involved in the endocytosis thanks to clathrin and the adaptive protein 2 (Fig. 10B-C) (Prokic et al., 2014). The exon 11 encodes for the PI which is a muscle specific domain and is included only in BIN1 isoform 8 (Fig. 10B-C) (Prokic et al., 2014; Toussaint et al., 2011; Wechsler-Reya et al., 1997).The MBD domain is transcribed by the exon 17 and 18. However not always the exon 17 is expressed in adult skeletal muscle isoform (Fig. 10B-C) (Prokic et al., 2014; Toussaint et al., 2011; Wechsler-Reya et al., 1997). The exon 19 and 18 encode for the SH_3 domain. It is responsible for recruiting proline-rich domain (PRD) of other proteins such as synaptojanin and dynamin2. This domain is also interacting with neuronal Wiskott–Aldrich syndrome protein (N-WASP) and with MTM1 (Fig. 10B-C) (Prokic et al., 2014). To date BIN1 mutations identified in patients were localized to the N-BAR, PI and SH3 domains. Mutations on N-BAR domain and SH3 domain of BIN1 have also been identified in ADCNM.

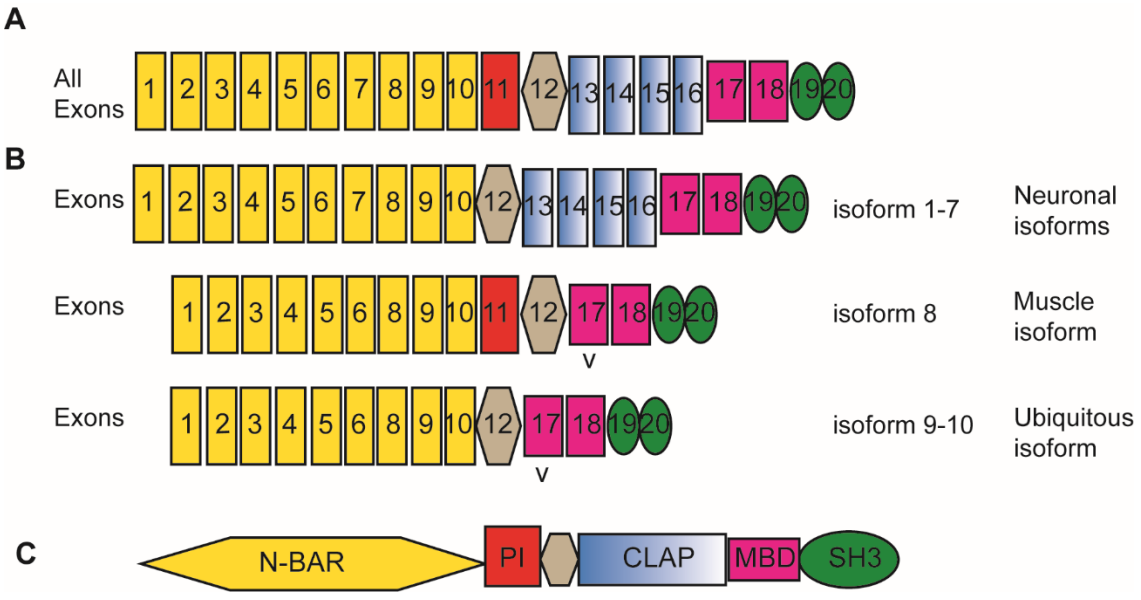

Figure 10: BIN1 isoforms and protein domains.

A, BIN1 exons. The exons in yellow code for the N-BAR domain, in red for the PI domain, in light blue for the CLAP domain, in pink for the MBS domain and in green for the SH3 domain. **B,** Representation of the exons present in each transcript isoform. The isoform from 1 to 7 are the neuronal isoforms which do not contain exon 11. The muscle isoform is the isoform 8, it does not have the exon 7 and the exons which encode for the CLAP domain. The exon 17 is alternatively spliced. Isoforms 9 and 10 are ubiquitously expressed and do not contain exon 7, exon 11 (PI domain) or exons which encode for the CLAP domain. v correspond to alternative spliced exon. **C,** Schematic BIN1 protein domains.

Characterisation of the BIN1 function

BIN1 and membrane remodeling

The N-BAR domain of BIN1 is involved in homo and hetero-dimerization with other BAR domain proteins such as amphiphysin I (Fig. 11A). The dimerization allows the positively charged concave face of the BAR domain to interact with the negatively charged lipids of the membrane (Peter et al., 2004). Two CNM mutations in BIN1 BAR domain, D151N and R154Q, decrease the ability of BIN1 to form dimer and consequently to bind the phosphoinositide (Claeys et al., 2010; Nicot et al., 2007). The N-BAR domain of BIN1 can sense membrane curvature. Indeed, the banana shape of the N-BAR domain binds the membrane in a curvature dependent manner. Moreover, the N-BAR domain of BIN1 has an N-terminal amphipathic α helix which anchors to the membrane. Biophysics analysis demonstrated that the N-BAR α helix increases insertion ability when the membrane is curved (Nishimura et al., 2018). Cryo-EM reconstruction of BIN1 N-BAR domain showed that α helixes from different BIN1 forming homo-interactions stabilize BIN1 polymers (Adam et al., 2015). Three CNM mutations, K35N and D151N and ΔK21 were identified in the N-terminal amphipathic α helix (Nicot et al., 2007). All the three mutations cause the replacement or the loss of a positively charged amino acid, and probably interfere with the structure of α helix compromising its ability to bind and sense membrane curvature and to create the homo-helix interaction necessary to stabilize the polymers structure (Hohendahl et al., 2016).

The interaction of the N-BAR domain to the plasma membrane enriched with PtdIns(4,5)P_2 and PtdIns(4)P is enhanced by the high basic amino acid content (9 out of 15) of the exon 11 which is expressed only in skeletal muscle isoform (isoform 8) (Fig. 11B) (Lee et al., 2002) (PtdIns(4,5)P_2 and PtdIns(4)P localization describes in Introduction, Fig.4C). Moreover, overexpression of BIN1 isoform 8 induces the formation of membrane tubulation in cells (Fig. 11C) (Lee et al., 2002; Nicot et al., 2007) and BIN1 PI domain was identified as a key player for membrane tubulation in skeletal muscle promoting the biogenesis of T-tubules in myotubes (Lee et al., 2002) (T-tubule described in Introduction, Brief introduction to skeletal muscle biology). However, exon 11 alone was not able to form tubules but it required the presence of N-BAR domain (Fig. 11B). The role of BIN1 in T-tubule formation was also highlighted in *Drosophila* and in CNM muscle patients. The loss of exon 11 due to an intronic mutation, IVS10-1G > A, which causes mis-splicing of the PI domain, leads to CNM. These patients have disorganized muscle ultrastructure and abnormal BIN1 localization. Overexpression of this mutation in cells caused decreased membrane tubulation (Bohm et al., 2013). The overexpression of K35N and D151N BIN1 mutants also decreased membrane tubulation (Nicot et al., 2007). These results strongly suggest the necessary contribution of

both the N-BAR and PI domains together in BIN1 protein localization and curvature-sensing function to promote membrane binding in skeletal muscle (Hohendahl et al., 2016).

In addition to phosphoinositide binding, the PI domain also binds with its own SH_3 domain. This interaction is thought to be crucial in regulating the activity of both PI and SH3 domains. The SH_3 domain, as already mentioned, interacts with various proline rich domain proteins, among them dynamin which is mainly involved in membrane fission. Biochemical assay showed that the basic amino acids of exon 11 competes with dynamin in binding the SH3 domain. BIN1 is described to be in a "folded" conformation when it is not interacting with phosphoinositides or dynamin. However, this conformation is disrupted upon the addition of dynamin which binds to the SH3 domain allowing the PI domain to be available for interactions with phosphoinositide and to bind the membrane (Kojima et al., 2004; Wu et al., 2014).

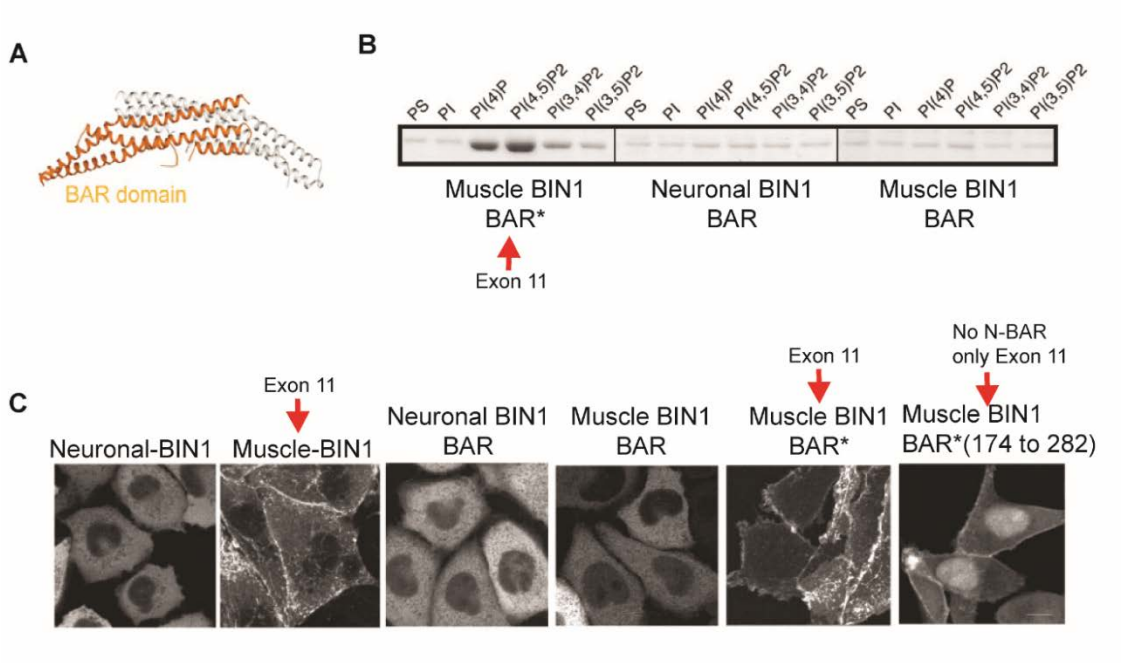

Figure 11: BIN1-BAR domain and phosphoinositide binding

A, Structure and assembly of N-BAR domain of amphiphysin I. Adapted from Daumke et al., 2014. **B,** Binding of the N-BAR and phosphoinositide. The N-BAR and PI domains of BIN1 (BIN1-BAR*) bind to PI(4)P and PI(4,5)P2. No binding occurs when the PI domain is missing as in the case of Neuronal BIN1-BAR and Muscle BIN1-BAR. Assessed using liposome binding assay. **C,** CHO cells transfected with different neuronal and muscle BIN1 GFP constructs. Muscle BIN1 and Muscle BIN1-BAR* (BIN1 N-BAR domain and PI domain) induce GFP positive membrane tubules on cells, these structures are not observed in cells transfected with Neuronal BIN1 isoform, Neuronal BAR and muscle BAR domain. The expression of the second half of the BAR* domain, which contains exon 11 Muscle BIN1-BAR* (174 to 282) localizes on the membrane but does not induce membrane tubules. Adapted from Lee *et al.*, 2002.

BIN1 and the cytoskeleton

BIN1 is involved in actin cytoskeleton and microtubule modulation. The SH3 domain of BIN1 interacts with N-WASP, an actin nucleation promoter factor and this interaction is disrupted by CNM mutation on this domain. Experiments on C2C12 cells showed that this interaction regulates triad formation and nuclear peripheral positioning in skeletal muscle (Triads description in Figure 1, Brief introduction to skeletal muscle biology). (Falcone et al., 2014). *In vitro* experiments showed that BIN1 binds and stabilizes actin filaments through its N-BAR domain. The BAR domain also modulates the microtubule network through the interaction with CLIP170 whose level is elevated in CNM patient fibroblasts. The ability of BIN1 to regulate microtubules and actin filaments and the interaction with nesprin, a protein localizing to the nuclear envelope, suggests a contribution of BIN1 in controlling nuclear positioning (D'Alessandro et al., 2015). This function of BIN1 is predicted to be lost in various CNM mutations on the *BIN1* gene. Indeed, a common characteristic of *BIN1* patients is the increase in centrally positioned nuclei in muscle fibers (ARCNM, Incidence, clinical and histological feature) (Romero and Bitoun, 2011).

In addition, in mouse brain and in human neuroblastoma cells, BIN1 colocalizes and interacts with TAU, a microtubule associated proteins implicated in microtubules assembly and maintenance. The hyper-phosphorylation of TAU in neurons causes the Alzheimer's disease (AD). Genome-wide association study linked BIN1 to the late-onset Alzheimer's disease and downregulation of BIN1 revealed an amelioration of Alzheimer's disease in *Drosophila* TAU neurotoxicity model (Chapuis et al., 2013). Recently, several studies underlay the important role played by BIN1 regarding the endocytosis and recycling of amyloid precursor protein (APP) in neurons whose aggregation is the main cause of Alzheimer's disease (Guimas Almeida et al., 2018).

BIN1 and membrane recycling:

The ability of N-BAR BIN1 domain to bind and remodels cells membranes and actin filaments suggests its involvement in endocytosis and endosome recycling. The neuronal BIN1 isoform 1, which contains the CLAP domain, is involved in clathrin mediated endocytosis (Prokic et al., 2014). In neuronal cells, the endocytosis activity of BIN1 has been well described. It can form homo-dimers or hetero-dimer with amphiphysin I or endophilin on the clathrin coated pits and interacts with clathrin, AP2 adaptor complex, synaptojanin, dynamin and N-WASP (Daumke et al., 2014; Nishimura et al., 2018; Wigge et al., 1997). In Hela cells, knock-down of the ubiquitous BIN1 isoform, which does not contain the CLAP domain, did not affect the cargo transferrin uptake. However, the intracellular transferrin levels were increased, and transferrin accumulated inside endosomes, suggesting that BIN1 plays a crucial role in endosome regulation (Pant et al., 2009). The role of BIN1 in membrane recycling was also

suggested by immufluorescence experiments in mammalian cells which showed that it could colocalise with early endosomal antigen 1 (EEA1) (early recycling marker), Ras-related protein 11 (Rab11) (recycling endosomal marker), CD63 (late endosomes and lysosome marker) (Leprince et al., 2003) and interact with Eps15 homology-domain protein 1 (EHD1) in skeletal muscle (Posey et al., 2014).

BIN1 and cancer:

BIN1 was initially identified as onco-suppressor interacting and blocking Myc. Cells culture experiments using carcinoma cells and primary breast cancer tumors showed that BIN1 level was dramatically reduced in those tumor cells (Sakamuro et al., 1996). Further studies showed that BIN1 is abnormally low expressed in a lot of tumors and its reduction increases cell proliferation, survival, and mortality, favoring tumor cell migration. Overexpression of BIN1 inhibits cells growth and induces cells apoptosis (Prokic et al., 2014).

Animal models

Several animal models have been generated to better study ARCNM and the role of BIN1 in muscle development and maintenance.

Drosophila mutants depleted of the only gene encoding for amphiphysin (*Amph)* were flightless. This model had abnormal skeletal muscle organization with a reduction in the number of T-tubules. This phenotype underlines the importance of BIN1 in T-tubule formation and maintenance (T-tubules: Brief introduction to skeletal muscle biology) (Zelhof et al., 2001).

To date three murine models have been published. The first, published in 2003, has a deletion of exon 3 in *Bin1*. Mice with the homozygous deletion did not express BIN1. Embryos developed normally but died at birth. Analysis conducted in the heart showed packed and disorganized cardiac myofibrils. Abnormality in endocytosis has not been observed (Muller et al., 2003). Because *Bin1*$^{-/-}$ prenatal death was associated with cardiomyopathy, a mouse with cardiomyocyte-specific loss of Bin1 was generated. This mouse had a mild phenotypes with a cardiomyopathy that began at 8-10 months (Laury-Kleintop et al., 2015).

The second mouse model was recently published. In this case the exon 20 was removed. *Bin1*$^{-/-}$ in mice was lethal at birth, most likely due to defects in skeletal muscle (Cowling et al., 2017).

A spontaneous dog model was found in 2003. A 3 year-old Great Dane dog had a mutation on the intron upstream exon 11 affecting the splicing of thee exon 11. The histology of the femoris muscle biopsy showed more than 40% of the fibers with centralized nuclei and muscle atrophy (Fig. 12A). As in patients, a radial staining was observed with NADH-TR staining (Fig.12B). The ultrastructure showed internalized nuclei with a surrounded area

depleted in myofibrills and accumulation of glycogen and organelles. In addition, Membrane invagination and autophagosmes were increased in the muscle (Bohm et al., 2013).

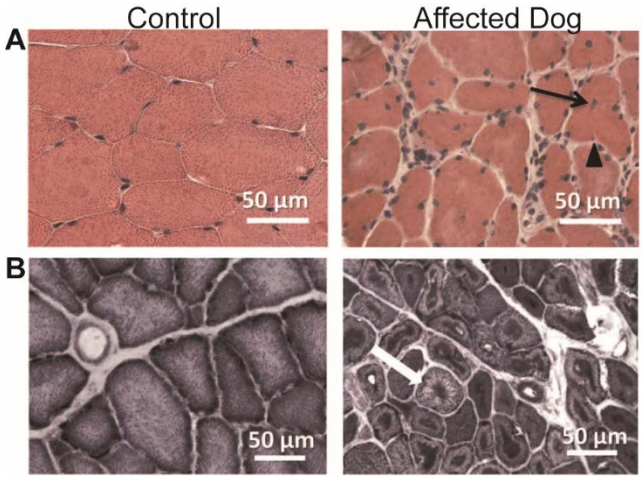

Figure 12: ADCNM canine skeletal muscle histology and structure

A, Transversal section of skeletal muscle from Control or ADCNM dogs stained with H&E (A) and NADH-TR (B). The H&E staining shows centralized nuclei and fiber atrophy. **B,** The NADH-TR staining shows dense staining in the center of the fiber. Scale bar 50 µm. Adapted from Bohm et al., 2014.

BIN1 mutations causes ARCNM and less extend studied some patients have ADCNM which can be due by mutations on *DNM2* gene.

Autosomal dominant centronuclear myopathy Dynamin 2-related (ADCNM)

Gain-of-function mutations in *Dynamin2* cause autosomal dominant form of centronuclear myopathy (ADCNM) (OMIM #16050). It is a form of congenital disorder characterized by a slow progression of muscle weakness.

Incidence, clinical and histological features

As other CNM, ADCNM Dynamin-related is a rare disease. Patients with a mild form develop the symptoms during adolescence or early adulthood. Patients with more severe ADCNM Dynamin 2-related form develop muscle weakness and hypertonia during infancy or in childhood, in these cases children required wheelchair and assistance.

Histological analysis showed abnormal NADH-TR staining. The center of the fiber is highly reactive to NADH-TR staining and displays a spoke of wheel staining from the center of the fiber (Fig.13A). The HE staining displayed nuclei positioned in center of the muscle fibers and often in a chain when observed on longitudinal muscle sections (Fig. 13 B-C). The ultrastructure pictures showed a disassembly of the myofibrillar organization around the nucleus (Fig. 13D) (Aghbolaghi and Lechpammer, 2017).

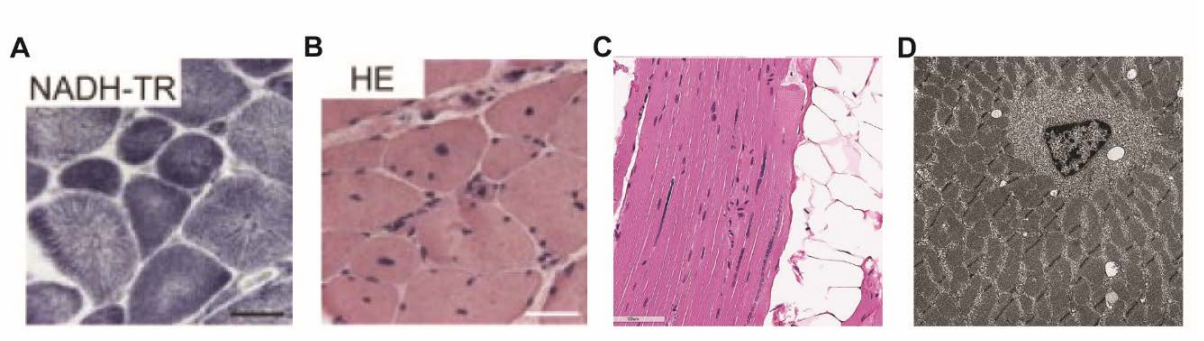

Figure 13: Skeletal muscle biopsy of ADCNM patient.

A, Transversal section of muscle stained with NADH-TR. Skeletal muscle has a radial arrangement of inter-myofibrillar network (spoke-like appearance) (scale bar 50 µm). Adapted from Cowling *et al*.,2011. **B,** Transversal section of muscle stained with HE. The picture shows fiber size variation with a high percentage of nuclei localized at the center of fibers, especially in small fibers (scale bar 50 µm). Adapted from Cowling *et al*.,2011. **C,** Longitudinal section of muscle stained with HE. The picture shows central nuclei often forming chains in a longitudinal section (scale bar 100 µm). Adapted from Aghbolaghi *et al*. 2017. **D,** Ultrastructure of muscle transversal section. Fibers with central nuclei and radial sarcoplasmic strands (X 6300). Adapted from Aghbolaghi *et al*. 2017.

Characterization of the Dynamin2 gene

Dynamin2 (*DNM2*) (OMIM #602378) is part of the large GTPase-binding family proteins with dynamin1 and dynamin3 in human. All three share a similar N-terminal sequence which codes for the GTPase domain. It is localized in the chromosome 19p13 and the sequence counts 22 exons (https://www.omim.org/entry/602378). *DNM2* gene codes for 5 possible DNM2 isoforms. The isoform 2 and 4 have an alternative splicing of the exon 10 which is substituted by a sequence of the same length and named exon 10 bis. The isoform 2 as well as the isoform 1 includes the exon 13bis while the isoform 3 and 4 do not have the exon 13bis (Cao et al., 1998). Recently another isoform has been detected specifically in skeletal muscle. It contains a new exon between exon 12 and exon 13, named exon 12B. The isoform including the exon 12B is increased during muscle differentiation and it is the main isoform expressed in adult skeletal muscle (Cowling et al., 2017).

Characterization of the Dynamin protein

Dynamin was discovered 30 years ago and was directly associated with its main function of membrane fission (Shpetner and Vallee, 1989). DNM2 is a protein of 100 kDa and it is ubiquitously expressed while DNM1and DNM3 are highly expressed in the brain and DNM3 also in testis (Cao et al., 1998). Most of the protein structure studies have been conducted on Dynamin1. Dynamins are formed by 5 domains: the GTPase domain, the middle domain, the pleckstrin homology (PH) domain, the GTPase effector (GED) domain and proline-rich sequence recognition domain (PRD) (Fig.14A).

The GTPase domain is at the N-terminal of the protein. It is reported to be constitutively loaded with GTP. The N-terminal and C-terminal helixes of the GTPase domain, together with the C-terminal helix of the GED domain, constitute the 3-helix buddle signaling element (BSE) (Chappie et al., 2009). The middle domain has an actin binding motif and, with part of the GED domain, composes the four-helix bundle called stalk. The BSE region controls the activity for membrane fission, transmitting the nucleotide-dependent conformational change received by the GTPase domain to the stalk. Depending on the information received by the BSA domain, the stalk mediates dimerization. The PH domain binds the PtdIns(4,5)P_2 (PtdIns(4,5)P_2 localization describes in Introduction, Fig. 4C). If the PH domain of DNM is not interacting with the lipid membrane, it assumes an auto-inhibitory conformation interacting with the interface 4 of the stalk region and preventing the formation the dimerization and oligomerization of the protein (Faelber et al., 2011). The PRD domain is a proline rich domain (PRD) which mediates the interaction with the SH_3 domain present in a lot of proteins such as BIN1 allowing the recruitment of DNM to the clathrin-coated pits (Antonny et al., 2016). Crystallography studies showed that DNMs dimerize thanks to the highly-conserved interface (called interface 2) of two stalks that assemble in a criss-cross fashion (Fig. 14 B-C) (Faelber et al., 2013). The

dimers oligomerize in a tetramer structure via two other stalk interfaces, named interface 1 and 3. The interface 1 interacts with the stalk of the neighbor DNM dimer while the interface 3 allows the formation of a ring-like oligomerization structure. The BSE of one DNM is interacting with the stalk region of the closest DNM dimer (interface 5). This contact allows the transmission of the conformational change of the GTPase domain to the other DNM dimers. In addition, two PH domains of the neighbor dimers are closed and may stabilize the oligomerization state of dynamin. Mutation in the PH domain interfere with the GTPase activity of DNM suggesting a cross-talk between these domains. DNM seems to assemble in a right-handed helical conformation. After one full helical turn around the membrane, the GTPase domain of DNMs localize in a turn dimerized with the one of the neighbor turn (Fig. 14D) (Faelber et al., 2013).

Most of the CNM mutations are cluster on the stalk region and in the PH domain. Mutations on the stalk region lead to the formation of more stable DNM2 oligomers, while mutation on the PH domain impacts on the GTP activity of DNM2 due to a conformational change of the protein (Kenniston and Lemmon, 2010; Wang et al., 2010). Several studies suggest ADCNM causing mutations may be gain-of-function and lead to more active DNM2 complexes (Buono et al., 2018; Cowling et al., 2011).

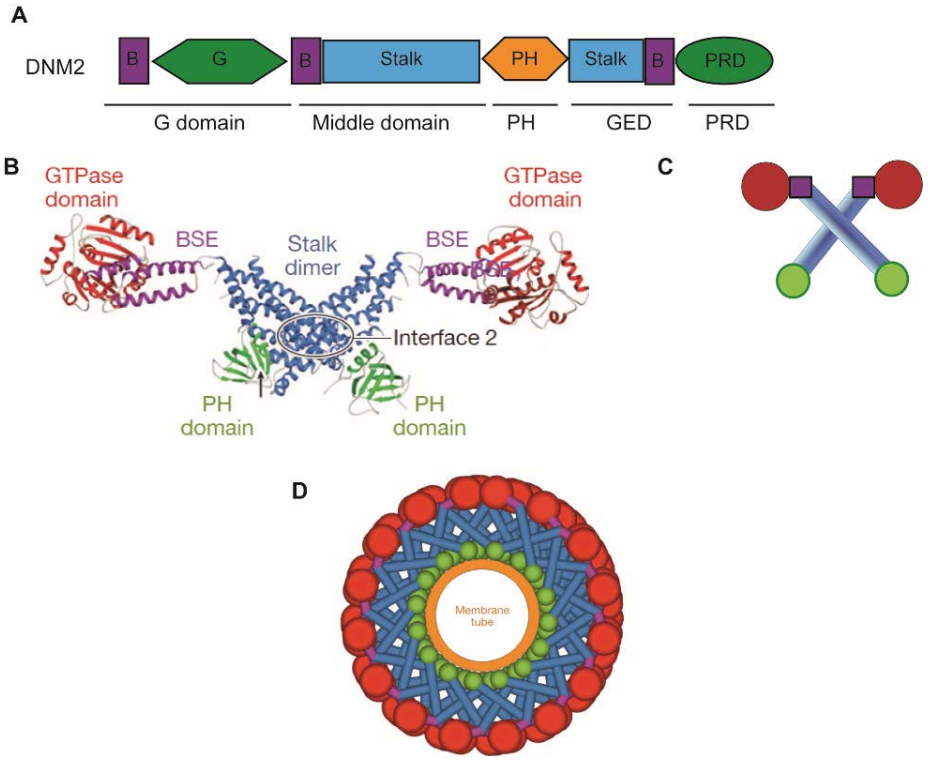

Figure 14: Structure and assembly of dynamin.

A, Representation of DNM2 protein domains. The G-domain is the GTPase domain, the PH domain is the pleckstrin-homology domain, the GED domain is the GTPase effector domain and the PRD domain is the proline/arginine-rich domain. **B,** Crystal structure of the dimer, showing the interfaces required for the assembly. **C**, A schematic representation of the dimer assembles. **D,** A schematic model for dynamin-mediated membrane fission. Adapted from Antonny *et al.*, 2016.(See main text)

Characterization of the DNM2 function

DNM2 and membrane fission

DNM oligomerization and GTPase activity are necessary for membrane fission which occurs during vesicle formation from clathrin-mediated endocytosis or caveolae-mediated endocytosis. DNM2 binds to membrane thanks to its interaction with the PtIns(4,5)P_2 and with BAR domain proteins such as BIN1 (Nicot et al., 2007).

GTP-bound DNM binds and forms helix around the membrane. Dynamin monomers do not hydrolyze the GTP cooperatively but independently. However, the GTPase domain of DNM interact with the neighbor DNM2s helix and this interaction is important for GTP hydrolyses. GTP hydrolysis allows a conformational change of DNM protein which lead to cascade events that imply twisting of the helical structure and constricting of the membrane. However, the mechanism of fission is still under discussion (Antonny et al., 2016). A recent publication reported that *in vitro* membrane fission is completed with the dissociation of the products of the GTP hydrolysis (the GDP and the P) (Takeda et al., 2018).

In COS-1 cell, the overexpression of CNM mutant DNM2 affects its localization and DNM2 presents cytosolic punctate pattern (Koutsopoulos et al., 2011). To evaluate if CNM mutation affected DNM2 activity in endocytosis, DNM2 mutants were overexpressed in different cell types but the results obtained were not homogeneous. Only a slight difference was detected between the mutant and the controls in clathrin independent endocytosis in *Dnm2* knock-out mouse fibroblast expressing DNM2 CNM mutant (E368K or R465W) (Liu et al., 2011). These results were not confirmed by a recent study conducted in mouse primary DNM2 $^{R465W/+}$ myoblasts and in human patient myoblast where an increase of transferrin uptake was observed (Rabai et al., 2018, accepted). This experiment suggests CNM R465W mutation in DNM2 is a gain-of-function mutation as it increases endocytosis activity in skeletal muscle.

In ADCNM DNM2 patient skeletal muscle, triads are abnormal, suggesting atypical DNM2 activity in membrane fission. In cells co-overexpression of CNM DNM2 mutants with BIN1 isoform 8 leads to fragmentation of BIN1 tubules (Chin et al., 2015). The same fragmented phenotype was also observed in *Drosophila* muscle which overexpressed DNM2 CNM mutant S619L (Gibbs et al., 2014).

DNM and recycling

In cells DNM2 is normally localizes close to the plasma membrane, at the endosomes, in the Golgi network and at the perinuclear region. Experiments conducted in Hela cells showed co-localization of DNM1 with early endosomes and in late endosomes. Defects in

transferrin recycling back to the plasma membrane was observed in cells expressing temperature sensitive mutant dynamin1 (dynamin-1^{G273D}) (van Dam and Stoorvogel, 2002).

DNM2 and cytoskeleton and microtubules

DNM2 was initially discovered through its co-localisation with microtubules. Further studies in Hela cells showed that depletion of DNM2 (using siRNA) could stabilize microtubules. Indeed, Microtubules depolymerization does not happen in cells not expressing DNM2 after treatment with the microtubule-depolymerizing drug nocodazole. This experiment suggests that microtubules stability correlates with the presence of DNM2 in the cells (Tanabe and Takei, 2009).

CNM *DNM2* mutants do not colocalize with microtubules in COS-1 cell. The decreased CNM *DNM2* mutant association with microtubules does not interfere with microtubule dynamic as ADCNM patients' fibroblast do not have any abnormalities in microtubules organization. Treatment with nicodazole causes a complete loss of microtubule while removal of the drug results in microtubule elongation for WT and mutant fibroblast (Koutsopoulos et al., 2011).

DNM2 localizes in clathrin-coated pits on the membrane thanks to the interaction with SH3 domain proteins. On this membrane compartment, DNM2 colocalizes also with proteins involved in actin polymerization, such as N-WASP (Hussain et al., 2001). These interactions suggest another possible role of DNM2 in actin filaments remodeling at sites of endocytosis. In addition, DNM2 associates with invadopodia and membrane ruffles during cell migration (Antonny et al., 2016; Durieux et al., 2010).

Animal model

The most frequent ADCNM mutation in *DNM2* is the missense mutation R465W where an arginine is exchanged by a tryptophan in the middle domain of DNM2. This CNM mutation increases the stability of DNM2 oligomer (Wang et al., 2010). Durieux *et al*. published in 2010 the first knock-in model expressing this gain-of-function mutation. Mice homozygous for this mutation died at birth and only few mice survived until 1 week of age while the heterozygous mice did not have any growth abnormalities and survived as the WT. The heterozygous mice (*Dnm2*$^{+/R465W}$) developed muscle atrophy around 8 weeks of age and had a slight reduction in *in situ* muscle force. The histology of *Dnm2*$^{+/R465W}$ muscle did not show internal nuclei but fibers had reduced NADH-TR staining and abnormal SDH staining (Fig. 15). Ultrastructural analysis showed abnormal T-tubule network and defect in calcium homeostasis (Durieux et al., 2010).

In the same year, Cowling *et al*. published a murine model of overexpression of DNM2 and DNM2^{R465W} in skeletal muscle. This model still expressed endogenous DNM2 at normal level. The overexpression of both DNM2 mutated or WT-DNM2 impacted on skeletal muscle

force, nuclei positioning and fiber size recapitulating a phenotype observed in ADCNM patients. However, a more severe phenotype was observed in muscle transduced with DNM2^{R465W} than with DNM2. The author concluded that overexpression of DNM2^{R465W} increased oligomerization and promoted its GTPase activity impacting in DNM2 normal muscle function. This data strongly suggested that CNM mutations cause gain-of-function of DNM2 activity (Cowling et al., 2011).

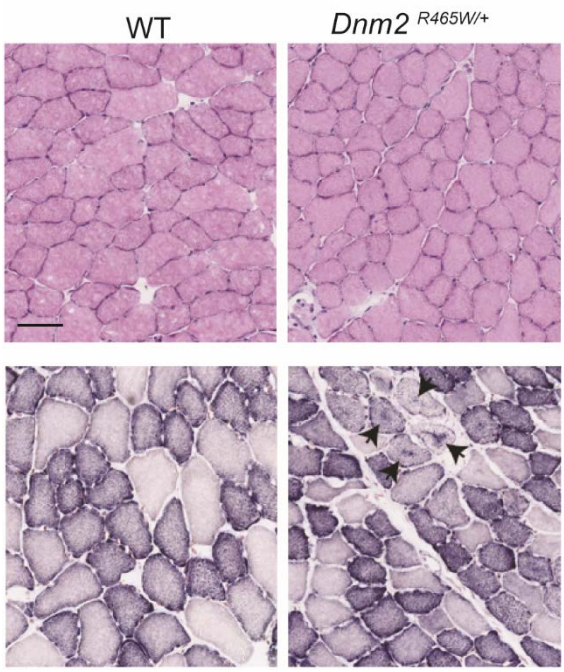

Figure 15 : Histology of Dnm2 R465W/+ mouse model.

Figure 15: Transversal section of Tibialis Anterior muscle from WT and Dnm2 R465W/+ stained with HE (upper pannel) and SDH (lower pannel). The mutant mice have smaller fiber compared to the WT control but no centralization of the nuclei. The SDH staining is abnormal in some fibers (arrow). Adapted from Buono *et al*., 2018.

The three proteins MTM1, BIN1 and DNM2 are related by common features. All three are involved in membrane remodelling and recycling and, when mutated, they all cause centronuclear myopathies. These data supports the hypothesis that they may be connected or involved in a common pathway, named the MAD pathway by our laboratory (Fig 16). The exact relationship between these three proteins however remains unclear.

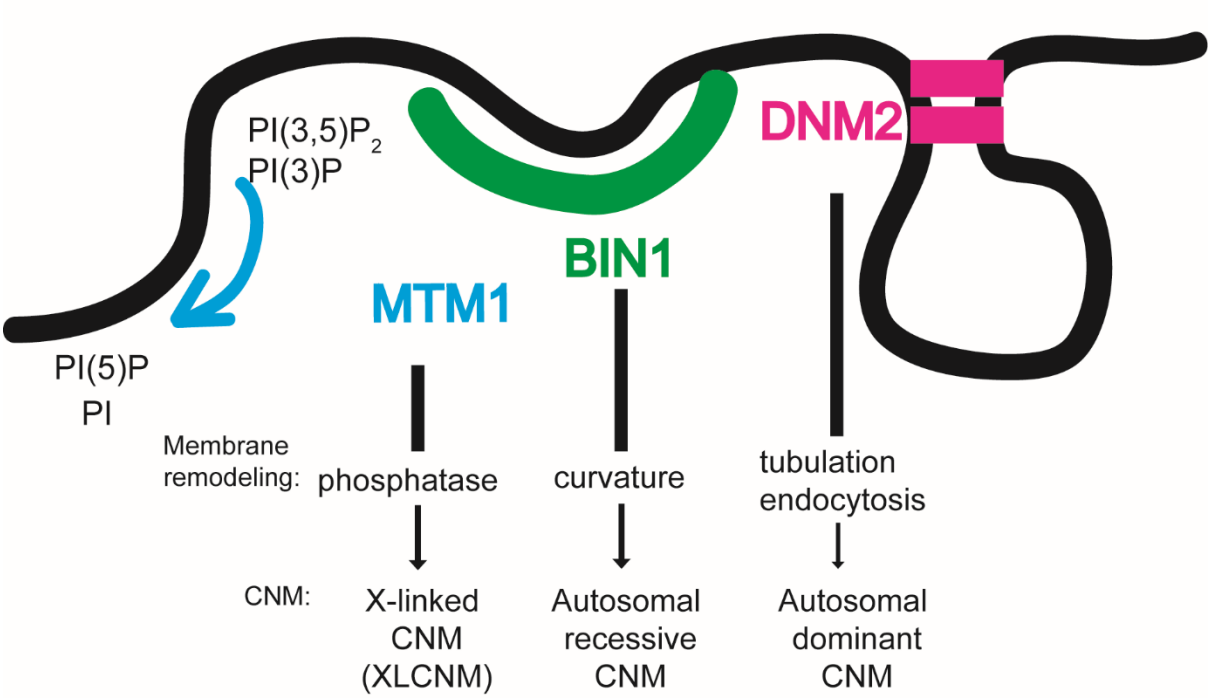

Figure 16: MTM1, BIN1 and DNM2 participate to membrane dynamics.

MTM1, BIN1 and DNM2 share common features: they interact with membranes, are involved in membrane remodelling and when mutated cause CNMs.

MTM1, BIN1 and DNM2 interact and regulate membrane remodeling

Following the identification of MTM1, BIN1 and DNM2 mutations in CNM, studies were conducted to understand if they could also interact in a common molecular pathway.

Pull-down experiments from skeletal muscle lysates suggested that MTM1 could bind BIN1 (Fig. 17A). This interaction may be crucial for the regulation of membrane tubulation in cells and, probably, also in skeletal muscle. In cells the co-transfection of BIN1 and MTM1 enhances membrane tubule formation (Fig. 17B) while in skeletal muscle it promotes the maintenance of the transversal orientation of the T-tubules. Indeed, at early stage of the disease, the skeletal muscle of the XLCNM model (*Mtm1-/y*), which do not express MTM1

but still have normal endogenous BIN1 level, display longitudinal oriented T-tubules instead of transversal. These data suggest that MTM1 may be implicated in maintaining the T-tubule in the correct orientation in skeletal muscle. MTM1 promotes the activity of BIN1 while BIN1 is not impacting on MTM1 phosphatase activity. Indeed, the presence of BIN1 does not influence the MTM1 production of PtdIns(3)P *in vitro* (Royer et al., 2013). In Royer et al., the authors evaluated if ARCNM mutations on BIN1 could alter the MTM1-BIN1 interaction. MTM1 interacted more efficiently with BIN1 mutated on its SH3 domain (p. Q573X and K575X) than with the WT-BIN1. *In* vitro experiments showed that the two ARCNM BIN1 mutations tested impaired the BIN1 intramolecular interaction PI-SH3 domain, promoting a constitutively open conformation of BIN1 which was always available to interact with MTM1. In this study, the expression of ARCNM BIN1 mutant and MTM1 still caused membrane tubulation in cells, but less efficiently than the co-expression of WT-BIN1 and MTM1. This data suggests that the interaction between MTM1 and BIN1 might have a pathological relevance (Royer et al., 2013).

In vitro binding analysis showed that BIN1 interacts with the PRD domain of DNM2 (Fig. 17C). It was observed by immunofluorescence analysis that DNM2 localized on BIN1 positive membrane tubules in COS-1 cells. The binding of DNM2 with ARCNM BIN1-mutant K575X was strongly reduced in comparison with the interaction of DNM2 and WT-BIN1. ARCNM BIN1-muttant K575X was still able to induce membrane tubulation in COS-1 cells, however without recruiting DNM2 on BIN1 positive membrane tubules, suggesting that ARCNM mutation caused not only loss of interaction but also loss of the regulatory function between BIN1 and DNM2. The author concluded that the ARCNM BIN1 loss-of-function mutation cause “a loss of function link” with DNM2 (Nicot et al., 2007).

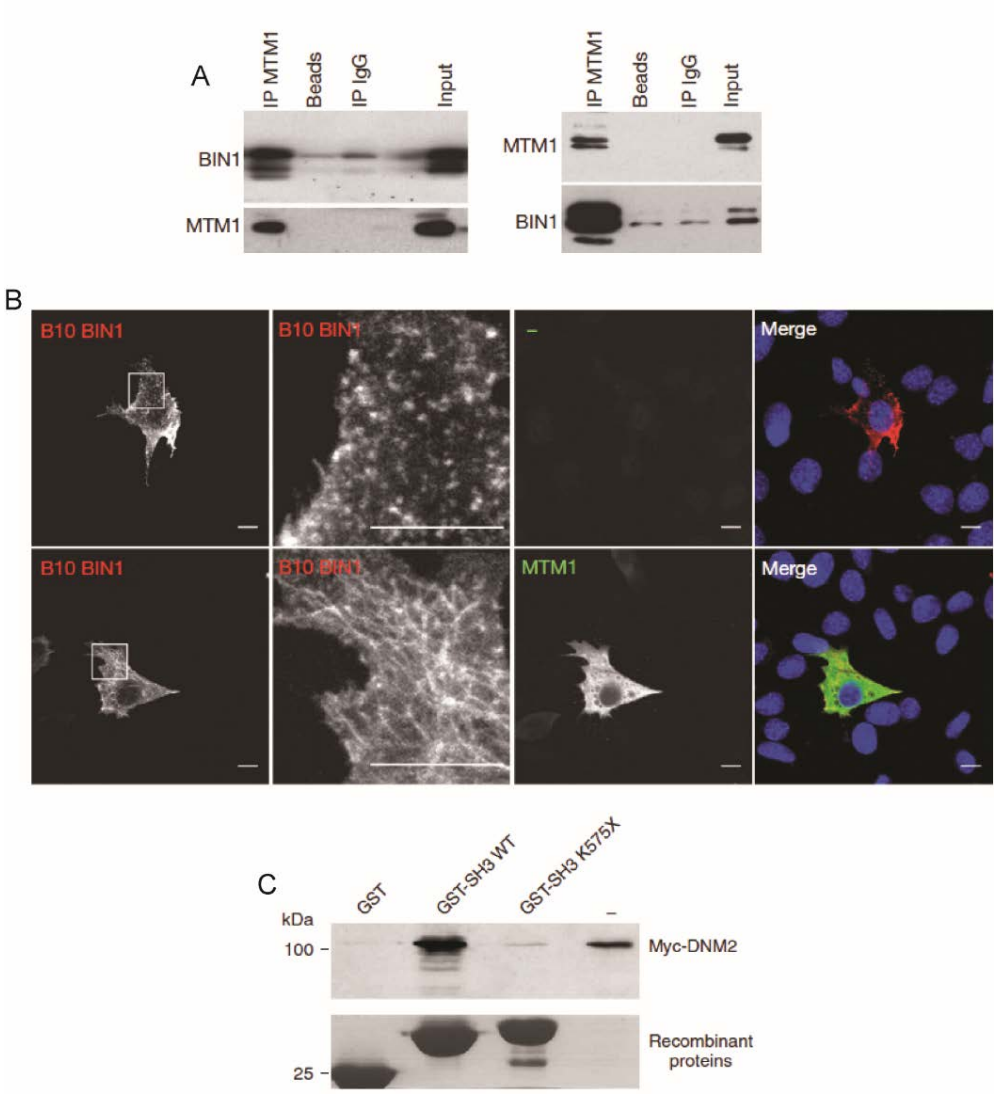

Figure 17: BIN1, MTM1 and DNM2 proteins interaction and membrane remodeling.

A, BIN1 interacts with MTM1 in vivo. Co-immunoprecipitation assays anti MTM1 (on the left) or anti-BIN1 (on the right) on membrane-enriched fractions of mouse muscle homogenates. The interaction was verified by immunoblot using BIN1 and MTM1 antibody. **B**, C2C12 transfected with B10-BIN1 alone displayed short tubules (upper panel). The co-expression of BIN1 and MTM1 promotes the formation of longer tubules in C2C12 (lower panel). Derived from Royer *et al*.2013. **C,** DNM2 interacts with BIN1 SH3 domain. GST-pulldown assay showed that the GST-tagged recombinant BIN1 SH3 domain was pulled down with Myc-tagged DNM2 overexpressed in COS-1 cells. Derived from Nicot *et al*., 2007

MTM1, BIN1 and DNM2 not only regulate the formation of tubules but participate in membrane recycling. Indeed, MTM1 localises on endosomes, binds and regulates phosphoinositides as it dephosphorylates in D3 position the PtdIns(3)P and PtdIns(3,5)P_2 to produce PtdIns and PtdIns(5)P, with the last one binding with BIN1. BIN1 has high affinity with membrane phosphoinositide PtdIns (4,5)P_2 , PtdIns (4)P and PtdIns (5)P. In addition to its role in endosome regulation and membrane recycling, BIN1 can bind and recruit DNM2 GTPase protein to the phosphoinositide membrane. The interaction between BIN1 and DNM2 is crucial for the regulation of DNM2 membrane fission ability crucial for endocytosis and membrane recycling. Recently *in vitro* lipids binding experiments showed that all muscle DNM2 isoforms (+ or – exon 12B) were activated by lipids binding, but DNM2 -12B activity decreased after the addition of BIN1 (Cowling et al., 2017). This study proposed that BIN1 negatively regulates the GTPase activity of the predominantly expressed DNM2 isoform during skeletal muscle development. However, no study has showed a co-participation of these three proteins for endosomal and membrane recycling to date.

It has been suggested that CNM mutations in MTM1 and BIN1 lead to loss-of-function of the proteins while CNM mutation on DNM2 lead to gain-of-function. In the membrane remodelling context, we can hypothesize that:

CNM mutations on *MTM1* gene result in most cases in loss of MTM1 protein expression. The lack of MTM1 causes an increase in PtdIns(3)P and PtdIns(3,5)P_2 in the cells. The transition between early to late endosomes is deficient and there is an accumulation of early endosomes in the cells as it was shown in XLCNM patient fibroblast by Ketel *et al.* in 2016. In addition, it is likely that not enough phosphoinositide are converted to PtdIns(5)P which is present in the plasma membrane. The lack of phosphoinositides may cause an impairment of recruitment of effector proteins necessary for membrane recycling and tubules formation (Ketel et al., 2016) (Phosphoinositides localization describes in Introduction, Fig. 4C).

ARCNM mutations in BIN1 BAR domain affects the ability of BIN1 to dimerize and to bind efficiently the membrane allowing membrane curvature and tubulation. Mutations on the SH3 domain of BIN1 impact on BIN1-DNM2 interaction (Nicot et al., 2007). In the XLCNM patients, BIN1 can still bind and interact with membrane but the lack of MTM1 is probably affecting the level of phosphoinositide on the endosomes and plasma membrane affecting the activity of BIN1 on membrane recycling and T-tubule formation in skeletal muscle.

ADCNM mutation on DNM2 generates proteins that dimerize in a more stable way than the WT-DNM2. This is an indication that DNM2 may be more active in the ADCNM patients, leading abnormal membrane fission in patients, preventing the correct organisation and architecture of the muscle fiber.

A better understanding the relationship between these 3 proteins has been obtained and potential novel therapies identified by playing on the expression of MAD proteins in animal models, termed ‘cross-therapies’.

Therapies

Cross therapies

It has been identified that *Mtm1-/y* mice and XLCNM patients had an increased level on DNM2 in their skeletal muscle (Cowling et al., 2014). In addition, intramuscular overexpression of DNM2 in mice causes a CNM phenotype (Cowling et al., 2011). These results raised the hypothesis that DNM2 may be more active in XLCNM mouse model and patients and its activity. To prove this idea, a cross-therapy strategy modulating the level of DNM2 in XLCNM model was developed.

In 2014, the first rescue using a cross therapy was published by Cowling *et a*l. In this study, the author proposed the downregulation of DNM2 as a new therapy strategy to cure XLCNM mouse model (Fig. 18 A). *Mtm1*-/y mouse, which die around 2 months of age, were crossed with HTZ *Dnm2* mice and the obtained *Mtm1*-/y *Dnm2-/+* mice survived as the WT control (Fig. 18 B). *Mtm1*-/y *Dnm2 -/+* mice have a rescue phenotype in muscle force, coordination and histology. This study strongly supported the hypothesis that MTM1 and DNM2 are probably in the same pathway and that MTM1 is negatively regulating DNM2 in skeletal muscle as when MTM1 is not expressed it is enough to reduce DNM2 to rescue XLCNM (Cowling et al., 2014).

Following on this study the same author tested if the downregulation of DNM2 was also rescuing the ARCNM mouse model due to loss of BIN1. In 2017, the downregulation of DNM2 was proposed as a therapy in an ARCNM mouse model (Fig. 18 C). In this publication, the author crossed the *Bin1-/+* with *Bin1+/- Dnm2 +/-.* The downregulation of DNM2 rescues life span and the growth of *Bin1*-/- mice (Fig. 18 D and E). As downregulating DNM2 in a *Bin1-/-* mouse model, these results suggest BIN1 may control DNM2 in a negative way (Cowling et al., 2017).

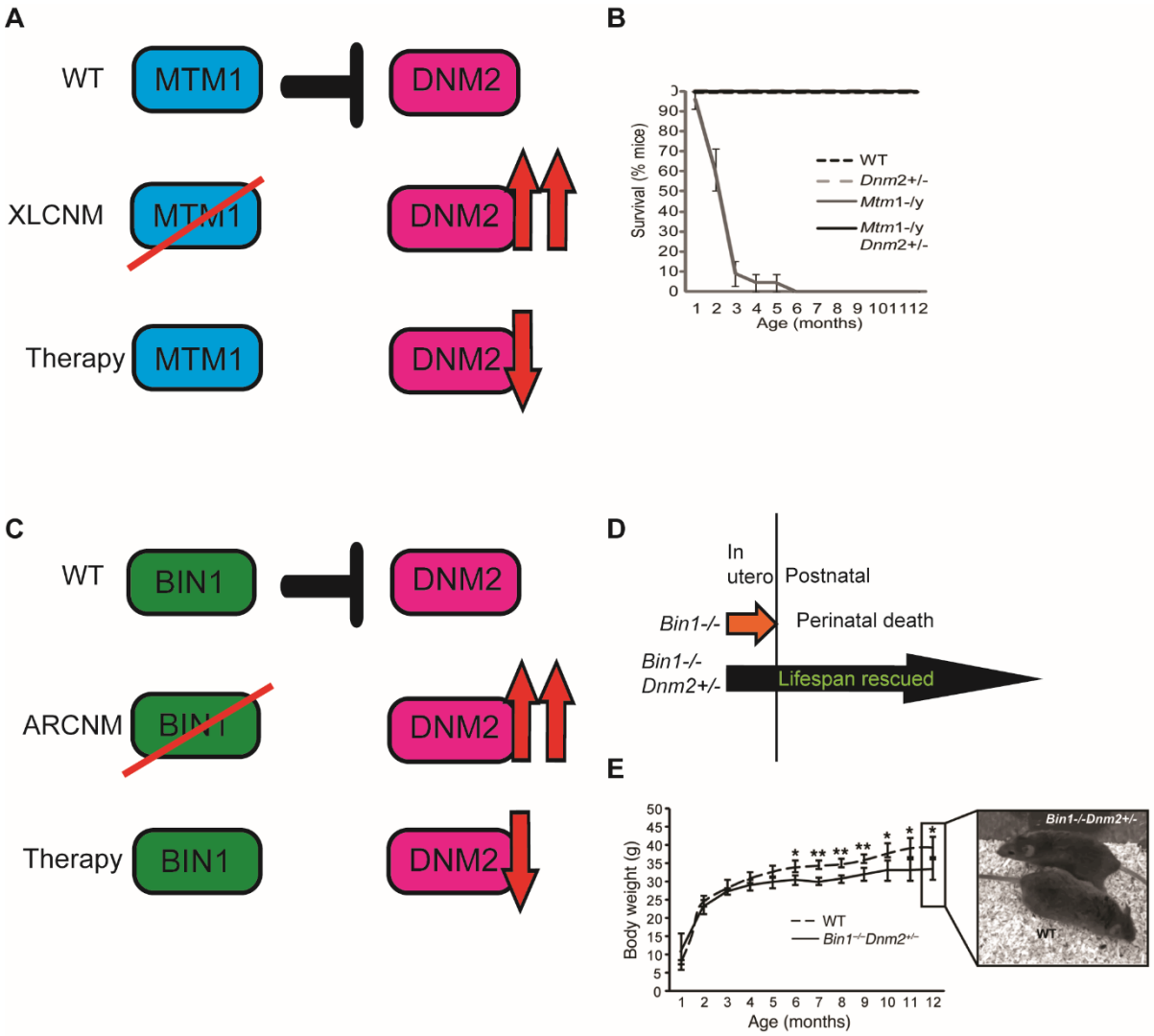

Figure 18: Cross therapy studies in CNM mouse models.

A, Schematic representation of the MTM1 and DNM2 level. In WT, MTM1 regulates DNM2. In XLCNM mouse model, DNM2 protein level is higher than the WT. In the rescue animal model, *Mtm1*–/y *Dnm2*+/– , DNM2 expression was decreased 50% in *Mtm1*–/y mouse model. **B,** Percentage of survival of WT, *Dnm2+/–,* and *Mtm1*–/y D*nm2*+/– mice. The reduction of DNM2 expression level rescues the life span of *Mtm1*–/y mice. Derived from Cowling *et al*., 2014. **C**, Schematic representation of BIN1 and DNM2 level. In WT, BIN1 regulates DNM2. In ARCNM mouse model, DNM2 is more active. In the rescue animal model, *Bin1*–/– *Dnm2*+/–, DNM2 expression was decreased 50% in *Bin1*–/– mouse mocel. **D,** Schematic representation of mice survival. All the *Bin1*–/– died at birth while the rescued Bin1–/– Dnm2+/–. Mice survived until 12 months. **E,** Body weight of WT and *Bin1*–/– *Dnm2*+/– mice. Adapted from Cowling *et al*., 2017.

Development of therapies

The encouraging results obtained by cross therapy helped to develop a new therapeutic strategy to cure XLCNM in the animal model. The post-birth DNM2 downregulation has been achieved with the injections of antisense oligonucleotide (ASO) which targets the mRNA of DNM2 (Tasfaout et al., 2017). The weekly systemic injections of ASO anti DNM2 were performed in *Mtm1-/y* mouse model from 3 week of age (pre-symptomatic age) or from 5 week of age (post-symptomatic age). In both cases this successful therapy drastically improved the life span and skeletal muscle force and histology and reverse the disease phenotypes (Tasfaout et al., 2017). This approach is now being developed for clinical trials in patients (https://www.dynacure.com/).

Recently, the downregulation of DNM2 was observed in human XLCNM muscle line treated with tamoxifen. Tamoxifen administrated to *Mtm1-/y* mouse model rescued the animal model life span and improved skeletal muscle force (Gayi et al., 2018; Maani et al., 2018).

Other therapies have been developed to rescue XLCNM using adeno associated virus (AAV) delivery. In 2008, BujBello *et al*. published a gene replacement therapy approach overexpressing MTM1 in *Mtm1-/y* mouse model. In this study, the systemic AAV delivery of MTM under the CMV promoter rescued muscle force, mass and histology in mice (Buj-Bello et al., 2008). Following studies showed new strategy to overexpressed MTM1 in muscle specific tissues using desmin promoter and the rescue was confirmed also in dog model (Childers et al., 2014; Mack et al., 2017). These positive results allow the gene therapy AAV-*MTM1* to enter into clinical trial; in September 2017 the first patient was injected with this AAV in USA (https://www.audentestx.com/).

Therapeutic strategy were also developed and tested to the *Dnm2*$^{R465W/+}$ mouse model for the ADCNM. As I presented before, ADCNM mutations DNM2 lead to an increase in protein stability; for this reason, an allele specific knockdown was proposed as possible therapy to decrease DNM2 protein level using shDNM2 delivered through AVV (Trochet et al., 2017). Improvement in the muscle mass and histology was visible 3 months post-intramuscular injection in *Dnm2*^{R465W} mouse. This therapeutic approach was also tested in *Dnm2*^{R465W} patient fibroblasts which have defect in endocytosis. The downregulation of DNM2 helps to rescue this abnormal phenotype.

The ASO used to downregulates DNM2 in XLCNM mouse model has been used to rescue also the *Dnm2*^{R465W} mouse model. Intramuscular and weekly systemic administration of ASO targeting the DNM2 mRNA rescued the muscle force, mass and histology of these mice (Buono et al., 2018).

An additional study was performed using *Dnm2*^{R465W} mutant myoblasts and CRISPR-Cas9 technology. An allele specific approach was used to target the mutated allele with siRNA via a CRISPR-Cas9 approach, to change the mutated allele. The abnormal increase on transferrin uptake described in *Dnm2*$^{R465W/+}$murine myoblasts and patient myoblasts was rescued thanks to the allele-specific genome editing (Rabai *et al*., 2018, accepted).

Focal adhesion

Focal adhesions are a multi- protein complex that anchor cells to extracellular matrix. They are a structural link between the external of cells and the inner part participating to cells migration, proliferation, growth and differentiation.

The first pictures of focal adhesion were published in 1971. Focal adhesions were initially described as “electrodense areas called plaque” located at the plasma membrane of lamellopodia in contact with the surface. (Abercrombie et al., 1971; Burridge, 2017; Couchman and Rees, 1979)

The identification of the “electrodense reagions” in the 70s arises curiosity for the identification of the transmembrane proteins involved in the connection between the extra-cellular matrix and the actin-based cytoskeleton.

Integrins

The discovery of integrin

During the 80s thanks to the used of monoclonal antibodies and cDNA library the transmembrane integrin proteins were identified

Integrins form heterodimers between an α and a ß integrin subunit, in vertebrate there are 8 ß integrin subunits and 18 α integrin subunits which can form 24 different heterodimers with different binding proprieties (Hynes, 2004).

Integrins protein structure

Integrins have three domains: an extracellular, a trans-membrane and a cytoplasmatic tail domains (Fig. 19).

The extracellular domains of integrins (α and ß) is composed by various subdomains which are organized in N-terminal globular head structures connected to the trans-membrane domain by two flexible legs. N-terminal globular heads allow integrins to interact with ligands and to form heterodimers. The transmembrane domains allow the homo and heterodimerize forming clusters on the membrane (Kim et al., 2011). The cytoplasmatic tails of α and ß subunits form a salt bridge that in some heterodimers maintain an inactive state of integrins.

The ß tail contains motifs necessary for phosphotyrosine-binding (PTB) and other binding proteins as talin (Fig. 19).

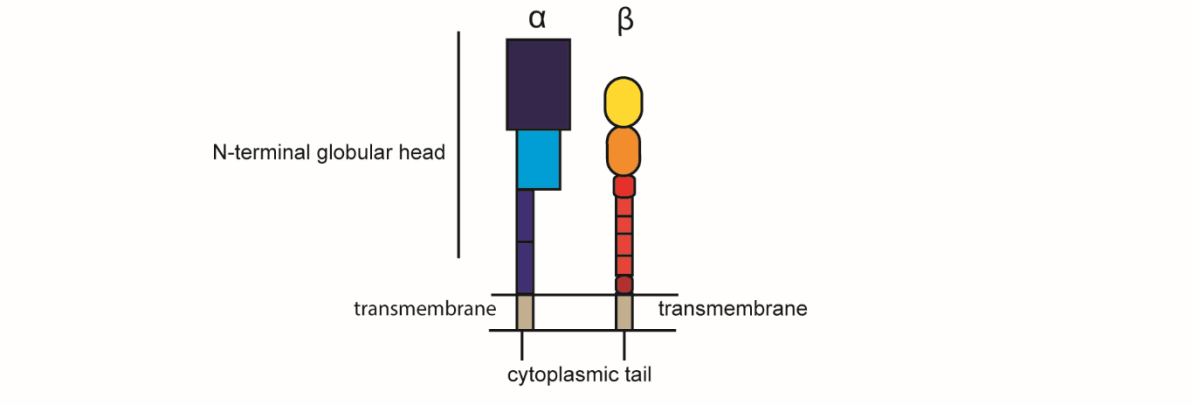

Figure 19: Integrins structure.

Schematic structure of α and β integrin subunit domains. Adapted from Anderson *et al.*, 2014.

Integrin signals

Integrins transmit signals from the outside to the cytoplasm (outside-in) or from the inside the cells to the outside (inside-out) depending on their ligands. The transmission of signal is due by the switch from an inactive to an active conformation. This transition happens after the binding of proteins to their cytoplasmic tail and to the interactions with ligands at the globular heads (Luo and Springer, 2006). After conformational change heterodimers of integrin can form cluster thanks to the homo-dimerization of the transmembrane domains.

Integrin functions

Integrins anchor cells to the extracellular matrix to allow cell adhesion or promote cell migration connecting actin cytosketron with the extracellular matrix (Huttenlocher and Horwitz, 2011). The binding with proteins of extracellular matrix drives signal from outside the cell to the cytoplasm (outside – in) modulating cytoskeleton structure arrangement and pathways through the proto-oncogene tyrosine-protein kinase (Src) and the focal adhesion kinase (FAK) (Luo and Springer, 2006; Shattil et al., 2010). In addition, intergins bind with the extracellular matrix proteins and promote their assembly. Experiments conducted in embryonic stem cells showed that ß1 integrin enhances fibronectin matrix assembly and controls the organization of laminin in a complex structure with the help of proteins part of dystroglycan complex, another cell surface receptor (Michael D. Henry et al., 2001) (Anderson et al., 2014).

Internalization and recycling of integrin

α_x and ß1 integrins can be endocytosed through a clathrine mediate endocytosis or through caveolin-1. Varoius mechanism regulates the endocytosis of ß1 integrin, one of those is mediated by the activity and phosphorylation of FAK, Src and DNM2. FAK auto-phosphorylates at the tyrosine 397 which is recognized by Src-homology 2 (SH2) domain of Src. The Src phosphorylates FAK in other sites allowing the interaction Src-FAK more stable and increases FAK kinase activity (Schaller MD. Et al., 1994). DNM2 is recruited at the focal adhesion site and is phosphorylated by Src at the tyrosin 231 and 597. These phosphorylations enhance DNM2 polymerization and promotes clathrine mediate endocytosis (Wang et al., 2011).

The integrins heterodimers internalized enter in early endosomes Rab-5 positive and they can be recycled back to the membrane or enter in the late endosomes and lysosomes trafficking. The destiny of integrin trafficking route depends on the proteins that interacts with integrin tails, for example the dissociation of kindlin from the ß1 integrin tail allow the binding of sortin nexin 17 to the ß1 integrin tail and mediates integrin recycling to the membrane (Bottcher et al., 2012). Depending on the type of heterodimers integrins follow the short or long loop of recycling. The short-loop recycling involved Rab 5, Rab21, Rab4 and PKD family members (Arjonen et al., 2012). After internalization, the tail of α integrin interacts with Rab21 in Rab5 positive endosomes and then to EEA1 positive endosomes. In the EEA1 positve endosomes, Rab 21 is displaced by p120RasGAP (RASA) which allows recycle back to the membrane via Rab4 dependent mechanism (Arjonen et al., 2012; Paul et al., 2015). The long loop is Rab11 dependent. ß1 integrin from the EEA1 positive early endosomes are transported to the middle body and then to the membrane by ARF6 and Rab11 positive late recycling endosomes (Powelka et al., 2004).

Integrins in skeletal muscle

In skeletal muscle the α_2, α_4 and α_5 have been identified and they dimerize with ß1 integrin. In adult skeletal muscle α_7 ß1 integrin heterodimer is the major laminin receptor ubiquitously expressed and it is normally localized at the costamere with the dystroglycan complex. In muscle integrins not only connect the extracellular matrix with the cytoskeletron but also provide the muscle stability during muscle contraction (Mayer, 2003).

In 1995, Fassler *et al*. analyzed ß1 null mice obtained from embryonic cells modified by homologous recombination. The embryos died around 5-6 days suggesting a problem before or around the implantation. To study the development of the embryos after the implantation period, the embryonic cells *ß1 integrin* KO were injected into normal blastocysts. The chimeric embryos with a contribution of *ß1 integrin* KO cells more than 25% displayed

defect on mouse morphogenesis while embryo with a contribution lower this percentage developed normally. In this study a high number of *ß1 integrin* KO cells was detected in skeletal muscle, they were however in a mosaic pattern with cells expressing normal level of ß1 integrin so no strong conclusions could be found on these mice regarding the role of integrin in skeletal muscle formation (Fassler and Meyer, 1995).

In vitro study showed that ß1 integrin contributes in myoblast fusion and myotubes formation. This result was then confirmed *in vivo* with the generation of mice ß1 integrin conditional KO in skeletal muscle. The mice died immediately after birth, no defect was observed in myoblast migration and proliferation but accumulation of not fused myoblasts were identified in limb muscle at embryonic day 16.5. To confirming that ß1 integrin contributes in myoblasts fusion, the author conducted experiments in vitro using primary myoblasts and observed that the mutant myoblasts do not fuse to form myotubes (Fig. 20) (Schwander et al., 2003).

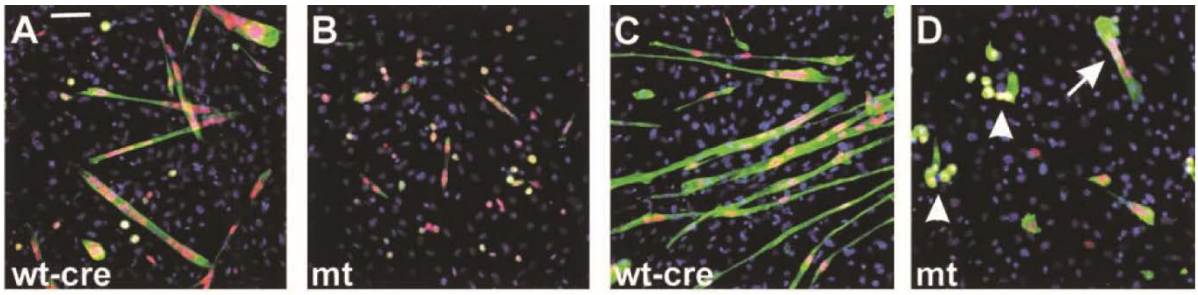

Figure 20: β1 integrin KO primary myoblasts.

Myoblasts were extracted from E18.5 wild-type and mutant embryos. The cells were differentiated on fibroblast layer for 1 (A and B) and 3 (C and D) days. The mutant myoblast do not fuse to form myotubes. There are only few shorts myotubes (D). The cells were stained with DAPI (nuclei), actinin (green) and Cre recombinase (red). Adapted from Schwander *et al*., 2003.

In parallel, studies were conducted to study the role of α 7 integrin in muscle. Mice lacking α 7 integrin developed normally and they were viable and fertile, they had progressive muscle dystrophy after birth. The main defect was observed in the myotendinous junctions, which connect the muscle to the tendon, in this side the sarcomere was retracted from the muscle membrane (Mayer et al., 1997). Patients with α7 integrin deficiency have been classified to have a congenital myopathy disorder. All the patients presented muscle weakness at birth and muscle atrophy predominantly in the proximal muscle (Hayashi et al., 1998; Nakashima et al., 2009). The gpatients' muscle fibers were slightly smaller compared to the control however the severity of the disease was hypothesized to be due by defect in the myotendinous junctions as the animal model α7 integrin KO displayed (Mayer et al., 1997). Even though these patients were classified with a congenital myopathy disorder, some clinicians considered them as dystrophic patients (Mayer, 2003; Nakashima et al., 2009; Pegoraro et al., 2002).

Recent study showed that myotubes with integrin silencing have abnormal central nuclei position. Integrins drive the peripheral nuclear positioning thanks to its ability to bind fibronectin and activate FAK, Src and paxillin to regulate cells cytoskeleton required for nuclei movement (Roman et al., 2018).

The MAD proteins and focal adhesion

MTM1, BIN1 and DNM2 have been identified to interact and regulate focal adhesion proteins and focal adhesion maintenance. The phosphatase activity of MTM1 is crucial for membrane recycling. Experiments conducted on *MTM* KO *Drosophila* model showed abnormal integrin protein localization in *Drosophila* muscle fibers (Ribeiro et al., 2011). This result was confirmed in XLCNM patient fibroblast where ß1 integrin accumulates in early recycling endosomes (Ketel et al., 2016). Focal adhesion turnover and trafficking dependent to DNM2 (Brinas et al., 2013). DNM2 is recruited in focal adhesion sites thanks to the direct interaction with FAK (Wang et al., 2011). Its recruitment is crucial for focal adhesion disassembling and integrin internalization. In addition, FAK directly interacts with the SH3 domain of Src and of amphiphysin 1 (Messina et al., 2003).

These results underline the importance of the equilibrium between MTM1, DNM2 and BIN1 in membrane remodeling, trafficking and recycling.

Goals of the PhD thesis

The greatest challenge in centronuclear myopathy field is the lack of available therapy for CNM patients. For this reason, the main aims of my PhD were to (1) identify novel therapeutic strategies to treat CNM and (2) investigate the *in vivo* molecular pathways implicated in CNM.

XLCNM (Results part 1 and 2) and ADCNM (Results part 3) are severe muscle disorders and, to date, there are no available therapies for patients. To identify novel therapeutical strategies, I focused on the role of DNM2 and BIN1 expression in CNMs. I contributed to DNM2 post-natal downregulation to rescue *Mtm1*$^{-/y}$ mice's phenotype (Tasfaout et al., 2018b) and I overexpressed BIN1 by genetic cross and adeno-associated virus (AAV) in *Mtm1*$^{-/y}$ mice (Lionello *et al.*, under second revision in Science Translational Medicine) , in *Dnm2* $^{R465W/+}$ and *Dnm2* $^{R465W/ R465W}$.

As previously described in the introduction, studies showed interactions between MTM1 and BIN1 (Royer et al., 2013) and between BIN1 and DNM2 (Nicot et al., 2007). In addition it has been reported that MTM1 and BIN1 negatively regulate DNM2 (Cowling et al., 2014; Cowling et al., 2017) (Introduction, Cross therapies). However no analysis were conducted on the relationship between MTM1 and BIN1. Thus, the second aim of my PhD was to investigate the relationship between MTM1 and BIN1 under normal and pathological conditions (Results part 2). To achieve this goal, I characterized the *Mtm1-/y* mice overexpressing *BIN1* and I performed mechanistic study on primary myoblasts. This experiment allowed us to understand that MTM1 and BIN1 are positively linked and their involvement in integrin recycling.

Results

Part 1. Single intramuscular injection of AAV-shRNA reduces DNM2 and prevents myotubular myopathy in mice.

Introduction

Loss-of-function mutation on *MTM1* gene caused a severe congenital myopathy form, X-linked centronuclear myopathy (Introduction, XLCNM). Patients have muscle weakness and atrophy at birth. Most of the patients die in the first years of age, unlikely no therapy has been developed yet.

Previous study showed that patients and XLCNM animal model muscle lysate have an increase DNM2 protein expression (Cowling et al., 2014). DNM2 protein is coded by *DNM2* gene which gain-of-function mutations can lead to autosomal dominant centronuclear myopathy (Bitoun et al., 2005). DNM2 is implicated in endocytosis, cytoskeleton organization and autophagy (Durieux et al., 2010). In addition, studies showed a link between MTM1 and DNM2. Cowling *et al*. reported that the downregulation of DNM2 rescues *Mtm1-/y* mouse model survival. In addition, *Mtm1-/y Dnm2+/-* mice had an improvement in muscle force and rescue of the histological defects compared the *Mtm1-/y* littermate (Cowling et al., 2014). These results strongly suggested that the upregulation of DNM2 negatively impact on the disease.

Aim of the study

The main aim of this study was to identify a post-natal therapeutic strategy to reduce disease features in an XLCNM mouse model, by downregulating DNM2.

Results

In this study, several shDNM2 GFP tagged were generated and tested on human embryonic kidney 293T cells and C2C12 myoblast to verify their effects on DNM2 downregulation. The best AAVs selected were injected intramuscularly on the *Mtm1-/y* TA at 3 weeks of age. Analysis was than conducted 2 weeks post- injection. Muscle force, histology, and ultrastructure were rescued in *Mtm1-/y* injected with AAV-GFP-sh*DNM2* compared to the *Mtm1-/y* injected with AAV-GFP control. In addition, the abnormal protein aggregates visible in *Mtm1-/y* injected with AAV-GFP control were rescued by downregulating DNM2 protein level.

Conclusion

In summary this study confirmed DNM2 as a potential therapeutic target for XLCNM, and provided an alternative therapeutic option to rescue *Mtm1-/y* by downregulating DNM2 using an AAV approach.

Contribution

We observed that WT muscle injected with sh*Dnm2* GFP tagged had decrease in skeletal muscle force compared the WT muscle injected with NaCl.

I verified if the abnormal general absolute muscle force measured in the WT was a consequence of DNM2 reduction or of the overexpression of the GFP tag in the skeletal muscle. To assess if GFP negatively impacted on muscle contraction, I generated a WT control cohort intramuscularly injected in one leg with AAV-*GFP* and in the control leg with NaCl. I showed that the injection of AAV-*GFP* in the WT Tibialis Anterior muscle negatively impacted on skeletal muscle contraction.

Molecular Therapy
Original Article

Single Intramuscular Injection of AAV-shRNA Reduces DNM2 and Prevents Myotubular Myopathy in Mice

Hichem Tasfaout,[1,2,3,4] Valentina M. Lionello,[1,2,3,4] Christine Kretz,[1,2,3,4] Pascale Koebel,[2,3,4] Nadia Messaddeq,[2,3,4,6] Deborah Bitz,[2,3,4,5] Jocelyn Laporte,[1,2,3,4,7] and Belinda S. Cowling[1,2,3,4,7]

[1]Institut de Génétique et de Biologie Moléculaire et Cellulaire (IGBMC), Illkirch 67400, France; [2]INSERM U964, Illkirch 67400, France; [3]CNRS UMR7104, Illkirch 67400, France; [4]Strasbourg University, Illkirch 67400, France; [5]Celphedia, Phenomin, Institut Clinique de la Souris (ICS), Illkirch 67400, France; [6]Imaging Center, Institut de Génétique et de Biologie Moléculaire et Cellulaire (IGBMC), Illkirch 67400, France

Myotubular myopathy, or X-linked centronuclear myopathy, is a severe muscle disorder representing a significant burden for patients and their families. It is clinically characterized by neonatal and severe muscle weakness and atrophy. Mutations in the myotubularin (*MTM1*) gene cause myotubular myopathy, and no specific curative treatment is available. We previously found that dynamin 2 (DNM2) is upregulated in both *Mtm1* knockout and patient muscle samples, whereas its reduction through antisense oligonucleotides rescues the clinical and histopathological features of this myopathy in mice. Here, we propose a novel approach targeting *Dnm2* mRNA. We screened and validated *in vitro* and *in vivo* several short hairpin RNA (shRNA) sequences that efficiently target *Dnm2* mRNA. A single intramuscular injection of AAV-sh*Dnm2* resulted in long-term reduction of DNM2 protein level and restored muscle force, mass, histology, and myofiber ultrastructure and prevented molecular defects linked to the disease. Our results demonstrate a robust DNM2 knockdown and provide an alternative strategy based on reduction of DNM2 to treat myotubular myopathy.

INTRODUCTION

Centronuclear myopathies (CNMs) are a group of rare congenital disorders characterized clinically by severe muscle atrophy and generalized muscle weakness.[1,2] Muscle biopsies from affected patients present numerous myofibers with nuclei abnormally located at the center, without excessive regeneration. Different forms of CNM have been characterized to date. The most common and severe form is the X-linked CNM (XLCNM), also called myotubular myopathy.[3] XLCNM patients present with severe hypotonia and respiratory distress at birth, strongly impacting on life expectancy. More than 200 mutations in *MTM1* have been identified to cause XLCNM, most of them leading to a strong decrease or absence of the MTM1 protein.[4–9] MTM1 is a phosphoinositide phosphatase involved in key cellular processes, including endosomal trafficking,[10] excitation contraction coupling,[11,12] intermediate filament organization,[13] neuromuscular junction (NMJ) structure,[14,15] satellite cell proliferation,[16] apoptosis,[16,17] and autophagy.[18,19] Mutations in *DNM2* have been associated with a less severe autosomal dominant form.[20,21] It is characterized by moderate muscle weakness with late onset[20]; however, several neonatal cases have been reported with very severe phenotype. *DNM2* encodes for dynamin 2, a mechanoenzyme implicated in endocytosis,[22] exocytosis,[23,24] as well as cytoskeleton organization.[25–27] Different *in vitro* studies have proposed CNM-causing DNM2 mutations increase dynamin 2 guanosine triphosphatase (GTPase) activity and oligomer stability, suggesting a gain of function of the mutated forms.[28,29] This hypothesis is sustained by the fact that overexpression of wild-type DNM2 in mice recapitulates a CNM-like phenotype.[30,31] To date, no effective and specific therapy is available for patients with CNM.

The *Mtm1* knockout (*Mtm1*KO) mice present a severe muscular phenotype and have been extensively used to understand the physiopathology of XLCNM and to test therapeutic approaches.[32–37] They develop a severe progressive myopathy starting from week 3 that is clinically reflected by a severe muscle atrophy and weakness.[32] They present a short lifespan and die between 1 and 3 months of age. Transversal muscle sections of *Mtm1*KO exhibit a typical XLCNM histology with predominance of hypotrophic and rounded fibers with centralized nuclei, abnormal organelle distribution, and aggregated proteins, including caveolin 3 (Cav3) and desmin.[13,36] In addition, and similarly to muscle biopsies from XLCNM patients, DNM2 was found to be upregulated at the symptomatic phase, pointing to DNM2 reduction as a therapeutic strategy.[36]

We have previously reported that reduction of DNM2 expression by genetic crossing rescues the early XLCNM lethality and ameliorates

Received 17 August 2017; accepted 9 February 2018;
https://doi.org/10.1016/j.ymthe.2018.02.008.

[7]These authors contributed equally to this work.

Correspondence: Belinda S. Cowling, Institut de Génétique et de Biologie Moléculaire et Cellulaire (IGBMC), Illkirch 67400, France.
E-mail: belinda@igbmc.fr
Correspondence: Jocelyn Laporte, Institut de Génétique et de Biologie Moléculaire et Cellulaire (IGBMC), Illkirch 67400, France.
E-mail: jocelyn@igbmc.fr

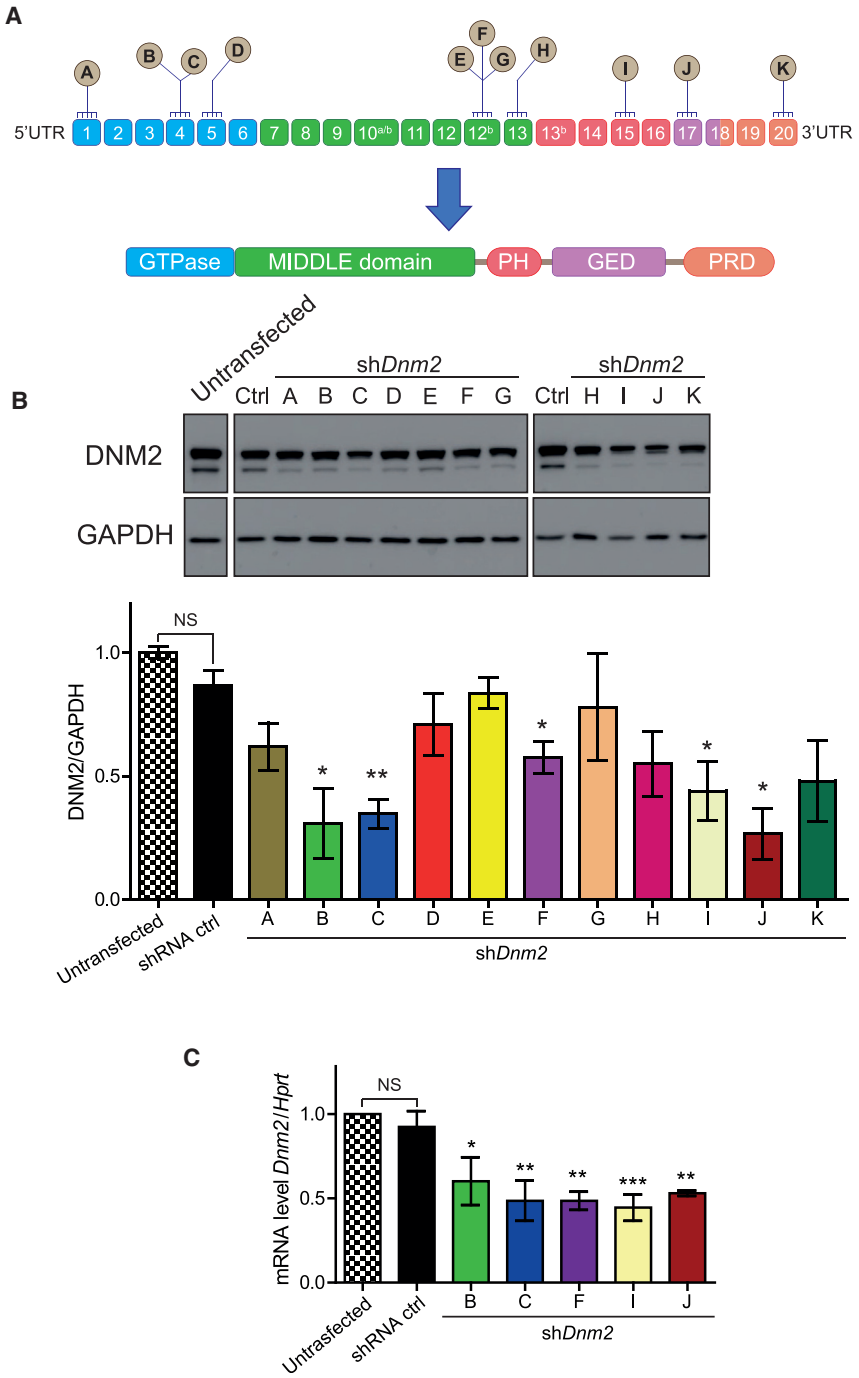

Figure 1. *In Vitro* Validation of shRNA Targeting *DNM2*

(A) Location of shRNA-targeting sequences in *Dnm2* mRNA. Exons are depicted as boxes, and exons 10a, 10b, 12b, and 13b are alternative exons. Below, the protein domains encompass a GTPase domain, a middle and GTP effector (GED) domains forming the stalk, a pleckstrin homology (PH), and a proline-rich (PRD) domain. (B) Representative western blot from HEK293T cells co-transfected with two plasmids is shown: one encoding human *DNM2* and the second expressing the different shRNA. DNM2 protein levels were determined by densitometry and standardized to GAPDH. (C) Endogenous *Dnm2* mRNA levels in shRNA-treated C2C12 mouse myoblast cells were determined by qRT-PCR and standardized to *Hprt*. Cells were electroporated with shRNA ctrl or sh*Dnm2* (B, C, F, I, or J). n = 3 biological replicates per each group. Data represent an average of three independent experiments ± SEM. *p < 0.05; **p < 0.01 for sh*Dnm2*-treated versus shRNA ctrl-treated cells (ANOVA test).

most CNM features, notably increased muscle force and correction of myofiber histology, indicating an epistasis between *MTM1* and *DNM2*.[36] These data have been recently confirmed using antisense oligonucleotides (ASOs) that target the nuclear pre-mRNA of *Dnm2*. Repeated injections of ASO targeting *Dnm2* into *Mtm1*KO mice efficiently reduced the DNM2 protein level and revert the CNM features.[35] However, such ASO strategy would require repeated injections in patients, potentially on a long-term basis, and an efficient biodistribution in patients to reach all muscles of the body.

Here, we tested another approach of reducing DNM2 expression based on AAV-short hairpin RNA (shRNA). Adeno-associated virus (AAV) vectors have been intensively used to re-express the defective gene in many monogenic disorders.[38] In addition, an increasing number of studies showed their efficacy to repress gene expression when they encode for shRNA complementary to the target mRNA.[39–42] In the present study, we evaluated the potential of AAV-shRNA to knockdown DNM2 in mice. A single intramuscular injection of AAV-sh*Dnm2* resulted in long-term reduction of DNM2 protein level and restored different CNM features. Our data validate the epistasis between *Mtm1* and *Dnm2* and propose an alternative approach to target DNM2 for therapeutic approaches.

RESULTS

Design and *In Vitro* Validation of shRNA Targeting *DNM2* Conserved Regions

To target *DNM2* mRNA for degradation, eleven highly conserved regions between the human and mouse *DNM2* mRNA were selected to design the different shRNA sequences (Figure 1A; Table 1). All shRNA-*Dnm2* sequences as well as a scrambled sequence (shRNA ctrl) had an identical nine-nucleotide hairpin or loop sequence.

To evaluate the efficacy of shRNA to knockdown DNM2 protein level *in vitro*, HEK293T cells were co-transfected with a plasmid expressing human DNM2 and plasmids expressing the sh*Dnm2* under the control of the mouse U6 promoter. DNM2 protein level

Table 1. Selected shRNA and Target Sequences

shRNA	Target Sequence (Mouse)	Remarks	Top 3 of Potential Off-Target mRNA (Mouse)	Sequence Homology (%)
shRNA ctrl	GGGCTATCCCAACGCTATTAGT	no target	UTP23 small subunit processome component (*Utp23*)	68
			Von Willebrand factor A domain containing 2 (*Vwa2*)	63
			B cell CLL/lymphoma 11A (zinc finger protein) (*Bcl11a*)	59
sh*Dnm2* A	AACCGCGGGATGGAAGAGCT	identical to human sequence	transmembrane protein 67 (*Tmem67*)	70
			family with sequence similarity 206, member A (*Fam206a*)	70
			protein phosphatase 1F (PP2C domain containing) (*Ppm1f*)	70
sh*Dnm2* B	AACTTGACCCTCATCGACCTC	identical to human sequence	potassium voltage-gated channel, subfamily G, member 1 (*Kcng1*)	76
			IKAROS family zinc finger 1 (*Ikzf1*)	76
			DnaJ heat shock protein family (Hsp40) member C2 (*Dnajc2*)	71
sh*Dnm2* C	AAGGACATGATCCTGCAGTTCAT	identical to human sequence	adaptor-related protein complex 3, delta 1 subunit (*Ap3d1*)	78
			suppressor of glucose, autophagy-associated 1 (*Soga1*)	65
			adhesion G protein-coupled receptor G2 (*Adgrg2*)	60
sh*Dnm2* D	TCGGTGTCATCACCAAGCT	identical to human sequence	myosin IA (*Myo1a*)	78
			ankyrin repeat domain 52 (*Ankrd52*)	73
			zinc finger protein 407 (*Zfp407*)	73
sh*Dnm2* E	TGCCAACTGTTTCTATACT	1 nucleotide different to human (underlined)	protocadherin 17 (*Pcdh17*)	73
			folliculin interacting protein 1 (*Fnip1*)	73
			zeta-chain (TCR)-associated protein kinase (*Zap70*)	73
sh*Dnm2* F	AACTGTTTCTATACTGAGGAG	2 nucleotides different to human (underlined)	protocadherin 17 (*Pcdh17*)	71
			tenascin R (*Tnr*)	71
			ligand-dependent nuclear receptor corepressor-like (*Lcorl*)	66
sh*Dnm2* G	TTTCTATACTGAGGAGCTGGT	2 nucleotides different to human (underlined)	WNK lysine-deficient protein kinase 2 (*Wnk2*)	71
			TRAF3 interacting protein 2 (*Traf3ip2*)	66
			trans-2,3-enoyl-CoA reductase-like (*Tecrl*)	66
sh*Dnm2* H	GCACGCAGCTGAACAAGAA	identical to human sequence	HGF-regulated tyrosine kinase substrate (*Hgs*)	78
			two-pore segment channel 2 (*Tpcn2*)	73
			interleukin-1 alpha (*Il1a*)	73
sh*Dnm2* I	AAGAAGTACATGCTGCCACTGGA	1 nucleotide different to human (underlined)	zinc finger, C3H1-type containing (*Zfc3h1*)	69
			DENN/MADD domain containing 5A (*Dennd5a*)	69
			small G protein signaling modulator 1 (*Sgsm1*)	65
sh*Dnm2* J	AACACCTTCTCCATGGACCC	identical to human sequence	proteasome (prosome, macropain) 26S subunit, non-ATPase, 12 (*Psmd12*)	75
			GTP cyclohydrolase 1 (*Gch1*)	75
			acyl-CoA synthetase medium-chain family member 3 (*Acsm3*)	70
sh*Dnm2* K	CCATTATCCGCCCAGCCGAGC	identical to human sequence	poly (ADP-ribose) polymerase family, member 6 (*Parp6*)	66
			RAP2B, member of RAS oncogene family (*Rap2b*)	66
			arylsulfatase i (*Arsi*)	66

CoA, coenzyme A.

was measured 72 hr post-transfection. A statistically significant decrease of DNM2 protein level was observed with five sh*Dnm2* constructs (B, C, F, I, and J) out of the 11 sh*Dnm2*s tested (Figure 1B). In addition, selected sh*Dnm2*s elicited a strong decrease of the endogenous murine *Dnm2* mRNA when electroporated into mouse C2C12 myoblasts (Figure 1C). However, protein level was unchanged 48 hr after electroporation, most likely due to longer stability of endogenous DNM2 (Figure S1). These results indicate that five shRNAs (B, C, F, I, and J) target efficiently both human and murine *DNM2* mRNA.

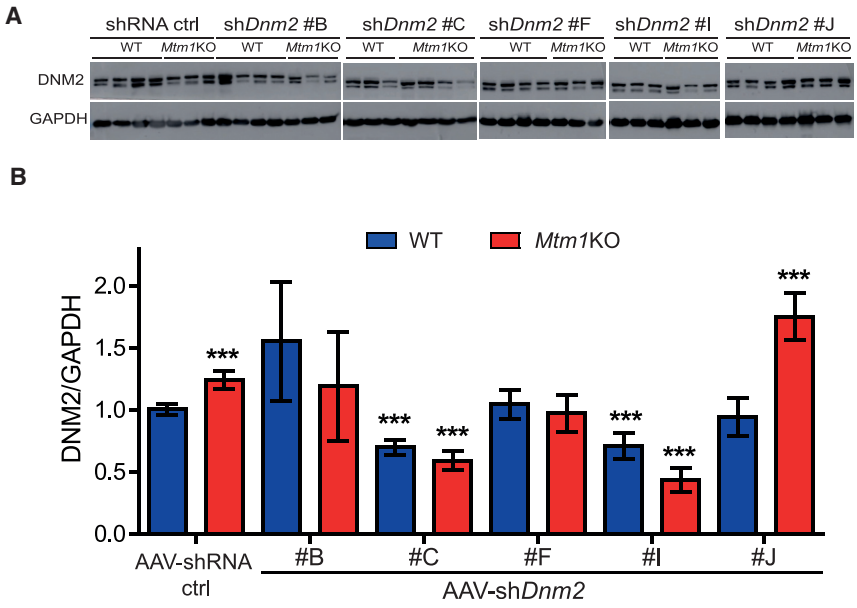

Figure 2. *In Vivo* Validation of shRNA Targeting *Dnm2* following Intramuscular Injection

(A) Representative western blot of 7-week-old WT or *Mtm1*KO TAs injected with either AAV-shRNA ctrl or AAV-sh*Dnm2* (B, C, F, I, or J). (B) DNM2 densitometries were quantified and standardized to the loading control GAPDH (n = 5–7 mice/group). ***p < 0.01 versus WT muscles treated with AAV-shRNA ctrl (ANOVA test).

Efficient *In Vivo Dnm2* Knockdown following a Single Intramuscular Injection of AAV shRNA

To test the *in vivo* efficacy of the five best sh*Dnm2*s, AAV serotype 2/9 vectors encoding the selected sh*Dnm2* or shRNA ctrl were produced. AAV2/9 serotype efficiently transduces skeletal muscle.[43] The AAV-sh*Dnm2*s (B, C, F, H, or I) were administrated locally into right tibialis anterior muscles (TAs) of 3-week-old wild-type (WT) or *Mtm1*KO mice at a dose of 1.2×10^{11} viral genome per TA while the same dose of AAV-shRNA ctrl was injected into the contralateral TA. Four weeks later, GFP expression was visualized in the injected TAs to ensure an effective viral transduction (Figure S2). TAs were weighed, and *in situ* muscular force as well as DNM2 protein level were measured. DNM2 protein levels in TA injected with AAV-sh*Dnm2* B, F, and J were not reduced below TA injected with AAV-shRNA ctrl (Figures 2A and 2B). Accordingly, these muscles remain atrophic (Figures 3A, 3B, and S3). Conversely, muscles of WT or *Mtm1*KO injected with sh*Dnm2* C or I presented a strong decrease of DNM2 protein level (Figures 2A and 2B). In addition, improvement of muscle mass and force were noted for *Mtm1*KO injected with sh*Dnm2* C or I. *Mtm1*KO muscles injected with AAV-sh*Dnm2* C or I were remarkably bigger and exhibit an increase of specific muscle force compared to the contralateral TA injected with shRNA ctrl (Figures 3A–3C and S3). Nevertheless, we noted that the absolute force of WT muscles injected with AAV was reduced when compared to those injected with NaCl, whereas muscle mass and histology were similar (Figure S4). This may indicate a deleterious effect of AAV injection and GFP expression specifically on muscle force.[44,45] Moreover, these results validate *in vivo* the efficiency of several shRNA sequences targeting *Dnm2* mRNA and show that reducing DNM2 after a single injection of AAV-sh*Dnm2* efficiently ameliorates muscle mass and force of the *Mtm1*KO XLCNM model.

AAV shRNA-Mediated Knockdown of *Dnm2* Rescues *Mtm1*KO Muscle Histology

To assess whether the functional amelioration of *Mtm1*KO muscles is linked to an improved muscle histology, transversal sections of TA 4 weeks post-injection were stained with H&E. *Mtm1*KO muscles treated with AAV-shRNA ctrl exhibited small and rounded fibers with a 3-fold reduction in fiber size compared to WT muscles (Figures 4A–4C). In addition, approximately 20% of the myofibers presented with abnormal internal localization of nuclei (Figure 4D). Succinate dehydrogenase (SDH) staining showed abnormal mitochondrial distribution with aggregated staining in the center or forming a halo at the periphery of the myofiber (Figures 4A and 4E). These abnormal histological features are reminiscent of the typical histology seen in XLCNM patients[46] and were corrected in *Mtm1*KO TA when treated with two different AAV-sh*Dnm2*. Muscles injected with AAV-sh*Dnm2* C or I showed a normalization of the myofiber size with nuclei positioned at the periphery (Figures 4A–4D). In addition, TAs injected with AAV-sh*Dnm2* C exhibit a normal muscle histology similar to WT with normal mitochondrial distribution and a decreased number of fibers with central or peripheral accumulation of mitochondria (Figures 4A and 4E). Injection of sh*Dnm2* I correlated with an increase of myofiber size and a strong improvement of mitochondria distribution; however, few myofibers still presented an intermediate size with mitochondrial oxidative staining in the center or forming a halo at the periphery (Figures 4A–4E). These results suggest only a slight difference in efficacy between sh*Dnm2* C and I based on SDH staining and show overall a strong rescue of muscle histology following a single injection of two different AAV-sh*Dnm2*s.

Dnm2 Reduction through AAV-shRNA Rescues Myofiber Organization in *Mtm1*KO Muscles

MTM1 deficiency was documented to induce disorganization of muscle fiber in several species.[12,32,47] MTM1-deficient fibers present with misalignment of Z-line; mislocalization of organelles, including nuclei and mitochondria; and a strong defect in triad structure (formed by one T-tubule and two sarcoplasmic reticulum cisternae) implicated in excitation-contraction coupling. In agreement with the literature, misalignment of the Z-line was observed in the *Mtm1*KO TAs by transmission electronic microscopy (TEM) in this study (Figure 5A) and confirmed by immunolabeling of alpha-actinin (Z-line marker; Figure 6). Well-organized triads are seldom observed in this model

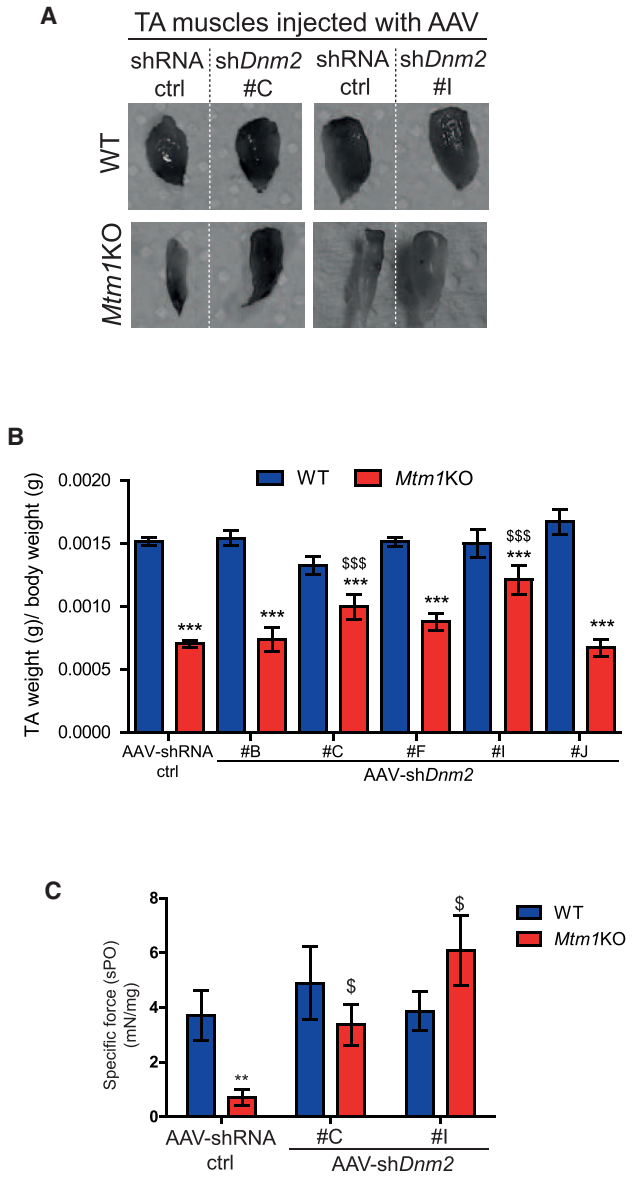

Figure 3. Positive Physiological Effects of AAV shRNA-Mediated *Dnm2* Knockdown

(A) Photography of TAs from WT or *Mtm1*KO mice treated with AAV-shRNA ctrl or sh*Dnm2* (C or I). (B) TA weight relative to body weight is shown (n = 6). (C) Specific muscle force of TA was measured after sciatic nerve stimulation. The specific muscle force was calculated by dividing the absolute force by TA weight (n = 5–7 mice/group). **p < 0.01; ***p < 0.001 versus WT TA treated with shRNA ctrl. $p < 0.05; $$$p < 0.01 *Mtm1*KO treated with AAV-sh*Dnm2* versus *Mtm1*KO treated with AAV-shRNA ctrl (ANOVA test).

(Figures 5A and 5B), and this finding parallels the perturbed localization of the junctional sarcoplasmic reticulum calcium channel RYR1 and caveolin 3 implicated in T-tubule biogenesis (Figure 6).

AAV-sh*Dnm2* injection into *Mtm1*KO mice restored the disorganized ultrastructure observed in untreated mice. Using TEM, myofiber ultrastructure revealed a well-organized structure with increased ratio of normal and well-positioned triads in treated *Mtm1*KO mice (Figures 5A and 5B), equivalent to the rescue observed targeting *Dnm2* systemically by ASO at higher doses.[35] RYR1 and caveolin 3 were also correctly localized as in WT muscle (Figure 6). Furthermore, Z-line alignment and alpha-actinin labeling were also normal. DNM2 localized normally in both untreated and treated *Mtm1*KO muscles, in a transverse localization. In addition, the desmin aggregation observed in the *Mtm1*KO mice treated with AAV-shRNA ctrl was also rescued upon injection with AAV-sh*Dnm2* (Figure 6).

Altogether, these findings underline a complete amelioration of the XLCNM-like phenotypes in the *Mtm1*KO model at the structural and molecular levels upon DNM2 reduction through AAV-shRNA treatment and fully correlate with the rescue in muscle mass and force.

DISCUSSION

Myotubular myopathy is the most severe form of CNM with highest incidence, and no available effective treatment exists. Among the different therapeutic approaches that were tested in preclinical trials on animal models, few showed significant histological and functional improvements. Here, we provide evidence showing that a single injection of AAV-sh*Dnm2* rescues the CNM phenotype of *Mtm1*KO mice at the functional, histological, and ultrastructural level when analyzed four weeks after injection. Molecular defects were greatly ameliorated with a strong improvement of the localization of desmin, caveolin 3, and RYR1. The structural alterations of the myofibers were rescued, including normalization of mitochondria and nuclei positioning and triad shape and distribution. Furthermore, the different histological hallmarks of CNM were absent upon AAV-sh*Dnm2* injection, with an increase in myofiber size and decrease in frequency of fibers with mislocalized nuclei. These effects correlated with a normalization of muscle mass and force. Nonetheless, muscles injected with AAV showed a reduction in general absolute muscle force. This could be due to GFP overexpression, as previous studies showed that GFP expression impairs contractile activity of the muscle by affecting actin-myosin interaction.[44,45]

Our results demonstrate that reduction of DNM2 level, through local injection of AAV-sh*Dnm2*, prevents the disease progression. These data confirmed the therapeutic potential of DNM2 knockdown and are concordant with those obtained with ASO targeting *Dnm2* or genetic reduction of *Dnm2*.[35,36] Furthermore, it is noteworthy that, using this approach, we almost fully rescued the CNM phenotype targeting DNM2 in one muscle alone, despite the severe phenotype still observed in other muscles of the mouse. DNM2 protein levels are increased in muscles from both XLCNM patients and *Mtm1*KO mice at symptomatic ages. The fact that reducing DNM2 level promotes disease prevention strongly supports the observed increase in DNM2 as a significant cause of the disease initiation and/or progression. This finding is sustained by the fact that overexpression of DNM2 in WT mice by transgenesis or AAV injections creates a CNM phenotype.[30,31] Moreover, *in vitro* experiments showed that

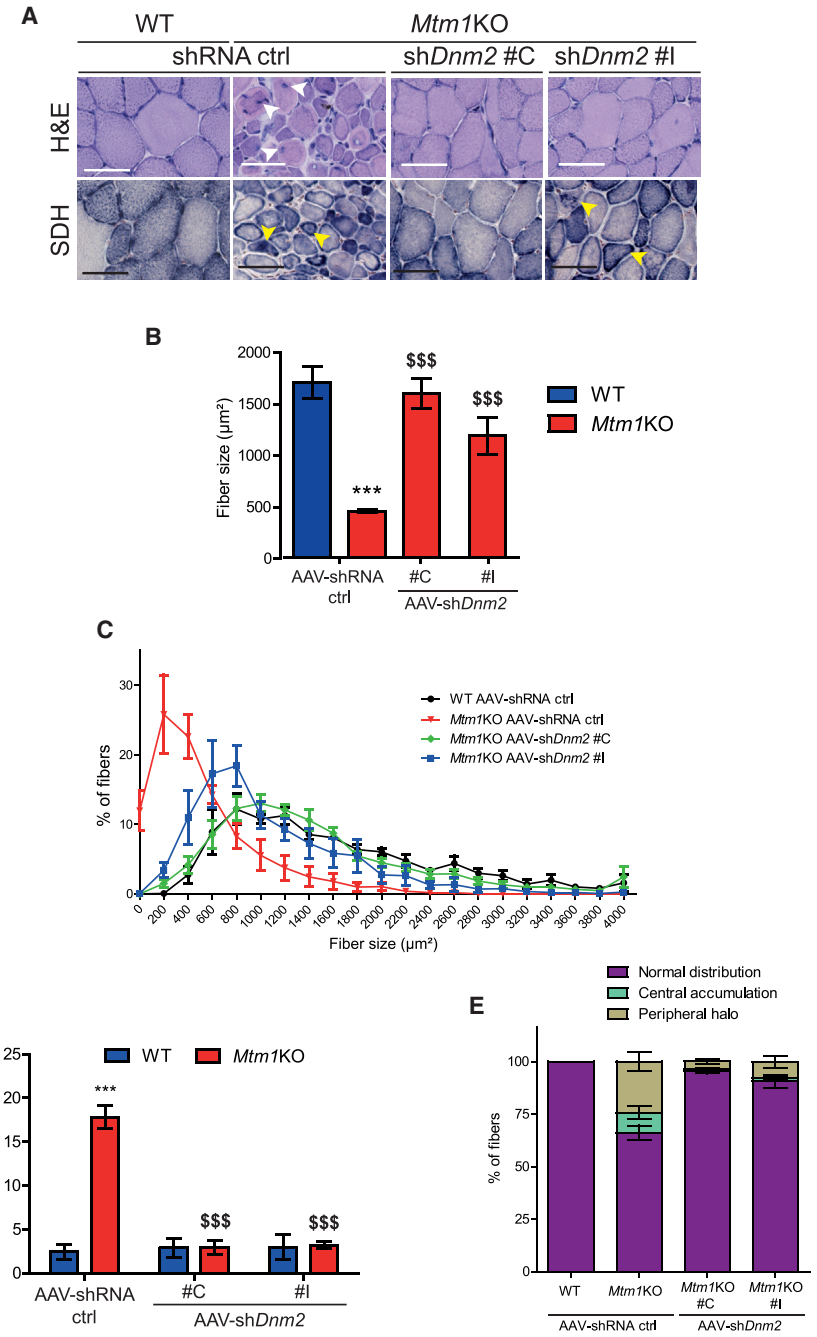

Figure 4. Histology Amelioration of TA Treated with AAV sh*Dnm2*

(A) TA sections of WT or *Mtm1*KO mice treated with AAV-shRNA ctrl or sh*Dnm2* (C or I) were stained with H&E and SDH to visualize fiber size, shape, nuclei positioning, and mitochondrial oxidative activity. Arrows show mislocalized nuclei or aggregated mitochondria (scale bars: 50 µm). (B) TA myofiber area was calculated on 300–400 fibers per sample (n = 5 mice/group). (C) Fiber size distribution of WT or *Mtm1*KO TAs according to size groups. Affected *Mtm1*KO TAs have more small fibers and less medium-size or large fibers. (D) Percentage of fibers with mislocalized nuclei was determined in 1,000 fibers (n = 5–6 mice/group). (E) Percentage of fibers with abnormal mitochondrial distribution was determined in 1,000 fibers (n = 5 mice/group). ***p < 0.001 versus WT TA treated with shRNA ctrl. $$$p < 0.01 *Mtm1*KO treated with AAV-sh*Dnm2* versus *Mtm1*KO treated with AAV-shRNA ctrl (ANOVA test).

DNM2 mutations leading to a dominant CNM form increase its GTPase activity and oligomerization stability.[28,29] We thus hypothesize that either increase in DNM2 protein level upon impairment of MTM1 or increase in DNM2 activity following mutations trigger the CNM phenotypes in XLCNM or ADCNM, respectively.

The present results confirm the epistasis between *Mtm1* and *Dnm2* and place DNM2 downstream of MTM1 in the pathological pathway causing CNM. To date, the functional link between MTM1 and DNM2 and the molecular mechanism underlying this rescue remain unclear. However, MTM1 deficiency was reported to cause an alteration of autophagy and protein accumulation.[18,19] One could hypothesize that autophagy defects lead to imbalance between transcription and clearance of DNM2, causing its accumulation and increased overall activity. Alternatively, MTM1 might somehow regulate *DNM2* transcription or translation. However, this is less likely, as *Dnm2* mRNA is not elevated in *Mtm1*KO mice.[36] In addition, one cannot exclude that MTM1 directly regulates DNM2 activity or transport in addition to its expression.

Here, we validated several shRNA sequences targeting *Dnm2* mRNA *in vitro* and *in vivo* for efficient DNM2 knockdown. In particular, we identified shRNA sequences partially (I) or fully (C) improving the molecular, cellular, and physiological phenotypes. These data provide the proof of concept that targeting *Dnm2* mRNA for degradation using AAV as a delivery method is efficient to ameliorate XLCNM, thus validating a novel approach to tackle this disease. Compared to the recently reported ASO targeting nuclear *Dnm2* pre-mRNA, shRNA targets the cytoplasmic mRNA, and both approaches efficiently decrease DNM2 level. Moreover, AAVs have two main advantages: they can have a good muscle tropism and they can sustain long-term expression following a single injection. Indeed, tissue specificity can be further achieved by modulating the AAV serotype and the promoter controlling the expression of the transgene. Numerous AAV serotypes have been identified, and several showed a strong skeletal muscle tropism.[48] In addition, several promoter and regulatory cassettes have been reported to have a high

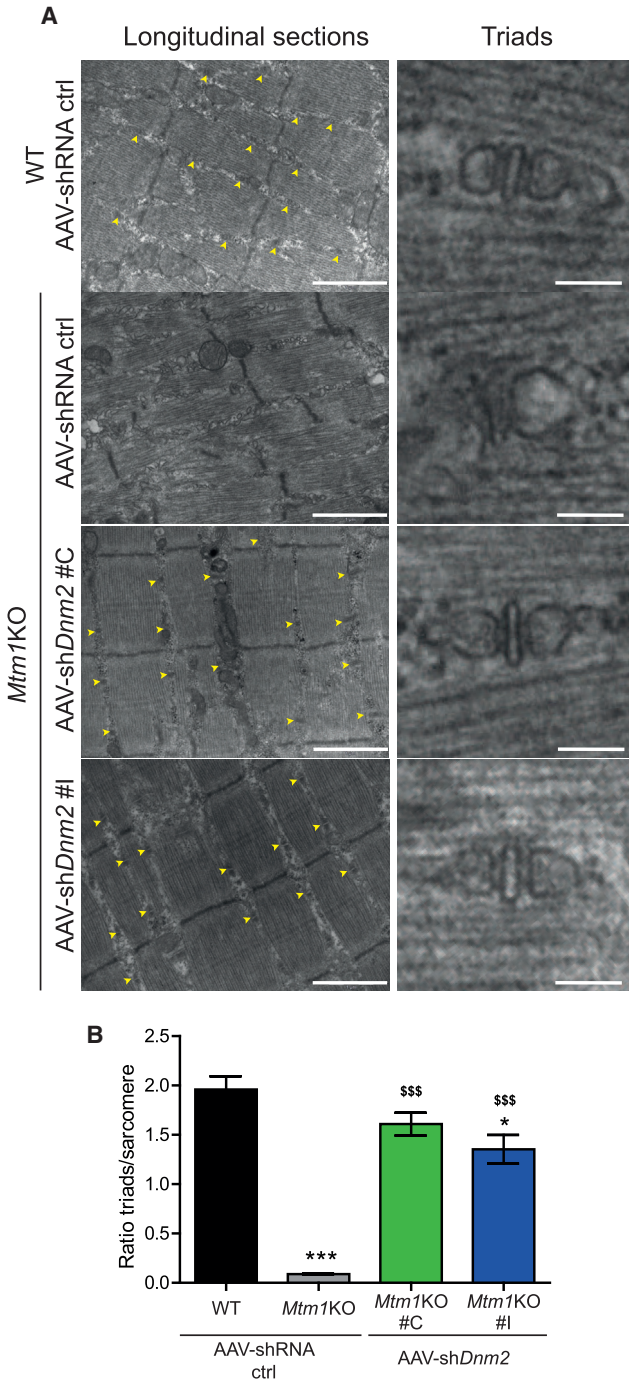

Figure 5. Amelioration of Muscle Ultrastructure through AAV-sh*Dnm2* Injections

(A) Electron microscopy was used to assess the general ultrastructure of myofibers and to count the triads formed (yellow arrows, scale bar: 1 μm for left panels and 100 nm for right panels). (B) Graph representing the number of triad well formed and localized per sarcomere is shown (n = 3 per group). *p < 0.05; ***p < 0.001 for *Mtm1*KO treated with AAV-shRNA ctrl or AAV-sh*Dnm2* versus WT treated with AAV-shRNA ctrl. $$$p < 0.001 *Mtm1*KO treated with AAV-sh*Dnm2* versus *Mtm1*KO treated with AAV-shRNA ctrl (ANOVA test).

activity in skeletal muscle.[49] Together, the combination of these two elements would largely restrict the delivery of shRNA to skeletal muscles, which may improve the efficacy while decreasing the required dose and minimizing potential side effects related to reduction of DNM2 in other organs. Of note, reduction of DNM2 by 50% through transgenesis or ASO injection did not induce a detectable toxicity.[35,36]

Many studies showed the potential of AAV to maintain a long-term and robust transgene expression,[50–53] which implies avoiding multiple injections that may trigger immune reaction against these vectors. Moreover, several reports claim the safety of recombinant AAV vector. Unlike other viral vectors, they do not integrate the genome of the host cell, and they elicit a mild and manageable immune response.[52–54] However, they represent some limitations. Following their transduction into host cells, AAVs are mostly present as non-integrated episomes. Loss of the transgene expression could be expected due to normal muscle turnover. In addition, it has been reported that AAVs do not transduce satellite cells, which are multipotent cells able to differentiate and give rise to myofibers.[55] Thus, re-administration of these vectors after the initial infusion might be needed. Furthermore, human administration of AAV requires a large amount and high-titer production, which represent a manufacturing challenge and costly process. Also, expression of shRNA to downregulate DNM2 level using ubiquitous RNA polymerase III promoters (like U6 or H1) might have some side effects in non-muscle tissues. These promoters do not provide a spatial or temporal control, and they show a high transcription activity in some cell types causing microRNA processing factors (Exportin-5 and RNA-induced silencing complex [RISC]) saturation, which leads to cytotoxicity and tissue damage.[56–58] Transcription of shRNA from polymerase II promoters could be an alternative for effective and safer RNAi therapeutics.[59]

In conclusion, this study shows once again the usefulness of *Mtm1*KO as a bio-assay for screening of therapeutic agents and provides the first proof of principle that using AAV encoding for sh*Dnm2* in this XLCNM mouse model shows a strong and robust reduction of DNM2 protein level following a single injection. These shRNA-targeting *Dnm2*s exhibit a strong affinity to human *DNM2* transcript as shown *in vitro* (Figure 1), which might be relevant for human application in future clinical trials.

MATERIALS AND METHODS

Cell Transfection

HEK293Ts were co-transfected by plasmid encoding human DNM2 and another plasmid expressing either shRNA ctrl or different sh*Dnm2* using Lipofectamine 2000 and following the manufacturer's instructions. Cells were seeded in 6-well plates. At 80% of confluency, a mixture of Lipofectamine reagent and opti-minimum essential medium (MEM) medium containing 2 μg of plasmid expressing human *DNM2* and 2 μg of plasmid encoding the different shRNA was incubated for 4 hr. Then, the mixture was removed and replaced by DMEM containing 20% fetal calf serum (FCS). The transfected cells were incubated at 37°C for 72 hr before harvesting for protein analysis.

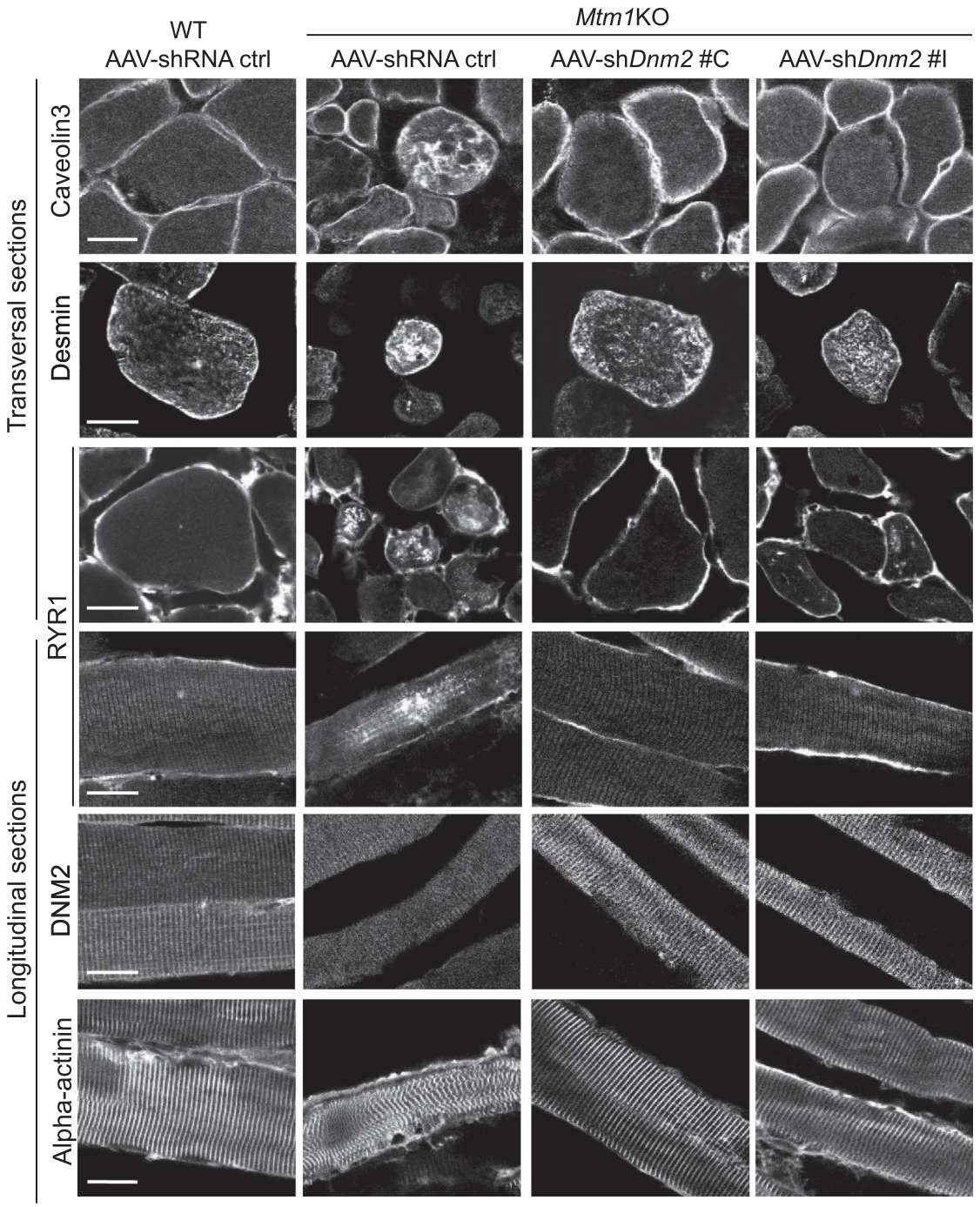

Figure 6. Improvement of Molecular Defects in *Mtm1*KO Mice Treated with AAV sh*Dnm2*

Immunolabeling of CAV3, desmin, RYR1, DNM2, and alpha-actinin was performed on 8 μm transversal or longitudinal sections. The staining was visualized using confocal microscopy (scale bar: 20 μm).

C2C12 mouse myoblast were electroporated with plasmids encoding the different shRNA candidates using Amaxa nucleofector2B Kit V and following the manufacturer's instructions. Briefly, cells were trypsinized and 1×10^6 cells per sample were gently centrifuged at 90 *g* for 10 min at room temperature. Cell pellet was resuspended in 100 μL of the solution provided in the kit. Then, 2 μg of plasmid expressing shRNA ctrl or different sh*Dnm2*s were added to the cell suspension and transferred immediately to an electroporation

cuvette. Electroporation was performed using the B-032 program of Nucleofector I Device. The electroporated cells were incubated for 48 hr in DMEM medium containing 20% FCS at 37°C before harvesting the electroporated cells for protein and RNA analysis.

Animals

Animal experiments were conducted on male *Mtm1*KO or WT 129SvPAS mice according to the French and European legislation on animal care and experimentation. Protocol nos. Com'Eth IGBMC-ICS 2012-132, 2013-034, and 2016-5453 were approved by the Institutional Ethics Committee. Mice were housed in a temperature-controlled room and ventilated cages with 12 hr day light/darkness cycle and given free access to food.

Intramuscular Injection of AAV

3-week-old male *Mtm1*KO or WT was weighed and then an anesthetic solution of ketamine 20 mg/mL and xylazine 0.4% at 5 μL/g of body weight was administrated by intraperitoneal injection. Right TAs were injected with 1.2×10^{11} vg/TA in 20 μL of AAV2/9 expressing sh*Dnm2* (either B, C, F, I, or J), and the same dose of AAV2/9 expressing shRNA ctrl was injected in the contralateral TA. As an additional control, 20 μL of NaCl 0.9% was administrated into WT TA. At 7 weeks of age, mice were humanely killed by CO2 suffocation followed by cervical dislocation. The TAs were dissected and weighed. They were snap frozen in liquid nitrogen-cooled isopentane and stored at −80°C for H&E and SDH histology analysis as well as protein extraction and quantification. For immunostaining, TAs were stored in paraformaldehyde (PFA) 4% for 24 hr, and then they were transferred to sucrose 30% overnight and stored at 4°C.

Immunostaining of Muscle Sections

8 μm transversal or longitudinal cryosections of TA were stained with antibodies against CAV3 (Santa Cruz Biotechnology N-18 sc-7665; 1:500), RYR1 (34C abcam2668; 1:500), desmin (Santa Cruz sc-7559; 1:500), DNM2 (homemade antibody R2680; 1:500), and alpha-actinin (anti-α-actinin sarcomeric clone EA-53; 1:500). Images were taken with a Leica SP8-UV confocal microscope.

Muscle Histology

8 μm transversal cryosections were prepared and stained by H&E or SDH. Entire muscle sections were imaged with the Hamamatsu NanoZoomer 2HT slide-scanner. The percentage of TA fibers with mislocalized (centralized or internalized) nuclei or abnormal mitochondrial distribution was counted using the cell counter plugin in Fiji image analysis software. The fiber area was measured using the Fiji software.

TA Contractile Properties

TA contraction properties were evaluated *in situ* after sciatic nerve stimulation using Complete1300A Mouse Test System from Aurora. Briefly, mice were anesthetized with intraperitoneal (i.p.) injection of pentobarbital (60 mg/kg) and maintained under deep anesthesia during the experiment. The distal tendon of TA was detached and tied to the isometric transducer using a silk ligature. The knee and foot were fixed with clamps. All isometric contraction measurements were made at an initial muscle length of L0 (length at which maximal tension was obtained during the twitch). Then, sciatic nerves were stimulated by pulses of 50– 200 Hz, and the absolute maximal force was measured. The specific maximal force was determined by dividing the absolute muscle force on the TA weight.

Protein Extraction and Western Blot

TA cryosections or transfected HEK293T cells were lysed in radio immunoprecipitation assay (RIPA) buffer supplemented with PMSF 1 mM and complete mini EDTA-free protease inhibitor cocktail (Roche Diagnostic). Protein concentrations were determined with the Bio-Rad Protein Assay Kit. Samples were denaturated at 95°C for 5 min. Then, 20 μg of protein was loaded in buffer containing 50 mM Tris-HCl, 2% SDS, and 10% glycerol, separated in 10% SDS-PAGE electrophoretic gel, and transferred on nitrocellulose membrane for 1.5 hr at 200 mA. Membranes were blocked for 2 hr in Tris-buffered saline (TBS) containing 5% non-fat dry milk and 0.1% Tween20 before an incubation for 2 hr with primary rabbit polyclonal antibodies against DNM2 (homemade antibody R2865; 1:500) or mouse antibody against GAPDH (1:100,000) diluted in blocking buffer containing 5% milk. Secondary antibodies coupled to horseradish peroxidase were goat anti-rabbit (for DNM2; 1:10,000) or goat anti-mouse (for GAPDH; 1:10,000) and were incubated overnight. Nitrocellulose membranes were visualized in Amersham Imager 600.

Production and Purification of rAAV

Recombinant adeno-associated virus (rAAV)2/9 vectors were generated by a triple transfection of AAV-293 cell line with pAAV2 insert containing either shRNA control (scrambled sequence) or sh*Dnm2* (B, C, F, I, and J) under the control of the mouse U6 promoter, a GFP gene under the control of cytomegalovirus (CMV) promoter as a reporter and flanked by serotype-2 inverted terminal repeats, pXR1 containing rep and cap genes of AAV serotype-9, and pHelper encoding the adenovirus helper functions. Cell lysates were subjected to 3 rounds of freeze/thaw and then treated with 50 U/mL Benzonase (Sigma) for 30 min at 37°C and clarified by centrifugation. Viral vectors were purified by iodixanol gradient ultracentrifugation followed by dialysis and concentration against Dulbecco's phosphate-buffered saline (DPBS) using centrifugal filters (Amicon Ultra-15 Centrifugal Filter Devices 30K). Physical particles were quantified by real-time PCR, and titers are expressed as viral genomes per mL (vg/mL).

RNA Extraction and qRT-PCR

Total RNA was isolated from transfected HEK293T or C2C12 cells using TRIzol reagent according to the manufacturer's instruction (Invitrogen, UK). RT-PCR was carried out on 1–1.5 μg aliquot using SuperscriptII Reverse Transcriptase (Thermo Fisher Scientific). qRT-PCR was performed in Lightcycler 480 (Roche) using *Dnm2* (F): CCAACAAAGGCATCTCCCCT, *Dnm2* (R): TGGTGAGTAG ACCCGAAGGT, *Hprt*(F): GTAATGATCAGTCAACGGGGG-AC, and *Hprt* (R): CCAGCAAGCTTGCAACCTTAACCA mixed in SybrGreen (QIAGEN).

Statistical Analysis

For *in vitro* studies, n = 3 biological replicates. Bar charts depict mean ± SEM. For *in vivo* studies, n = 5–8 were used. Curves and graphs were made using GraphPad Prism software. Difference between groups was analyzed by t test or two-way ANOVA followed by post hoc Bonferroni.

SUPPLEMENTAL INFORMATION

Supplemental Information includes four figures and can be found with this article online at https://doi.org/10.1016/j.ymthe.2018.02.008.

AUTHOR CONTRIBUTIONS

Conceptualization, B.S.C. and J.L.; Investigation, H.T.; Resources, V.M.L., C.K., P.K., N.M., and D.B.; Writing – Original Draft, H.T.; Writing – Review & Editing, B.S.C. and J.L.

CONFLICTS OF INTEREST

H.T., J.L., and B.S.C. are inventors of a patent on targeting *DNM2* for the treatment of centronuclear myopathies. J.L. and B.S.C. are scientific advisors for Dynacure.

ACKNOWLEDGMENTS

We thank Pascal Kessler, William Magnant, and Olivia Wendling for excellent technical assistance and Julie Johnston (Penn Vector Core at University of Pennsylvania) for providing pAAV2/9 plasmid. This study was supported by ANR-10-LABX-0030-INRT, a French state fund managed by the Agence Nationale de la Recherche under the frame program Investissements d'Avenir ANR-10-IDEX-0002-02, ANR-14-CE12-0009, Myotubular Trust and Sparks the Children's Medical Research Charity, Association Française contre les Myopathies (AFM 20323), and the SATT Alsace Conectus. H.T. was supported by a MRT fellowship.

REFERENCES

1. Romero, N.B. (2010). Centronuclear myopathies: a widening concept. Neuromuscul. Disord. *20*, 223–228.
2. Jungbluth, H., Wallgren-Pettersson, C., and Laporte, J. (2008). Centronuclear (myotubular) myopathy. Orphanet J. Rare Dis. *3*, 26.
3. Spiro, A.J., Shy, G.M., and Gonatas, N.K. (1966). Myotubular myopathy. Persistence of fetal muscle in an adolescent boy. Arch. Neurol. *14*, 1–14.
4. Laporte, J., Hu, L.J., Kretz, C., Mandel, J.L., Kioschis, P., Coy, J.F., Klauck, S.M., Poustka, A., and Dahl, N. (1996). A gene mutated in X-linked myotubular myopathy defines a new putative tyrosine phosphatase family conserved in yeast. Nat. Genet. *13*, 175–182.
5. Laporte, J., Kress, W., and Mandel, J.L. (2001). Diagnosis of X-linked myotubular myopathy by detection of myotubularin. Ann. Neurol. *50*, 42–46.
6. Buj-Bello, A., Biancalana, V., Moutou, C., Laporte, J., and Mandel, J.L. (1999). Identification of novel mutations in the MTM1 gene causing severe and mild forms of X-linked myotubular myopathy. Hum. Mutat. *14*, 320–325.
7. Laporte, J., Biancalana, V., Tanner, S.M., Kress, W., Schneider, V., Wallgren-Pettersson, C., Herger, F., Buj-Bello, A., Blondeau, F., Liechti-Gallati, S., and Mandel, J.L. (2000). MTM1 mutations in X-linked myotubular myopathy. Hum. Mutat. *15*, 393–409.
8. Tsai, T.C., Horinouchi, H., Noguchi, S., Minami, N., Murayama, K., Hayashi, Y.K., Nonaka, I., and Nishino, I. (2005). Characterization of MTM1 mutations in 31 Japanese families with myotubular myopathy, including a patient carrying 240 kb deletion in Xq28 without male hypogenitalism. Neuromuscul. Disord. *15*, 245–252.
9. Tosch, V., Vasli, N., Kretz, C., Nicot, A.S., Gasnier, C., Dondaine, N., Oriot, D., Barth, M., Puissant, H., Romero, N.B., et al. (2010). Novel molecular diagnostic approaches for X-linked centronuclear (myotubular) myopathy reveal intronic mutations. Neuromuscul. Disord. *20*, 375–381.
10. Tsujita, K., Itoh, T., Ijuin, T., Yamamoto, A., Shisheva, A., Laporte, J., and Takenawa, T. (2004). Myotubularin regulates the function of the late endosome through the gram domain-phosphatidylinositol 3,5-bisphosphate interaction. J. Biol. Chem. *279*, 13817–13824.
11. Al-Qusairi, L., Weiss, N., Toussaint, A., Berbey, C., Messaddeq, N., Kretz, C., Sanoudou, D., Beggs, A.H., Allard, B., Mandel, J.L., et al. (2009). T-tubule disorganization and defective excitation-contraction coupling in muscle fibers lacking myotubularin lipid phosphatase. Proc. Natl. Acad. Sci. USA *106*, 18763–18768.
12. Dowling, J.J., Vreede, A.P., Low, S.E., Gibbs, E.M., Kuwada, J.Y., Bonnemann, C.G., and Feldman, E.L. (2009). Loss of myotubularin function results in T-tubule disorganization in zebrafish and human myotubular myopathy. PLoS Genet. *5*, e1000372.
13. Hnia, K., Tronchère, H., Tomczak, K.K., Amoasii, L., Schultz, P., Beggs, A.H., Payrastre, B., Mandel, J.L., and Laporte, J. (2011). Myotubularin controls desmin intermediate filament architecture and mitochondrial dynamics in human and mouse skeletal muscle. J. Clin. Invest. *121*, 70–85.
14. Robb, S.A., Sewry, C.A., Dowling, J.J., Feng, L., Cullup, T., Lillis, S., Abbs, S., Lees, M.M., Laporte, J., Manzur, A.Y., et al. (2011). Impaired neuromuscular transmission and response to acetylcholinesterase inhibitors in centronuclear myopathies. Neuromuscul. Disord. *21*, 379–386.
15. Dowling, J.J., Joubert, R., Low, S.E., Durban, A.N., Messaddeq, N., Li, X., Dulin-Smith, A.N., Snyder, A.D., Marshall, M.L., Marshall, J.T., et al. (2012). Myotubular myopathy and the neuromuscular junction: a novel therapeutic approach from mouse models. Dis. Model. Mech. *5*, 852–859.
16. Lawlor, M.W., Alexander, M.S., Viola, M.G., Meng, H., Joubert, R., Gupta, V., Motohashi, N., Manfready, R.A., Hsu, C.P., Huang, P., et al. (2012). Myotubularin-deficient myoblasts display increased apoptosis, delayed proliferation, and poor cell engraftment. Am. J. Pathol. *181*, 961–968.
17. Lawlor, M.W., Viola, M.G., Meng, H., Edelstein, R.V., Liu, F., Yan, K., Luna, E.J., Lerch-Gaggl, A., Hoffmann, R.G., Pierson, C.R., et al. (2014). Differential muscle hypertrophy is associated with satellite cell numbers and Akt pathway activation following activin type IIB receptor inhibition in Mtm1 p.R69C mice. Am. J. Pathol. *184*, 1831–1842.
18. Al-Qusairi, L., Prokic, I., Amoasii, L., Kretz, C., Messaddeq, N., Mandel, J.L., and Laporte, J. (2013). Lack of myotubularin (MTM1) leads to muscle hypotrophy through unbalanced regulation of the autophagy and ubiquitin-proteasome pathways. FASEB J. *27*, 3384–3394.
19. Fetalvero, K.M., Yu, Y., Goetschkes, M., Liang, G., Valdez, R.A., Gould, T., Triantafellow, E., Bergling, S., Loureiro, J., Eash, J., et al. (2013). Defective autophagy and mTORC1 signaling in myotubularin null mice. Mol. Cell. Biol. *33*, 98–110.
20. Bitoun, M., Maugenre, S., Jeannet, P.Y., Lacène, E., Ferrer, X., Laforêt, P., Martin, J.J., Laporte, J., Lochmüller, H., Beggs, A.H., et al. (2005). Mutations in dynamin 2 cause dominant centronuclear myopathy. Nat. Genet. *37*, 1207–1209.
21. Böhm, J., Biancalana, V., Dechene, E.T., Bitoun, M., Pierson, C.R., Schaefer, E., Karasoy, H., Dempsey, M.A., Klein, F., Dondaine, N., et al. (2012). Mutation spectrum in the large GTPase dynamin 2, and genotype-phenotype correlation in autosomal dominant centronuclear myopathy. Hum. Mutat. *33*, 949–959.
22. Warnock, D.E., Baba, T., and Schmid, S.L. (1997). Ubiquitously expressed dynamin-II has a higher intrinsic GTPase activity and a greater propensity for self-assembly than neuronal dynamin-I. Mol. Biol. Cell *8*, 2553–2562.
23. Di, A., Nelson, D.J., Bindokas, V., Brown, M.E., Libunao, F., and Palfrey, H.C. (2003). Dynamin regulates focal exocytosis in phagocytosing macrophages. Mol. Biol. Cell *14*, 2016–2028.
24. Arneson, L.N., Segovis, C.M., Gomez, T.S., Schoon, R.A., Dick, C.J., Lou, Z., Billadeau, D.D., and Leibson, P.J. (2008). Dynamin 2 regulates granule exocytosis during NK cell-mediated cytotoxicity. J. Immunol. *181*, 6995–7001.

25. McNiven, M.A., Kim, L., Krueger, E.W., Orth, J.D., Cao, H., and Wong, T.W. (2000). Regulated interactions between dynamin and the actin-binding protein cortactin modulate cell shape. J. Cell Biol. *151*, 187–198.

26. Mooren, O.L., Kotova, T.I., Moore, A.J., and Schafer, D.A. (2009). Dynamin2 GTPase and cortactin remodel actin filaments. J. Biol. Chem. *284*, 23995–24005.

27. Yamada, H., Takeda, T., Michiue, H., Abe, T., and Takei, K. (2016). Actin bundling by dynamin 2 and cortactin is implicated in cell migration by stabilizing filopodia in human non-small cell lung carcinoma cells. Int. J. Oncol. *49*, 877–886.

28. Kenniston, J.A., and Lemmon, M.A. (2010). Dynamin GTPase regulation is altered by PH domain mutations found in centronuclear myopathy patients. EMBO J. *29*, 3054–3067.

29. Wang, L., Barylko, B., Byers, C., Ross, J.A., Jameson, D.M., and Albanesi, J.P. (2010). Dynamin 2 mutants linked to centronuclear myopathies form abnormally stable polymers. J. Biol. Chem. *285*, 22753–22757.

30. Cowling, B.S., Toussaint, A., Amoasii, L., Koebel, P., Ferry, A., Davignon, L., Nishino, I., Mandel, J.L., and Laporte, J. (2011). Increased expression of wild-type or a centronuclear myopathy mutant of dynamin 2 in skeletal muscle of adult mice leads to structural defects and muscle weakness. Am. J. Pathol. *178*, 2224–2235.

31. Liu, N., Bezprozvannaya, S., Shelton, J.M., Frisard, M.I., Hulver, M.W., McMillan, R.P., Wu, Y., Voelker, K.A., Grange, R.W., Richardson, J.A., et al. (2011). Mice lacking microRNA 133a develop dynamin 2–dependent centronuclear myopathy. J. Clin. Invest. *121*, 3258–3268.

32. Buj-Bello, A., Laugel, V., Messaddeq, N., Zahreddine, H., Laporte, J., Pellissier, J.F., and Mandel, J.L. (2002). The lipid phosphatase myotubularin is essential for skeletal muscle maintenance but not for myogenesis in mice. Proc. Natl. Acad. Sci. USA *99*, 15060–15065.

33. Childers, M.K., Joubert, R., Poulard, K., Moal, C., Grange, R.W., Doering, J.A., Lawlor, M.W., Rider, B.E., Jamet, T., Danièle, N., et al. (2014). Gene therapy prolongs survival and restores function in murine and canine models of myotubular myopathy. Sci. Transl. Med. *6*, 220ra10.

34. Buj-Bello, A., Fougerousse, F., Schwab, Y., Messaddeq, N., Spehner, D., Pierson, C.R., Durand, M., Kretz, C., Danos, O., Douar, A.M., et al. (2008). AAV-mediated intramuscular delivery of myotubularin corrects the myotubular myopathy phenotype in targeted murine muscle and suggests a function in plasma membrane homeostasis. Hum. Mol. Genet. *17*, 2132–2143.

35. Tasfaout, H., Buono, S., Guo, S., Kretz, C., Messaddeq, N., Booten, S., Greenlee, S., Monia, B.P., Cowling, B.S., and Laporte, J. (2017). Antisense oligonucleotide-mediated Dnm2 knockdown prevents and reverts myotubular myopathy in mice. Nat. Commun. *8*, 15661.

36. Cowling, B.S., Chevremont, T., Prokic, I., Kretz, C., Ferry, A., Coirault, C., Koutsopoulos, O., Laugel, V., Romero, N.B., and Laporte, J. (2014). Reducing dynamin 2 expression rescues X-linked centronuclear myopathy. J. Clin. Invest. *124*, 1350–1363.

37. Sabha, N., Volpatti, J.R., Gonorazky, H., Reifler, A., Davidson, A.E., Li, X., Eltayeb, N.M., Dall'Armi, C., Di Paolo, G., Brooks, S.V., et al. (2016). PIK3C2B inhibition improves function and prolongs survival in myotubular myopathy animal models. J. Clin. Invest. *126*, 3613–3625.

38. Samulski, R.J., and Muzyczka, N. (2014). AAV-mediated gene therapy for research and therapeutic purposes. Annu. Rev. Virol. *1*, 427–451.

39. Koornneef, A., Maczuga, P., van Logtenstein, R., Borel, F., Blits, B., Ritsema, T., van Deventer, S., Petry, H., and Konstantinova, P. (2011). Apolipoprotein B knockdown by AAV-delivered shRNA lowers plasma cholesterol in mice. Mol. Ther. *19*, 731–740.

40. Grimm, D., Pandey, K., and Kay, M.A. (2005). Adeno-associated virus vectors for short hairpin RNA expression. Methods Enzymol. *392*, 381–405.

41. Yang, Q., Tang, Y., Imbrogno, K., Lu, A., Proto, J.D., Chen, A., Guo, F., Fu, F.H., Huard, J., and Wang, B. (2012). AAV-based shRNA silencing of NF-κB ameliorates muscle pathologies in mdx mice. Gene Ther. *19*, 1196–1204.

42. Saal, K.A., Koch, J.C., Tatenhorst, L., Szegő, E.M., Ribas, V.T., Michel, U., Bähr, M., Tönges, L., and Lingor, P. (2015). AAV.shRNA-mediated downregulation of ROCK2 attenuates degeneration of dopaminergic neurons in toxin-induced models of Parkinson's disease in vitro and in vivo. Neurobiol. Dis. *73*, 150–162.

43. Koo, T., Malerba, A., Athanasopoulos, T., Trollet, C., Boldrin, L., Ferry, A., Popplewell, L., Foster, H., Foster, K., and Dickson, G. (2011). Delivery of AAV2/9-microdystrophin genes incorporating helix 1 of the coiled-coil motif in the C-terminal domain of dystrophin improves muscle pathology and restores the level of α1-syntrophin and α-dystrobrevin in skeletal muscles of mdx mice. Hum. Gene Ther. *22*, 1379–1388.

44. Agbulut, O., Huet, A., Niederländer, N., Puceat, M., Menasché, P., and Coirault, C. (2007). Green fluorescent protein impairs actin-myosin interactions by binding to the actin-binding site of myosin. J. Biol. Chem. *282*, 10465–10471.

45. Agbulut, O., Coirault, C., Niederländer, N., Huet, A., Vicart, P., Hagège, A., Puceat, M., and Menasché, P. (2006). GFP expression in muscle cells impairs actin-myosin interactions: implications for cell therapy. Nat. Methods *3*, 331.

46. Lawlor, M.W., Beggs, A.H., Buj-Bello, A., Childers, M.K., Dowling, J.J., James, E.S., Meng, H., Moore, S.A., Prasad, S., Schoser, B., and Sewry, C.A. (2016). Skeletal muscle pathology in X-linked myotubular myopathy: review with cross-species comparisons. J. Neuropathol. Exp. Neurol. *75*, 102–110.

47. Beggs, A.H., Böhm, J., Snead, E., Kozlowski, M., Maurer, M., Minor, K., Childers, M.K., Taylor, S.M., Hitte, C., Mickelson, J.R., et al. (2010). MTM1 mutation associated with X-linked myotubular myopathy in Labrador Retrievers. Proc. Natl. Acad. Sci. USA *107*, 14697–14702.

48. Zincarelli, C., Soltys, S., Rengo, G., and Rabinowitz, J.E. (2008). Analysis of AAV serotypes 1-9 mediated gene expression and tropism in mice after systemic injection. Mol. Ther. *16*, 1073–1080.

49. Salva, M.Z., Himeda, C.L., Tai, P.W., Nishiuchi, E., Gregorevic, P., Allen, J.M., Finn, E.E., Nguyen, Q.G., Blankinship, M.J., Meuse, L., et al. (2007). Design of tissue-specific regulatory cassettes for high-level rAAV-mediated expression in skeletal and cardiac muscle. Mol. Ther. *15*, 320–329.

50. Rivera, V.M., Gao, G.P., Grant, R.L., Schnell, M.A., Zoltick, P.W., Rozamus, L.W., Clackson, T., and Wilson, J.M. (2005). Long-term pharmacologically regulated expression of erythropoietin in primates following AAV-mediated gene transfer. Blood *105*, 1424–1430.

51. Husain, T., Passini, M.A., Parente, M.K., Fraser, N.W., and Wolfe, J.H. (2009). Long-term AAV vector gene and protein expression in mouse brain from a small pan-cellular promoter is similar to neural cell promoters. Gene Ther. *16*, 927–932.

52. Penaud-Budloo, M., Le Guiner, C., Nowrouzi, A., Toromanoff, A., Chérel, Y., Chenuaud, P., Schmidt, M., von Kalle, C., Rolling, F., Moullier, P., and Snyder, R.O. (2008). Adeno-associated virus vector genomes persist as episomal chromatin in primate muscle. J. Virol. *82*, 7875–7885.

53. Nathwani, A.C., Tuddenham, E.G., Rangarajan, S., Rosales, C., McIntosh, J., Linch, D.C., Chowdary, P., Riddell, A., Pie, A.J., Harrington, C., et al. (2011). Adenovirus-associated virus vector-mediated gene transfer in hemophilia B. N. Engl. J. Med. *365*, 2357–2365.

54. Nowrouzi, A., Penaud-Budloo, M., Kaeppel, C., Appelt, U., Le Guiner, C., Moullier, P., von Kalle, C., Snyder, R.O., and Schmidt, M. (2012). Integration frequency and intermolecular recombination of rAAV vectors in non-human primate skeletal muscle and liver. Mol. Ther. *20*, 1177–1186.

55. Arnett, A.L., Konieczny, P., Ramos, J.N., Hall, J., Odom, G., Yablonka-Reuveni, Z., Chamberlain, J.R., and Chamberlain, J.S. (2014). Adeno-associated viral (AAV) vectors do not efficiently target muscle satellite cells. Mol. Ther. Methods Clin. Dev. *1*, 14038.

56. Yi, R., Doehle, B.P., Qin, Y., Macara, I.G., and Cullen, B.R. (2005). Overexpression of exportin 5 enhances RNA interference mediated by short hairpin RNAs and microRNAs. RNA *11*, 220–226.

57. Hutvágner, G., Simard, M.J., Mello, C.C., and Zamore, P.D. (2004). Sequence-specific inhibition of small RNA function. PLoS Biol. *2*, E98.

58. Grimm, D., Streetz, K.L., Jopling, C.L., Storm, T.A., Pandey, K., Davis, C.R., Marion, P., Salazar, F., and Kay, M.A. (2006). Fatality in mice due to oversaturation of cellular microRNA/short hairpin RNA pathways. Nature *441*, 537–541.

59. Giering, J.C., Grimm, D., Storm, T.A., and Kay, M.A. (2008). Expression of shRNA from a tissue-specific pol II promoter is an effective and safe RNAi therapeutic. Mol. Ther. *16*, 1630–1636.

YMTHE, Volume *26*

Supplemental Information

Single Intramuscular Injection of AAV-shRNA Reduces DNM2 and Prevents Myotubular Myopathy in Mice

Hichem Tasfaout, Valentina M. Lionello, Christine Kretz, Pascale Koebel, Nadia Messaddeq, Deborah Bitz, Jocelyn Laporte, and Belinda S. Cowling

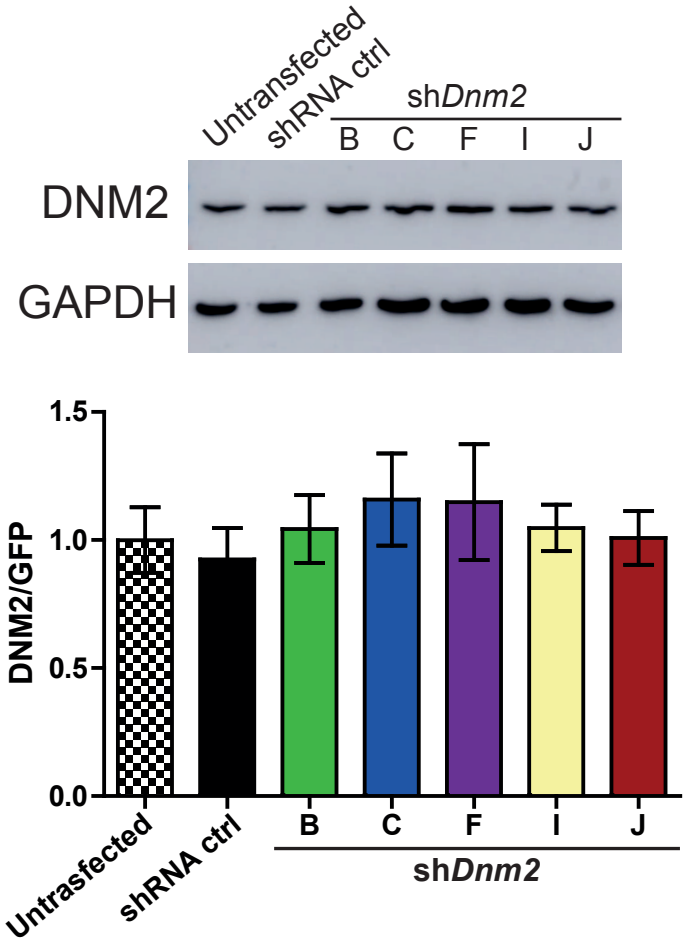

Supplemental figure S1: *In vitro* validation of shRNA targeting *Dnm2*.
Representative western blot from shRNA-treated C2C12 mouse myoblast. Cells were electroporated with shRNA ctrl, or sh*Dnm2* (B, C, F, I or J). DNM2 protein levels was determined by densitometry and standardized to GAPDH. *n*=3 per each group. Data represent an average of three independent experiments ± SEM.

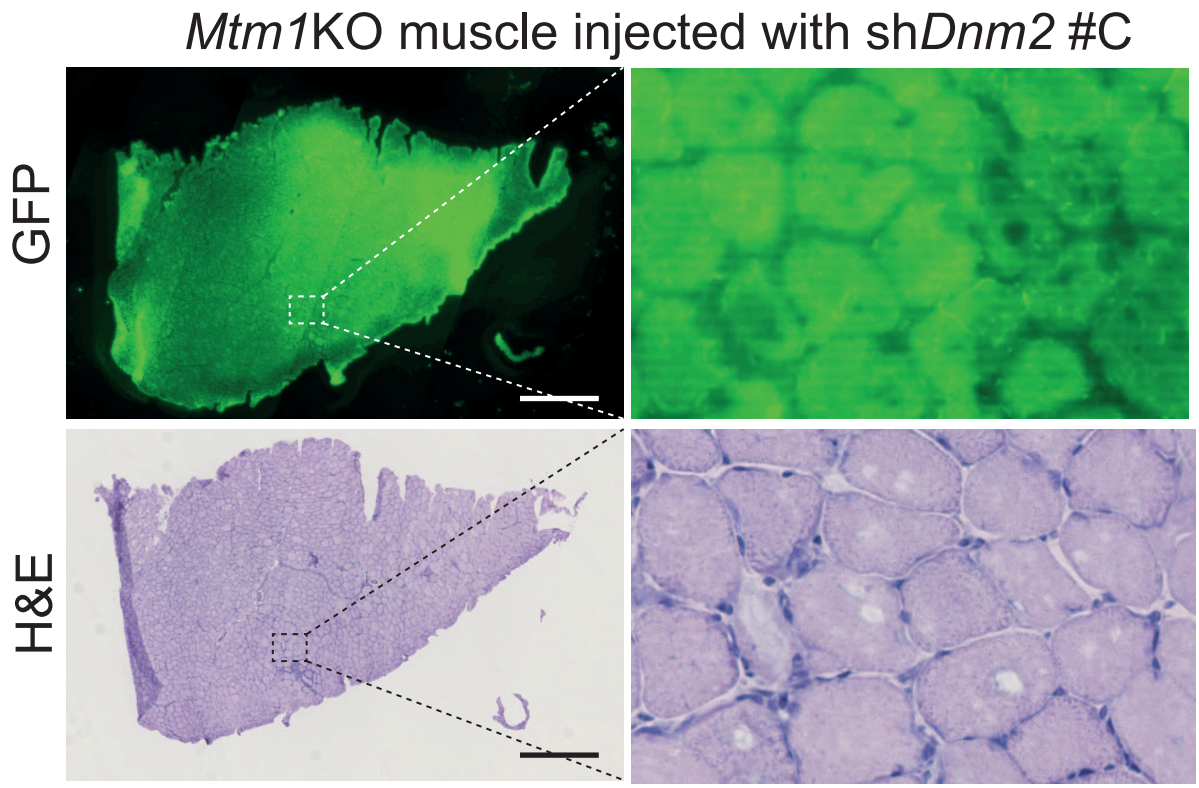

Supplemental figure S2: GFP expression and H&E staining of serial sections at 4 weeks after AAV-sh***Dnm2*** injection.**
Heterogeneous GFP expression was visualized on 8µm TA cross section of 7-weeks old *Mtm1*KO.

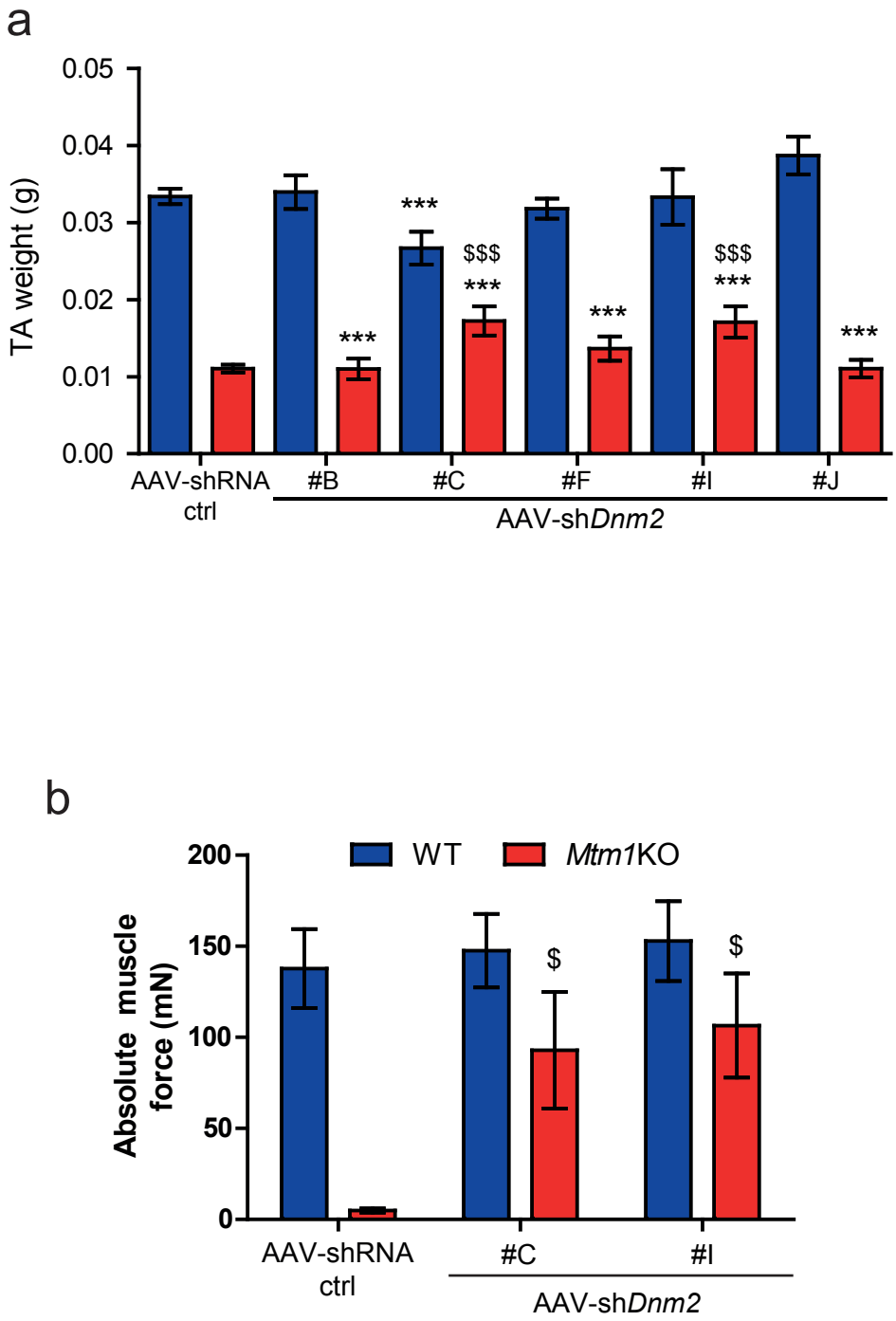

Supplemental Figure S3: Positive effects of AAV shRNA-mediated *Dnm2* knockdown on *Mtm1*KO muscle mass and absolute force.

4 weeks after AAV-sh*Dnm2* #C or #I injections, improvements in absolute muscle mass (a) and muscle maximal force (measured at 150 Hz) (b) were noted in *Mtm1*KO muscles. n=5-7 mice/group, ***p<0.001 vs WT TA treated with shRNA ctrl. $p<0.05, $$$p<0.01 *Mtm1*KO treated with AAV-sh*Dnm2* vs *Mtm1*KO treated with AAV-shRNA ctrl (ANOVA test).

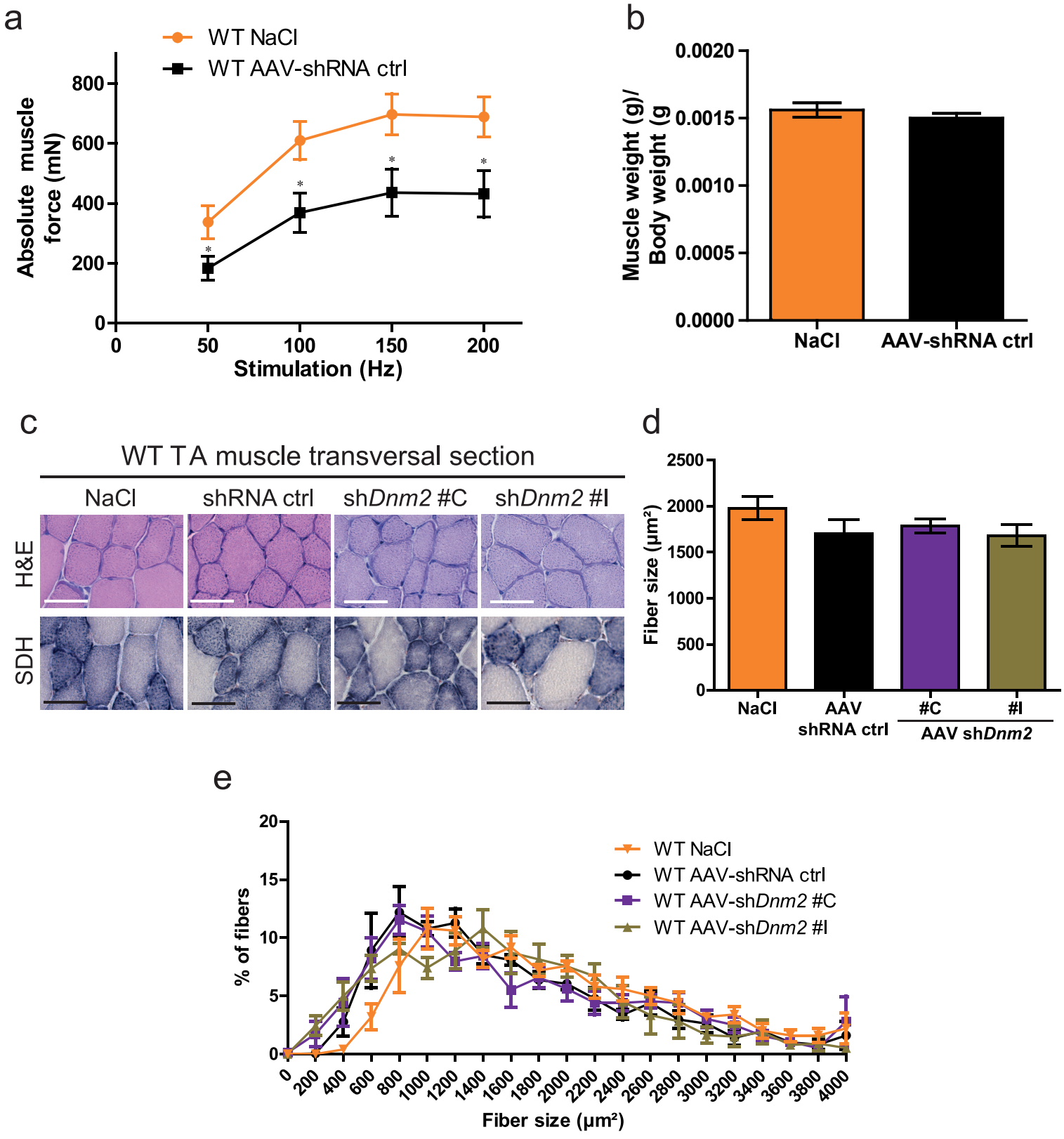

Supplemental figure S4: Characterization of AAV-shRNA ctrl and AAV-sh*Dnm2* impact on muscle mass, force and histology. (a) TA muscle of WT mice treated with NaCl or AAV-shRNA ctrl were weighed 4 weeks after a single injection. (b) Absolute muscle forces of TA muscle were recorded after sciatic nerve stimulation with 50, 100, 150 and 200Hz. *n*=5-7 mice/group. (c) TA muscle sections of WT mice treated with AAV-shRNA ctrl, AAV-sh*Dnm2* (#C or #I) or NaCl were stained with H&E and SDH to visualize fiber size, shape, nuclei positioning and mitochondrial distribution (scale bars: 50µm). (d) Myofiber area was calculated on 300-400 fibers per sample. (e) Fiber size distribution of WT TA muscles according to size groups. n=5 mice/group. *p<0.05 vs WT TA treated with NaCl (*t*-test).

Part 2a: Amphiphysin 2 (BIN1) modulation rescues MTM1 myotubular myopathy and prevents focal adhesion defects

Introduction

As described in the introduction, the XLCNM myopathy is the most severe form of centronuclear myopathy, it is due to mutations in the *MTM1* gene (Laporte et al., 1996) (Introduction, XLCNM). Currently no therapy is available for XLCNM patients and the pathophysiological mechanisms underline the disease is still not clear. Mutations on *BIN1* gene also caused CNM (Introduction, Autosomal CNM forms BIN1-related). A previous study showed that MTM1 and BIN1 interact in skeletal muscle and this interaction is crucial for BIN1 activities (Royer et al., 2013) (Introduction, MTM1,BIN1 and DNM2 interact regulate membrane remodeling). However, the pathomechanisms linking MTM1 and BIN1 in CNM remained unclear.

Aim of the study

The main goal of this study was to better understand the molecular mechanism between BIN1 and MTM1 *in vivo*, and to identify a novel therapeutic strategy to rescue XLCNM in mice. In addition, we aimed to elucidate the mechanism for this rescue by investigating the link between MTM1 and BIN1 and their involvement in focal adhesion recycling.

Results

In this study, I identified a new therapeutic strategy to rescue XLCNM in mice (*Mtm1*-/y). We crossed the *Mtm1* heterozygous female with Tg *BIN1* male mice to generate *Mtm1-/y* Tg *BIN1* mouse model. *Mtm1*-/y mouse died around 7 week of age because of a progressive myopathy that appear around 3 week of age. The overexpression of BIN1 rescued the lifespan, the growth and the muscle force of the *Mtm1-/y* mice. The abnormal muscle histological features were also rescued in the *Mtm1-/y* Tg *BIN1* model. Thanks to the positive and encouraging results obtained in the genetic cross model, we next developed a translated approach to increase BIN1 expression, using adeno associated virus (AAV). AAV-*BIN1* was injected postnatally by intramuscular injection at 3 weeks of age and systemically in pups 1 day post-birth (P1). In both experiments, skeletal muscle force was rescued by overexpressing *BIN1*. The systemic injection showed that the postnatal overexpression of BIN1 rescued the life span, as *Mtm1-/y* mice survived for more than 1.5 years.

I next investigated the molecular mechanism for this rescue. XLCNM histological muscle hallmarks are small rounded fibers with increased inter-fiber space suggesting a defect of adhesion to the extracellular matrix. We observed an increase in ß1 integrin protein level

and abnormal localization in *Mtm1-/y* skeletal muscle fibers. To confirm if MTM1 loss impacted on focal adhesion recycling and activity *Mtm1-/y* primary myoblasts were phenotyped. *Mtm1-/y* primary myoblasts displayed adhesion, migration and fusion defects. Abnormalities in focal adhesion proteins level and localization were rescued overexpressing BIN1.

Conclusion

This work suggests BIN1 as novel therapeutic target for XLCNM. Furthermore a functional link between MTM1 and BIN1 and focal adhesion homeostasis was identified.

Contribution

In this study, I performed all the mice phenotyping, muscle force, histological and ultrastructural analysis, AAV injections (intramuscular and systemic), immunofluorescence and primary myoblasts characterization.

Anne –Sophie Nicot supervised me on the focal adhesion chapter and performed Western blot of focal adhesion proteins and extracellular matrix proteins. Maxime Sartori phenotyped the line *Bin1*-/- Tg *BIN1* mice. Christine Kretz and Suzie Buono helped me with the mice genotyping and phenotyping. Pascale Kessler designed a macro in Fiji software to perform automated analysis of muscle morphometry. Sarah Djeroud contributed with primary cell maintenance. Pascale Koebel prepared the AAV-*BIN1*. Nadia Massaddeq prepared and acquired the EM pictures.

This work was supervised by Jocelyn Laporte and Belinda Cowling.

Amphiphysin 2 modulation rescues myotubular myopathy and prevents focal adhesion defects

Valentina M. Lionello[1,2,3,4], Anne-Sophie Nicot[1,2,3,4,8,9], Maxime Sartori[1,2,3,4], Christine Kretz[1,2,3,4], Pascal Kessler[1,2,3,4], Suzie Buono[1,2,3,4,10], Sarah Djerroud[1,2,3,4], Nadia Messaddeq[1,2,3,4], Pascale Koebel[1,2,3,4], Ivana Prokic[1,2,3,4,], Yann Hérault[1,2,3,4], Norma B Romero[5,6,7], Jocelyn Laporte[1,2,3,4,*,†], Belinda S. Cowling[1,2,3,4,10†]

[1]IGBMC (Institut de Génétique et de Biologie Moléculaire et Cellulaire), 67404 Illkirch, France.

[2]INSERM U1258, 67404 Illkirch, France

[3]CNRS UMR7104, 67404 Illkirch, France

[4]Strasbourg University, 67404 Illkirch, France

[5]Université Sorbonne, UPMC Univ Paris 06, INSERM UMRS974, CNRS FRE3617, Center for Research in Myology, GH Pitié-Salpêtrière, 47 Boulevard de l'hôpital, 75013 Paris, France

[6]Centre de référence de Pathologie Neuromusculaire Paris-Est, Institut de Myologie, GHU Pitié-Salpêtrière, Assistance Publique-Hôpitaux de Paris, 75013 Paris, France

[7]Neuromuscular Morphology Unit, Institut de Myologie, GHU Pitié-Salpêtrière, Assistance Publique-Hôpitaux de Paris, 75013 Paris, France

[8]Grenoble Institute des Neurosciences, Université Grenoble Alpes, 38706 Grenoble, France

[9]INSERM, U1216, 38706 Grenoble, France

[10]Dynacure, CS 10413, 67412, Illkirch, France (present address).

*Correspondence to Jocelyn Laporte (jocelyn@igbmc.fr)

†equal contributors

Overline: myopathies

One Sentence Summary:

Modulation of human Amphiphysin 2 expression by genetic cross and viral delivery rescues all hallmarks of X-linked centronuclear myopathy in mice.

Abstract

Centronuclear myopathies (CNM) are severe diseases characterized by muscle weakness and myofiber atrophy. Currently there are no approved treatments for these disorders. Mutations in the phosphoinositides phosphatase myotubularin (MTM1) are responsible for X-linked CNM (XLCNM), also called myotubular myopathy, whereas mutation in the membrane remodeling Bin/amphiphysin/Rvs (BAR) protein amphiphysin 2 (bridging integrator 1, BIN1) are responsible for an autosomal form of the disease. Here we investigated the functional relationship between MTM1 and BIN1 in healthy skeletal muscle and in the physiopathology of CNM. Genetic overexpression of human BIN1 efficiently rescued the muscle weakness and lifespan in a mouse model of XLCNM. Exogenous human BIN1 expression with adeno-associated virus (AAV) after birth also prevented the progression of the disease, suggesting that human BIN1 overexpression can compensate for the lack of reduced Mtm1 expression in this mouse model. Our results showed that MTM1 controls cell adhesion and integrin localization in mammalian muscle. Alterations in this pathway in *Mtm1*-/y mice was associated with defects in myofiber shape and size. BIN1 expression rescued integrin and laminin alterations and restored myofiber integrity, supporting the idea that MTM1 and BIN1 are functionally linked and necessary for focal adhesions in skeletal muscle. BIN1 modulation rescues XLCNM mouse model providing a proof-of-concept for future trials in XLCNM patients.

Introduction

Centronuclear myopathies (CNM) are severe congenital disorders characterized by muscle weakness, hypotonia, respiratory insufficiency, myofiber atrophy and abnormal nuclei position (Jungbluth et al., 2008). Currently no specific therapy is available for patients and the pathophysiology of these disorders is not well understood.

The most severe form of CNM is the X-linked form, also called myotubular myopathy (XLCNM, OMIM 310400). XLCNM is caused by mutations in the phosphoinositide 3-phosphatase myotubularin (*MTM1*) (Blondeau et al., 2000; Laporte et al., 1996; Raess et al., 2017; Taylor et al., 2000). Other forms of CNM are mainly due to mutations in *BIN1* (bridging integrator 1), ryanodine receptor (*RYR1*) and dynamin 2 (*DNM2*). Mutations in *BIN1* cause both autosomal recessive and dominant forms (OMIM 255200) (Bohm et al., 2014; Nicot et al., 2007). *BIN1* encodes amphiphysin 2, a BAR domain protein that senses and induces membrane curvature and remodeling (Daumke et al., 2014; Lee et al., 2002; Peter et al., 2004; Prokic et al., 2014). Among the various tissue-specific isoforms of BIN1, the skeletal muscle isoform 8 contains a phosphoinositides (PI) binding domain important for the formation of transverse (T)-tubules, a highly specialized muscle structure crucial for excitation-contraction coupling (Lee et al., 2002; Razzaq et al., 2001). BIN1 is also important for clathrin-mediated endocytosis (McMahon et al., 1997; Wigge et al., 1997) and is linked to nuclei positioning (D'Alessandro et al., 2015).

No similarity has been identified between MTM1 and BIN1 protein structure (Royer et al., 2013). MTM1 and BIN1 bind directly, and this interaction is important for membrane tubulation (Royer et al., 2013). Furthermore, BIN1 mutations leading to CNM disrupt this interaction (Royer et al., 2013), suggesting that the MTM1-BIN1 binding might be important for normal muscle function.

The muscle weakness of XLCNM correlates with a strong reduction in muscle fiber size, rounder fibers with increased inter-fiber space, abnormal centralization of nuclei or organelles such as mitochondria, and altered T-tubule structure (Romero, 2010). These hallmarks have been reproduced faithfully in the *Mtm1*-/y knockout mouse, which develops a progressive muscle weakness starting at 2-3 weeks of age, leading to death by 1-3 months of age (Buj-Bello et al., 2002b; Lawlor et al., 2016).

We hypothesize that the main defects of fiber shape and size are due to an alteration in focal adhesions. One of the key focal adhesion components and regulators are integrins (Mayer, 2003; Sun et al., 2016). Recently, MTM1 has been implicated in the exit of β1 integrin from endosomes (Ketel et al., 2016), and depletion of *mtm*, the ortholog of *MTM1*, in drosophila muscle caused accumulation of integrin on endosomes (Ribeiro et al., 2011). These results raise the possibility that MTM1, through

integrins, is required for myofiber attachments. Integrins are part of the focal adhesion complex responsible for maintaining the connection between the cytoskeleton and the extracellular matrix (Campbell and Humphries, 2011). Integrins bind extracellular matrix proteins such as fibronectin, laminin and collagen, change their conformation and recruit cytoskeletal regulators (such as vinculin) and kinases (such as focal adhesion kinase (FAK)) to activate downstream pathways (Graham et al., 2015). Integrins are actively recycled and can also signal from endosomes (Alanko and Ivaska, 2016). As such, they are key regulators of mechano-transduction, tissue integrity, cell shape and migration (Sun et al., 2016). In muscle, β1 integrin is important for myoblast fusion, nuclei peripheral positioning and sarcomere assembly (Perkins et al., 2010; Roman et al., 2018; Schwander et al., 2003), and is part of the costamere that couples sarcomeric forces to the extracellular matrix (Bloch and Gonzalez-Serratos, 2003).

The aim of this study was to investigate the relationship between MTM1 and BIN1 in skeletal muscle, under normal and pathological conditions. As loss-of-function mutations in *MTM1* or *BIN1* cause CNM , we hypothesized that increasing BIN1 expression may compensate for loss of MTM1. This hypothesis was tested by increasing BIN1 either through a genetic cross with a humanized *BIN1* transgenic mouse or by exogenous expression of human *BIN1* in *Mtm1*-/y mice using adeno-associated virus (AAV), and characterizing the CNM motor and histological phenotypes. We also investigated the focal adhesion pathway in the pathological model and upon BIN1-mediated rescue.

Results

Increased expression of human BIN1 rescues *Mtm1*-/y survival

To study the epistasis between *MTM1* and *BIN1*, we modulated the expression of these genes in mice. We first investigated the effect of downregulation of *Bin1* in *Mtm1-/y* mice. *Mtm1*-/y mice start developing a progressive muscle disease closely resembling XLCNM from 3-4 weeks and die usually by 2 months of age (Buj-Bello et al., 2002b). *Mtm1+/-* females were crossed with *Bin1+/-* males to obtain WT, *Mtm1*-/y, *Bin1*+/- and *Mtm1*-/y *Bin1*+/-mice. At embryonic day 18.5 (18.5 E), 8.3% of embryos were *Mtm1*-/y *Bin1*+/- while no pups *Mtm1*-/y *Bin1*+/- were obtained at 10 days post birth showing that concomitant downregulation of *Mtm1* and *Bin1* was not compatible with postnatal life (Table S1).

Conversely, to upregulate BIN1, we created transgenic mice expressing the human BIN1 gene (*TgBIN1*) by insertion of a human bacterial artificial chromosome (BAC) containing the human *BIN1* gene with its flanking sequence into the mouse genome (fig. S1A). RT-PCR, cloning and sequencing from tibialis anterior (TA) muscles showed the presence of the human *BIN1* isoform 8 (fig. S1B) that is the main muscle isoform (Cowling et al., 2017). *TgBIN1* mice are viable with no overt motor phenotypes (Movie S1). Crossing *TgBIN1* with *Bin1*-/- mice that die at birth from muscle defects (Cowling et al., 2017) efficiently rescued the lethality as at 4 months we observed 10 *Bin1*-/- Tg*BIN1* and no *Bin1*-/- mice. (fig. S1C). Furthermore no difference was observed in body weight, tibialis anterior (TA) weight and specific muscle force between WT and *Bin1*-/- Tg*BIN1* mice at 4 months (fig. S1D-I), suggesting that human *BIN1* is functional in a mouse context.

To investigate if increased expression of BIN1 rescues the survival of *Mtm1*-/y mice, we generated *Mtm1*-/y *TgBIN1* mice. Most *Mtm1*-/y *TgBIN1* mice survived more than 12 months and survival was indistinguishable from wildtype (WT) and *TgBIN1* mice (**Fig. 1A**). There was no difference in body weight between WT, *TgBIN1* and *Mtm1*-/y *TgBIN1* mice throughout their 2 year lifespan, whilst *Mtm1*-/y mice weighed significantly less before dying (p-value < 0.0001) (**Fig. 1B**, Movie S2, fig. S2A). BIN1 expression was increased approximately 4-fold in *TgBIN1* and *Mtm1*-/y *TgBIN1* mice compared to WT (**Fig. 1C, D**). These results show that increased expression of BIN1 alone is sufficient to rescue the postnatal lethality and growth defects observed in *Mtm1*-/y mice.

Increased expression of BIN1 rescues muscle strength and coordination in *Mtm1*-/y mice

We next investigated if muscle strength was rescued in *Mtm1*-/y mice by BIN1 expression. At 5 weeks, *Mtm1*-/y mice had strong defects in rotarod (neuromuscular analysis) and footprint (gait analysis) tests, while the *Mtm1-/y* Tg*BIN1* mice performed similarly to WT and Tg *BIN1* mice in rotarod, footprint, bar test and grip test (**Fig. 2A**, fig. S2A-E). *Mtm1*-/y mice could not perform the bar test. At 5 months of age, *Mtm1*-/y Tg*BIN1* were still able to perform all tests (rotarod, and footprint), indicating a long-term improvement in their motor function (fig. S2F, G). *Mtm1*-/y mice had difficulties to perform the hanging test (a test indicating whole body strength), while the *Mtm1-/y* Tg*BIN1* mice performed similarly to WT.

Overexpression of BIN1 in *Mtm1*-/y mice which normally present with strong muscle atrophy, rescued the TA muscle atrophy back to WT (**Fig. 2B**). Specific muscle force, measured in situ in the TA muscle, was extremely low in *Mtm1*-/y mice at 2 months, and rescued to WT levels in 2, 7 and 24 month old *Mtm1*-/y Tg*BIN1* mice (**Fig. 2C**, fig. S2H). No difference was detected in the muscle force between

Tg*BIN1* and WT mice. The time to muscle exhaustion during continuous stimulation was similar between *Mtm1*-/y Tg*BIN1*,Tg*BIN1* and WT mice at 2 and 7 months of age (fig. S2I). Overall, the severe muscle weakness phenotype of *Mtm1*-/y mice was fully rescued by increased expression of BIN1 in *Mtm1*-/y mice.

Increased BIN1 rescues histological and ultrastructural defects in *Mtm1*-/y mice

At 8w, *Mtm1*-/y TA muscles present with small rounded fibers with abnormal subsarcolemmal and central accumulation of oxidative staining as it was previously described (Buj-Bello et al., 2002b; Lawlor et al., 2016) (**Fig. 3A**, fig. S3A). Fiber size distribution (minimum ferret's diameter) was shifted towards smaller fibers (peak diameter 20-25 µm), whilst it increased to 25-30 µm in *Mtm1*-/y Tg*BIN1,* similar to WT and Tg*BIN1* muscles (**Fig. 3B**, fig. S3A, B). *Mtm1*-/y TA muscles exhibit approximately 22% of fibers with abnormal nuclei position, whereas *Mtm1*-/y Tg*BIN1* were indistinguishable from WT (**Fig. 3C**). Similar defects in *Mtm1*-/y mice were found in other muscles (gastrocnemius, diaphragm) and were efficiently rescued in *Mtm1*-/y Tg*BIN1* mice (fig. S3C-F). Later at 7 months of age, no differences were found in TA and gastrocnemius muscles between the *Mtm1*-/y Tg*BIN1* and WT mice (fig. S3G-J).

We next investigated myofiber organization by transmission electron microscopy (TEM) in TA at 8w (**Fig. 3D**). In contrast to *Mtm1*-/y mice that had misaligned Z lines and general sarcomere disorganization, *Mtm1*-/y Tg*BIN1* mice displayed normal myofiber ultrastructure (fig. S3K). As several studies highlighted an important role for BIN1 in T-tubule biogenesis (Lee et al., 2002; Razzaq et al., 2001) and as T-tubule defects were observed in several forms of centronuclear myopathies (Toussaint et al., 2011), we next analyzed the triads that are composed of one T-tubule and two sarcoplasmic reticulum cisternae. *Mtm1*-/y triads were barely distinguishable (**Fig. 3D**, fig.S3L). However, normal triads and T-tubule shape and localization were observed in Tg*BIN1* and *Mtm1*-/y Tg*BIN1* mice (fig. S3M). BIN1 and the T-tubule receptor DHPR colocalized at T-tubules in WT, Tg*BIN1* and *Mtm1*-/y Tg*BIN1* mice whereas *Mtm1*-/y mice had some fibers with disorganized staining (**Fig. 3E**) (fig. S3N). Overall, increased expression of human BIN1 rescued the muscle atrophy, histopathology and ultrastructure alterations observed in *Mtm1*-/y mice.

Postnatal muscle overexpression of human BIN1 rescues muscle force and myofiber organization in *Mtm1-/y* mice.

The expression of *BIN1* during development in *Mtm1*-/y mice by genetic cross rescued the muscle strength and all CNM hallmarks. We next investigated if postnatal BIN1 expression was sufficient to rescue the *Mtm1*-/y defects. The human BIN1 isoform 8 was the main isoform expressed in the rescued *Mtm1*-/y Tg*BIN1* mice and was cloned into adeno-associated virus (AAV) serotype 9. AAV-*BIN1* was injected intramuscularly in TA muscles of 3w old *Mtm1*-/y mice and analysis was performed 2 or 4w post-injection, compared to empty AAV. BIN1 was expressed 4 fold higher than in control muscles (**Fig. 4A**). Two weeks post-injection, there was no significant difference in TA muscle weight in *Mtm1*-/y injected with AAV-*BIN1* and the *Mtm1-/y* injected with the AAV-Ctrl (p=0.1216) (**Fig. 4C, D**).While the specific muscle force of *Mtm1-/y* mice injected with the AAV-Ctrl was significant difference compared to the WT control (p=0.0056), no difference was measured between the WT and the *Mtm1-/y* injected with AAV-*BIN1* (p=0.9288)(**Fig. 4E**). AAV-*BIN1* greatly improved the general aspect of the muscle (HE) including fiber size, and to a lesser extent nuclei position and the oxidative staining (SDH) (**Fig. 4F-H**, fig. S4A). Myofiber organization was improved in *Mtm1*-/y TA muscles injected with AAV-*BIN1* compared with AAV-empty control and WT and *Mtm1*-/y injected with AAV-*BIN1* had the same number of triads per sarcomere (**Fig. 4I,** fig. S4B). Similar effects on improvement of skeletal muscle force and muscle histology were also observed 4 weeks post-injection (fig. S4C-H). Overall, these results show that the intramuscular overexpression of BIN1 after birth is sufficient to improve muscle force and myofiber organization in the *Mtm1*-/y mice. These results suggest that increasing BIN1 postnatally is sufficient to reduce the myopathic phenotype in *Mtm1*-/y mice.

Postnatal systemic overexpression of BIN1 prolongs *Mtm1*-/y lifespan and rescues CNM muscle defects.

As increasing BIN1 by intramuscular injection of AAV-*BIN1* improved CNM features in *Mtm1-/y* muscles, we tested whether systemic AAV-*BIN1* transduction after birth could rescue the muscle defects and extend lifespan of *Mtm1*-/y mice. AAV-*BIN1* or AAV-empty control were injected into pups at postnatal day 1 by intraperitoneal injection and the effects of the injection were analyzed until 10 weeks of age, an age never reached by untreated *Mtm1*-/y mice. The systemic overexpression of BIN1 post-birth rescued the premature death of *Mtm1*-/y mice (**Fig. 5A**). The oldest treated *Mtm1-/y* mouse died at 1.5 years old (Movie S3). A slight amelioration of body weight was noted for *Mtm1*-/y mice injected with AAV-*BIN1* compared to mice injected with AAV-control (**Fig. 5B**). In addition, no difference in organ weight (brain, heart, liver) were observed between *Mtm1*-/y mice injected with AAV-*BIN1* and WT mice at 10w (fig. S5A).

To evaluate if the positive effect on growth and survival correlated with an increase in muscle function and structure, TA and GAS muscles were dissected. BIN1 overexpression was confirmed in the AAV-*BIN1* injected animals from TA muscle lysate (**Fig. 5C,D**). TA muscle weight relative to body weight of surviving treated *Mtm1*-/y mice was smaller than WT control whilst no difference was observed in the GAS weight between the WT and the treated *Mtm1-/y* (**Fig. 5E**, fig.S5B). *Mtm1*-/y mice presented a severe TA muscle weakness at 7 weeks of age whereas no difference was observed in situ in TA absolute or specific muscle force or time to fatigue between *Mtm1*-/y mice injected with AAV-*BIN1* and WT injected with AAV control at 10 weeks (**Fig. 5F**, **G** fig. S5C), indicating a complete rescue in muscle force. We analyzed the histology at 10w when no untreated *Mtm1*-/y mice were alive for direct comparison. In AAV-*BIN1* treated *Mtm1*-/y mice, the general organization was normal. There was no difference in nuclei position and the majority of the fibers had a muscle diameter between 30 to 50 µm as the WT control(**Fig. 5H-J**). Furthermore only an average of 5% of abnormal oxidative staining fibers were counted in the treated *Mtm1-/y* (fig. S5D). Ultrastructural analysis revealed the sarcomere organization was rescued by AAV-*BIN1* injection, and the number of triads per sarcomere was normalized, with most triads presenting a normal shape and localization (**Fig. 5K, L**). The correct T-tubule organization was confirmed through DHPR and BIN1 immunofluorescence (**Fig. 5M**, fig S5E.). In conclusion, systemic injection of AAV-*BIN1* extended *Mtm1*-/y lifespan, normalized TA muscle force and rescued the main histological and ultrastructural defects of the TA muscle.

Focal adhesion is impaired following loss of *Mtm1* and rescued in mice overexpressing *BIN1*.

Hypotrophic (smaller) and rounder fibers with increased inter-fiber space are the main histological defects in XLCNM patients (Romero and Bitoun, 2011), suggesting a defect in cell adhesion (**Fig. 6A**). The *Mtm1*-/y mouse faithfully recapitulates these hallmarks. To better understand if these defects correlate with an increase of extracellular matrix, we stained transverse TA sections from WT and *Mtm1*-/y mice with collagen and laminin, two main components of the extracellular matrix in skeletal muscle (Carmignac and Durbeej, 2012) (fig. S6A). *Mtm1*-/y muscle presented an increased inter-fiber space occupied by collagen labelled with Masson staining or a specific antibody (**Fig. 6B-D**, fig. S6A-B). We next quantified the distance between muscle fibers using collagen fluorescence staining. *Mtm1*-/y TA muscle presented an increase in the thickness of collagen interfiber staining compared to WT control (fig. S6C). Proteins from the extracellular matrix connect to proteins of focal adhesion including α7/β1 integrins and adaptor proteins such as vinculin (fig. S6C) (Harburger and Calderwood, 2009). In WT, vinculin and integrins localize at the sarcolemma, specifically at the costamere. *Mtm1*-/y muscles exhibited internalized vinculin (**Fig. 6E**, fig. S7A-C) and β1 integrin (**Fig. 6F**).

We next investigated if the modulation of BIN1 expression rescued the localization defects in the extracellular matrix and focal adhesion proteins. The muscle of *Mtm1*-/y Tg*BIN1* mice showed a normalization of inter-fiber space and consequently reduced collagen accumulation between fibers (**Fig. 6G-I**), in addition to a rescue in fiber size. We next verified the localization of vinculin and β1 integrin in *Mtm1*-/y Tg*BIN1* skeletal muscle. Vinculin and β1 integrin localized on the plasma membrane in *Mtm1*-/y Tg*BIN1* as observed in WT (**Fig. 6J, K**). Twenty percent of muscle fibers had abnormal β1 integrin localization in *Mtm1*-/y while no fibers with abnormal staining were identified in *Mtm1*-/y Tg *BIN1* (**Fig. 6L**).

To investigate in which intracellular compartment β1 integrin accumulates, endosomal markers were labelled on muscle sections and the early endosome marker EEA1 was found to colocalize with β1 integrin (**Fig. 6M**, fig. S7D-E). EEA1-positive endosomes also aggregated in several *Mtm1*-/y myofibers compared to WT (fig. S7F). Overall, these results highlight that β1 integrin abnormally accumulates at early endosomes in *Mtm1*-/y muscles, indicating a defect in β1 integrin turnover that may induce the abnormality in fiber shape and the increase in inter-fiber space.

To further decipher the mechanisms responsible for the defects in the focal adhesion pathway, the activation of the focal adhesion kinase (FAK), a downstream effector of β1 integrin, was measured. No difference in FAK protein quantity was detected between the *Mtm1*-/y and WT (**Fig. 6N, O**). The activation of the focal adhesion complex leads to the auto-phosphorylation of FAK on tyrosine 397 (Graham et al., 2015). *Mtm1*-/y muscles exhibited decreased auto-phosphorylation of FAK, confirming activation of the focal adhesion pathway is altered (**Fig. 6 P**). We also verified if phosphoY397-FAK was present on endosomes accumulating β1 integrin in *Mtm1*-/y skeletal muscle fibers. A colocalization of internalized β1 integrin and phosphoY397-FAK was detected in some *Mtm1*-/y fibers suggesting that β1 integrin signaling was still maintained in endosomes (fig. S7G).

Consequences in focal adhesion defects in *Mtm1*-/y skeletal muscle.

To better understand the functional impact of focal adhesion defects observed in skeletal muscle, experiments on primary myoblasts were conducted. *Mtm1*-/y myoblasts exhibited larger β1 integrin vesicles than WT myoblasts (**Fig. 7A,** fig. S7H), confirming the accumulation of β1 integrin observed in adult skeletal muscle. No difference was detected in β1 integrin plasma membrane signal between WT and *Mtm1*-/y skeletal muscles (fig. S7I). Focal adhesions are important for cell adhesion, migration and fusion (Perkins et al., 2010; Ratcliffe et al., 2016; Schwander et al., 2003). Cell adhesion was checked by allowing WT and *Mtm1*-/y myoblasts to adhere for 10, 20, 40 min on laminin coated dishes.

The surface area of *Mtm1*-/y myoblasts was lower than for WT cells at 20 minutes while no difference was detected at 1, 40 and 60 minutes (**Fig. 7B**). As studies showed that defects in β1 integrin localization affected cell migration (Ratcliffe et al., 2016), a migration assay was performed with WT and *Mtm1*-/y myoblasts plated on laminin-coated dishes. A significant (P value: 0.0126) reduction of migrating distance was observed in *Mtm1*-/y myoblasts compared to WT (**Fig. 7C**). Finally, the ability of myoblasts to fuse was analyzed over time on matrigel-coated dishes. A significant (P value: 0.0001) defect in myoblast fusion was identified at 24 and 48 hours of differentiation in *Mtm1*-/y cells but not at 72 hours (**Fig. 7D**). Overall, these results suggest *Mtm1*-/y myoblasts exhibit defects in cell adhesion, migration and fusion that are related to a defect in β1 integrin localization and turnover in muscle.

We next analyzed the protein levels of laminin, vinculin and β1 integrin and found an increase in their amount in the *Mtm1*-/y skeletal muscle which was normalized to WT levels upon BIN1 expression (**Fig. 7E-H**, fig. S7J). *Mtm1*-/y skeletal muscle exhibited a higher β1 integrin protein level compared to the WT control. No difference in β1 integrin transcription was identified between WT and *Mtm1-/y* skeletal muscle (fig. S7K). We next investigated if the postnatal overexpression of BIN1 rescued the β1 integrin intracellular accumulation observed in *Mtm1-/y* mice. A normalization of β1 integrin localization in *Mtm1*-/y muscle was observed upon AAV-*BIN1* systemic injection after birth (**Fig. 7I**, fig. S7L), suggesting this rescue was not dependent on the methodology used for BIN1 expression. Overall, BIN1 expression efficiently rescued the defects of extracellular matrix and focal adhesion in addition to the muscle weakness and fiber histopathology in the *Mtm1*-/y mouse model of XLCNM.

Discussion

This study reports a genetic and functional link between MTM1 and BIN1 in skeletal muscle. Increased expression of BIN1 by genetic cross or viral delivery after birth prolongs the lifespan of *Mtm1*-/y mice and rescued the muscle force and the main histological hallmarks of CNM in this mouse model. *Mtm1*-/y mice showed defects in integrin turnover and focal adhesion functions, myofiber hypotrophy and abnormal shape, and these phenotypes were rescued upon BIN1 overexpression.

Loss-of-function mutations in *BIN1* and *MTM1* cause different forms of CNM (Laporte et al., 2000; Nicot et al., 2007); however, whether a functional connection existed between these genes was not clear. While *Mtm1*-/y mice present with progressive muscle weakness from 2-3w of age and die by 2 months (Buj-Bello et al., 2002b), increased expression of human BIN1, either by transgenesis or AAV-

mediated transduction, rescued the lifespan, the motor defects, most of the histological and ultrastructural defects, and the molecular alterations. These results show that increasing BIN1 compensates for the lack of MTM1, suggesting that MTM1 and BIN1 might be in a common pathway where MTM1 is a positive regulator of BIN1. Previously, we showed decreased expression of DNM2, a third protein mutated in CNM, rescued both the CNM phenotypes due to MTM1 or BIN1 loss (Cowling et al., 2014; Cowling et al., 2017), supporting that MTM1 and BIN1 are negative regulators of DNM2. Taken together with the present data, we propose a CNM pathway where MTM1 would activate BIN1 that in turn inhibits DNM2. This hypothesis is supported by the fact that MTM1 binds BIN1 (Royer et al., 2013) and that BIN1 is a known interactor of DNM2 (Lee et al., 2002; Nicot et al., 2007). In addition, *BIN1* mutations reduce the interaction with MTM1 or DNM2 (Nicot et al., 2007; Royer et al., 2013). However, we cannot rule out that MTM1 and BIN1 act on parallel pathways converging to regulate DNM2.

We observed a 1.9 fold increase in BIN1 protein amount in *Mtm1*-/y muscle at 8w (advanced disease stage) but normal quantity at 5w, suggesting a potential compensatory mechanism that is insufficient for reaching a rescue that can be obtained by increasing exogenous BIN1 by about 3.5 fold through transgenesis or AAV injection.

Here we identified *BIN1* as a modifier for *MTM1*-related CNM, and thus *BIN1* as a potential therapeutic target. We showed that *BIN1* expression could rescue the postnatal muscle maintenance defects linked to MTM1 loss. Following the positive proof-of-concept based on a transgenesis approach, we used AAV delivery of human *BIN1* after birth to validate a potentially translational approach. *BIN1* was first overexpressed intramuscularly and then through systemic delivery, and both strategies rescued muscle force and myofiber structural defects; in addition, the systemic injection greatly prolonged the lifespan. Of note, AAV injection at 3 weeks, after the onset of the disease, was sufficient to reduce disease severity, suggesting that early treatment in symptomatic patients may provide a benefit. The positive results obtained here using a human *BIN1* transgene in an AAV9 vector, a serotype already used in clinical trial, suggest that this approach could be tested in larger animals that more closely mimic the human condition. However, it is not clear how long the AAV-mlediated expression remains active in the body.

DNM2 modulation also rescued BIN1 or MTM1 loss in animal models (Cowling et al., 2017; Tasfaout et al., 2017; Tasfaout et al., 2018b). In this study we identified an additional “cross therapy” concept where modulation of a CNM gene (*BIN1*) rescues the loss of another CNM gene (*MTM1*). Moreover, AAV-mediated *MTM1* gene therapy was shown to be effective in animal models of XLCNM and is

currently in clinical trials (Childers et al., 2014). XLCNM patients barely express MTM1 protein and its delivery might trigger an immune response against an unknown protein. Using AAV-*BIN1* strategy could avoid a potential immune response as in the case of AAV-*MTM1*, or the potential secondary effects of DNM2 reduction (Tasfaout et al., 2018a).

Small rounded fibers and increased inter-fiber space are main histological hallmarks in patients for the diagnosis of XLCNM, and suggest a defect of adhesion to the extracellular matrix. β1 integrin is the major integrin molecule of skeletal muscle and links the extracellular matrix with the intracellular cytoskeleton and the sarcomeres at focal adhesions termed costameres (Carmignac and Durbeej, 2012). Focal adhesions integrity is indeed important for muscle as they mediate mechano-transduction and are a platform for intracellular signaling (Olsen et al., 2019). Alteration of β1 integrin quantity and localization in muscle was seen in 5w and 8w old *Mtm1*-/y mice, together with increased collagen and inter-fiber space. Of note, correct sarcomere alignment and integrity depends on costameres. Indeed myofibril formation can be inhibited by antagonizing integrin dimers alone, suggesting integrin-ECM interaction is important for correct sarcomere formation during muscle development (Schwander et al., 2003). Sarcomeres are greatly altered in XLCNM and *Mtm1*-/y muscles, which probably contributes to the severe muscle weakness (Cowling et al., 2012; Romero and Bitoun, 2011). In addition, a recent report proposed that integrins regulate peripheral nuclear positioning in myofibers differentiated in vitro, suggesting that integrin defects may also mediate the centralization of nuclei in CNM (Roman et al., 2018). Importantly, all these defects were rescued by increased BIN1 expression, supporting defects in the focal adhesion pathway are an important cause of the disease. MTM1 and BIN1 thus appear as important regulators of focal adhesions, in addition to their recognized roles in maintenance of the T-tubule structure (Al-Qusairi et al., 2009; Dowling et al., 2009; Lee et al., 2002; Razzaq et al., 2001). Mice that lack β1 integrin specifically in skeletal muscle had reduced muscle mass and alteration of sarcomere ultrastructure and died at birth with non-inflated lungs (Schwander et al., 2003); such phenotypes are typical from XLCNM patients (Jungbluth et al., 2008). Also, compound heterozygous mutations in α7 integrin cause muscular dystrophy (Hayashi et al., 1998). Altogether, the literature supports the rationale that defects in the functions of focal adhesions is an important component of the pathomechanism leading to the MTM1-related myopathy.

Both MTM1 and BIN1 are involved in membrane remodeling and recycling in cells (Ketel et al., 2016; Pant et al., 2009; Ribeiro et al., 2011), and we observed that β1 integrin is blocked in EEA1-positive endosomes in *Mtm1*-/y muscles. This defect is potentially due to the fact that MTM1 is implicated in

the conversion of early to late or recycling endosomes (Ketel et al., 2016). This function appears conserved in evolution as a previous study found that the drosophila ortholog of MTM1 was necessary for integrin turnover (Ribeiro et al., 2011). In this study, we showed that integrin downstream effectors as vinculin and FAK were altered in *Mtm1*-/y muscles, supporting that integrin trafficking defects lead to alteration of focal adhesion signaling. Subsequently, alteration of focal adhesions caused a defect in adhesion, migration and fusion of myoblasts lacking MTM1, leading to a decrease in myoblast to myotube fusion index that is reminiscent of the myofibers hypotrophy typically seen in patient muscles (Romero and Bitoun, 2011).

Overall, this study underlines a key role for MTM1 and BIN1 in the regulation of integrin trafficking and focal adhesion in skeletal muscle, and points to the defect in these mechanisms as an important cause of XLCNM that can be efficiently rescued by increasing BIN1 expression through viral delivery. As MTM1 homologs and BIN1 are implicated in other diseases, especially in peripheral neuropathies or late-onset Alzheimer and arrhythmia, these findings suggest that the approach proposed here might provide benefits in other disorders.

Material and Methods

Study Design

The sample size for each experiment is included in the figure legends. In this study we used mice (WT, *Mtm1*-/y Tg*BIN1* mice) and primary myoblasts obtained from WT and *Mtm1*-/y pups. The number of mice used was selected based on previous phenotyping analyses conducted in the same model and calculating the statistical power of the experiment.. *Mtm1*-/y mice died before 2-3 months of age and were analyzed in this study until 2 months. The other genotypes studied (WT, Tg*BIN1*, *Mtm1*-/y , *Mtm1-/y* Tg*BIN1, Mtm1*-/y injected with AAV-Ctrl and *Mtm1*-/y injected with AAV-*BIN1* systemically*)* were phenotyped and sacrificed at the ages noted. Blind phenotyping tests were conducted on mice (WT, Tg*BIN1*, *Mtm1-/y* Tg*BIN1* and *Mtm1*-/y*)* and on primary cells. Each experiment was repeated at least 3 times. Sample collection, treatment and processing information are included in the main text or in other sections of Material and Methods. No outliers were excluded in the study.

Chemicals

Primary antibodies used were mouse anti-DHPRα_1 ($Ca_v1.1$) subunit (abcam2862, Abcam), BIN1 (C99D, Abcam), and glyceraldehyde-3-phosphate dehydrogenase (GAPDH, MAB374; Chemicon), β_1 integrin (MAB1997, Chemicon), vinculin (V9131, Sigma), laminin (ab11575, Abcam), collagen VI (NB120-6588, Novus Biologicals), FAK (3285S, Cell Signaling), pY397 FAK (44-624G, Invitrogen), EEA1 (sc-137130, Santa Cruz Biotechnology, Inc.), dystrophin (ab15277, Abcam), Rhodamine Phalloidin (PHDR1, Cytoskeleton) and anti-BIN1 (R2405), rabbit anti-DNM2 antibodies (R2680 and R2865) were made onsite at the polyclonal antibody facility of the IGBMC. Alexa Fluor–conjugated secondary antibodies were purchased from Invitrogen (Alexa Fluor 488, Alexa Fluor 594 , Alexa Fluor 647). Secondary antibodies against mouse and rabbit IgG, conjugated with horseradish peroxidase (HRP) were purchased from Jackson ImmunoResearch Laboratories (catalog 115-035-146 and 111-036-045). An ECL kit was purchased from Pierce.

Primary myoblasts

Primary myoblasts from WT and *Mtm1-/y* newborn mice were prepared as previously described in Cowling et al. 2017 (Cowling et al., 2017). After extraction, primary cells were plated in IMDM with 20% FCS and 1% Chicken Embryo Extract (MP Biomedical) onto 1:200 Matrigel Reduced Factor (BD) and Laminin (354232, Corning).

Primary myoblasts adhesion experiments

The experiments were conducted following the protocol adapted from Ratcliffe, 2016 (Ratcliffe et al., 2016). WT and *Mtm1-/y* primary myoblasts were trypsinized and resuspended in IMDM with 20% FCS and 1% Chicken Embryo Extract. 2.5 x 10^4 primary myoblasts were diluted in 500 µl media and plated in laminin coated dishes. Cells were allowed to adhere for 10, 20, 30 and 60 minutes. Primary myoblasts were then washed with warmed medium and fixed with 4% PFA. Immunofluorescence was conducted and cells were stained with Rhodamine Phalloidin (Cystoskeleton). After confocal acquisition cells surface were measured using ImageJ program.

Primary myoblasts fusion index

Primary myoblasts were plated at 4 x 10^4 on matrigel. Primary myoblasts differentiation was triggered when cells reach 70% by switching the medium to IMDM with 2% horse serum and 24 hours later a

thick layer of matrigel (1:3 in IMDM) was added. Brightfield picture were acquired in living myotubes at 24, 48 and 72 hours post differentiation.

Primary myoblasts migration

2 x 10^4 primary myoblasts were plated in IMDM with 20% FCS and 1% Chicken Embryo Extract on laminin coated dishes. Migration of cells were observed by Time lapse with a Leica microscope for 24 hours, Pictures were taken every 15 minutes. The migration velocity was measured using Fiji program.

Mouse lines

Mtm1-/y mouse line (129PAS) was previously generated and characterized (Buj-Bello et al., 2002b; Tasfaout et al., 2017). *TgBIN1* (B6J) mice were obtained by the insertion of human BAC (n° RP11-437K23 Grch37 Chr2: 127761089-127941604) encompassing the full *BIN1* gene with 180.52 Kb of genomic sequence. The *Bin1*+/- mice were previously published (Cowling et al., 2017). *Mtm1* heterozygous female mice were crossed with *TgBIN1* males to generate 4 genotypes: WT, *TgBIN1, Mtm1*-/y *TgBIN1* and *Mtm1*-/y. Animals were maintained at room temperature with 12 hours light/ 12 hours dark cycle. Animals were sacrificed by cervical dislocation following European legislation on animal experimentation and experiments approved by ethical committees (APAFIS#5640-2016061019332648; 2016031110589922; Com'Eth 01594).

Animal phenotyping

The phenotyping experiments were conducted blinded and all the experiments were repeated three time for each mouse to ensure reproducibility. The tests were performed by the same examiners in order to avoid stress and to ensure reproducibility. The daily phenotyping experiments were performed in the same part of the day for all the mice in the cohort while the weekly experiments were always performed on the same day of the week. The following phenotyping tests were performed: hanging test, grip test, rotarod test, bar test and footprint test. The Hanging test was performed each week from 3 weeks to 16 weeks of age and monthly from 4 to 12 months. The mice were suspended from a cage lid for maximum 60 seconds and the test was repeated three times. The average time each mouse fall from the grid is presented in the graph. The grip test was conducted each month from 3 to 12 months. The 4-paw strength was measured using a dynamometer; and the test was repeated 3 times for each animal in each time point. The average of the 3 repetitions is

reported in the graph. Results are represented as force (g) relative to body weight in grams (g). The rotarod test was conducted at 5 weeks and 5 months of age. The mice performed the test for 5 days. During day 1 mice were trained to run in acceleration mode on the rotarod. From day 2-5 mice ran for a maximum of 5 minutes with increasing speed (4-40rpm). Each mouse performed the test 3 times, and the average of 3 repetitions was represented. We did not use the same cohort of mice at 5 weeks and 5 months. The data reported in the graph correspond to the amount of time the animal run on the rotarod. The bar test was performed placing the mice in a suspended bar. The time to walk along the bar was measured, the experiment was performed only at 5 weeks of age. In this experiment only WT, Tg *BIN1* and *Mtm1-/y* Tg *BIN1* mice were tested as *Mtm1-/y* mice could not walk on a suspended bar. The footprint test was performed at 5 weeks and 5 months of age. For this test the mice hindpaw placement was analyzed as previously described (Cowling et al., 2017). Hindlimbs were coloured with ink, and the placement of mice hindlimbs were recorded. The angle between the hindlimb position was measured using ImageJ.

Muscle force measurement

Mice were anesthetized using Pentobarbital (50mg/kg) by intraperitoneal injection, the force of tibialis anterior (TA)was measured using a force transducer (Aurora Scientific) as described previously (Tasfaout et al., 2017). The absolute maximal force of the TA was measured after tetanic stimulation of the sciatic nerve with a pulse frequency from 1 to 125 Hz. The specific maximal force was determined dividing the absolute maximal force with the TA weight. The fatigue was measured stimulating continuously the sciatic nerve with a frequency of 50 Hz.

AAV transduction of TA muscle

Intramuscular injection: 3 weeks old male wild-type or *Mtm1*-/y mice were anesthetized by intraperitoneal injection of ketamine 20mg/ml and xylazine 0,4% (5 µl/g of body weight). The TA muscle was injected with 20 µl of AAV9 (7x10^11 vg/mL) CMV human *BIN1* isoform 8 without exon 17 or empty AAV9 control diluted in PBS. Systemic injection: Pups were injected intraperitoneally (IP) in the first 24 hours after birth. A volume of 50 µL of AAV9 (10^13vg/ mL) CMV human *BIN1* isoform 8 without exon 17 or with empty AAV control was used(Long et al., 2016). The pups were immediately housed in the cage with their mother after the injection.

Tissue collection

Cervical dislocation was used to sacrifice mice after carbon dioxide suffocation. TA and GAS (gastrocnemius) muscles were extracted and then frozen in isopentane cooled in liquid nitrogen. The diaphragm was collected and directly frozen in OCT on dry ice. Heart, liver and brain were collected and directly frozen in liquid nitrogen. All tissues were then stored at -80°C.

Histology

8 µm cryosections of TA, GAS and diaphragm muscles were cut and stained with Haematoxylin and Eosin (HE) and succinate dehydrogenase (SDH) for histological analysis. After staining the images were acquired with the Hamamatsu Nano Zoomer 2HT slide scanner. The percentage of internalized nuclei were counted using Cell Counter Plugin in Fiji software. A Macro was used to measure the TA fiber diameter foe each genotype. The TA fiber diameter was calculated (>100 fibers per mouse) from 3–5 mice per group. The percentage of TA muscle fibers with centralized or internalized nuclei was counted in >350 fibers using the cell counter plugin in Image.

Immunostaining

Transversal 8 µm cryosections were prepared from TA frozen in isopentane. For longitudinal staining the TA was incubated overnight in PFA at 4°C and after 3 PBS 1X washing transferred into 30% sucrose overnight at 4°C. The sections were permeabilized with PBS-Triton 0,5% and then saturated with BSA 5% in PBS. The primary antibodies diluted in BSA 1% used were: laminin (ab11575, 1:200), EEA1 (sc-137130, 1:50), α7 integrin (ab195959, 1:50), β1 integrin (MAB1997, 1:50), vinculin (V9131, 1:200), DHPR (abcam2862, 1:50), BIN1 (C99D, 1:50). The secondary antibodies were anti-mouse, rabbit or rat Alexa 488, Alexa 594 and Alexa 647 were diluted 1:250 in 1% BSA.

Electron microscopy

TA was stored in 2.5 % paraformaldehyde and 2.5 % glutaraldehyde in 0,1M cacodylate buffer. Sections were observed by electron microscopy. To observe T-tubules, potassium ferrocyanide was added to the buffer (K3Fe(CN) 6 0.8% , Osmium 2%, cacodylate 0.1M)(Al-Qusairi et al., 2009). The triad number per sarcomere and T-tubule direction were measured manually.

RNA extraction and *BIN1* isoform 8 detection

TA muscles were lyzed in TRIzol reagent (Invitrogen) to extract RNA and the reverse transcriptase (Thermofisher Scientific) was used to obtain cDNA. To identify human *BIN1* isoform overexpressed in *Mtm1*-/y *TgBIN1* mice, *BIN1* cDNA was amplified using human *BIN1* primers (5'ACGGCGGGAAAGATCGCCAG, 3' TTGTGCTGGTTCCAGTCGCT). Human *BIN1* cDNAs were cloned into pENTR1A vector and then sequenced using GATC service.

Protein Extraction and western blotting

TA muscle was lysed in RIPA buffer with 1mM DMSO, 1mM PMSF and mini EDTA free protease inhibitor cocktail tablets (Roche Diagnostic) on ice. The protein concentration was measured using the BIO-RAD Protein Assay Kit (BIO-RAD). Loading buffer (50 mM Tris-HCl, 2% SDS, 10% glycerol) was added to protein lysates, and proteins were separated by 8% or 10% in SDS-polyacrylamide gel electrophoresis containing 2,2,2-Trichloroethanol (TCE) in order to visualize all tryptophan-containing proteins. After transfer to nitrocellulose, saturation was done with 3% BSA or 5% milk, primary antibody and secondary antibody was added: β1 integrin (MAB1997, 1:500), vinculin (V9131, 1:1000), BIN1 (2405, 1:1000; IGBMC), MTM1 (2827, 1:1000; IGBMC), GAPDH (MAB374, 1:100000).

Statistical Analysis

The data are expressed as mean ± s.e.m. Graph and curves were made using GraphPad Prism software versions 5&6. The unpaired students *T-test* was used to compare two groups. Non parametric test and Kruskal Wallis post-hoc were used to compare different groups. One-way ANOVA and Bonferroni test post-hoc were used to compared different groups if the data followed a normal distribution and if the samples analyzed had the same genetic background. P values smaller than 0.05 were considered significant. The number of mice and the tests used for each experiments are listed for each experiment in the figure legends.

Supplementary Materials

Table S1: Breeding strategy and outcome for *Mtm1-/y Bin1*+/-

Fig. S1: Creation of transgenic mice expressing human BIN1 (Tg*BIN1*).

Fig. S2: Increased BIN1 expression rescues the motor function and muscle force of *Mtm1-/y* mice.

Fig. S3: Increased BIN1 expression rescues muscle histology of *Mtm1-/y* mice at 2 and 7 months old.

Fig. S4: Postnatal intramuscular overexpression of BIN1 rescues muscle force and myofiber organization in *Mtm1-/y* mice.

Fig. S5: Organ weights and muscle fatigue in the *Mtm1-/y* mice expressing BIN1 after systemic AAV delivery

Fig. S6: Extracellular matrix defects in *Mtm1-/y* muscle

Fig. S7: Focal adhesion defects in Mtm1-/y myofibers

Movie S1: Expression of human *BIN1* did not generate any obvious clinical phenotypes in mice. Tg*BIN1* mice at 8 weeks.

Movie S2: Increased *BIN1* expression rescues *Mtm1*-/y phenotype.

Movie S3: Postnatal systemic injection of AAV-*BIN1* rescued *Mtm1*-/y mice clinical phenotypes.

References

1. H. Jungbluth, C. Wallgren-Pettersson, J. Laporte, Centronuclear (myotubular) myopathy. *Orphanet J Rare Dis* **3**, 26 (2008).
2. J. Laporte *et al.*, A gene mutated in X-linked myotubular myopathy defines a new putative tyrosine phosphatase family conserved in yeast. *Nat Genet* **13**, 175-182 (1996).
3. F. Blondeau *et al.*, Myotubularin, a phosphatase deficient in myotubular myopathy, acts on phosphatidylinositol 3-kinase and phosphatidylinositol 3-phosphate pathway. *Hum Mol Genet* **9**, 2223-2229. (2000).
4. G. S. Taylor, T. Maehama, J. E. Dixon, Inaugural article: myotubularin, a protein tyrosine phosphatase mutated in myotubular myopathy, dephosphorylates the lipid second messenger, phosphatidylinositol 3-phosphate. *Proc Natl Acad Sci U S A* **97**, 8910-8915. (2000).
5. M. A. Raess, S. Friant, B. S. Cowling, J. Laporte, WANTED - Dead or alive: Myotubularins, a large disease-associated protein family. *Adv Biol Regul* **63**, 49-58 (2017).
6. J. Bohm *et al.*, Adult-onset autosomal dominant centronuclear myopathy due to BIN1 mutations. *Brain* **137**, 3160-3170 (2014).
7. A. S. Nicot *et al.*, Mutations in amphiphysin 2 (BIN1) disrupt interaction with dynamin 2 and cause autosomal recessive centronuclear myopathy. *Nat Genet* **39**, 1134-1139 (2007).
8. E. Lee *et al.*, Amphiphysin 2 (Bin1) and T-tubule biogenesis in muscle. *Science* **297**, 1193-1196 (2002).

9. B. J. Peter *et al.*, BAR domains as sensors of membrane curvature: the amphiphysin BAR structure. *Science* **303**, 495-499 (2004).

10. I. Prokic, B. S. Cowling, J. Laporte, Amphiphysin 2 (BIN1) in physiology and diseases. *J Mol Med (Berl)* **92**, 453-463 (2014).

11. O. Daumke, A. Roux, V. Haucke, BAR domain scaffolds in dynamin-mediated membrane fission. *Cell* **156**, 882-892 (2014).

12. A. Razzaq *et al.*, Amphiphysin is necessary for organization of the excitation-contraction coupling machinery of muscles, but not for synaptic vesicle endocytosis in Drosophila. *Genes Dev* **15**, 2967-2979 (2001).

13. P. Wigge *et al.*, Amphiphysin heterodimers: potential role in clathrin-mediated endocytosis. *Mol Biol Cell* **8**, 2003-2015 (1997).

14. H. T. McMahon, P. Wigge, C. Smith, Clathrin interacts specifically with amphiphysin and is displaced by dynamin. *FEBS letters* **413**, 319-322 (1997).

15. M. D'Alessandro *et al.*, Amphiphysin 2 Orchestrates Nucleus Positioning and Shape by Linking the Nuclear Envelope to the Actin and Microtubule Cytoskeleton. *Dev Cell* **35**, 186-198 (2015).

16. B. Royer *et al.*, The myotubularin-amphiphysin 2 complex in membrane tubulation and centronuclear myopathies. *EMBO Rep* **14**, 907-915 (2013).

17. N. B. Romero, Centronuclear myopathies: a widening concept. *Neuromuscul Disord* **20**, 223-228 (2010).

18. A. Buj-Bello *et al.*, The lipid phosphatase myotubularin is essential for skeletal muscle maintenance but not for myogenesis in mice. *Proc Natl Acad Sci U S A* **99**, 15060-15065. (2002).

19. M. W. Lawlor *et al.*, Skeletal Muscle Pathology in X-Linked Myotubular Myopathy: Review With Cross-Species Comparisons. *J Neuropathol Exp Neurol* **75**, 102-110 (2016).

20. Z. Sun, S. S. Guo, R. Fassler, Integrin-mediated mechanotransduction. *J Cell Biol* **215**, 445-456 (2016).

21. U. Mayer, Integrins: redundant or important players in skeletal muscle? *J Biol Chem* **278**, 14587-14590 (2003).

22. K. Ketel *et al.*, A phosphoinositide conversion mechanism for exit from endosomes. *Nature* **529**, 408-412 (2016).

23. I. Ribeiro, L. Yuan, G. Tanentzapf, J. J. Dowling, A. Kiger, Phosphoinositide regulation of integrin trafficking required for muscle attachment and maintenance. *PLoS Genet* **7**, e1001295 (2011).

24. I. D. Campbell, M. J. Humphries, Integrin structure, activation, and interactions. *Cold Spring Harb Perspect Biol* **3**, (2011).

25. Z. A. Graham, P. M. Gallagher, C. P. Cardozo, Focal adhesion kinase and its role in skeletal muscle. *J Muscle Res Cell Motil* **36**, 305-315 (2015).

26. J. Alanko, J. Ivaska, Endosomes: Emerging Platforms for Integrin-Mediated FAK Signalling. *Trends Cell Biol* **26**, 391-398 (2016).

27. A. D. Perkins *et al.*, Integrin-mediated adhesion maintains sarcomeric integrity. *Dev Biol* **338**, 15-27 (2010).

28. M. Schwander *et al.*, Beta1 integrins regulate myoblast fusion and sarcomere assembly. *Dev Cell* **4**, 673-685 (2003).

29. W. Roman, J. P. Martins, E. R. Gomes, Local Arrangement of Fibronectin by Myofibroblasts Governs Peripheral Nuclear Positioning in Muscle Cells. *Dev Cell* **46**, 102-111 e106 (2018).

30. R. J. Bloch, H. Gonzalez-Serratos, Lateral force transmission across costameres in skeletal muscle. *Exerc Sport Sci Rev* **31**, 73-78 (2003).

31. B. S. Cowling *et al.*, Amphiphysin (BIN1) negatively regulates dynamin 2 for normal muscle maturation. *J Clin Invest*, (2017).

32. A. Toussaint *et al.*, Defects in amphiphysin 2 (BIN1) and triads in several forms of centronuclear myopathies. *Acta Neuropathol* **121**, 253-266 (2011).

33. N. B. Romero, M. Bitoun, Centronuclear myopathies. *Semin Pediatr Neurol* **18**, 250-256 (2011).

34. V. Carmignac, M. Durbeej, Cell-matrix interactions in muscle disease. *J Pathol* **226**, 200-218 (2012).

35. D. S. Harburger, D. A. Calderwood, Integrin signalling at a glance. *J Cell Sci* **122**, 159-163 (2009).

36. C. D. Ratcliffe, P. Sahgal, C. A. Parachoniak, J. Ivaska, M. Park, Regulation of Cell Migration and beta1 Integrin Trafficking by the Endosomal Adaptor GGA3. *Traffic* **17**, 670-688 (2016).

37. J. Laporte *et al.*, MTM1 mutations in X-linked myotubular myopathy. *Hum Mutat* **15**, 393-409 (2000).

38. B. S. Cowling *et al.*, Reducing dynamin 2 expression rescues X-linked centronuclear myopathy. *J Clin Invest* **124**, 1350-1363 (2014).

39. H. Tasfaout *et al.*, Antisense oligonucleotide-mediated Dnm2 knockdown prevents and reverts myotubular myopathy in mice. *Nat Commun* **8**, 15661 (2017).

40. H. Tasfaout *et al.*, Single Intramuscular Injection of AAV-shRNA Reduces DNM2 and Prevents Myotubular Myopathy in Mice. *Mol Ther* **26**, 1082-1092 (2018).

41. M. K. Childers *et al.*, Gene therapy prolongs survival and restores function in murine and canine models of myotubular myopathy. *Sci Transl Med* **6**, 220ra210 (2014).

42. H. Tasfaout, B. S. Cowling, J. Laporte, Centronuclear myopathies under attack: A plethora of therapeutic targets. *J Neuromuscul Dis*, (2018).

43. L. A. Olsen, J. X. Nicoll, A. C. Fry, The skeletal muscle fiber: a mechanically sensitive cell. *Eur J Appl Physiol*, (2019).

44. B. S. Cowling, A. Toussaint, J. Muller, J. Laporte, Defective membrane remodeling in neuromuscular diseases: insights from animal models. *PLoS Genet* **8**, e1002595 (2012).

45. L. Al-Qusairi *et al.*, T-tubule disorganization and defective excitation-contraction coupling in muscle fibers lacking myotubularin lipid phosphatase. *Proc Natl Acad Sci U S A* **106**, 18763-18768 (2009).

46. J. J. Dowling *et al.*, Loss of myotubularin function results in T-tubule disorganization in zebrafish and human myotubular myopathy. *PLoS Genet* **5**, e1000372 (2009).

47. Y. K. Hayashi *et al.*, Mutations in the integrin alpha7 gene cause congenital myopathy. *Nat Genet* **19**, 94-97 (1998).

48. S. Pant *et al.*, AMPH-1/Amphiphysin/Bin1 functions with RME-1/Ehd1 in endocytic recycling. *Nat Cell Biol* **11**, 1399-1410 (2009).

49. C. Long *et al.*, Postnatal genome editing partially restores dystrophin expression in a mouse model of muscular dystrophy. *Science* **351**, 400-403 (2016).

Acknowledgements

We thank the imaging, animal and histological platforms of the IGBMC for help and Frédéric Saudou for support.

Funding

This study was supported by INSERM, CNRS, University of Strasbourg, ANR-10-LABX-0030-INRT, a French State fund managed by the ANR under the frame program Investissements d'Avenir (10-IDEX-0002), Myotubular Trust and Sparks the Children's Medical Research Charity.

Author contributions

B.S.C., A.S.N. and J.L. designed and supervised research; V.M.L., A.S.N., M.S., C.K., S.B., S.D., I.P., N.M. and N.B.R. performed research. V.M.L performed the animal characterization, injections, protein immunofluorescence and primary myoblast experiments. A.S.N performed protein quantity analysis by western blot. M.S. and I.P. characterized the *Bin1-/-* Tg *BIN1* mice. C.K., S.B. performed mice genotyping and helped with animal phenotyping tests. S.D. contributed to primary myoblasts extraction. N.M. acquired electron microscopy pictures. N.B.R. provided the Masson staining on human skeletal muscle. P.Ke, P.Ko. and Y.H. provided materials and analysis tools. P.Ke designed a macro to analyze fiber size. P.Ko. generated the AAVs to inject in mice. Y.H. provided the Tg*BIN1* mice. V.M.L., A.S.N., B.S.C. and J.L. analyzed data; V.M.L., B.S.C. and J.L. wrote the paper.

Competing financial interests

V.M.L., B.S.C. and J.L. submitted a patent on the rescue of centronuclear myopathies by BIN1 modulation.which title: Compositions and methods for the treatment of X-linked centronuclear myopathy, the European patent filing number is 17 306 566.5 and the initial submission date was 11 november 2017. B.S.C. and J.L are co-founders of Dynacure. B.S.C. is now a Dynacure employee (Dynacure, 67400 Illkirch, France). J.L. is a scientific advisor for Dynacure.

Data and material availability: All the data used for this study are included in the main text or in the supplementary material. The AAV serotype 9 used in this study was received from the University of Pennsylvania under a MTA.

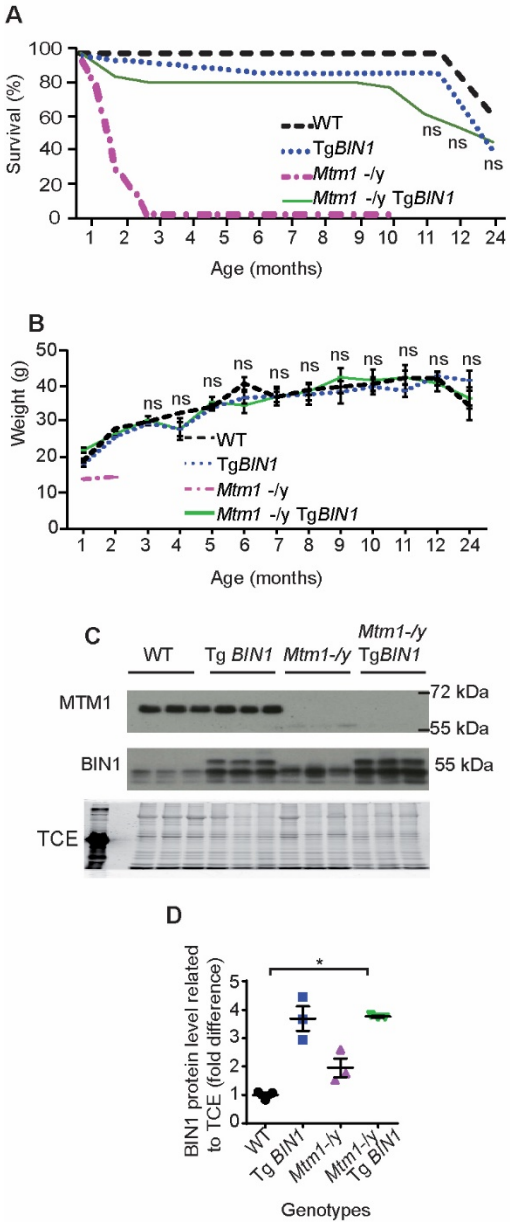

Figure 1. BIN1 overexpression rescues the lifespan of *Mtm1-/y* mice. (A), Lifespan represented as percentage of survival. Survival of *Mtm1*-/y was statistically impaired compared to the 3 other genotypes from 1 month of age ($p<0.01$). (B), Body weight with age ($n > 4$). The body weight of *Mtm1*-/y was statistically impaired compared to the 3 other genotypes from 1 month of age ($p<0.01$). There was no significant difference between the other genotypes studied.(C), Western blot from tibialis anterior (TA) muscles probed with anti BIN1 and MTM1 antibodies. (D), BIN1 quantification normalized on TCE (2,2,2-Trichloroethanol) fluorescence labeling all tryptophan-containing proteins. Statistical analysis: One-way Anova and Bonferroni post-hoc test was performed for data represented in graph, *$p<0.05$, ** $p<0.01$, *** $p<0.001$, **** $p<0.0001$.

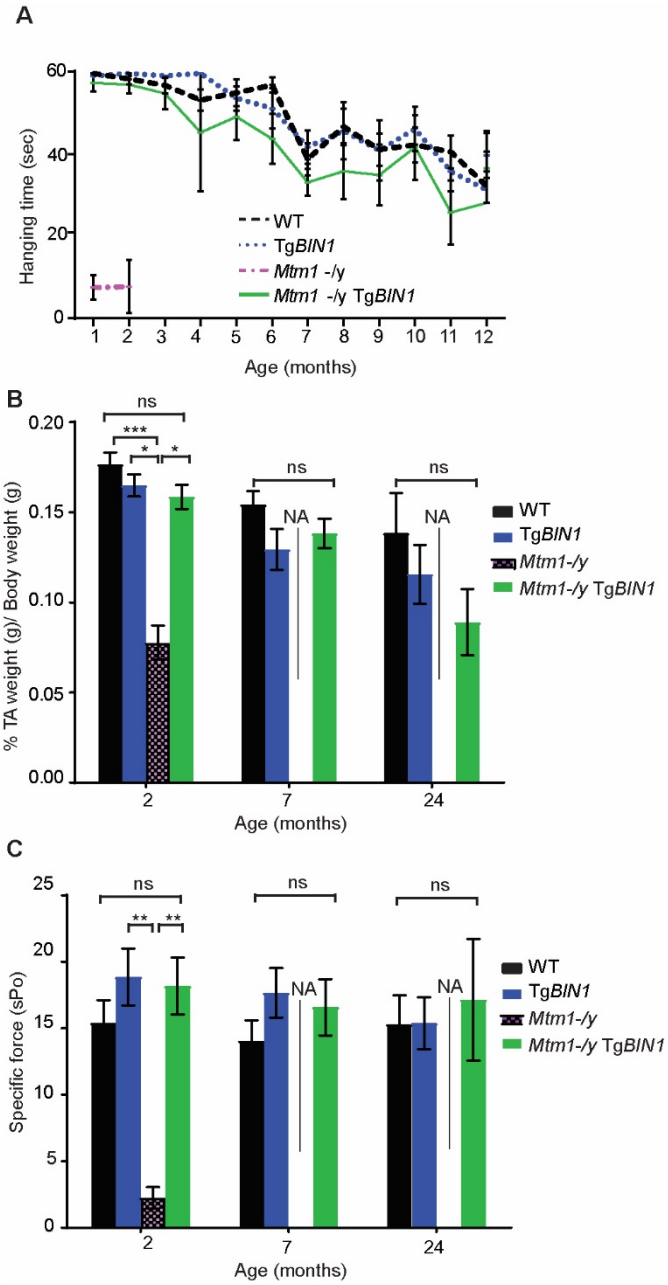

Figure 2. Overexpression of BIN1 rescues muscle force of *Mtm1-/y* mice. (A), Hanging test. Mice were suspended from a cage lid for maximum 60s and each mouse repeated the test three times (n ≥ 4). The hanging test of *Mtm1*-/y was statistically impaired compared to the 3 other genotypes from 1 month of age ($p<0.001$). There was no significant difference between the other genotypes in all the months analyzed. (B), Weight of TA muscle normalized on total body weight (n > 5). (C), Specific muscle force of the TA at 2 months (n > 5), 7 months (n > 5) and 24 months (n = 4). NA: not applicable as Mtm1-/y mice died before. Statistical analysis: One-way Anova and Bonferroni post-hoc test was performed for data represented in graph A. Non parametric Kruskal Wallis test and Dunn'spost-hoc test was performed for data represented in graph B and C; ns: not significant, *$p<0.05$, ** $p<0.01$, *** $p<0.001$, **** $p<0.0001$.

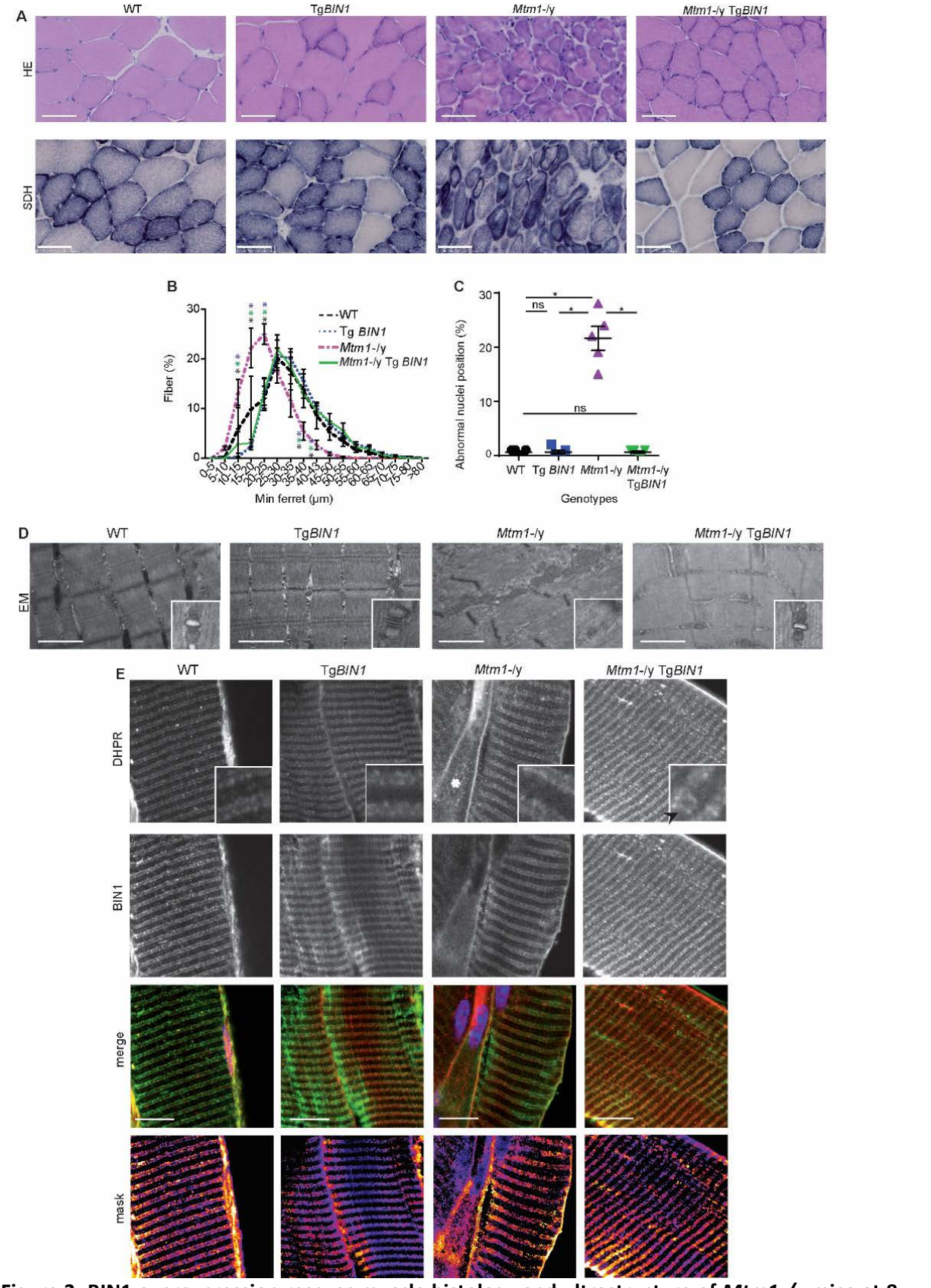

Figure 3: BIN1 overexpression rescues muscle histology and ultrastructure of *Mtm1-/y* mice at 8w old. (A), Transversal TA muscle sections stained with HE and SDH. Scale bar, 500 µm. (B), Minimum ferret of TA fibers grouped into 5 µm intervals (n=5). (C), Frequency of fibers with abnormal (internalized and centralized) nuclei position in TA (n=5). (D), TA muscle ultrastructure observed by

electron microscopy. Scale bar 1µm. High magnification insert for triads. (E), Longitudinal TA muscle sections stained for DHPR (red) and BIN1 (green). The star indicates disorganized DHPR staining. Pictures were taken with different laser intensity. Scale bar 10 µm. Statistical analysis: Non parametric Kruskal Wallis test and Dunn's post-hoc test; ns: not significant, *p<0.05, ** p<0.01.

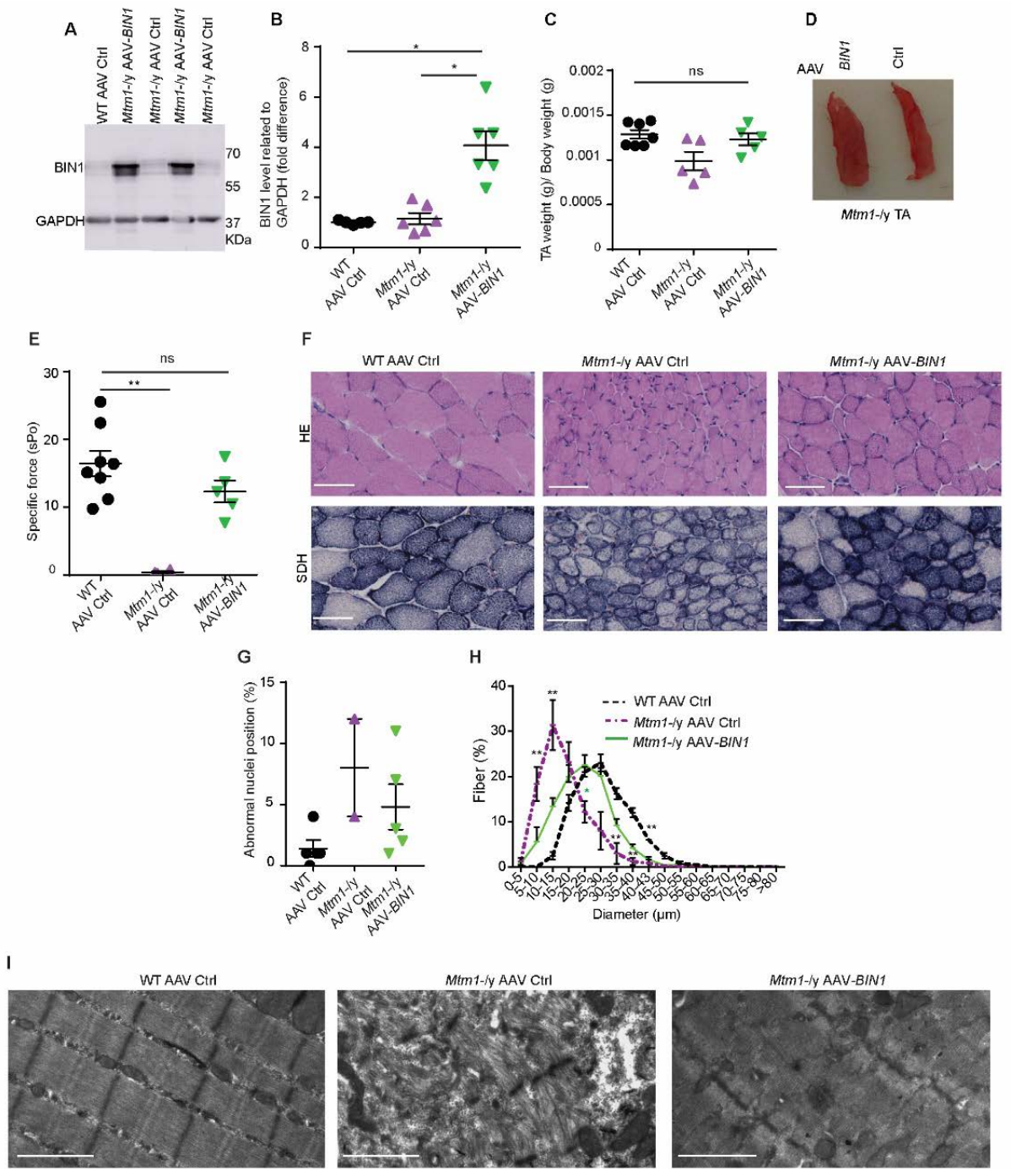

Figure 4: Postnatal intramuscular BIN1 overexpression rescues muscle force and myofiber organization in *Mtm1-/y* mice. (A), Western blot with anti-BIN1 antibody(n=5) (B), Quantification of BIN1 on GAPDH. (C), TA muscle weight normalized on total body weight (n≥5). (D), Photo of *Mtm1-/y* TA muscles injected with AAV-*BIN1* (left) or AAV empty control (right) 5w post injection. (E), Specific

TA muscle force (n≥5). (F), Transversal TA sections stained with HE and SDH. Scale bar, 500 µm. (G), Frequency of fibers with abnormal (internalized and centralized) nuclei position in TA of WT mice and *Mtm1-/y* mice (n≥2). (H), Minimum ferret of TA fibers grouped into 5 µm intervals (n≥4). (I), TA muscle ultrastructure observed by electron microscopy (n=1). Scale bar 1 µm. Statistical analysis: Non parametric test Kruskal-Wallis test and Dunn's post-hoc statistic; ns: not significant, *p<0.05, ** p<0.01.

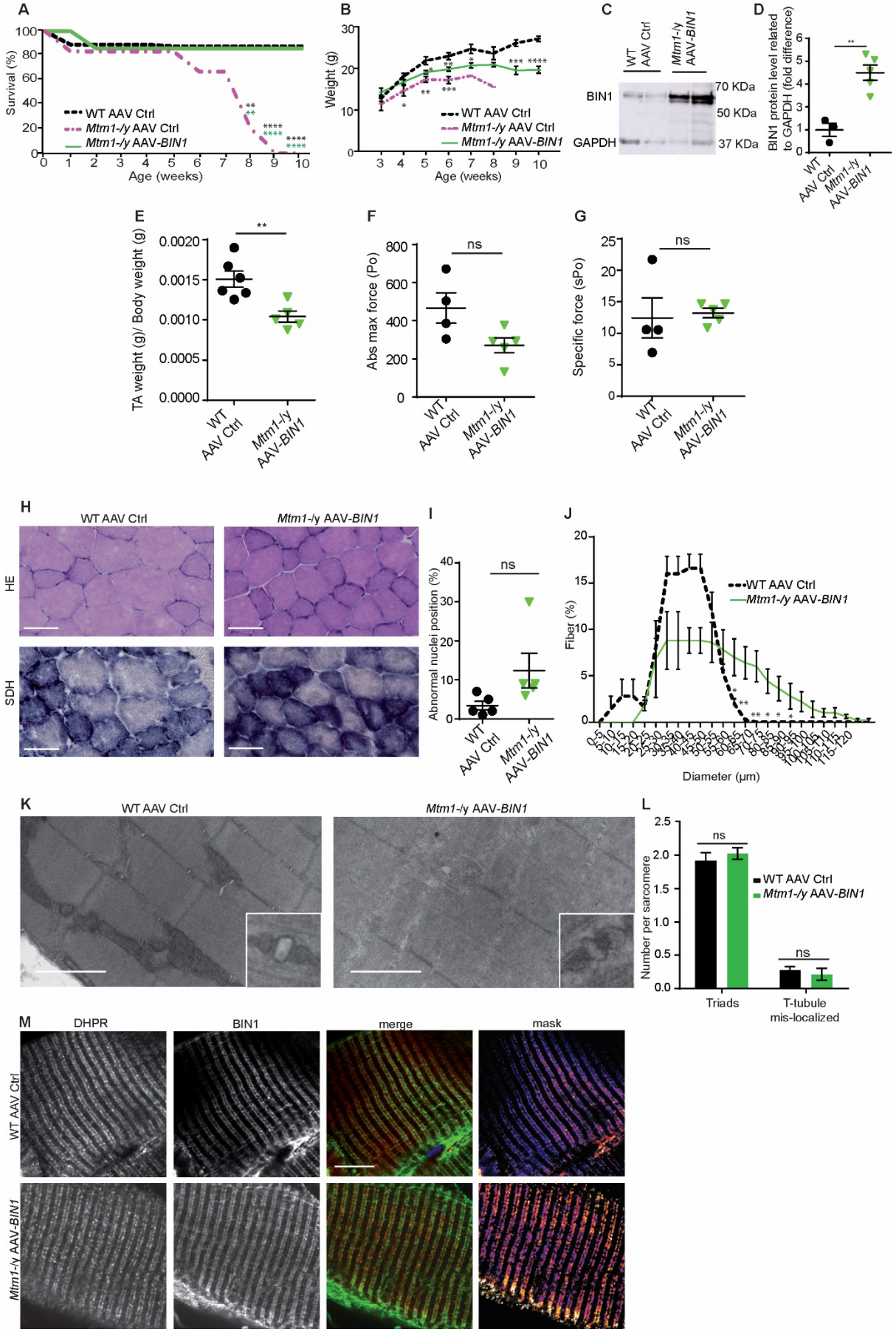

Fig. 5: Postnatal systemic BIN1 overexpression rescues the survival and muscle defects of *Mtm1-/y*

mice. (A), Percentage of survival before sacrifice at 10w. (B), Body weight. (C), Western blot probed with anti-BIN1 and GAPDH antibodies, and (D), BIN1 quantification normalized to GAPDH. (E), Ratio of TA muscles weight on total body weight (n≥5). (F), Absolute TA muscle force. (G), Specific TA muscle force (n≥4). (H), Transversal TA muscle sections stained with HE and SDH. Scale bar, 500 µm. (I), Percentage of fibers with abnormal (internalized and centralized) nuclei position (n=5). (J), Minimum ferret of TA fibers grouped into 5 µm intervals (n=5). (K), TA muscle ultrastructure observed by electron microscopy. Scale bar 1µm. High magnification insert for triads. (L), Frequency of triads per sarcomere. (M), Longitudinal TA muscle sections stained with DHPR and BIN1 antibodies. Scale bar 10 µm. Statistical analysis: One-way Anova, Turkey post-hoc test for graph B (until 8w time point). T-test for graph B (for 9w and 10w time points), C, D, E, F, H, I; ns: not significant, ** $p<0.01$.

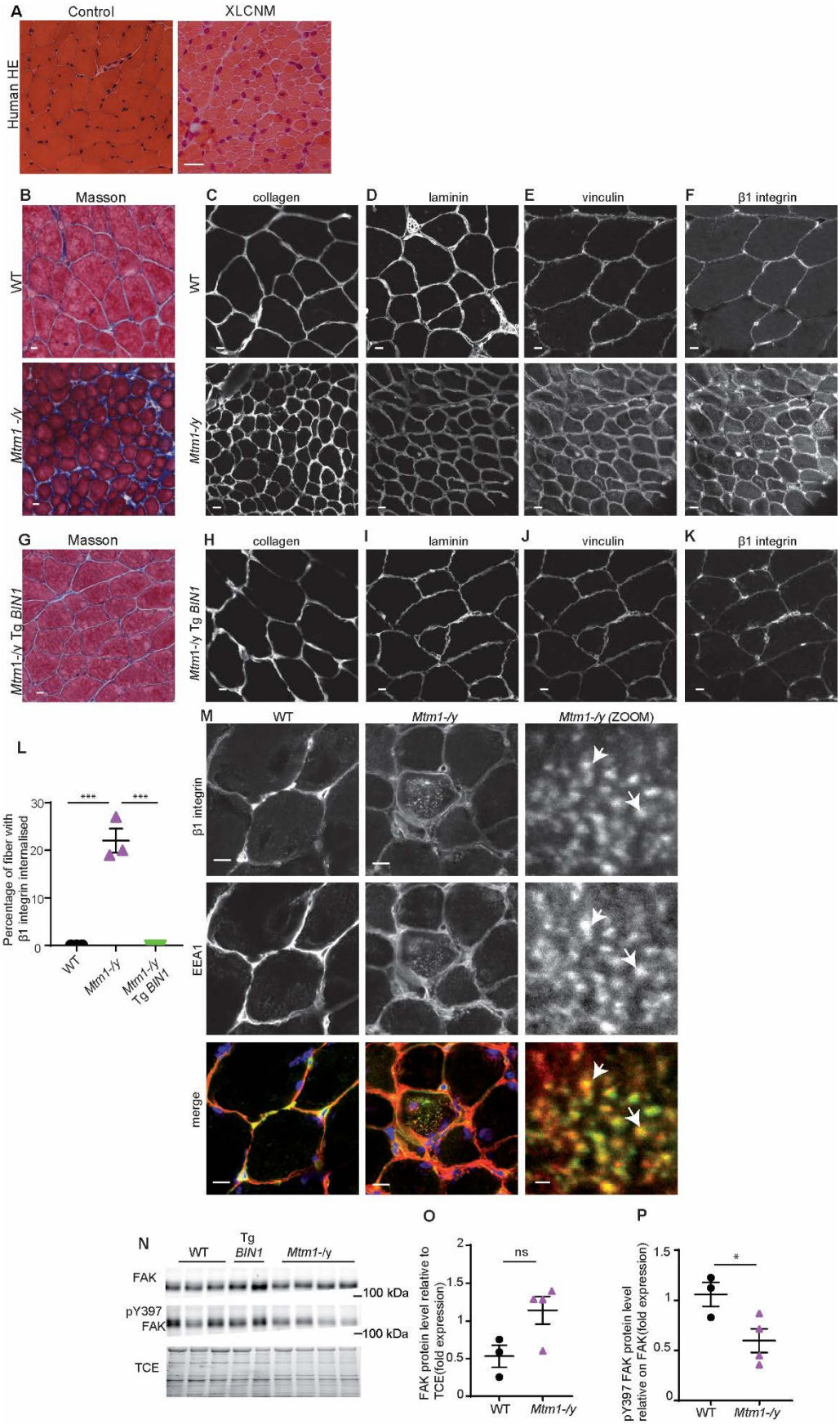

Figure 6: MTM1 and BIN1 are essential for β1 integrin trafficking in mammalian muscle. (A), Comparison of transversal muscle sections from a control human skeletal muscle with X-linked centronuclear myopathy patient (mutation c.141-144delAGAA p.Glu48LeufsX24 in MTM1). Scale bar

20µm. (B), 8w WT and *Mtm1-/y* TA muscle stained with Masson trichrome. Scale bar 10 µm. (C), Transversal WT, *Mtm1-/y* TA muscle stained for the extracellular matrix proteins collagen, (D), laminin, (E), vinculin and (F), β1 integrin. Scale bar 10µm. (G), Transversal TA 8w *Mtm1*-/y Tg *BIN1* muscle sections stained with Masson trichrome. Scale bar 10 µm. (H), Transversal WT, *Mtm1-/y* TA muscle stained for the extracellular matrix proteins collagen, (I), laminin, (J) vinculin and (K) β1 integrin. Scale bar 10µm. (L), Percentage of muscle fiber with β1 integrin internalised. (M), Transversal TA muscle sections stained for β1 integrin (green) and EEA1 (red). Scale bar, 10µm. Scale bar for the Mtm1-/y (zoom) pannel, 1 µm. Arrows point to abnormal intracellular accumulation of β1 integrin on EEA1-positive endosomes. Scale bar, 10µm and 1 µm (zoom). (N), Western blot probed with anti-FAK and anti-p-FAK (Tyr397) antibodies. (O), Quantification of FAK on TCE and. (P) quantification of p-FAK (Tyr397) on total FAK. Statistical analysis: one-way Anova test, Turkey's post hoc. *$p<0.05$, ** $p<0.01$, *** $p<0.001$,

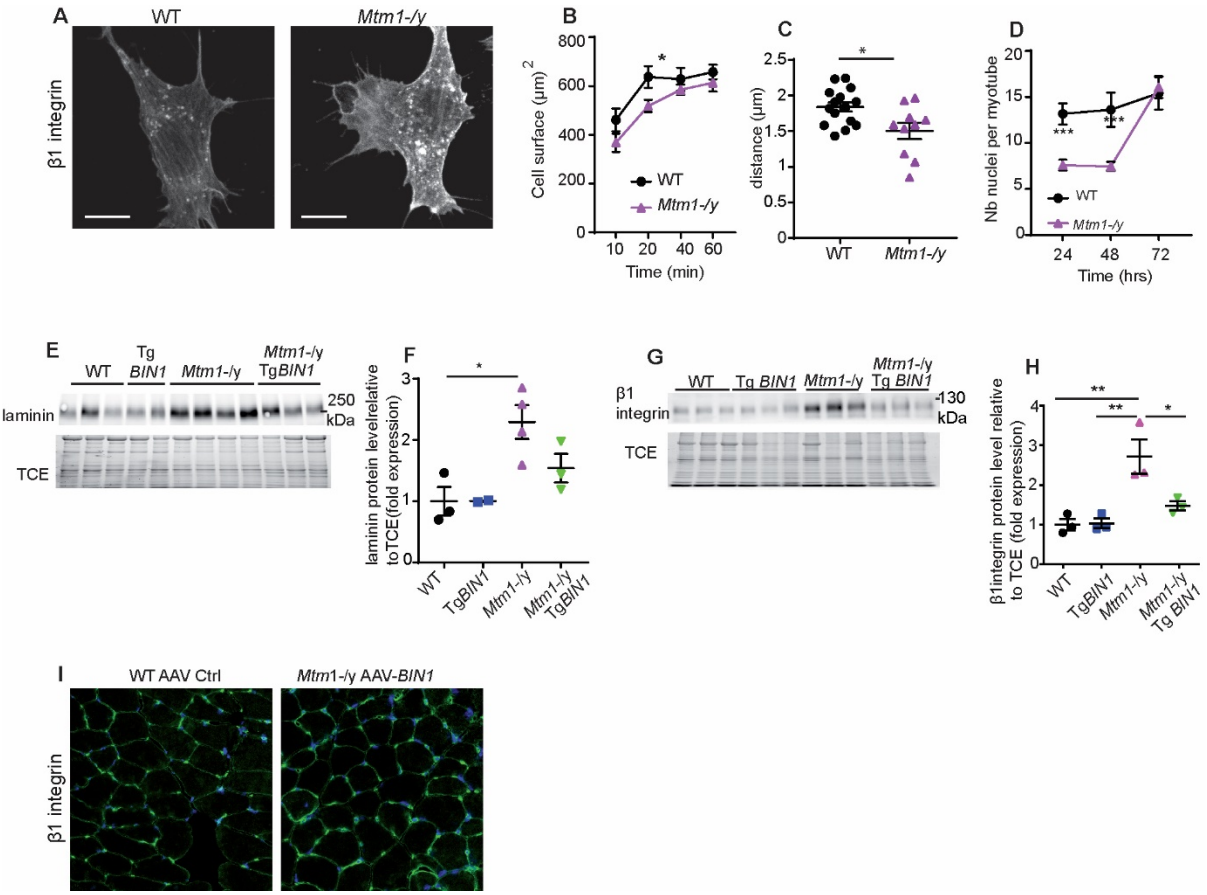

Figure 7: BIN1 increased expression rescues focal adhesion deficit in the Mtm1-/y muscle. (A), WT and *Mtm1-/y* primary myoblasts probed for β1 integrin. Scale bar, 10 µm. (B), Adhesion assay: adherent surface of primary myoblasts at different timepoints after plating (n ≥25 from n>=2 mice). (C), Migration assay: distance (µm) migrated by WT and *Mtm1-/y* myoblasts during 24 hours (n ≥20 from n=3 mice). (D), Fusion index: number of nuclei in WT and *Mtm1-/y* myotubes at 3 time points after differentiation was started (24, 48, 72 hrs) (n >36 from n≥2 mice). (E), Western blot probed with anti-laminin antibodies. (F), Quantification of laminin on TCE. (G), Western blots probed for β1 integrin. (H), Quantification of β1 integrin normalized to the TCE of the same gel. (I), Transversal TA muscle of WT mice injected systemically with AAV empty as control, and Mtm1-/y mice injected systemically with AAV-*BIN1* and probed with anti-β1 integrin antibody. Scale bar, 10 µm. Statistical analysis: T-test; one-way Anova test, Bonferroni post hoc. *p<0.05, ** p<0.01, *** p<0.001.

Supplementary Table 1: Breeding strategy and outcome for Mtm1-/y x Bin1-/+ with expected mice and obtained at E18.5 and 10 days post-natal.

Breeding	***Mtm1+/- x Bin1 +/-***			
Offspring	WT	*Bin1 +/-*	*Mtm1 -/y*	*Mtm1+/- Bin1+/-*
Expected genotype	12.5%	12.5%	12.5%	12.5%
Obtained at E18.5	13.3%	13.3%	15%	8.3%
Obtained at PN 10 days	19.5%	19%	13%	0%

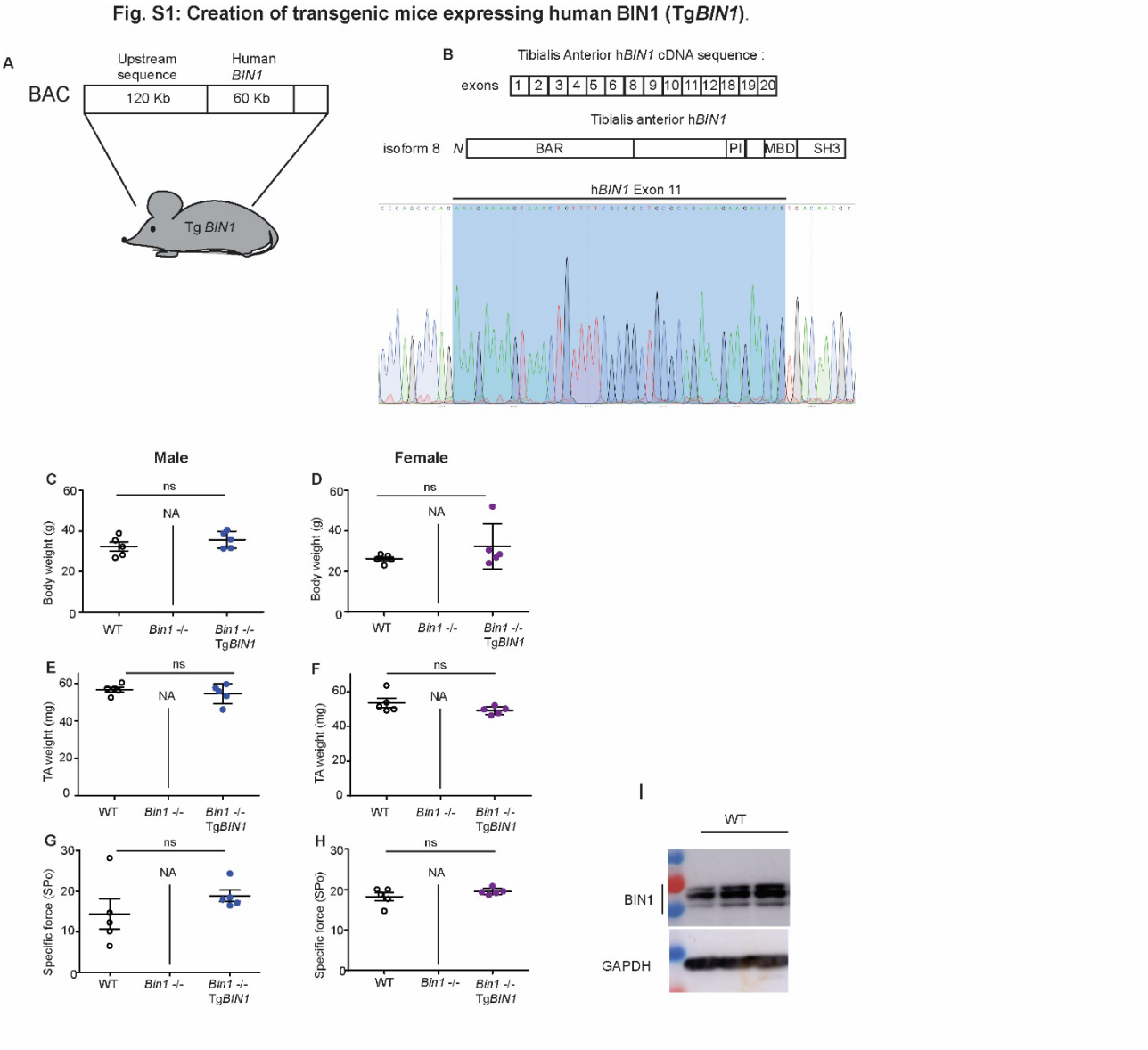

Fig. S1: (A), Drawing of the bacterial artificial chromosome (BAC) encompassing the whole BIN1 locus. (B), Human BIN1 isoform sequence expressed in tibialis anterior (TA) muscle, identified by cloning and sequencing RT-PCR products; chromatopherogram of BIN1 exon 11 identified in Mtm1-/y TgBIN1 TA. (C), Male body weight at 4 months (n=5). NA: not applicable as Bin1-/- mice died at birth. (D), Female body weight at 4 months (n=5). NA: not applicable as Bin1-/- mice died at birth. (E), Male Tibialis anterior weight at 4 months (n=5). NA: not applicable as Bin1-/- mice died at birth. (F), Female Tibialis anterior weight at 4 months (n=5). NA: not applicable as Bin1-/- mice died at birth. (G), Specific muscle force of the male TA at 4 months (n=5). NA: not applicable as Bin1-/- mice died at birth. (H), Specific muscle force of the female TA at 4 months (n=5). (I), Western blot probed anti BIN1 and GAPDH antibody. NA: not applicable as Bin1-/- mice died at birth. Statistical analysis: T-test; ns: not significant.

Fig. S2: Increased BIN1 expression rescues the motor function and muscle force of *Mtm1*-/y mice.

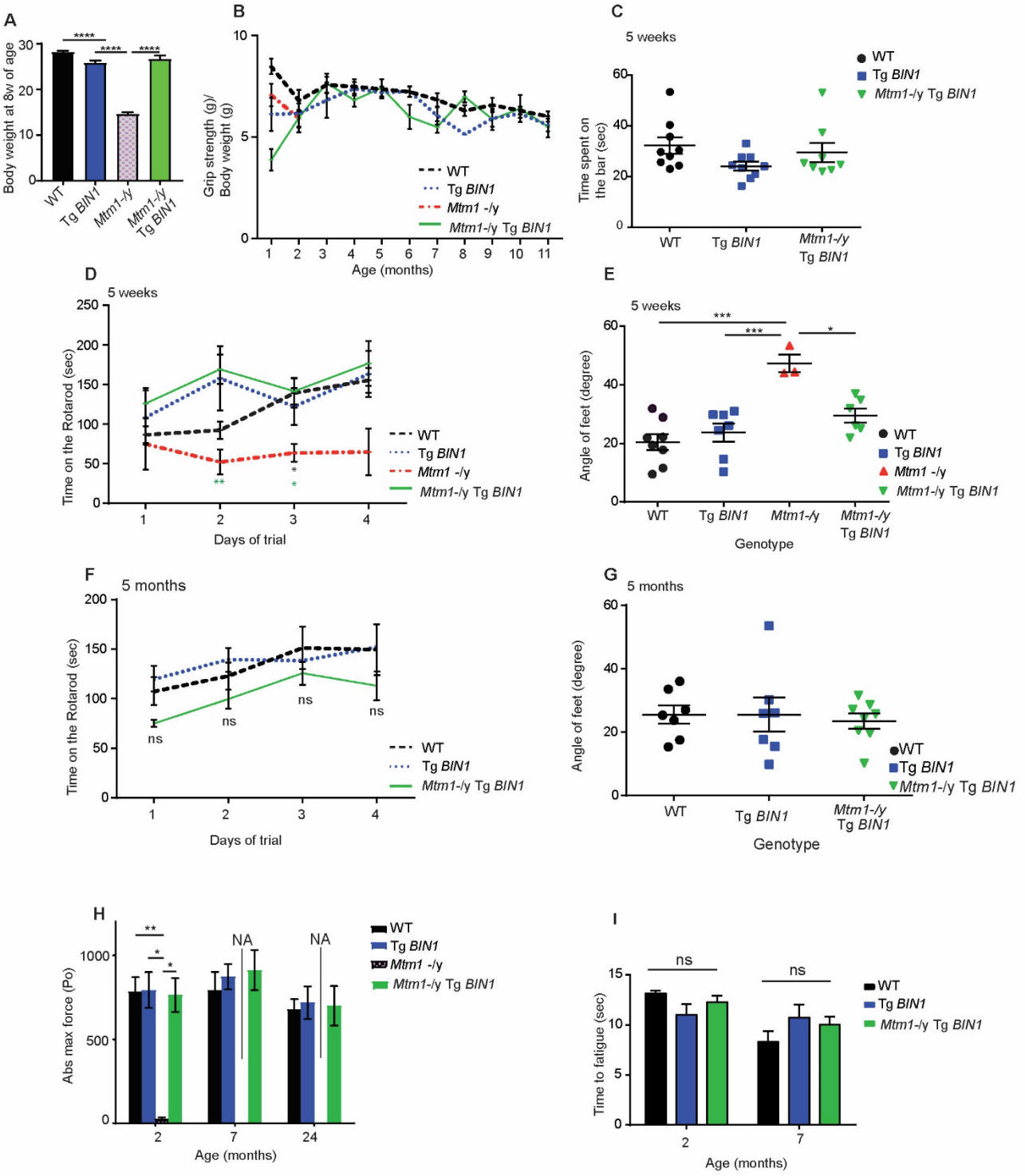

Fig. S2: Increased BIN1 expression rescues the motor function and muscle force of Mtm1-/y mice. Note that Mtm1-/y mice die by 8w and are not available for comparison with Mtm1-/y TgBIN1 mice at late ages. (A), Body weight. (B), Grip test performed every month from 1 month to 12 months. The test was repeated 3 times for each mouse (n>7). (C), Bar test performed at 5w. Mtm1-/y mice cannot walk on the bar. D and F, Rotarod tests performed at 5w (D), and 2 month old (F). (E) and (G), Footprint tests performed at 5w (E) and 2 months (G) (n≥5). (H), Absolute maximal force of the TA muscles (n≥3). (I), Time to fatigue for the TA muscles(n≥3). Statistical analysis: non parametric test Kruskal Wallis test and Dunn's post-hoc. *p-Value < 0.05, **p<0.01, ***p<0.001.

Fig. S3: Increased BIN1 expression rescues muscle histology of *Mtm1-/y* mice at 2 and 7 months old.

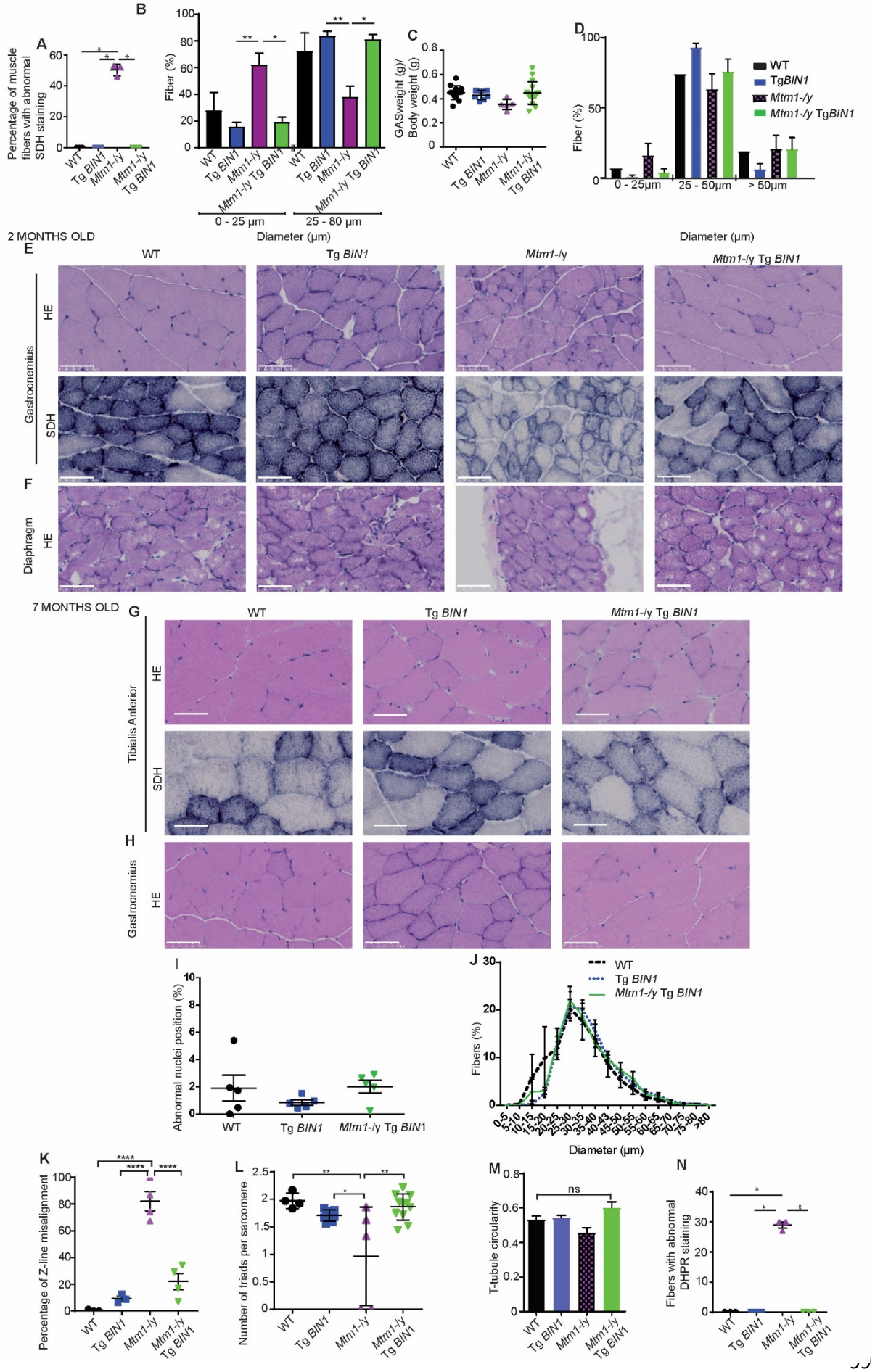

Fig. S3: Increased BIN1 expression rescues muscle histology of Mtm1-/y mice at 2 and 7 months old. Note that Mtm1-/y mice die by 8w and are not available for comparison with Mtm1-/y TgBIN1 mice at later ages. (A), Percentage of fiber with abnormal SDH stain. (B), Minimum ferret of TA fibers grouped as small (0-25 µm) or large (25-80 µm) fibers at 2 months (n=5). SDH pictures are in Fig. 3A; (C), Gastrocnemius weight normalized to total body weight at 2 month old (n≥3). (D), Minimum ferret of Gastrocnemius fibers grouped as small (0-25 µm),medium (25-50 µm) and large (> 50µm)fibers at 2 months. Animals analyzed: 1 WT, 2 Tg *BIN1*, 3 *Mtm1-/y* and 3 *Mtm1-/y* Tg *BIN1*. (E), Transversal Gastrocnemius (GAS) muscle sections stained with HE and SDH at 2 month old. Scale bar, 50 µm. (F), Transversal diaphragm muscle sections stained with HE at 2 month old. Scale bar, 50 µm. (G), Transversal TA muscle sections stained with HE and SDH at 7 months old. (H), Transversal GAS muscle sections stained with HE at 7 month old. (I), Percentage of abnormal nuclei position (internal or central) in TA muscle at 7 month old (n=5). (J), Fiber size diameter of TA muscle at 7 month old (n=5). (K), Percentage of Z line misaligned observed in EM pictures (animals per genotype=3). (L), Number of triads counted per sarcomere (animals per genotype=2). (M), Circularity of the T-tubule in the triads (only 1 *Mtm1-/y* mouse was analysed as triads were difficult to distinguish in other animals while n ≥ 2 for the other genotypes). Scale bar, 50 µm. (N), Percentage of muscle fibers with abnormal DHPR staining Statistical analysis: One-way Anova and Bonferroni test. * p-value < 0.05,**<0.001.

Fig. S4: Postnatal intramuscular overexpression of BIN1 rescues muscle force and myofiber organization in *Mtm1*-/y mice

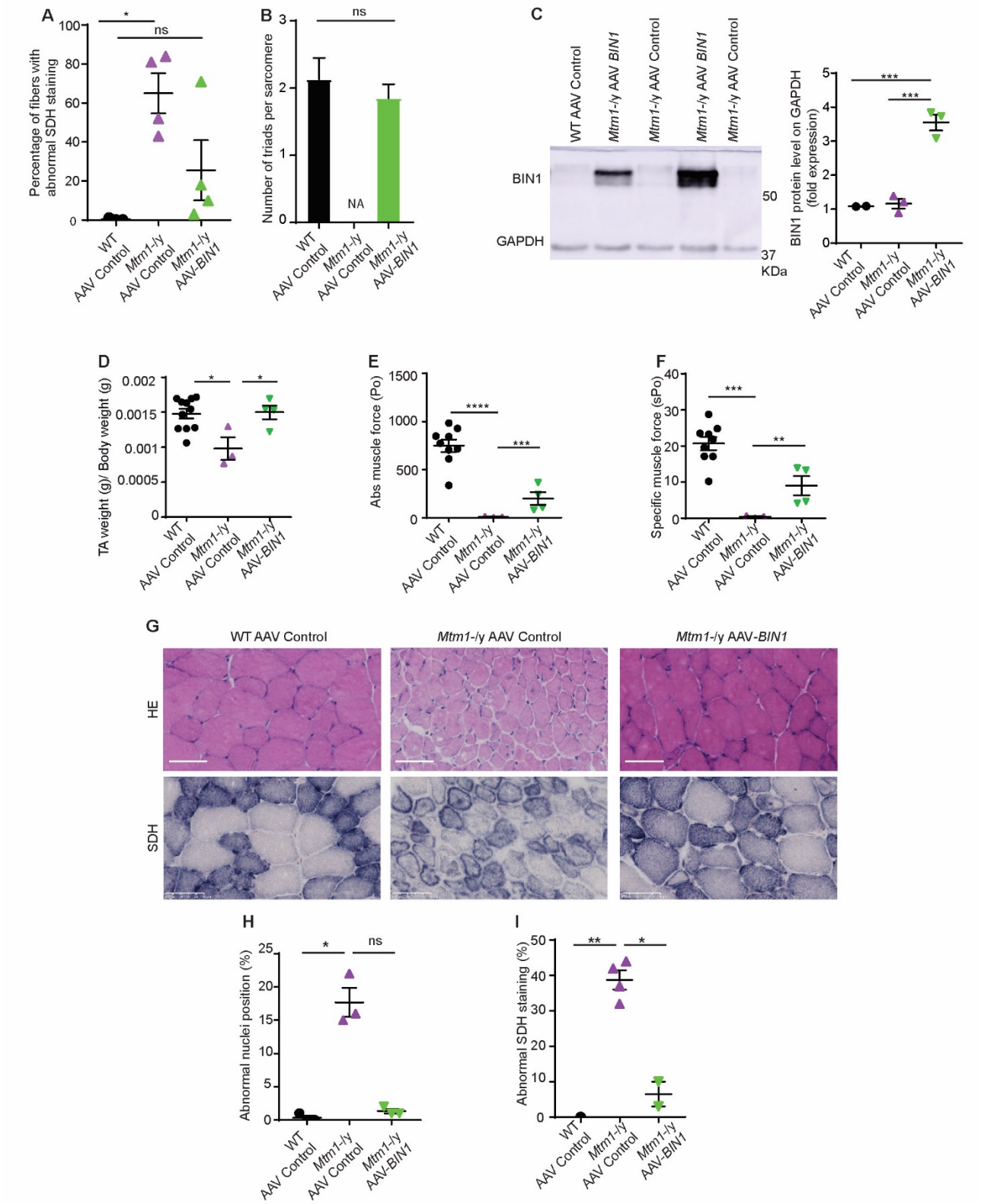

Fig. S4: Postnatal intramuscular overexpression of BIN1 rescues muscle force and myofiber organization in Mtm1-/y mice. Mtm1-/y were injected at 3 weeks with either AAV empty as control or AAV-BIN1, and mice were analyzed 2 to 4 weeks post-injection (n ≥3). (A), Percentage of fibers with abnormal SDH staining 2w post injection (n ≥2). The SDH staining pictures are in Fig. 4E. (B), Number

of triads counted per sarcomere (animals per condition=1, triads counted ≥ 90). *Mtm1-/y* muscle injected with AAV Ctrl was disorganized and triads difficult to be counted. (C) to (H): analysis at 3-4 weeks. (B), Western blot with anti-BIN1 antibody. BIN1 level was normalized on GAPDH. (C), TA muscle weight normalized on total body weight (n ≥3). (D), Absolute TA muscle force. (E), Specific TA muscle force (n ≥3). (F), Transversal TA sections stained with HE and SDH. (G), Percentage of fiber with abnormal nuclei position. (H), Percentage of fiber with abnormal SDH staining. Scale bar, 50 µm. Statistic test: One-Way Anova and Bonferroni test; ns: not significant, *p<0.05, ** p<0.01, *** p<0.001.

Fig. S5: Organ weights and muscle fatigue in the *Mtm1*-/y mice expressing *BIN1* after systemic AAV delivery

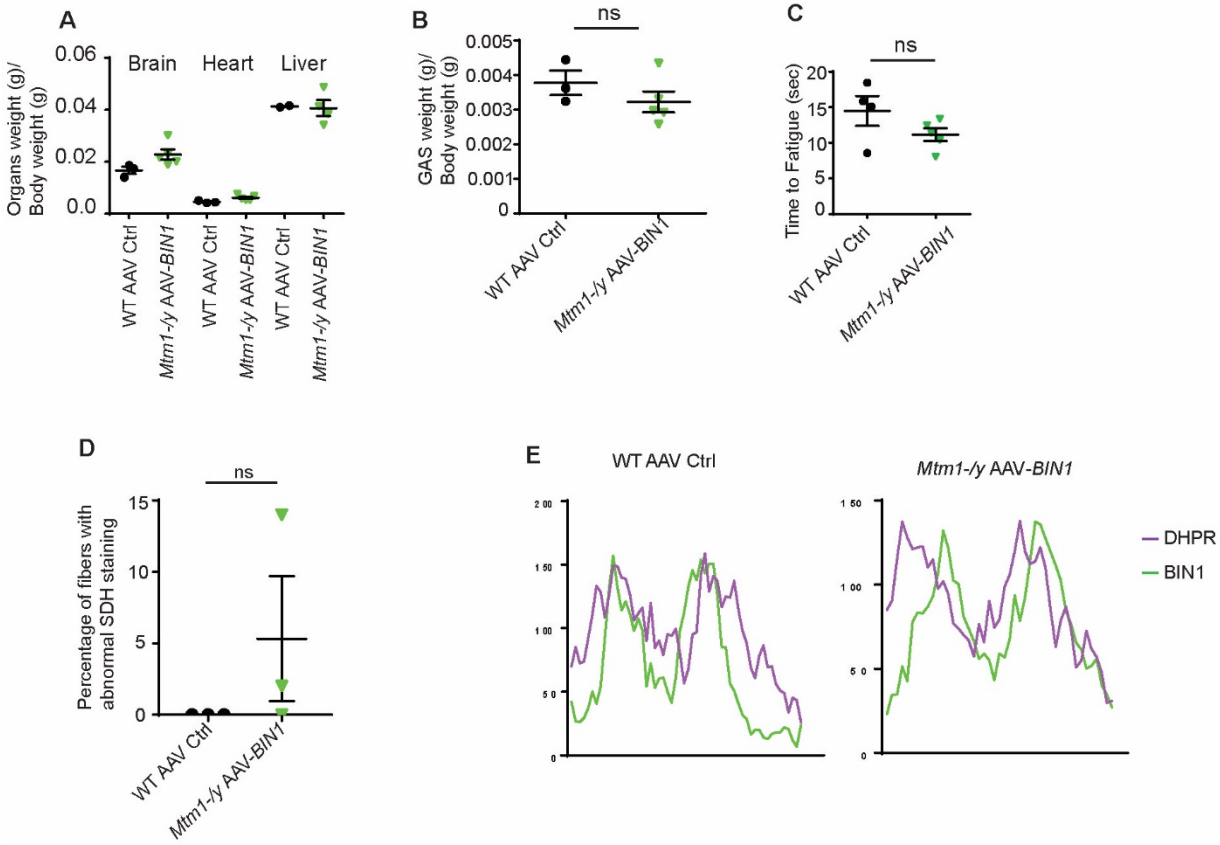

Fig. S5: Organ weights and muscle fatigue in the Mtm1-/y mice expressing BIN1 after systemic AAV delivery. Mice were analyzed at 10w old (n≥2). Mtm1-/y mice do not survive until 10w age. (A), Brain, heart and liver weights on total body weight (n≥2). (B), Gastrocnemius weight on total body weight (n≥3). (C), Time to fatigue for the TA muscle. (D), Percentage of fibers with abnormal SDH staining. The SDH pictures are in Fig. 5G. (E), Intensity plot showing the colocalisation of BIN1 and DHPR signal in immunofluorescence pictures. Statistic test:Unpaired T-test, Mann-Whitney test : ns = no significant difference.

Fig. S6: Extracellular matrix defect in *Mtm1*-/y muscle .

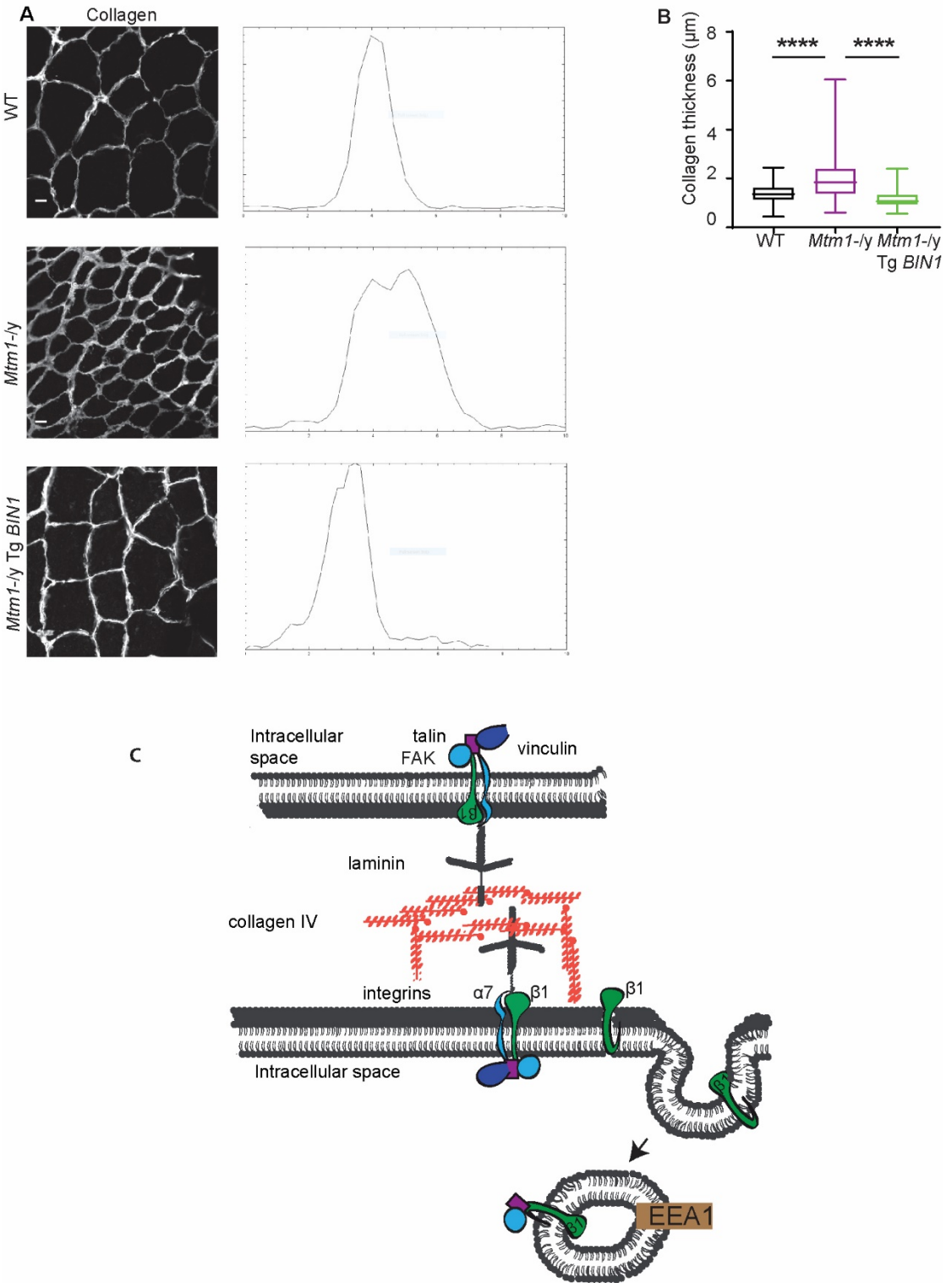

Fig. S6: Extracellular matrix defect in Mtm1-/y muscle. (A), Transversal TA stained with Collagen (Scale bar 10µm) and intensity plot showing collagen stained area profile. (B), Quantification of extracellular collagen thickness (fiber counted for WT and Mtm1-/y=140, Mtm1-/y Tg BIN1=50). (C), Drawing of the main costamere constituents. Statistical test, no-parametric test Kruskal Wallis test; ns: not significant, *p<0.05, ** p<0.01, *** p<0.001

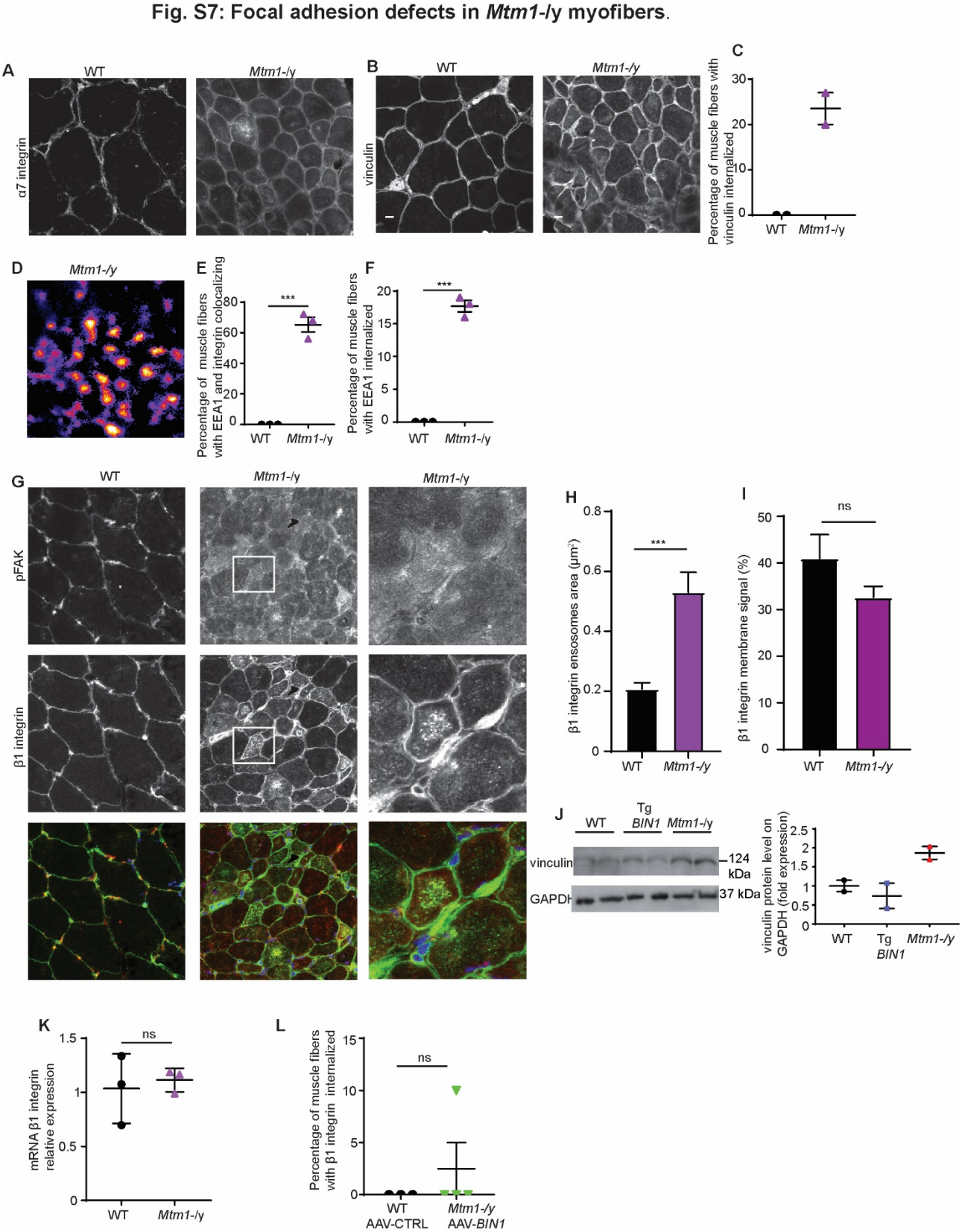

Fig. S7: Focal adhesion defects in Mtm1-/y myofibers. (A), Transversal TA muscle sections stained for α7 integrin. Scale bar, 10µm. (B), Transversal TA muscle sections stained for vinculin. (C), Percentage of fibers with vinculin internalized (n=2). (D), Transversal TA muscle section mask of EEA1 and β1 integrin, merge of Fig. 6M. (E), Percentage of abnormal β1 integrin stained muscle fibers with EEA1 and β1integrin colocalization. (F), Percentage of fibers with abnormal EEA1 staining (n=3), (G),

Transversal TA muscle sections staining for p-FAK (Tyr397) (Red) and β1integrin (Green). (H), Area of endosomes stained with β1 integrin in primary myoblast (n=2, endosomes counted ≥ 100). (I), Percentage of β1 integrin plasma membrane signal in WT and Mtm1-/y primary myoblasts. (J), Western blot probed for vinculin and quantification of vinculin normalized to the GAPDH of the same gel. (K), mRNA expression level of β1 integrin (Itgb1) relative to Rpl27 housekeeping gene. (L), Percentage f fibers with abnormal β1 integrin aggregates inside the muscle fibers of WT injected with AAV-Ctrl and *Mtm1-/y* injected with AAV-*BIN1* systemically (n≥3). .Unpaired T-test, Mann-Whitney test : ns = no significant difference, *** $p<0.001$.

Supplementary videos. Supplementary video 1. Expression of human *BIN1* did not generate any obvious clinical phenotypes in mice. Tg*BIN1* mice at 8 weeks.

Supplementary video 2. Increased *BIN1* expression rescues *Mtm1*-/y phenotype. WT mouse (left), *Mtm1*-/y Tg*BIN1* mouse (center) and *Mtm1*-/y mouse (right cage) of six weeks old. Tg*BIN1* mouse (left), WT mouse (center) and *Mtm1*-/y Tg*BIN1* mouse (right) of seven months old. *Mtm1*-/y Tg*BIN1* mouse of twelve months old performing hanging test.

Supplementary video 3. Postnatal systemic injection of AAV-*BIN1* rescued *Mtm1*-/y mice phenotypes. A 5w old *Mtm1*-/y mouse injected with AAV empty control was affected with kyphosis and had difficulties to move in the cage while 5w old *Mtm1*-/y mice injected with AAV-*BIN1* did not display any particular phenotypes. The postnatal overexpression of *BIN1* rescued *Mtm1*-/y life span. One year old *Mtm1*-/y injected with AAV-*BIN1* and WT injected with AAV Ctrl.

Part 2b: Characterization of WT and *Mtm1-/y* skeletal muscle force upon post-natal overexpression of alternative BIN1 constructs

Introduction

In the previous study, we overexpressed the BIN1 isoform 8 by intramuscular and systemic injections as it corresponds to the human isoform identified in the rescued TA of Mtm1-/y TgBIN1 mice model. The modulation of BIN1 isoform 8 expression in *Mtm1-/y* rescued the life span and improved their skeletal muscle force. To better understand if other isoforms may also rescue the myopathy and to investigate if a specific domain of BIN1 was enough to ameliorate the phenotype in mice I tested additional BIN1 isoforms. I injected BIN1 BAR* domain, BIN1 isoform 8 with inclusion of exon 7 and BIN1 isoform 9 through AAV delivery in the Tibialis Anterior of XLCNM mouse model (Fig 21).

The BIN1 BAR* domain contains the N terminal BAR domain of the isoform 8 including the PI domain coded by exon 11. The BIN1 N-BAR domain does not contain the exon 7 (Fig. 21).

Abnormal BIN1 splicing was observed in Myotonic dystrophy (DM1) patients (Fugier et al., 2011). Myotonic dystrophy (MD) is an autosomal disorder characterized by skeletal muscle weakness, atrophy and myotonia. This disease is caused by an intronic expansion of CTG or CCTG repeats in the *CNBP* gene which repeats in skeletal muscle enrolled a splicing regulator family Muscleblind-like. This recruitment causes abnormal splicing of various pre-mRNAs (Miller et al., 2000; Ho et al., 2004; Goodwin et al., 2015). RNA sequencing of skeletal muscle from Myotonic dystrophy patients revealed a splicing alteration in BIN1 skeletal muscle isoform which includes exon 7 in its BAR domain (Fugier et al., 2011) (Michel Ney, et al. in preparation). We decided to inject BIN1 isoform 8 with the presence of exon 7 to verify if the inclusion of this exons was impairing skeletal muscle force. BIN1 isoform 9 is the isoform ubiquitously express, it does not contain the exon 7 and exon 11.

I performed the intramuscular injection of the BIN1 AAVs and control at 3 weeks of age in WT and *Mtm1-/y* mouse model. 2 weeks post-injection *in situ* TA muscle force was measured.

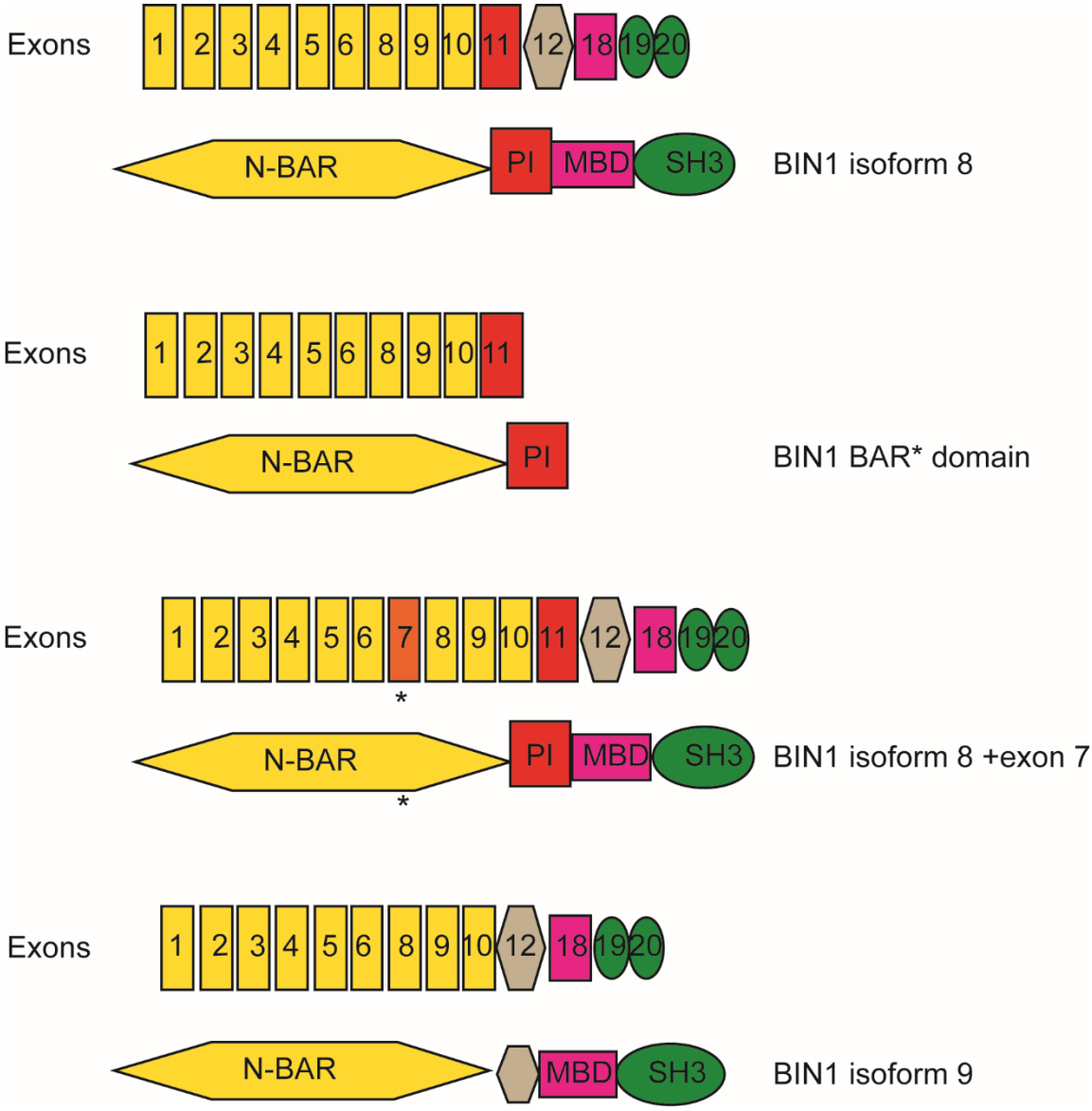

Figure 21: BIN1 exons and constructs injected in skeletal muscle intramuscularly.

BIN1 isoform 8 contains the N-BAR domain (exons 1, 2, 3, 4, 5, 6, 8, 9, 10), PI domain (exon 11), exon 12, MBD domain (exon 18 only), SH3 domain (exon 19, 20). BIN1 BAR* constructs contains the N-BAR domain (exons 1, 2, 3, 4, 5, 6, 8, 9, 10) and PI domain (exon 11). BIN1 isoform 8 + exon 7 has the same exons of isoform 8 with the inclusion of exon 7 in the BAR domain. BIN1 isoform 9 contains the N-BAR domain (exons 1, 2, 3, 4, 5, 6, 8, 9, 10), PI domain (exon 11), exon 12, MBD domain (exon 18 only), SH3 domain (exon 19, 20).

The overexpression of BIN1 constructs impacts on muscle weight differently

The weight of WT TA muscle injected with AAV control was significantly higher than the *Mtm1-/y* TA muscle. The overexpression of BIN1 constructs in WT leg did not impact the TA muscle weight as no significant difference was detected between the legs injected with the AAVs and with the control 2 week post injection. The overexpression of *BIN1* BAR* domain in *Mtm1-/y* improved TA muscle weight which was significantly higher than the *Mtm1-/y* control legs and it reached the weight of the WT control legs. High variability was measured for the *Mtm1-/y* legs injected with AAV-*BIN1* isoform 9 and no significant difference was detected with the *Mtm1-/y* control muscles. The inclusion of exon 7 in BIN1 isoform 8 did not improve the muscle weight as any difference was detected with the leg injected with AAV-Ctrl (Fig. 22).

To conclude, the overexpression of different BIN1 constructs did not impact on the WT TA muscle weight 2 weeks post injections. In contrast, a significant increase in TA weight was measured in *Mtm1-/y* injected with AAV- *BIN1* BAR* domain and a slight amelioration on the TA injected with AAV-*BIN1* isoform 9.

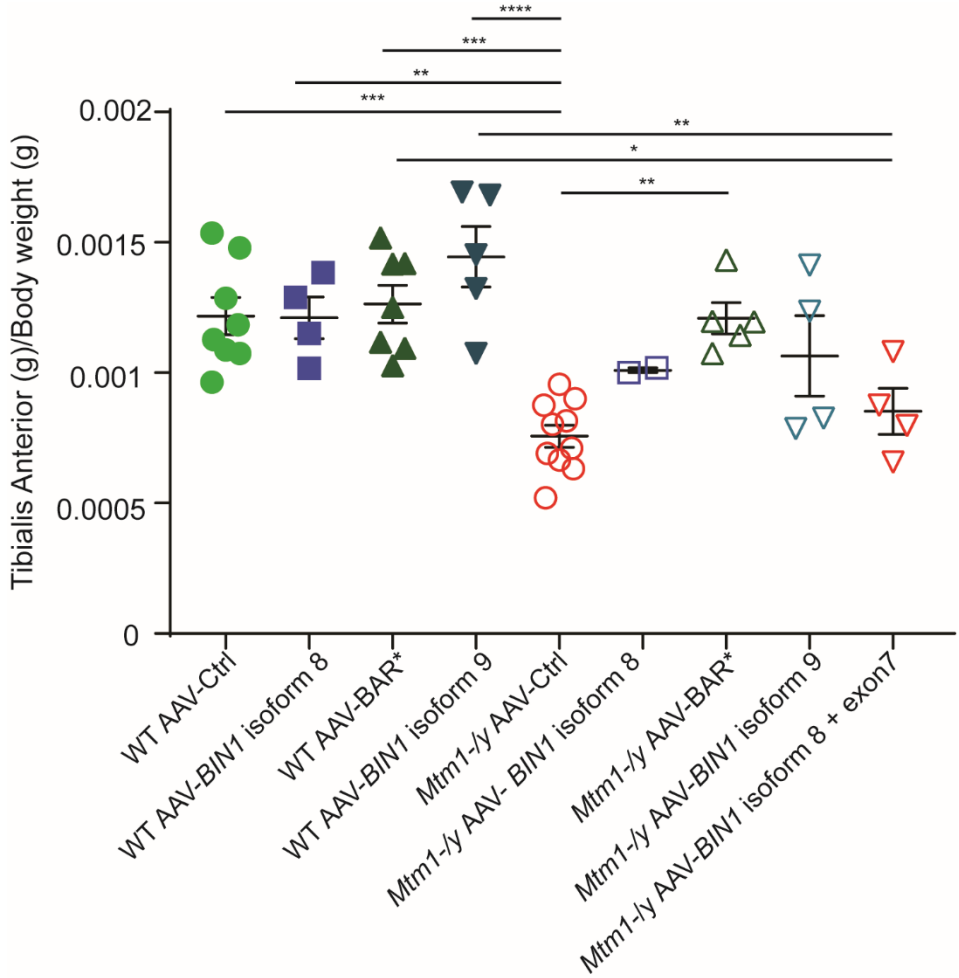

Figure 22: Tibialis Anterior weight

Ratio of TA weight (g) to total body weight (g) of WT and *Mtm1*-/y muscles injected with AAV BIN1 constructs.

The overexpression of various BIN1 constructs induce different in situ muscle strength

To verify if the overexpression of different BIN1 constructs impacted on muscle force, we performed *in situ* TA force analysis. The 5 weeks old WT and *Mtm1*-/y mice injected with control AAV- Ctrl had TA muscle force respectively of 350 mN and around 20 mN at 5 weeks of age.

WT legs injected with AAV-*BIN1* isoform 8, AAV-*BIN1* BAR* domain and AAV-*BIN1* isoform 9 had a strong reduction of TA muscle force compared to the WT injected with the control (Fig.23 A).

The intramuscular overexpression of BIN1 isoform 8 rescued the muscle strength of *Mtm1-/y* (Fig 23 A and in Results part 2a: Fig. 4 and Supplementary Fig. 4). The injection of BIN1 BAR* domain slightly improved the muscle force which reached almost 100 mN more than the force measured in the *Mtm1-/y* control leg (Fig. 23 A). In addition, similar values were obtained in WT injected with the same construct, AAV-*BIN1* BAR* domain. A strong improvement in muscle force was measured in *Mtm1-/y* legs injected with BIN1 isoform 9. This construct improved more efficiently the muscle force than the BIN1 BAR* domain as the muscles injected had an average of 200 mN force. Even in this case the *Mtm1*-/y muscle force was indistinguishable with the average data obtained in WT legs injected with AAV-*BIN1* isoform 9. The only construct that did not ameliorate the muscle force was BIN1 isoform 8 including exon 7. No difference in muscle force was observed in *Mtm1-/y* mice leg injected with AAV- *BIN1* isoform 8 with including exon 7 and the *Mtm1-/y* control leg (Fig. 23A).

Next, we calculated the specific muscle force of the TA dividing the absolute force with the TA weight. The results confirmed that WT legs injected with AAV-*BIN1* isoform 8 and AAV-*BIN1* BAR* significant reduced the specific muscle force. The *Mtm1-/y* legs injected with the AAV-*BIN1* BAR* and AAV BIN1 isoform 9 had a strong improvement in the specific force (Fig. 23B).

Therefore, the overexpression of BIN1 in WT muscles caused a dramatic decrease in muscle force without compromising the skeletal muscle weight. In *Mtm1-/y* muscles the overexpression of BIN1 BAR* domain and BIN1 isoform 9 allowed improvement in muscle force and increased of muscle weight. The inclusion of exon 7 did not improve the skeletal muscle force which was undistinguishable from the *Mtm1-/y* injected with AAV-Ctrl.

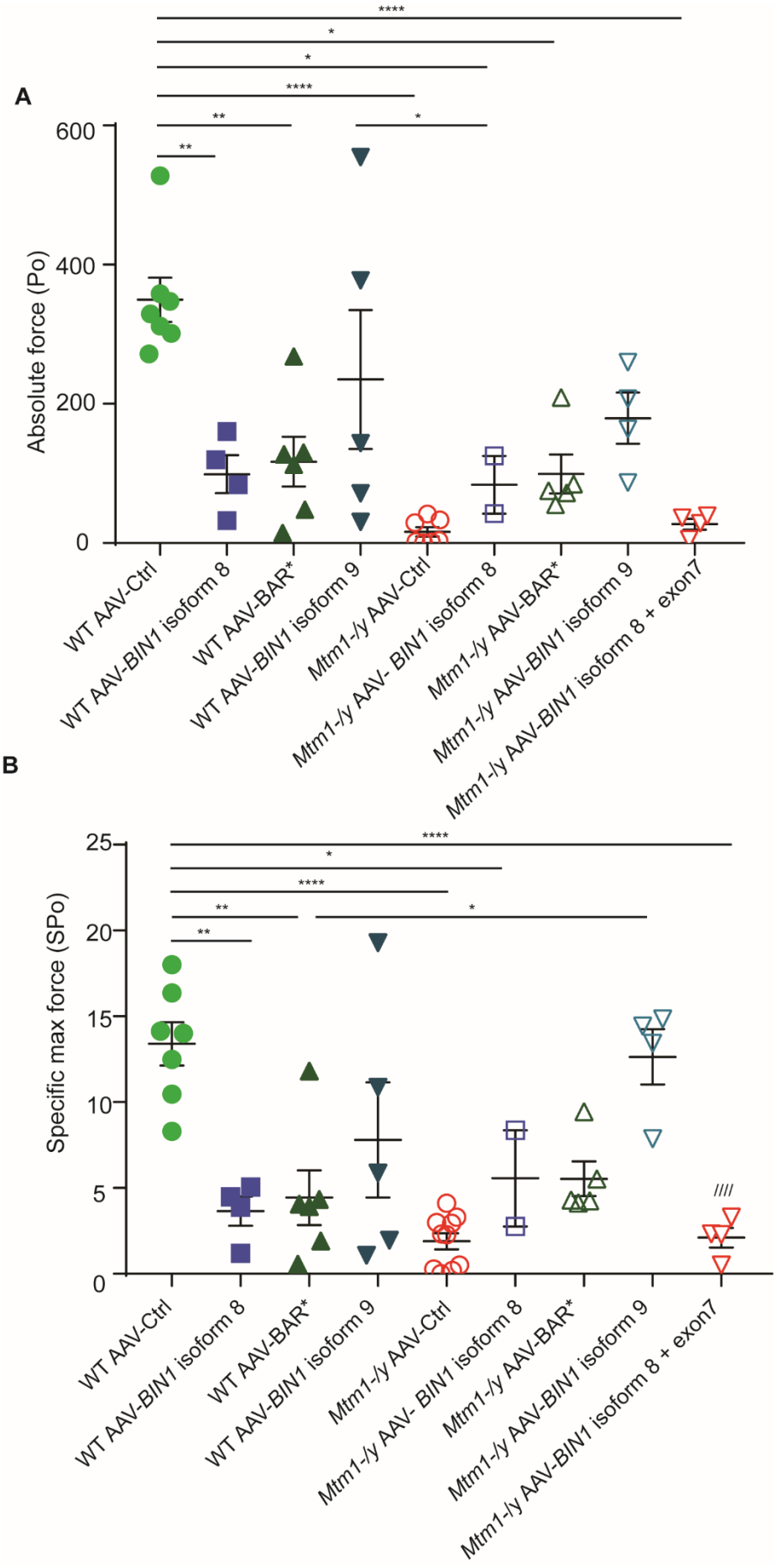

Figure 23: TA muscle force.

A, Absolute force of TA muscle injected with AAV-Ctrl, AAV-*BIN1* isoform 8, AAV-*BIN1* BAR* domain, AAV-*BIN1* isoform 8 inclusion of exon 7 and AAV-*BIN1* isoform 9. **B**, Specific muscle force measured in WT and *Mtm1*-/y intramuscularly injected; Statistical test: One way Anova. Bonferroni post-hoc test.

Histological feature of TA overexpressing BIN1 constructs

As previously described, the main histological differences between WT and *Mtm1-/y* skeletal muscle are the nuclei position and the fiber dimension and shape. WT skeletal muscle have hexagonal muscle fibers with nuclei localized in the periphery of the fibers (arrow) (Fig.24A). The injection of AAV-Ctrl did not affect WT skeletal muscle histology stained with HE, a slight increase of inflammation was detected in the area touched by the needle. The overexpression of the BIN1 isoform 8 and BIN1 BAR* domain caused a dramatic increase in inflammation in the TA muscle. In addition, muscle transduced had two types of muscle fibers, small fibers with nuclei localized in the center (arrows) and larger fibers with nuclei still in the periphery (Fig. 24A). HE coloration was not homogeneous as for muscle transduced with AAV-Ctrl, some fibers had central aggregates. To sum up, the overexpression of full length BIN1 isoform 8 or only BIN1 BAR* domain induced abnormalities observed by HE staining.

Mtm1-/y TA muscle histological pictures reveal small and rounder fibers with nuclei abnormally localized at the center of the fibers (Buj-Bello et al., 2002b) and an increase in interfiber space (Results Part 2a). As it was shown in Fig. 4 in Result Part 2a, AAV-*BIN1* isoform 8 improved TA muscle histology decreasing the number of nuclei in the center of the fiber and improving the fiber size diameter. To evaluate if the overexpression of BIN1 BAR* domain and BIN1 isoform 9 was rescuing these features, TA histology was analyzed 2 weeks post intramuscular injection. The injection of AAV BIN1 BAR* domain in *Mtm1-/y* muscle did not ameliorate fiber size as the picture showed (Fig. 24B). No difference in nuclei position was detected and some fibers had nuclei localized in the center (arrow) as the *Mtm1-/y* control legs. In contrary, the overexpression of the BIN1 isoform 9 increased fiber size dimension and rescued the fiber shape reducing interfiber space (Fig. 24B). In addition, no centralized nuclei were identified.

To conclude, BIN1 isoform 9 improved skeletal muscle histology in *Mtm1-/y* as described for the injection of BIN1 isoform 8 in *Mtm1-/y* while the injection of BIN1 BAR* domain did not rescue the nuclei position and fiber size diameter.

Analysis were also conducted in transversal muscle stained with succinate dehydrogenase (SDH) (Fig. 24A). WT muscle injected with AAV-Ctrl had homogeneous distribution of SDH staining inside the muscle fibers. In contrast, WT muscle transduced with BIN1 isoform 8 and BIN1 BAR* domain had abnormal dark aggregates distributed either around the fibers either in the center area (arrow) (Fig. 24A). Previous studies already demonstrated that *Mtm1-/y* muscle have an increase of SDH staining in the center of the fiber and a dark ring on the periphery (Buj-Bello et al., 2002b). This abnormal staining was still visible in muscle injected with AAV-*BIN1* BAR* domain while reduced in muscle injected with

AAV-BIN1 isoform 8. The injection of AAV-*BIN1* isoform 9 in *Mtm1*-/y rescued completely this phenotype (Fig. A).

In summary, the SDH staining showed that the overexpression of BIN1 affected the oxidative activity in WT muscle while a rescue was observed in *Mtm1*-/y muscle injected with AAV BIN1 isoform 9.

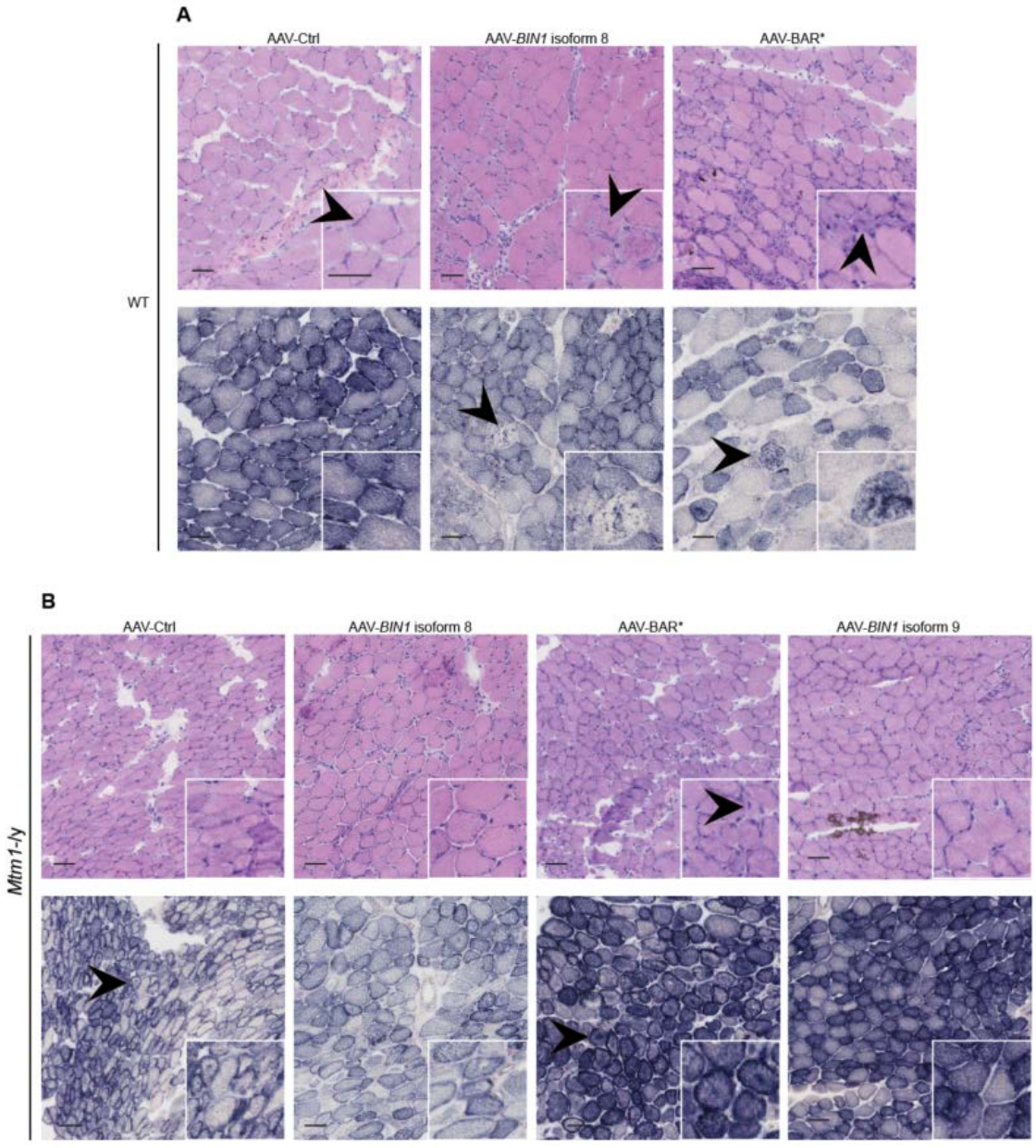

Figure 24: Transversal TA muscle sections stained with H&E and SDH

A, WT injected with AAV-*BIN1* isoform 8 and AAV-BAR* domains have unusual HE (upper panel) and SDH (lower panel) staining and a dramatic increase in inflammation. The arrows indicate the nuclear position and the abnormal SDH staining. **B**, *Mtm1-/y* muscle injected with AAV-Ctrl, AAV-*BIN1* isoform 8 and AAV-BAR* domain have central localized nuclai and some abnormalities in SDH staining while there XLCNM features were rescued in *Mtm1-/y* muscle injected with AAV-*BIN1* isoform 9. The arrows indicate the abnormal nuclei position and SDH staining. Scale bar: 50µm

Conclusion

Here we confirmed that post-natal overexpression of BIN1 isoform 8 rescued the muscle force of *Mtm1-/y* mice. Furthermore the inclusion of exon 7 in BIN1 isoform 8 did not improve the skeletal muscle force when overexpress postnatally in *Mtm1-/y* muscle. The best rescue of muscle force and histology was observed overexpressing BIN1 isoform 9 which does not express exon 11. The BIN1 BAR* domain slightly improved the skeletal muscle force of *Mtm1-/y* mice but did not ameliorate muscle histology.

The positive improvement in muscle force observed in *Mtm1-/y* muscle strongly suggest that the muscles were properly injected, however further analysis will be required to examine the protein level to confirm that the muscles were properly transduced with the AAVs.

The overexpression of BIN1 in WT skeletal muscle may cause inflammatory reaction. It can be due to postnatal expression of human protein in mice. However, this phenotype was never observed in *Mtm1-/y* muscle.

These results highlight protein domains of BIN1 that may be important in the rescue of *Mtm1-/y* muscle phenotypes, and suggest further work is necessary to understand the pathomechanism underlying the results presented here.

Part 3: The overexpression of BIN1 rescues the life span of *Dnm2*$^{R465W/R465W}$ and improve the force of *Dnm2* $^{R465W/+}$ mice.

Introduction

BIN1 overexpression rescued the life span, ameliorated muscle mass and muscle force and improved the histology of the TA muscle of XLCNM mouse model (Result part 2a). These positive results suggest that BIN1 and MTM1 may be part of a common pathway. Previous study showed a genetic and functional link between BIN1 and DNM2. The negative modulation of DNM2 rescues the life span of ARCNM mouse model, *Bin1*$^{-/-}$ mouse (Cowling et al., 2017) (Introduction, Cross therapy). This result proposes that BIN1 and DNM2 are part of the same pathway in skeletal muscle. In addition, *in vitro* study suggests that BIN1 may regulates the GTPase activity of DNM2 during skeletal muscle development (Cowling et al., 2017).

Previous studies showed that the gain-of-function mutation on *DNM2* in the position 465 (mutation R465W) favors DNM2 oligomerization and enhances endocytosis (Rabai *et al*., 2018, accepted). Durieux *et al.,* created and characterized a knock-in mouse model carrying this mutation. *Dnm2* $^{R465W/+}$ mice are viable and have a normal life span and body weight; they start to present muscle force and histological defects during the 2nd month (Durieux et al., 2010). Recently, Buono *et al*., proposed a novel therapeutic strategy to downregulating the total pool of DNM2 through oligonucleotide (ASO) or AAV-shRNA targeting the pre-mRNA and mRNA of DNM2 in *Dnm2* $^{R465W/+}$ mice. These approaches allowed the rescue of skeletal muscle force and muscle histology (Buono et al., 2018) and suggested that DNM2 is more active in *Dnm2* $^{R465W/+}$ as the reduction of total protein level (not specific for mutated allele) rescued the CNM skeletal muscle phenotype.

However, the studies conducted up to now have been focused on mice with heterozygous *Dnm2* ^{R465W} mutation because the homozygous mouse *Dnm2* ^{R465W} dies a few days after birth. Durieux *et al.,* observed that six homozygous *Dnm2* $^{R465W/R465W}$ survived for 2 weeks after birth. Only one mouse was analyzed and it showed an increase in connective tissue inside the muscle and reduced fiber size diameter compared to the WT control. The ultrastructure analysis showed a disorganization on the myofiber and an increase in tubular structure closed to the Z-line (Durieux et al., 2010). No further investigations have been conducted on *Dnm2* $^{R465W/R465W}$ mouse model. To date no study has presented a rescue in the life span of homozygous $^{R465W/R465W}$ mice.

The aim of the study was to investigate a novel therapeutic strategy for ADCNM mouse model and to investigate the relationship between BIN1 and DNM2 in skeletal muscle. We

hypothesized that the overexpression of BIN1 may ameliorate the pathophysiology in ADCNM mouse model. This hypothesis was tested overexpressing BIN1 in *Dnm2* $^{R465W/+}$ and in *Dnm2* $^{R465W/R465W}$ by genetic cross and verified the effect of overexpressing BIN1 post-natal using AAV delivery in *Dnm2* $^{R465W/+}$. These results highlight that BIN1 and DNM2 are part of the same pathway and that BIN1 regulates DNM2 activity.

Generation of Dnm2 $^{R465W/+}$ Tg BIN1 mouse line

To study the effect of BIN1 overexpression in *Dnm2* $^{R465W/+}$ mouse model, female *Dnm2* $^{R465W/+}$ mice (Durieux et al., 2010) were crossed with Tg *BIN1* mice to produce *Dnm2* $^{R465W/+}$ Tg *BIN1* mice. BIN1 protein level was measured in this line as done for the *Mtm1*-/y Tg *BIN1* study (Fig 1 of Result part 2a). No differences were observed in BIN1 protein level between the Tibialis Anterior (TA) lysate of WT and the *Dnm2* $^{R465W/+}$ mice (data not shown). An increase of 8-fold and 3-fold was detected in Tg BIN1 mice and in *Dnm2* $^{R465W/+}$ Tg *BIN1* compared to *Dnm2* $^{R465W/+}$respectively (Figure 25 A-B).

Most of the mice analyzed survived until the end fixed time-point 7 months of age, only some WT and *Dnm2* $^{R465W/+}$ died for unknown problems (Fig. 25C). No difference was identified in body weight between WT, Tg BIN1, *Dnm2* $^{R465W/+}$ and *Dnm2* $^{R465W/+}$ Tg BIN1 mice throughout the 7 months analyzed in this study (Fig. 25D).

Characterization of Dnm2 $^{R465W/+}$*Tg BIN1 mouse model phenotypes*

As previous results showed that *Dnm2* $^{R465W/+}$ have normal growth but decrease TA muscle force compared to the WT (Durieux et al., 2010), we performed phenotyping analysis (hanging test and rotarod) to verify if *Dnm2* $^{R465W/+}$ mice had a defect in total body strength and if the overexpression of BIN1 ameliorated the total body strength of the *Dnm2* $^{R465W/+}$ mice. *Dnm2* $^{R465W/+}$ hang on the grid slightly less than the *Dnm2* $^{R465W/+}$ Tg *BIN1*, the Tg *BIN1* and the WT control (Fig. 25E). To assess if the *Dnm2* $^{R465W/+}$ exhibited a problem in general coordination, the rotarod test was performed at 4 and 8 month mice using different mice cohort. Mice were placed on the rotarod for 5 minutes in acceleration mode and the test was repeated for 4 days for each cohort. No difference in time spent on the rotarod have been identified between the mice; the *Dnm2* $^{R465W/+}$ performed better than the WT and Tg *BIN1* control mice (Fig. 25F-G). We than verified if the force of the TA muscle was impaired. Previous publications showed atrophy in *Dnm2* $^{R465W/+}$ TA muscle from the second months of age (Durieux et al., 2010) (Buono et al., 2018). We analysed the TA muscle at 4 months of age, the overexpression of BIN1 significantly rescued the TA muscle weight of *Dnm2* $^{R465W/+}$ mice (Fig. 26A). We than tested the absolute TA muscle force. The absolute muscle force was significantly reduced in *Dnm2* $^{R465W/+}$ mice compared to the Tg *BIN1* at 4month and to the control genotypes at 8 month. The overexpression of BIN1 in *Dnm2* $^{R465W/+}$ ameliorated the muscle force at 4 and 8

month (Fig. 26B). Next, the specific *in situ* TA muscle force was measure and no significant difference was identified at 4 month of age between the *Dnm2* $^{R465W/+}$ Tg *BIN1* mice and the *Dnm2* $^{R465W/+}$ mice while a trend of improvement was observed in the *Dnm2* $^{R465W/+}$ Tg *BIN1* at 8 month compared to the control mice (Fig. 26C). To conclude, *Dnm2* $^{R465W/+}$ mice exhibited a slight defect in total body strength and no difference in coordination and motor activity with the WT control. The overexpression of BIN1 rescued TA muscle weight and slightly improved absolute muscle force at 4 and 8 month of age.

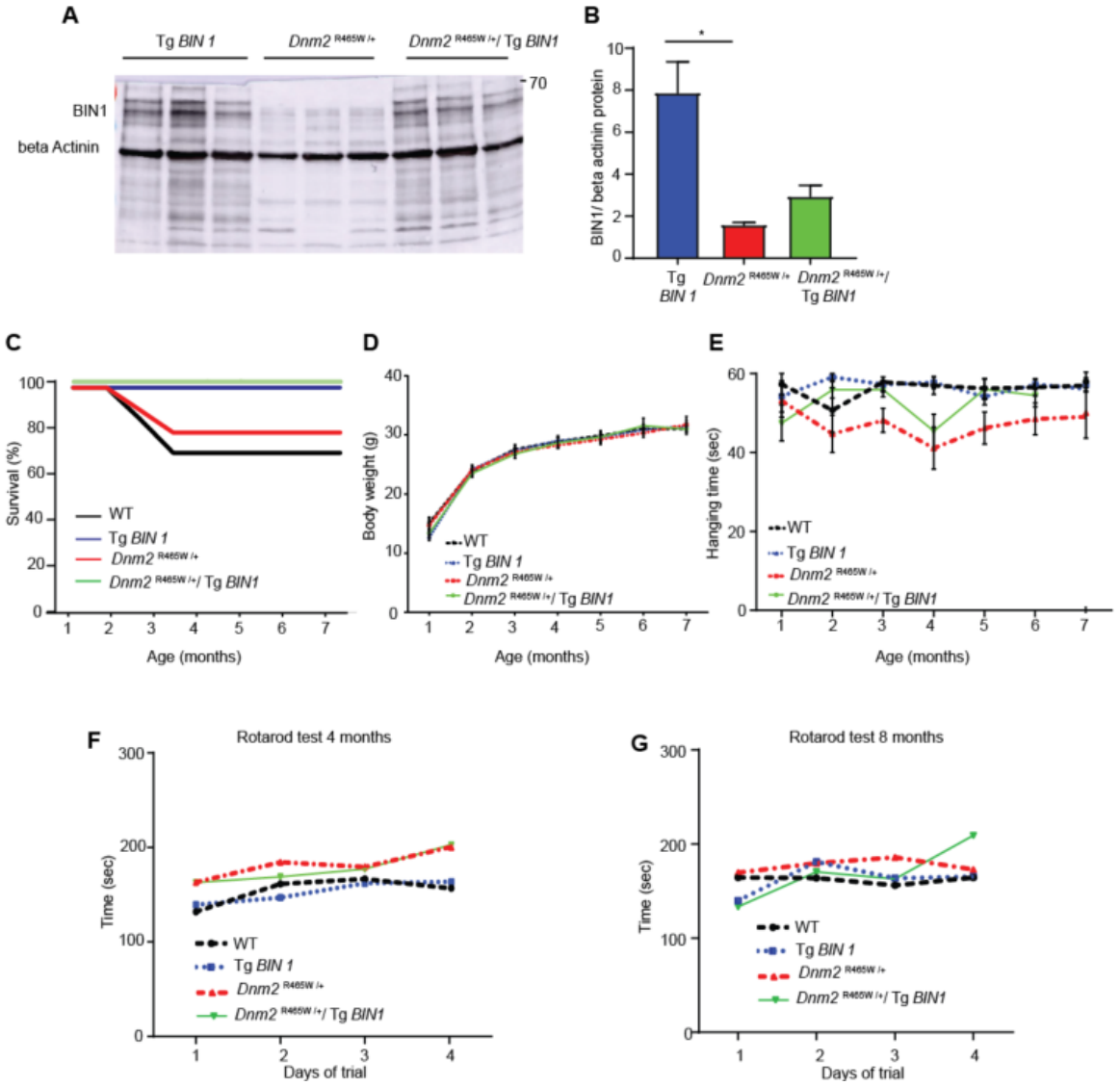

Figure 25: Characterization of Dnm2 $^{R465W/+}$ Tg BIN1 mice.

A, Western blot from Tibialis Anterior (TA) probed with anti BIN1 and DNM2 antibodies. **B,** BIN1 quantification normalized to beta actin. Statistic test: Non parametric test for the graph B, Kruskall-Wallis post-hoc test. *p<0.05. **C,** Lifespan represented as percentage of survival. **D,** Mouse body weight from 1 to 7 months (n ≥ 5). **E,** Hanging test. **F-G,** Rotarod test at 4 (F) and 8 months (G) of age.

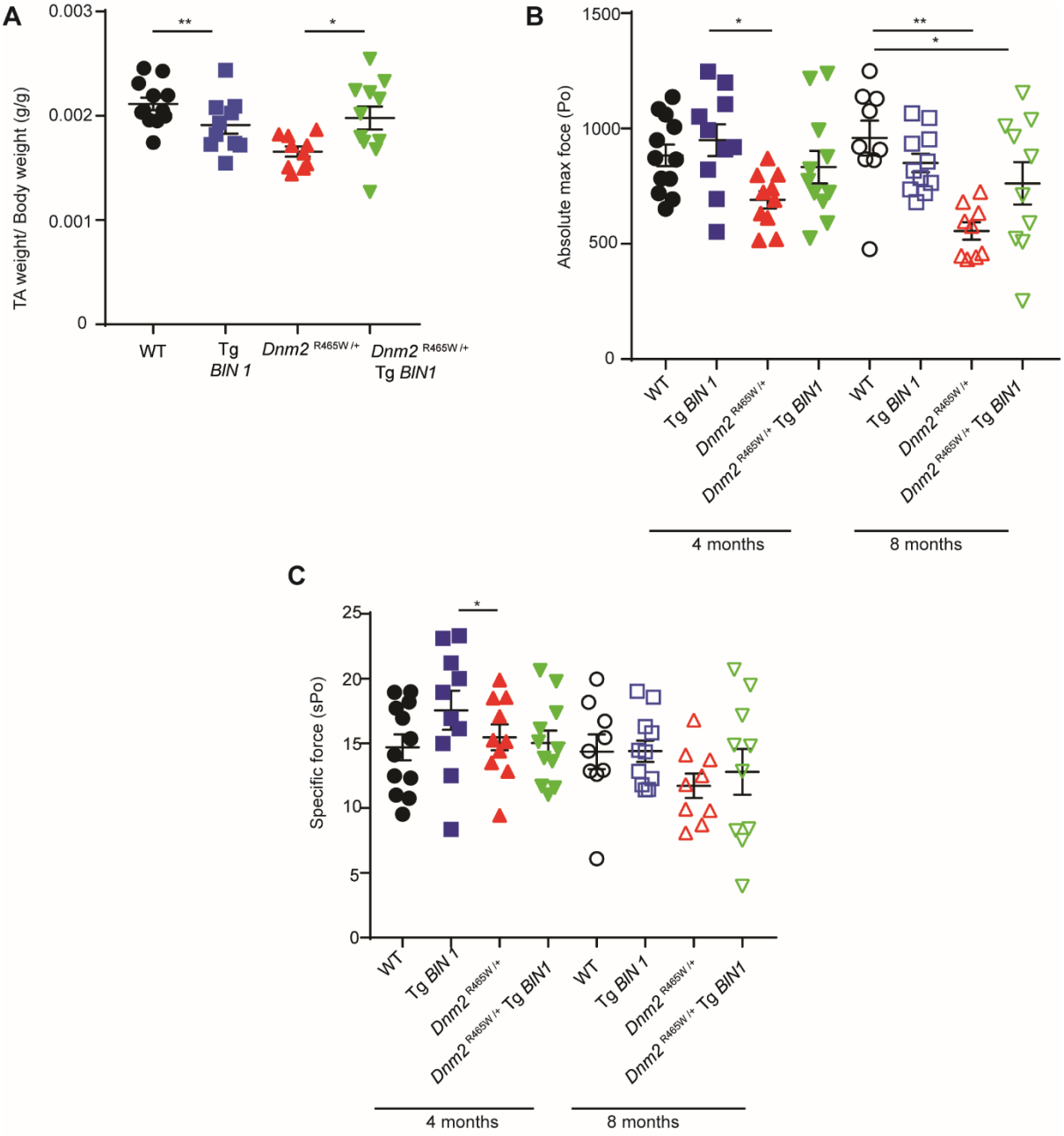

Figure 26: Overexpression of BIN1 in Dnm2 R465W /+ improves in situ muscle force.

A, TA muscle weight on total body weight at 4 months (g/g). **B**, Absolute maximal force at 4 months and 8 months. (C), Specific TA muscle force at 4 months and 8 months of age (n ≥ 7). Statistic test: One-way Anova and Bonferroni post-hoc test. *p<0.05, **p < 0.01. Mean ± SEM.

Overexpression of BIN1 level rescues the histological features in Dnm2 $^{R465W/+}$ muscles

To verify if the amelioration in TA muscle weight and muscle force observed in *Dnm2* $^{R465W/+}$ Tg *BIN1* mice was link with an improvement in *Dnm2* $^{R465W/+}$ muscle structure, we analyzed the TA muscle histology. *Dnm2* $^{R465W/+}$ TA muscle did not exhibit internal nuclei but did exhibit a decrease in fiber diameter (Durieux et al., 2010) (Fig. 27 A-B). The main histological feature was the abnormal aggregation of NADH-TR and SDH staining in the middle of the muscle fibers (Durieux et al., 2010). This abnormal staining was detectable at 4m and 8m of age in *Dnm2* $^{R465W/+}$ TA (Fig. 27 C, arrows and Fig. 27D). The overexpression of BIN1 in *Dnm2* $^{R465W/+}$ mice restored the control phenotype (Tg *BIN1*) (Fig. 27 C-D). Therefore, overexpression of BIN1 by genetic cross improves the histological defects observed in *Dnm2* $^{R465W/+}$ mice.

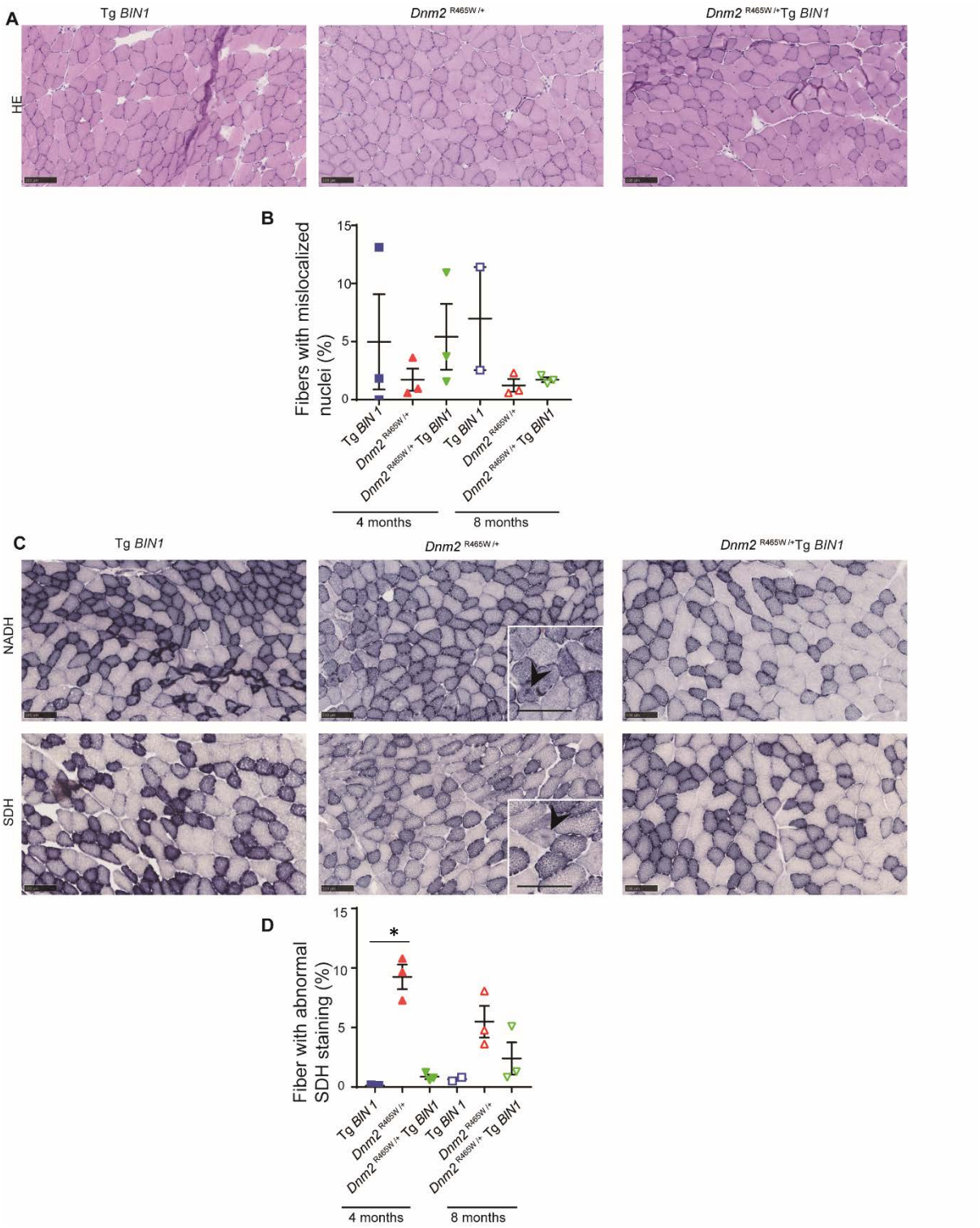

Figure 27: Transversal TA muscle sections stained with H&E and SDH.

A, Transversal TA muscle sections stained with HE at 4 months. Scale bar: 100µm. **B,** Percentage of fibers with abnormally localized nuclei. **C**, Transversal TA muscle sections stained with NADH-TR and SDH. (Arrows showed abnormal aggregates). **D**, Percentage of fibers with abnormal SDH staining. Scale bar: 100µm. Statistic test: Non parametric test for the graph B, Kruskall-Wallis post-hoc test. *p<0.05. Mean ± SEM.

The post-natal overexpression of BIN1 ameliorates muscle atrophy and histological muscle defects of Dnm2 $^{R465W/+}$ mice

Dnm2 $^{R465W/+}$ Tg *BIN1* mice were obtained by genetic cross and BIN1 was overexpressed since *in utero.* To develop a translated therapeutic approach we aimed to modulate BIN1 expression after birth. We decided to overexpress BIN1 isoform 8 (without exon 17), the same isoform that was successfully used to rescue the XLCNM mouse model (Fig.4 in Result part 2a). We overexpressed BIN1 by AAV delivery, the AAV-*BIN1* was injected intramuscularly in 3 week old *Dnm2* $^{R465W/+}$ mice and analyzed 4 weeks post-injection. A 4-fold of increase in BIN1 expression was detected in the muscles of *Dnm2* $^{R465W/+}$ injected with AAV-*BIN1* compared to the leg injected with AAV-Ctrl (Fig. 28 A-B). The increase of BIN1 expression allowed a slight improvement of TA muscle weight in *Dnm2* $^{R465W/+}$ leg injected with AAV-*BIN1* compared to the leg injected with AAV-Ctrl (Fig. 28 C). The WT TA injected with AAV-*BIN1* weighted more than the control leg (Fig.28 C). No difference in absolute and specific muscle force was measured between the *Dnm2* $^{R465W/+}$ leg injected with AAV-*BIN1* and the control leg (Fig. 28 D-E).

The injection of AAV-*BIN1* ameliorated the skeletal muscle histological defect feature observed in *Dnm2* $^{R465W/+}$. The fiber size of *Dnm2* $^{R465W/+}$ TA injected with AAV-*BIN1* appeared increased compared to the leg injected with the AAV-Ctrl (qualitative analysis only). The NADH-TR and SDH staining aggregations observed in *Dnm2* $^{R465W/+}$ TA were not visible in *Dnm2* $^{R465W/+}$ leg injected with AAV-*BIN1* (Fig. 29 B-C). The WT injected with AAV-*BIN1* presented an increase number of centralized nuclei and inflammation on the TA muscle compared to the control leg (Fig. 29 A). Quantification should be performed to confirm these qualitative observations.

In summary, the intramuscular injection of AAV-BIN1 in *Dnm2* $^{R465W/+}$ TA muscle improved the TA muscle weight and ameliorated the NADH-TR and SDH aggregation observed by histological pictures. However, the increase of BIN1 expression did not rescue the muscle force of *Dnm2* $^{R465W/+}$ injected leg compared to the control leg. The intramuscular overexpression of BIN1 in the WT causes an increase in TA muscle weight with a great TA inflammation response.

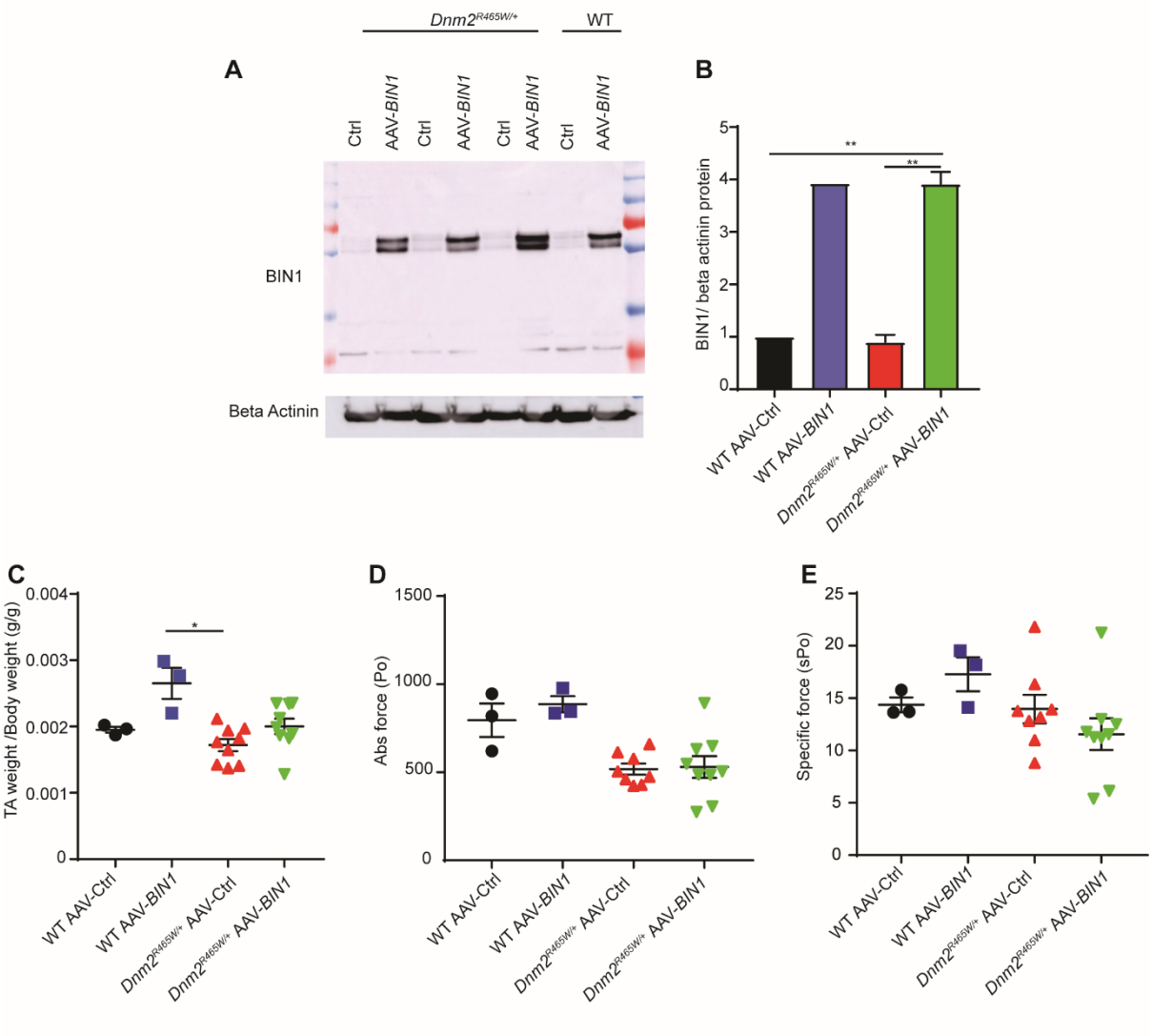

Figure 28: Post-natal overexpression of BIN1 in Dnm2 $^{R465W/+}$ mouse model.

A,Western blot from Tibialis Anterior (TA) probed with anti BIN1 and beta actinin antibodies. **B**, Western blot quantification graph of and BIN1 normalized on beta actinin. **C**, TA muscle weight on total body weight (g/g). **D**, Absolute TA muscle force 4 weeks post intramuscular injection (n ≥ 3). **E**, Specific TA muscle force at 8 weeks old mice (n ≥ 3). Statistic test: Non parametric test for the graph B, Kruskall-Wallis post-hoc test. *p<0.05. Mean ± SEM.

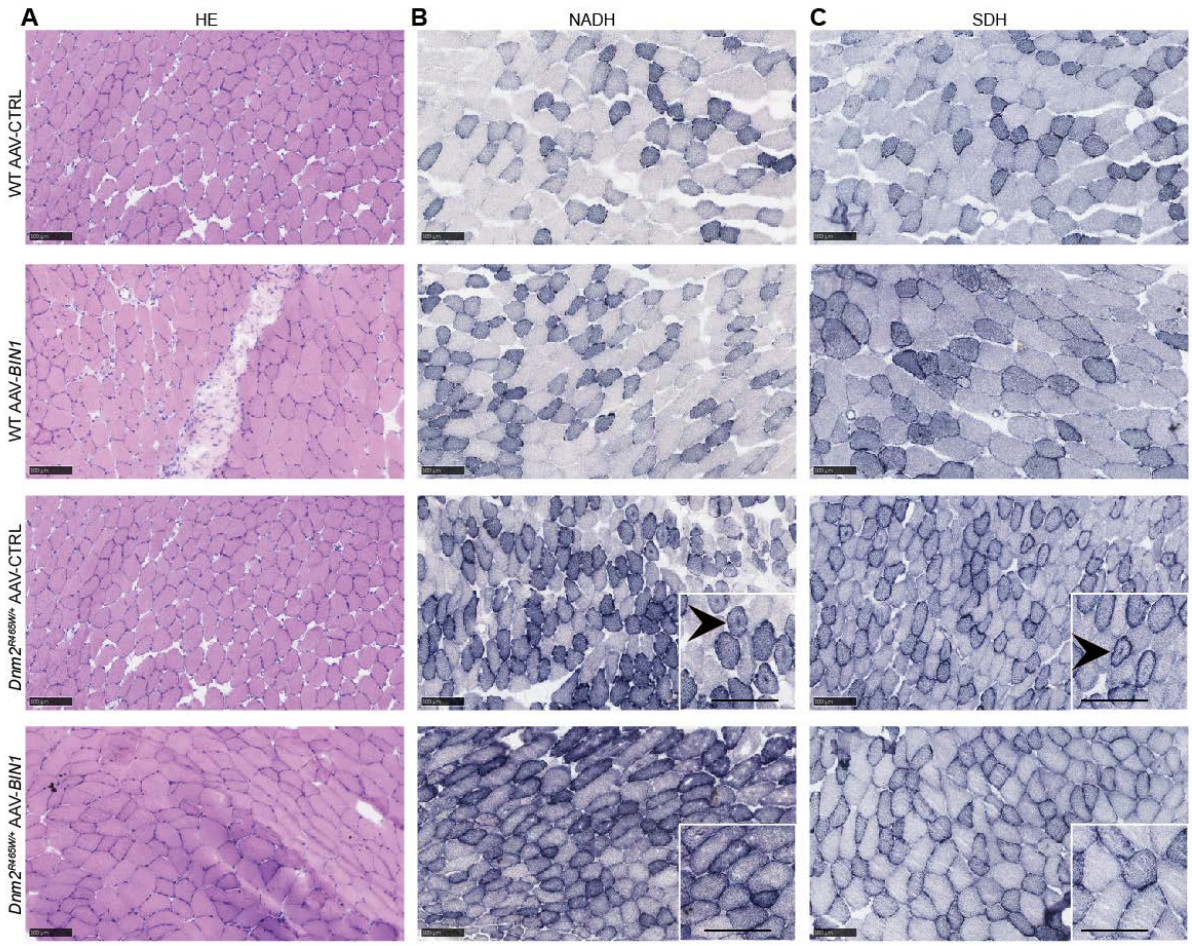

Figure 29: Transversal TA muscle sections stained with HE and SDH.

A, Transversal TA muscle sections stained with HE. WT and Dnm2R465W/+ injected with AAV Ctrl and AAV-*BIN1* isoform 8. **B-C**, Transversal TA muscle sections stained with NADH-TR and SDH. *Dnm2*$^{R465W/+}$ muscles injected with AAV-CTRL have abnormal aggregates in the center of the fibers (arrow) which are not detectable in muscles injected with AAV-*BIN1* isoform 8. Scale bar: 100µm.

Overexpression of BIN1 prevents the premature lethality of Dnm2 R465W/ R465W mouse model

As the overexpression of BIN1 *in utero* was able to improve the *Dnm2*$^{R465W/+}$ muscle weight, we next tested if the overexpression of BIN1 rescues the life span of *Dnm2* $^{R465W/ R465W}$ mice. The *Dnm2* $^{R465W/ R465W}$ mice were previously described to survive for a maximum of 2 weeks postnatally, and surviving mice presented severe muscle phenotypes (Durieux et al., 2010). Here, we generate *Dnm2* $^{R465W/ R465W}$ overexpressing BIN1 *in utero;* female *Dnm2*$^{R465W/+}$ were crossed with male *Dnm2*$^{R465W/+}$ Tg *BIN1* mice. In our cohorts, only 0.3% of 10 days pups were *Dnm2* $^{R465W/ R465W}$ suggesting that the majority died before (Table 1). The overexpression of BIN1 was confirmed by Western Blot (Fig. 30 F); a 3 fold overexpression of BIN1 rescued the life span of the *Dnm2* $^{R465W/ R465W}$ mice. The mice survived until the fixed time point 8 weeks (maximum aged analyzed in this study). A slight difference was observed in the growth of *Dnm2* $^{R465W/ R465W}$ Tg *BIN1* and WT control, the *Dnm2* $^{R465W/ R465W}$ Tg *BIN1* weighed less than the WT littermate from 6 weeks of age (Fig. 30 A). A small cohort of *Dnm2* $^{R465W/ R465W}$ Tg *BIN1* mice were maintained alive to verify their life span and surprisingly survived until 2 years of age. These results suggest that increasing BIN1 expression is sufficient to rescue neonatal lethality of *Dnm2* $^{R465W/ R465W}$ mice.

Dnm2 $^{R465W/+}$ X *Dnm2* $^{R465W/+}$ Tg *BIN1*

	WT	*Dnm2* $^{R465W/+}$	*Dnm2* $^{R465W/ R465W}$	Tg *BIN1*	*Dnm2* $^{R465W/+}$ Tg *BIN1*	*Dnm2* $^{R465W/ R465W}$ Tg *BIN1*
Expected	8.3%	8.3%	8.3%	8.3%	8.3%	8.3%
Obtained at PN 10 days	12.3%	13.4%	0.3%	9.4%	5.4%	9%

Table 1: Percentage of male pups genotyped at 10 days post-birth

Characterization of Dnm2 R465W/ R465W Tg BIN1 mice phenotype and muscle force.

As the overexpression of BIN1 rescue the *Dnm2* R465W/ R465W survival, the total body force and specific *in situ* muscle force were measured. To assess the total body strength, the hanging test was performed. At 4 weeks old *Dnm2* R465W/ R465W Tg *BIN1* were able to hang for up to 20 seconds to the grid. At 8 weeks of age no difference was observed between the *Dnm2* R465W/ R465W Tg *BIN1* and the WT control (Fig. 30 B). We next analyzed the TA muscles, *Dnm2* R465W/ R465W Tg *BIN1* had smaller TA muscles compared to the WT control (Fig. 30 C). A significant difference was obtained between the WT and *Dnm2* R465W/ R465W Tg *BIN1* TA muscle absolute and specific force (Fig. 30 D-E). *Dnm2* R465W/ R465W Tg *BIN1* mice had a TA absolute force of 600 mN which was a similar value measured in *Dnm2* R465W/+ mice (Fig. 26 B). In addition, we verified the level of DNM2 on the TA lysates of *Dnm2* R465W/ R465W Tg *BIN1* mice and it was significantly higher compared to WT (Fig. 30 G). To conclude, the *Dnm2* R465W/ R465W Tg *BIN1* have normal body strength but lower TA muscle strength than the WT control at 8 week.

Characterization of Dnm2 R465W/ R465W Tg BIN1 muscle histology and ultrastructure

To assess the skeletal muscle histology and structure, TA muscle was analyzed after histological staining. HE transversal muscle sections staining (Fig. 31 A) showed small percentage of fibers with nuclei abnormally positioned (around 7%) in *Dnm2* R465W/ R465W Tg *BIN1* TA muscle (Fig. 31 C). In addition, abnormal internal dark staining was visible in some muscle fibers stained with HE and SDH (arrows) (Fig.31 A-B). Around 15% of *Dnm2* R465W/ R465W Tg *BIN1* TA muscle fiber had abnormal SDH aggregates (Fig. 31 D). I noticed that the fiber with abnormal aggregates were mainly situated on the periphery of the TA muscle. The electron microscopy pictures did not reveal abnormalities in muscle ultrastructure. The longitudinal pictures showed aligned Z-line in *Dnm2* R465W/ R465W Tg *BIN1* as the WT control and normal muscle triads localization. In conclusion, *Dnm2* R465W/ R465W Tg *BIN1* had defects in nuclei position and SDH staining compared the WT control.

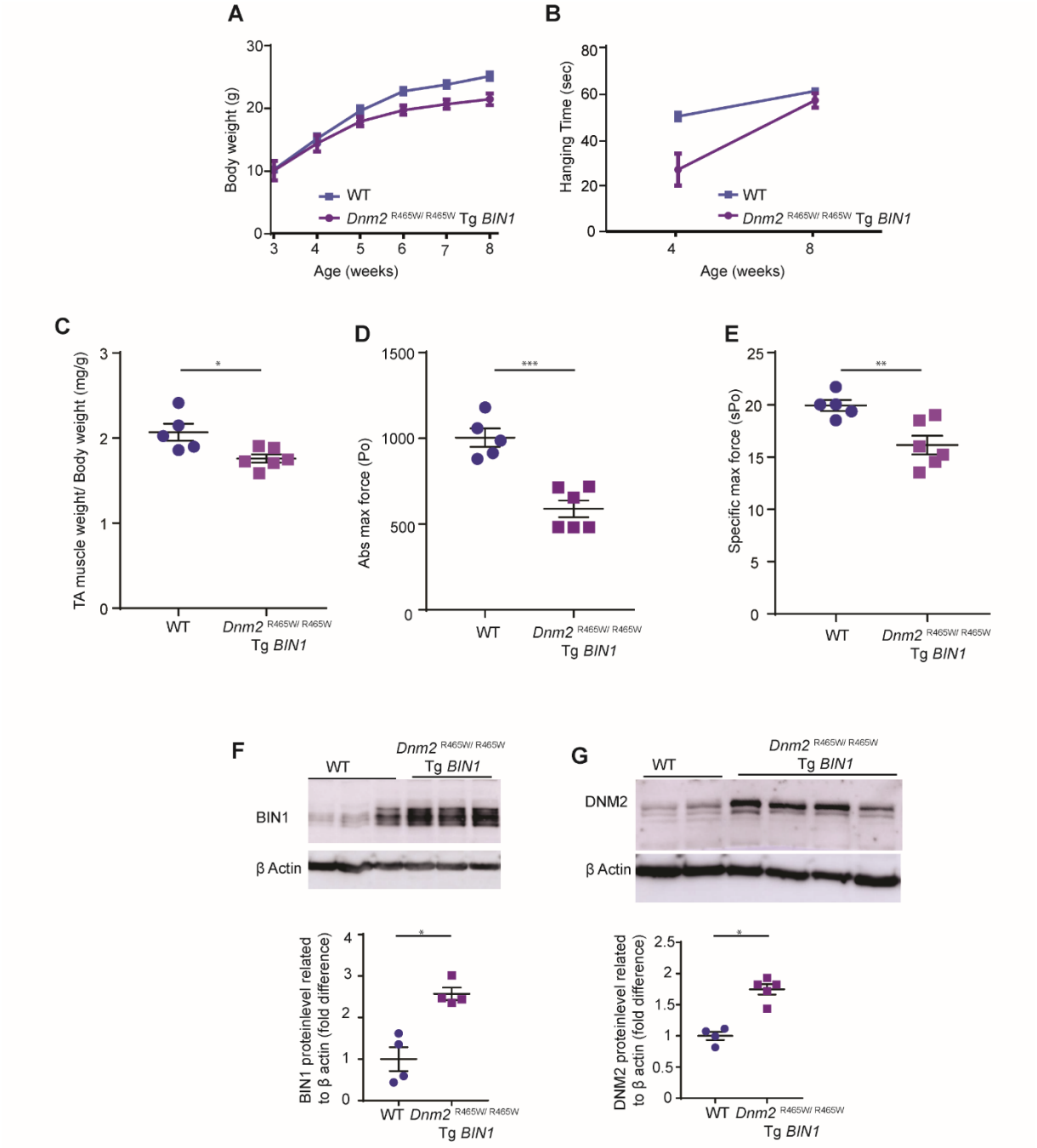

Figure 30: The overexpression of BIN1 improves Dnm2 R465W/ R465W mice life span and growth.

A, Mouse body weight from 1 to 8 weeks (n ≥ 7). **B,** Hanging test. Mice were suspended from a grid for maximum 60 seconds. n=3 repeats/mouse. **C,** TA muscle weight/total body weight ratio (g/g). **D,** Absolute TA muscle force at 8 weeks of age (n ≥ 7). **E**, Specific TA muscle force at 8 weeks of age (n ≥ 7). **F-G**, Western blot from Tibialis Anterior (TA) probed with anti DNM2 and BIN1 antibodies. Quantification graph of DNM2 and BIN1 normalized to beta actin. Statistic test: Non parametric test. Mann-Whitney post-hoc test. *p<0.05, **p < 0.01, ***p < 0.001

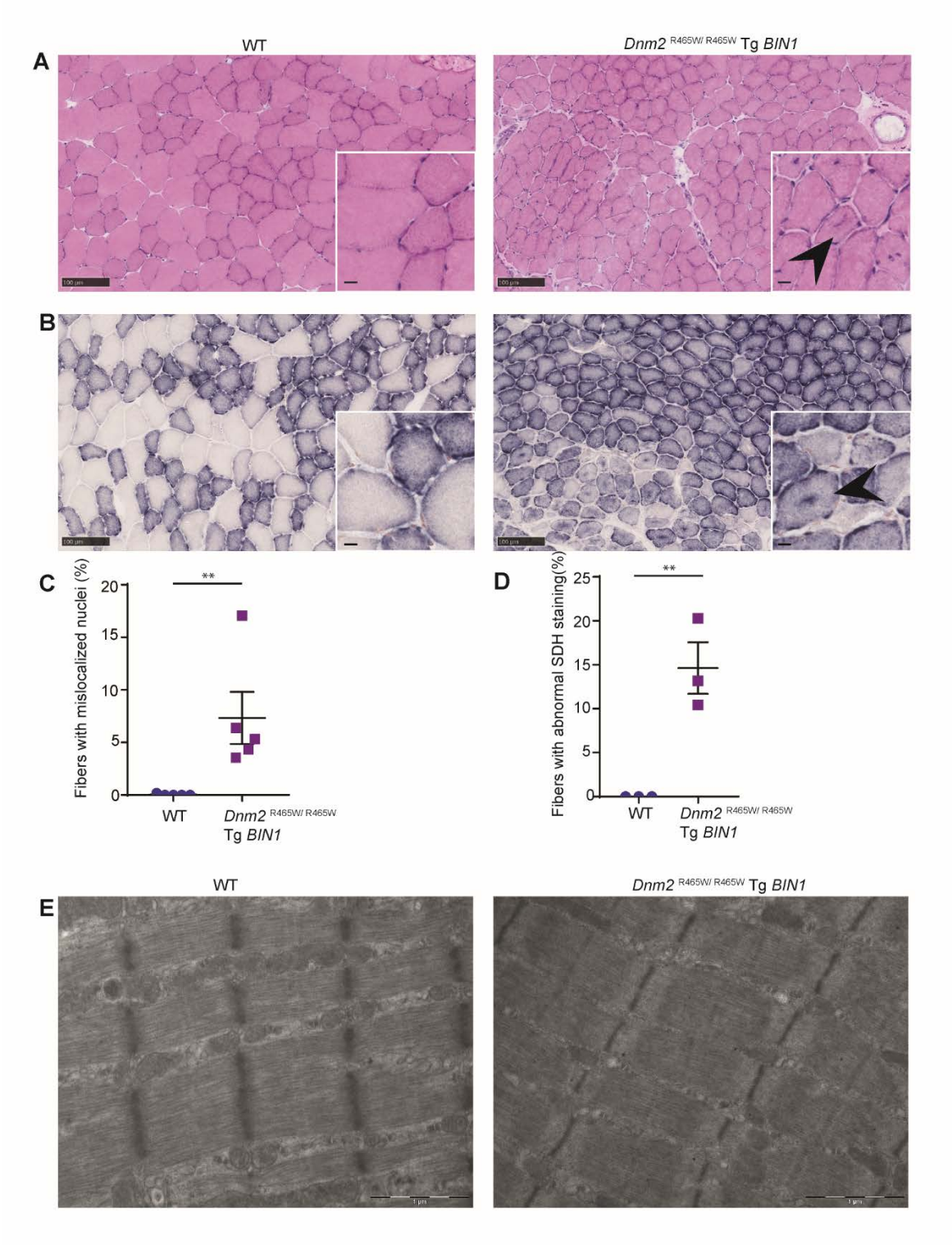

Figure 31: Dnm2R465W/R465W Tg BIN1 muscle histology and structure

A-B, Transversal TA muscle sections stained with (A) HE and (B) SDH. (A), HE showed internalized nuclei. Arrows indicate abnormal internalized HE and (B), SDH staining in *Dnm2*$^{R465W/R465W}$ Tg *BIN1*. Scale bar 100 µm, insert zoom have a scale bar of 10µm. **C**, Fibers with abnormal localized nuclei. **D**, Abnormal SDH staining in the center of the fibers. **E**, Longitudinal muscle ultrastructure observed by electron microscopy. Scale bar: 1µm. Statistic test: Non parametric test for the graph, Kruskall-Wallis post-hoc test.**$p < 0.01$

Conclusion and perspectives

In this study we proposed that the overexpression of BIN1 *in utero* rescued the muscle atrophy and partially the histology defects of *Dnm2* $^{R465W/+}$ *BIN1* mice. Furthermore *Dnm2* $^{R465W/R465W}$ Tg *BIN1* mice survived until 2 years and exhibited only minor histological defects like the *Dnm2* $^{R465W/+}$ mice. Therefore overexpression of BIN1 rescued the neonatal lethality normally observed in this line.

I will complete the study with further molecular investigation. I will focus on the endocytosis propriety of DNM2. As it was recently reported by Rabai *et al*, the *Dnm2* $^{R465W/+}$ myoblasts exhibit defects in transferrin uptake, I will verify if *Dnm2* $^{R465W/+}$ myoblasts overexpressing BIN1 rescues this feature (Rabai *et al.,* 2018, accepted).

Contribution

To complete this study, I was strongly helped by Christine Kretz and Suzie Buono. Christine Kretz conduced the genotyping and phenotyping of the genetic cross mouse lines. The help of Suzie was crucial for muscle dissection of the genetic-cross line. I performed and analysed the phenotyping and *in situ* muscle force tests performed on the genetic cross models and I implemented the injection of AAV-*BIN1* intramuscularly.

The study has been conducted under the supervision of Jocelyn Laporte and Belinda Cowling.

Material and Methods

The following material and methods are referred to the Results part 2b and part 3. The material and methods of Results part 1 and 2a are included in the articles.

Chemicals

Primary antibodies used were rabbit anti-BIN1 (R2405), rabbit anti-DNM2 antibodies (R2680 and R2865), mouse β actin were made onsite at the polyclonal antibody facility of the IGBMC. Secondary antibodies against mouse and rabbit IgG, conjugated with horseradish peroxidase (HRP) were purchased from Jackson ImmunoResearch Laboratories (catalog 115-035-146 and 111-036-045). An ECL kit was purchased from Pierce.

Mouse lines

Mtm1-/y mouse line (129PAS) was previously generated and characterized (Buj-Bello, Laugel et al. 2002, Tasfaout, Buono et al. 2017). *Mtm1* heterozygous females were obtained by homologous recombination of a target sequence, they were crossed with WT male to generate *Mtm1*-/y mice.

TgBIN1 (B6J) mice were obtained by the insertion of human BAC (n° RP11-437K23 Grch37 Chr2: 127761089-127941604) encompassing the full BIN1 gene with 180.52 Kb of genomic sequence.

The Bin1+/- mice were created targeting the exon 20 of BIN1 with LoxP site. The deletion was trigger by recombinase expressed under the cytomegalovirus (CMV) promoter (Cowling, Prokic et al. 2017).

Dnm2R465W/+ was generated with an insertion of a point mutation in exon 11. The homozygous mice were generated by genetic cross of male and female *Dnm2*$^{R465W/+}$ mice. The *Dnm2*$^{R465W/+}$ Tg *BIN1* mice were generated by crossing the Tg *BIN1* with *Dnm2*$^{R465W/+}$ whereas the *Dnm2*$^{R465W/\ R465W}$ Tg *BIN1* mice by crossing *Dnm2*$^{R465W/+}$ Tg *BIN1* male and *Dnm2*$^{R465W/+}$ female.

Animals were maintained at room temperature with 12 hours light/ 12 hours dark cycle. Animals were sacrificed by cervical dislocation following European legislation on animal experimentation and experiments approved by ethical committees (APAFIS#5640-2016061019332648; 2016031110589922; Com'Eth 01594).

Animal phenotyping

The phenotyping experiments were conducted blinded and all the experiments were repeated three time for each mouse to ensure reproducibility. The tests were always performed by the same examiners in order to avoid stress and to ensure reproducibility. The daily phenotyping experiments were always performed in the same part of the day for all the mice in the cohort while the weekly experiments were always performed on the same day of the week. In the following section we will briefly described the Hanging test and rotarod test. The Hanging test was performed each week from 3 weeks to 16 weeks of age and monthly from 4 to 12 months. The mice were suspended from a cage lid for maximum 60 seconds and the test was repeated three times. The average time each mouse hang on the grid is presented in the graph. The rotarod test was conducted at 5 weeks and 5 months of age. The mice performed the test for 5 days. During the day 1 the mice were trained to run in acceleration mode on the rotarod. From day 2-5 mice ran for a maximum of 5 minutes with increasing speed (4-40rpm). Each mouse performed three times the test for each day in each time points. We did not use the same cohort of mice at 5 weeks and 5 months. The data reported in the graph corresponded to the amount of time the animal run on the rotarod.

Muscle force measurement

Mice were anesthetized using Domitor (1mg/kg), Fentanil (0.14mg/kg) and Diazepam (4mg/kg) by intraperitoneal injection, the force of tibialis anterior (TA)was measured using a force transducer (Aurora Scientific) as described previously (Tasfaout, Buono et al. 2017). The absolute maximal force of the TA was measured after tetanic stimulation of the sciatic nerve with a pulse frequency from 1 to 125 Hz. The specific maximal force was determined dividing the absolute maximal force with the TA weight.

AAV transduction of TA muscle

The intramuscular injection was performed at 3 weeks old male wild-type, Mtm1-/y or Dnm2R465W/+ mice. The mice were anesthetized by intraperitoneal injection of ketamine 20mg/ml and xylazine 0,4% (5 µl/g of body weight). The TA muscle was injected with 20 µl of AAV9 (7x10^11 vg/mL) CMV human BIN1 constructs or empty AAV9 control diluted in physiological solution. The virus were producted by the molecular biology facility of the IGBMC; Post-injection the animal were immediately housed in the ventilated cage.

Tissue collection

Cervical dislocation was used to sacrifice mice after carbon dioxide suffocation. TA muscle was extracted and then frozen in isopentane cooled in liquid nitrogen. The muscles were stored at -80°C.

Histology

8 µm cryosections of TA muscles were cut and stained with Haematoxylin and Eosin (HE), nicotinamide adenine dinucleotide (NADH-TR) and succinate dehydrogenase (SDH) for histological analysis. After staining the images were acquired with the Hamamatsu Nano Zoomer 2HT slide scanner. The percentage of internalized nuclei and abnormal SDH staining was counted using Cell Counter Plugin in Fiji software.

Electron microscopy

TA was stored in 2.5 % paraformaldehyde and 2.5 % glutaraldehyde in 0,1M cacodylate buffer. Sections were observed by electron microscopy. To observe T-tubules, potassium ferrocyanide was added to the buffer (K3Fe(CN) 6 0.8% , Osmium 2%, cacodylate 0.1M)(Al-Qusairi, Weiss et al. 2009). The triad number per sarcomere and T-tubule direction were measured manually.

Protein Extraction and western blotting

TA muscle was lysed in RIPA buffer with 1mM DMSO, 1mM PMSF and mini EDTA free protease inhibitor cocktail tablets (Roche Diagnostic) on ice. The protein concentration was measured using the BIO-RAD Protein Assay Kit (BIO-RAD). Loading buffer (50 mM Tris-HCl, 2% SDS, 10% glycerol) was added to protein lysates, and proteins were separated by 8% or 10% in SDS-polyacrylamide gel electrophoresis containing 2,2,2-Trichloroethanol (TCE) in order to visualize all tryptophan-containing proteins. After transfer to nitrocellulose, saturation was done with 3% BSA or 5% milk, primary antibody and secondary antibody was added: β1 integrin (MAB1997, 1:500), vinculin (V9131, 1:1000), BIN1 (2405, 1:1000; IGBMC), MTM1 (2827, 1:1000; IGBMC), GAPDH (MAB374, 1:100000).

Statistical Analysis

The data are expressed as mean ± s.e.m. Graph and curves were made using GraphPad Prism software versions 5&6. The unpaired students T-test was used to compare two groups. No parametric test and Kruskal Wallis post-hoc were used to compare different groups. One-way ANOVA and Bonferroni test post-hoc were used to compared different group if the data followed a normal distribution and if the sample analysed had the same background. P values smaller than 0.05 were considered significant. The number of mice and the tests used for each experiments are listed for each experiment in the figure legends.

Discussion and future perspectives

During my PhD, I investigated **new therapeutic strategies** to treat CNMs *in vivo* using mouse models of disease. I contributed to finalizing the analysis on DNM2 downregulation to treat XLCNM using a shRNA-AAV mediated approach (Results part 1) (Tasfaout et al., 2018b). I then explored for most of my PhD a novel strategy which targeting overexpression of *BIN1* in *Mtm1-/y* mice to rescue XLCNM (Results part 2) (Lionello et al., under second revision in Science Translational Medicine). Furthermore, I have applied the same therapeutic strategy developed for XLCNM in part 2, to test in ADCNM mice. I have shown the rescue of muscle histology and life span by overexpressing BIN1 respectively in *Dnm2*$^{R465W/+}$ and *Dnm2*$^{R465W/R465W}$ mice (Results part 3). Finally, I have investigated **the pathophysiological mechanisms to understand the rescue observed by increasing BIN1 expression** in XLCNM. I have confirmed defects in β1 integrin recycling in skeletal muscle of XLCNM model and I have observed that BIN1 as well as MTM1 are both involved in the integrin recycling pathway (Results part 2).

These results help explain the molecular **relationship** between MTM1, BIN1 and DNM2 and to identify novel therapeutic targets.

New therapeutic strategy to treat various forms of CNM

The main goal of my study was to test new therapeutic approaches to treat CNM. During my thesis I participated in the development of therapies overexpressing BIN1 and downregulating DNM2 in XLCNM and ADCNM mouse models.

BIN1 level modulation rescues Mtm1-/y life span and muscle force

We tested overexpression of human BIN1 in mice by analyzing transgenic mice expressing the human BAC containing the *BIN1* gene. Firstly we verified that the overexpression of human BIN1 did not affect life span, muscle strength and histology in transgenic mice. No abnormal phenotypes were identified in the Tg *BIN1* mice suggesting the overexpression of BIN1 during embryogenesis is not overtly toxic to mice. In addition, analysis conducted on the human BIN1 isoform expressed in Tg *BIN1* mice revealed that there was no difference between the human and mouse BIN1 isoforms expressed in the Tg *BIN1* mice. This result indicates that the mouse splicing machinery recognizes the splicing site on the human sequence.

Mtm1-/y mice develop a progressive myopathy from 3 weeks of age and survive approximately until 2 months (Buj-Bello et al., 2002b). *Mtm1-/y* Tg *BIN1* mice survived as long as WT and Tg *BIN1* controls. Phenotyping analysis conducted on *Mtm1-/y* Tg *BIN1* mice showed no difference on body growth, total muscle force and muscle histology to the controls. These positive results obtained by genetic cross provided the first proof-of-concept necessary for the development of a new therapeutic approach. To address if the BIN1 expression after

birth could be used as a therapeutic strategy, we decided to test if viral delivery of BIN1 could also rescue *Mtm1-/y* mice (Results part 2).

We successfully performed intramuscular injection of AAV-*BIN1* in the TA of 3 weeks old *Mtm1-/y* mice. We injected the TA because it is one of the most affected and studied muscles in the XLCNM mouse model. The overexpression of exogenous BIN1 for 2 weeks or 4 weeks rescued the *Mtm1-/y* muscle force and reduce fiber atrophy. However, the number of nuclei localized in the center of the muscle fibers were significantly reduced only after 4 weeks treatment post-injection. Having validated the rescue of the BIN1 overexpression with the intramuscular injection, we aimed for overexpression of BIN1 systemically in the mice. We initially performed retro-orbital injection at 3 weeks old *Mtm1-/y* mice, however, BIN1 protein level were not increased in the muscle of injected mice even upon expert injections. We thus hypothesize defects in *Mtm1-/y* vessel architectures or problem in blood circulation. For this reason we decided to proceed to injecting pups directly after birth at P1 by intraperitoneal injection. We obtained a significant rescue of the *Mtm1-/y* life span, one *Mtm1-/y* mouse has been maintained alive for controlling its life span study and it died at 1.5 years of age. *Mtm1-/y* mice overexpressing BIN1 after birth exhibited reduced total body weight compared the WT control mice. However, analysis of absolute muscle force revealed that the *Mtm1-/y* mice, injected post-birth with AAV-*BIN1* systemically, exhibited a significant improvement in *in situ* muscle force. The overexpression of BIN1 postnatally rescued muscle atrophy and ultrastructure and only approximately 10 % of the nuclei were still abnormally positioned in the center of the fibers. *Mtm1-/y* treated with the *AAV-BIN1* still developed kyphosis and ptosis but at late stage and without affecting the mouse movement. Further analyses are needed to understand how long the AAV-*BIN1* is stable inside the muscle fibers. I hypothesize that the BIN1 overexpression started to decrease when the first phenotyping symptoms typical of *Mtm1-/y* mice starts to appear. We did not perform any post-symptomatic rescue analyses. Before translating this approach to human, further investigations need to be conducted to understand if the AAV-*BIN1* could recue mice which have already developed symptoms as XLCNM patients are born with the disease. Reversion of the disease has been seen by other therapeutic strategy (Childers et al., 2014; Tasfaout et al., 2017) so may be possible here too.

The overexpression of BIN1 through AAV delivery could be an alternative to the *MTM1* gene replacement which is already in clinical trial to rescue the XLCNM myopathy (Buj-Bello et al., 2008; Childers et al., 2014; Mack et al., 2017). The majority of XLCNM patients have no detectable MTM1 protein expression, therefore it remains to be seen if overexpression of MTM1 by gene therapy may trigger an immune response in patients. We hypothesize that modulating BIN1 level may not cause any immune response as BIN1 is normally expressed in the XLCNM patients.

To further understand the BIN1 protein domain responsible for the rescue, I injected several AAV- *BIN1* isoforms/constructs (Results part 2b). I performed intramuscular injection of AAV-*BIN1* BAR* domain (BAR and PI domains), AAV-*BIN1* isoform 9 and AAV-*BIN1* isoform 8 with the inclusion of the exon 7 in WT and XLCNM mouse model. The injection of the BAR* constructs improves skeletal muscle force. However, the histology still displayed internal nuclei and small muscle fibers. The best rescue of the force and of the histology was obtained injecting AAV-*BIN1* ubiquitous isoform 9. The BIN1 isoform 9 does not include the PI domain (exon 11) but still has the same BAR and SH3 domain sequence of the BIN1 isoform 8. On the other hand, no rescue of the force and of the histological phenotype was observed in BIN1 isoform 8 with the inclusion of exon 7 (BIN1 isoform 8 + exon 7). The presence of exon 7 seems to reinforce the interaction of BIN1 with DNM2 (Ellis et al., 2012) which may sequester the pool of DNM2, necessary for other cellular mechanisms. Furthermore, as the best rescue of muscle force and histology was observed with BIN1 isoform 9, we can hypothesize that the PI domain is probably not needed for *Mtm1-/y* muscle rescue. The PI domain is known to increase the affinity of BIN1 with phosphoinositide and it interacts with SH3 domain of BIN1 itself (Kojima et al., 2004; Lee et al., 2002). This interaction masks the SH3 domain to its ligands promoting BIN1 closed conformation. For the *Mtm1-/y* rescue it is necessary that BIN1 is in open conformation to allow the BAR and SH3 domains to interacts with their partners. The BAR domain is involved in membrane remodeling and dimerizes with other BAR domain proteins. It is possible that the exogenous BAR* domain injected in muscle dimerizes with the endogenous full length BIN1 to bind phosphoinositide and initiates the membrane curvature. However, as the injection of the BAR* construct allows a rescue only of the *Mtm1*-/y muscle force, we can hypothesize that membrane remodeling activity is not the only one needed. Histological analysis of muscle injected with BAR* domain showed defects in nuclei position and SDH staining which may suggest that the lack of SH3 domain, involved in DNM2 interaction, impacts on muscle maintenance and mitochondria organization. Further assays need to be conducted to verify the overexpression of only SH3 domain can rescue *Mtm1* muscle phenotype. The identification of the domain necessary to rescue *Mtm1-/y* muscle will facilitate the therapeutic application. In addition, it will suggest which function of BIN1 is necessary for the rescue allowing to better understand the pathophysiological mechanism of the XLCNM. However, we cannot exclude the implication of more BIN1 domains in the XLCNM rescue.

In addition, further investigation need to be conducted in the WT muscle transduced with the different BIN1 constructs. The overexpression of human BIN1 caused high level of inflammation that was not observed in the *Mtm1*-/y mice.

BIN1 level modulation rescues Dnm2 $^{R465W/+}$ muscle histology and Dnm2 $^{R465W/R465W}$ life span.

The most common gain-of-function ADCNM mutation in *DNM2* is the R465W. This mutation causes a mild late onset form of the disease (Bitoun et al., 2005; Romero and Bitoun, 2011). The *Dnm2* $^{R465W/+}$ mouse model has been created to better investigate the mechanism of the disease. This mouse model has a mild phenotypes without defects in their life span and growth, however, this mutation mainly impact on muscle atrophy and histology (Durieux et al., 2010). The *Dnm2* $^{R465W/+}$ TA muscle weight is reduced compared the WT and transverse TA muscle sections has increased number of fibers with abnormal oxidative staining. Interestingly, overexpression of BIN1 during embryogenesis ameliorates the histological defects in *Dnm2* $^{R465W/+}$ mouse model. We verified if the overexpression of BIN1 after birth could improve the histological defects described in *Dnm2* $^{R465W/+}$ mouse model. As in the *Dnm2* $^{R465W/+}$ Tg *BIN1* mice*,* AAV-*BIN1* overexpression resulted in no improvement in *in situ* muscle force but improvement in skeletal muscle histology compared to the *Dnm2* $^{R465W/+}$ mice. To date the majority of the published studies on ADCNM have been conducted on the *Dnm2* $^{R465W/+}$ mice as the *Dnm2* $^{R465W/R465W}$ were shown to be lethal at birth. However, the *Dnm2* $^{R465W/+}$ have a mild phenotypes and the impacts on a therapy may be difficult to be studied. So, we decided to verify if the overexpression of BIN1 could rescue the severe *Dnm2* $^{R465W/R465W}$ mouse model by genetic cross. *Dnm2* $^{R465W/R465W}$ Tg *BIN1* rescued the premature death. Interestingly, skeletal muscle force and histology of *Dnm2* $^{R465W/R465W}$ Tg *BIN1* were similar to *Dnm2* $^{R465W/+}$ mice untreated. This data suggests that overexpressing BIN1 is sufficient to trigger a decrease in severity in the homozygous phenotype (Results part 3).

Further investigations need to address how BIN1 reduced the gain-of-function activity of Dnm2 $^{R465W/R465W}$ in mice. BIN1 was shown to inhibit the activity of DNM2 (Cowling et al., 2017) supporting the mutation R465W leads to gain-of function. Recently, Buono *et al*., proposed a genetic cross to reduce DNM2 expression in *Dnm2* $^{R465W/+}$ mice (Buono et al., 2018). *Dnm2* $^{R465W/+}$ mice were crossed with *Dnm2*$^{+/-}$, which are viable and do not have any visible phenotype, to produce *Dnm2* $^{R465W/-}$ (KI/KO). The author obtained reduction in pups proportion with the *Dnm2* $^{R465W/-}$ genotype at birth and the few mice surviving died before 3 weeks of age (Buono et al., 2018). This results suggest that the R465W mutation does not purely lead to a gain-of-function mechanism and that wild-type DNM2 protein is necessary for embryogenesis (Buono et al., 2018).

DNM2 as a therapeutic target for different CNMs

Another therapeutic strategy that has been identified in our laboratory is DNM2 reduction to treat XLCNM and ADCNM in animal models (Buono et al., 2018; Cowling et al., 2014; Tasfaout et al., 2017; Tasfaout et al., 2018b). Cowling *et al.,* rescued *Mtm1-/y* life span

and muscle force reducing DNM2 expressing to 50%. Thanks to this result, two translational approaches have been initiated to target DNM2 in *Mtm1-/y* mice model: the antisense oligonucleotide (ASO) or adeno-associated virus (AAV) using shRNA targeting the *Dnm2* transcript (Cowling et al., 2014; Tasfaout et al., 2017; Tasfaout et al., 2018b). The intramuscular downregulation of DNM2 using the AAVshDNM2 successfully rescue the muscle force and the histological defects. However, we did not conduct systemic injection of AAV-shDNM2 to verify if this approach could rescue also the life span and the total body force of the *Mtm1-/y* mice (Tasfaout et al., 2018b). The systemic DNM2 reduction was tested postnatally only using the ASO delivery and the injections were performed in pre-symptomatic and, more importantly, in post-symptomatic *Mtm1-/y* mice (Tasfaout et al., 2017).

In the last few years great advances have been achieved in the identification of new therapeutic strategy to cure various forms of CNMs (Introduction, Development of therapies). Indeed, recent publications showed that each of these described strategies have their pros and cons. The gene therapy approach allowed a single injection, however, we do not know how long the effect last. The AAV delivery allows more specific tissue targeting, as different AAV serotypes target specific tissues more than others. Furthermore the use of specific promoters can direct more tissue specific expression of transgenes. However, once performed the treatment cannot be modulated, and high doses of AAV are required which may be a limiting factor. In contrast dosing of ASO or other drugs such as tamoxifen can be modulated for each administration and can be withdrawn if needed. However, they require continuous injections or administration placing a heavy burden on the patient and medical system. Furthermore both AAV and ASO can accumulate in certain tissues such liver or kidney, which may cause undesirable side effects.

Recent studies have shown tamoxifen administration may improve XLCNM features in mice. Food supplemented with tamoxifen administered to *Mtm1-/y* mice improved the life span of XLCNM mouse model (Gayi et al., 2018; Maani et al., 2018)The tamoxifen-treated *Mtm1-/y* mice were maintained alive until 7 months of age. Tamoxifen has been already approved by EMA and FDA and it is already used for other diseases suggesting that this therapeutic strategy can be rapidly applied to patients (Gayi et al., 2018; Maani et al., 2018).

It could be interesting in the future to test this strategy for the other CNM forms. Additionally, CRISPR-Cas9 technology may be also developed to target and modify the mutated allele in these monogenic diseases. This innovative therapeutic strategy has been successfully tested in our lab to rescue the *Dnm2* $^{R465W/+}$ primary myoblasts (Rabai *et al*., 2018, accepted). In the future it may be useful to combine different drugs or gene therapy to better rescue the CNMs model.

Conclusion

The common clinical and histological features of the different CNM forms strongly suggest that the mutated proteins causing CNMs function in a common pathway in skeletal muscle. Modifying the expression level of a CNM gene to rescue the CNM myopathy caused by mutation of another CNM gene ('cross therapy') has greatly improved our knowledge of the function of this pathway and identified new therapeutic targets (Fig.32) (Buono et al., 2018; Cowling et al., 2014; Cowling et al., 2017; Tasfaout et al., 2017; Tasfaout et al., 2018b).

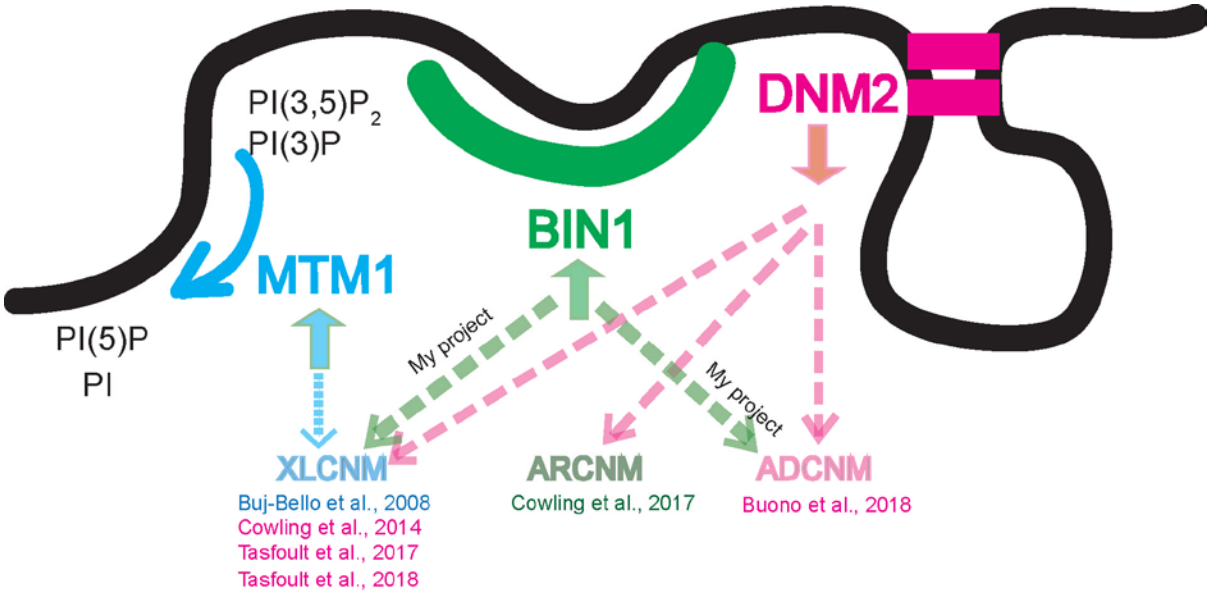

Figure 32: Cross-therapy strategies developed in the last 11 years of research to rescue XLCNM, ARCNM and ADCNM animal model.

The blue arrow refers to the AAV-*MTM1* therapy to rescue XLCNM form. The green arrows refers to the overexpression of BIN1 to rescue XLCNM and ADCNM mouse models. The pink arrows corresponds to the downregulation of DNM2 to cure XLCNM, ARCNM and ADCNM.

MTM1-BIN1- DNM2 protein level in the XLCNM mouse model.

Analysis conducted on *Mtm1-/y* skeletal muscle protein lysates showed an increase in DNM2 and BIN1 protein level in *Mtm1-/y* compared to WT control (Cowling et al., 2014) (Results part 2, Fig. 1).

As decreasing the genetic dosage of DNM2 (Cowling et al., 2014; Tasfaout et al., 2017; Tasfaout et al., 2018b)(Results part 1) improves the XLCNM phenotype of *Mtm1-/y* mice, we hypothesized that the increase of DNM2 expression level was probably pathogenic in XLCNM mouse model (Fig. 33 A). So, we expected that the downregulation strategy could be applied also for BIN1 level. We decreased BIN1 protein level in *Mtm1-/y* mice by genetic cross; the *Mtm1-/y Bin1-/+* mice die before birth suggesting that lowering BIN1 protein level strongly aggravates the *Mtm1-/y* phenotype (Fig.33 B) (Results part 2, Table 1). In contrast, when BIN1 protein level is positively modulated in *Mtm1-/y* mice, it rescues the *Mtm1-/y* mice life span and the XLCNM phenotype (Results part 2) (Fig.33 B). As increasing the level of BIN1 rescues the *Mtm1-/y* mouse model, we hypothesized that the increase of BIN1 protein level obtained in *Mtm1-/y* skeletal muscle is compensation for the lack of MTM1 in the pathology condition and it is not the cause of the pathological phenotype. BIN1 level is 2-fold higher in *Mtm1-/y* skeletal muscle compared to the WT control at 7 weeks. The increase of BIN1 protein level is not high enough to rescue the XLCNM phenotypes and life span. Around 3-fold overexpression is probably a threshold to overpass in order to rescue the *Mtm1-/y* mice phenotype and life span. Indeed, the level of BIN1 necessary to rescue the *Mtm1-/y* phenotype is 4 times more in the *Mtm1-/y* Tg *BIN1* and around 3 times more in the intramuscular and systemically injected mice. In addition, the increase of BIN1 level in *Mtm1-/y* skeletal muscle was not observed before 7 weeks of age which age corresponds to an advance stage of the disease. Indeed, 5 weeks old *Mtm1-/y* mice have the same BIN1 level than the WT control (Results part 2a, Fig. 4). We cannot exclude that the increase of BIN1 protein level happens in a late stage of the disease and it is not high enough to drive the reversion of the phenotype. However, we cannot exclude that the increased level of BIN1 is due to a defects in protein degradation. *Mtm1-/y* mice have defects in autophagy and proteasome in skeletal muscle causing an accumulation of misfolded and folded proteins.

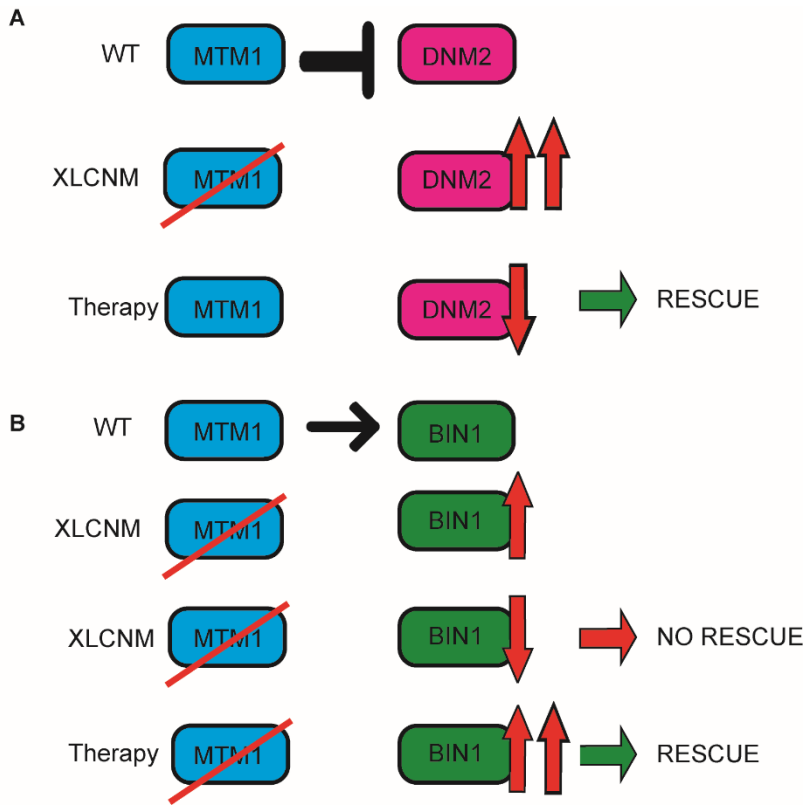

Figure 33: Cross-therapy strategies.

A, DNM2 protein level is higher in *Mtm1-/y* skeletal muscle lysate than the WT control. To rescue XLCNM mouse model, DNM2 level was decreased 50%. **B**, BIN1 level is higher in *Mtm1-/y* skeletal muscle lysate than the WT control. Downregulation of BIN1 level did not rescue XLCNM. Overexpression of BIN1 rescued XLCNM in mouse model.

MTM1-BIN1-DNM2 could be part of a common pathway.

Loss-of-functions mutations on *MTM1* and *BIN1* or gain-of-function mutations on *DNM2* cause different form of CNMs (Bitoun et al., 2005; Laporte et al., 2000; Nicot et al., 2007). The in vivo relationship between *MTM1-DNM2* and *BIN1-DNM2* was previously investigated (Cowling et al., 2014; Cowling et al., 2017). As lowering the level of DNM2 rescues the skeletal muscle phenotype and life span in *Mtm1-/y* mice, it suggests that in physiological conditions MTM1 is negatively regulating DNM2 (Cowling et al., 2014; Tasfaout et al., 2017; Tasfaout et al., 2018b) and (Results part 1). In addition, *Bin1*KO mouse model dies directly after birth but its life span is rescued by downregulating DNM2 protein level (Cowling et al., 2017) raising the possibility that BIN1 and DNM2 are linked and that BIN1 negatively regulates DNM2 (Introduction, Cross-therapies). This hypothesis is also confirmed by the data presented in Result part 3 where the histological phenotype and life span of the mice models *Dnm2* $^{R465W/+}$ *and Dnm2* $^{R465W/R465W}$ are rescued by overexpressing systemically BIN1 after birth. However, no investigation has been conducted on the relationship between MTM1-BIN1. Our recent results presented in the Results part 2 showed that modulation of BIN1 protein level rescues the lack of MTM1 in skeletal muscle suggesting that MTM1 positively regulating BIN1.

Based on all these results, we can conclude that MTM1, BIN1 and DNM2 are part of a common pathway. In the lab we like to call it the "MAD pathway" (MTM1, Amphiphysin 2, Dynamin pathway). We can imagine that MTM1 is positively regulating BIN1 which in turns negatively regulate DNM2 (linear pathway) (Fig. 34 A). We can also imagine that this pathway is not "linear" but that MTM1, BIN1 and DNM2 are part of a "triangular" pathway where MTM1 positively regulates BIN1 and both converge to negative regulate DNM2 (Fig.34 B). In order to better understand if this pathway is "linear" or "triangular" further experiments need to be conducted. Overexpression of MTM1 protein level in the severe *Bin1*KO mouse model would help to understand if the pathway is linear. If the overexpression of MTM1 does not rescue the *Bin1* KO mouse model, it would suggest that BIN1 is needed to regulate DNM2 and so the pathway MTM1, BIN1 and DNM2 is probably linear. In contrast, if *Bin1* KO mouse phenotype is rescued by the overexpression of MTM1, it suggests that MTM1 and BIN1 are both negatively regulating DNM2 ("triangular" pathway). We cannot exclude the presence of additional proteins which could mediate the relationship between MTM1, BIN1 and DNM2 and which may be involved in the MAD pathway.

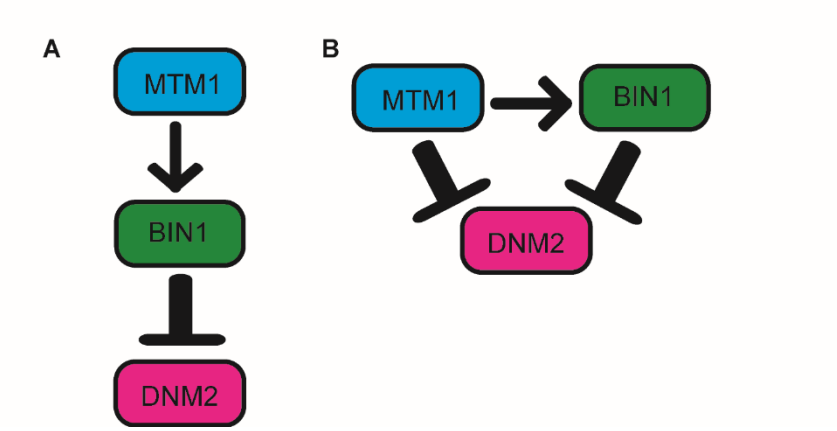

Figure 34: Linear or triangular MAD pathway.

A, Linear pathway: MTM1 positively regulates BIN1 which negatively regulates DNM2. **B**, Triangular pathway if MTM1 positively regulates BIN1 and both negatively regulate DNM2.

The pathological mechanisms in XLCNM.

The main histological feature of CNMs patients are the small and rounder skeletal muscle fibers which suggest defect in the adhesion between each other and defect in the extracellular matrix proteins. Our results showed that *Mtm1-/y* skeletal muscle have increased interfiber space, abnormal level of collagen and laminin (extracellular matrix proteins) and abnormal internalized β1 integrin.

Endosomal recycling defects in Mtm1-/y muscle

It is known that β1 integrin is part of the focal adhesion, in skeletal muscle focal adhesion proteins are important mechano-transduction and they are located in the costamere. β1 integrin abnormally accumulated in the center of *Mtm1-/y* muscle fibers in XLCNM patient fibroblasts and in XLCNM Drosophila model (Ketel et al., 2016; Ribeiro et al., 2011). We observed that β1 integrin is blocked in early recycling endosomes (EEA1 positive) in the *Mtm1-/y* muscle fibers. These endosomes are enriched of PtIns(3)P and PtIns(3,5)P_2 and as loss of MTM1 impacts on the cleavage of the phosphate, it affects the endosomal recycling. Ketel *et al*., showed β1 integrin colocalization with early endosomal marker Rab5 and with late endosomal marker Rab7 in XLCNM patient fibroblasts. As we did not have a specific late endosomal antibody, we could not get to the same conclusion. Our observation suggests that β1 integrin recycling is blocked from the early to late endosomes when MTM1 is not expressed.

Observations by confocal microscopy showed that β1 integrin positive endosomes were enlarged in *Mtm1-/y* skeletal muscle and primary myoblasts compared to WT muscle fiber and primary cells. I did not investigate further if the enlarged endosomes were the consequence of PtIns(3)P endosomes fusion when they are blocked inside the cells. However, the impairment of endosomal recycling affects the homeostasis of the cells as impacts on lysosomal activity and membrane trafficking. We cannot exclude that the blocked β1 integrin in *Mtm1-/y* muscle fibers is the consequence of a malfunction recycling to lysosome. In addition there was no difference in *β1 integrin* transcription level between the WT and *Mtm1-/y* muscle fibers whereas β1 integrin protein level is higher in *Mtm1-/y* skeletal muscle than in WT. These data raise the hypothesis that the endosomal recycling defect observed in *Mtm1-/y* muscle fiber affects β1 integrin shuttle through late endosomes to lysosomes for degradation.

Consequences of altered integrin trafficking

In skeletal muscle integrin turnover allows flexible response to muscle tension and helps the maintenance of muscle fibers adhesion to the extracellular matrix. In addition,

integrin turnover is important for maintaining tension between muscle fibers and tendons in the myotendinous junctions (Olsen et al., 2019).

We observed that the majority of the Mtm1-/y muscle fibers with abnormal β1 integrin accumulations corresponds to the fibers with the severe muscle phenotype, round shape and nuclei position in the center. It is still unclear when the aggregation of integrin start to accumulates inside the muscle fibers. We hypothesize that this phenotype worsen with the progression of the disease. *Mtm1-/y* mice have increase in laminin protein level and collagen staining which may be associated with integrin recycling defects. Integrins directly interact and promote the auto-phosphorylation of FAK which participate in regulating cell differentiation, proliferation, movement and proliferation. *Mtm1-/y* skeletal muscle have a reduction in FAK auto-phosphorylation compared to WT skeletal muscle (Results part 2).

As the investigation of integrin recycling defects are difficult to conduct in skeletal muscle fibers, we decided to continue our study in WT and *Mtm1-/y* primary myoblasts. Primary myoblasts were extracted from 6 days *Mtm1-/y* pups which still not manifest XLCNM phenotype. However, *Mtm1-/y* primary myoblasts recapitulated the abnormal integrin inclusion phenotype observed in adult skeletal muscle. In addition, they showed defects in cell adhesion and migration which confirm a problem in integrins recycling. In addition, *Mtm1-/y* primary myoblasts had fusion defects, a feature previously described in *β1 integrin* KO and FAK KO myoblasts (Introdustion, Integrins in skeletal muscle) (Schwander et al., 2003). The reduction in fusion index recapitulates the myofiber hypotrophy which is a typical XLCNM phenotype.

β1 integrin KO mice die at birth because of muscle atrophy and respiratory problems (Schwander et al., 2003), common phenotypes with XLCNM patients. Because of the post-birth dead, no study has been conducted on *β1 integrin* KO nuclear position in skeletal muscle, however, chimeric *α5 integrin* KO mice showed abnormal nuclear position in adult skeletal muscle (Taverna et al., 1998). Furthermore, depletion of *α5 integrin* or inhibition of FAK and Src negatively impact on positioning nuclei in the periphery of the myotubes suggesting the implication of the focal adhesion pathway in controlling nuclear position (Roman et al., 2018). Centralize nuclear position is a common feature of all the CNMs forms suggesting the involvement of MTM1, BIN1 and DNM2 in nuclei position pathway. Previous studies demonstrated that BIN1 bridges nesprin to the microtubules and interacts with actin cytoskeleton which allows to regulate nuclei position (D'Alessandro et al., 2015). We can hypothesize that the defects in focal adhesion recycling observed in XLCNM mouse model and primary cells not only impacts the adhesion of muscle fibers to the extracellular matrix but also plays a role on maintaining the nucleus on the periphery of muscle fibers. Indeed, the

majority of *Mtm1-/y* muscle fibers with internalized integrin in skeletal muscle accumulation are smaller, rounder and the nuclei position in the center of the fibers.

BIN1 overexpression rescue β1 integrin recycling

We observed that BIN1 overexpression rescued the life span, muscle force and histology abnormality of *Mtm1-/y* skeletal muscle. BIN1 is involved in membrane remodeling and trafficking binding the phosphoinositide in the plasma membrane. We observed that the overexpression of BIN1 rescues the abnormal integrin internalization observed in the *Mtm1-/y* muscle fibers (Results Part 2a) (Fig.35 B).

In vitro experiments proved that BIN1 preferably binds PtIns(4,5)P_2 and PtIns4P. On the contrary, β1 integrin positive endosomes are enriched with PtIns3P and PtIns(3,5)P_2 in *Mtm1-/y* skeletal muscle. Only small amount of PtIns(4,5)P_2 are localized on the sorting endosomes (Billcliff and Lowe, 2014). It may be possible that in non-treated *Mtm1-/y* mice, the recycling is blocked; the endogenous BIN1 does not bind the enlarged PtIns3P and PtIns(3,5)P_2 early endosomes. We hypothesize that in *Mtm1-/y* Tg *BIN1* mice the increased BIN1 protein level promotes unspecific binding of BIN1 to phosphoinositide which are normally not recognize by BIN1. The exogenous BIN1 binds the accumulated early endosomes and allows their sorting to late endosomes or lysosomes. In addition, we hypothesize that BIN1 does not act alone but may recruit or be recruited by other partners necessary for membrane recycling. One example could be DNM2 which interacts via its PRD domain with BIN1. Previous studies showed that DNM2 is involved in focal adhesion disassembling. After β1 integrin binding with its ligand, FAK auto-phosphorylates and recruits Src protein at the focal adhesion complex, which in turn recruits DNM2. As confocal pictures showed that FAK phosphoY397 colocalized with some internalized β1 integrin in skeletal muscle, we hypothesize that SRC, DNM2 and finally BIN1 are recruited in these early endosomes. BIN1 tubulates the membrane of the early endosomes and DNM2 surrounded the tubules causing membrane fission. In addition, the increased amount of BIN1 may impact on DNM2 activity such as membrane fission (Fig.35 B) (Cowling et al., 2017).

To confirm these hypotheses further experiments could be conducted to investigate if *Bin1*KO muscle fibers exhibit defects in endosome recycling. In addition, it would be interesting to investigate if DNM2 and the exogenous BIN1 localizes on β1 integrin endosomes in *Mtm1-/y* mice.

To conclude, our experiments confirmed that MTM1 and BIN1 are involved in endosome trafficking. We have also identified that integrin recycling pathway is abnormal in *Mtm1-/y* skeletal muscle and that *Mtm1-/y* primary myoblasts are a good model to study integrin defects. In addition, we have identified that focal adhesion integrity and pathway are

altered in XLCNM mouse model. Our results prove a relationship of MTM1, BIN1 and integrins and suggests that focal adhesion pathway may be downstream MTM1 and BIN1 in skeletal muscle. However, β1 integrin recycling is not the only pathway deregulated in the XLCNM muscle. It is plausible that MTM1 and BIN1 plays a broader role and that more pathways are

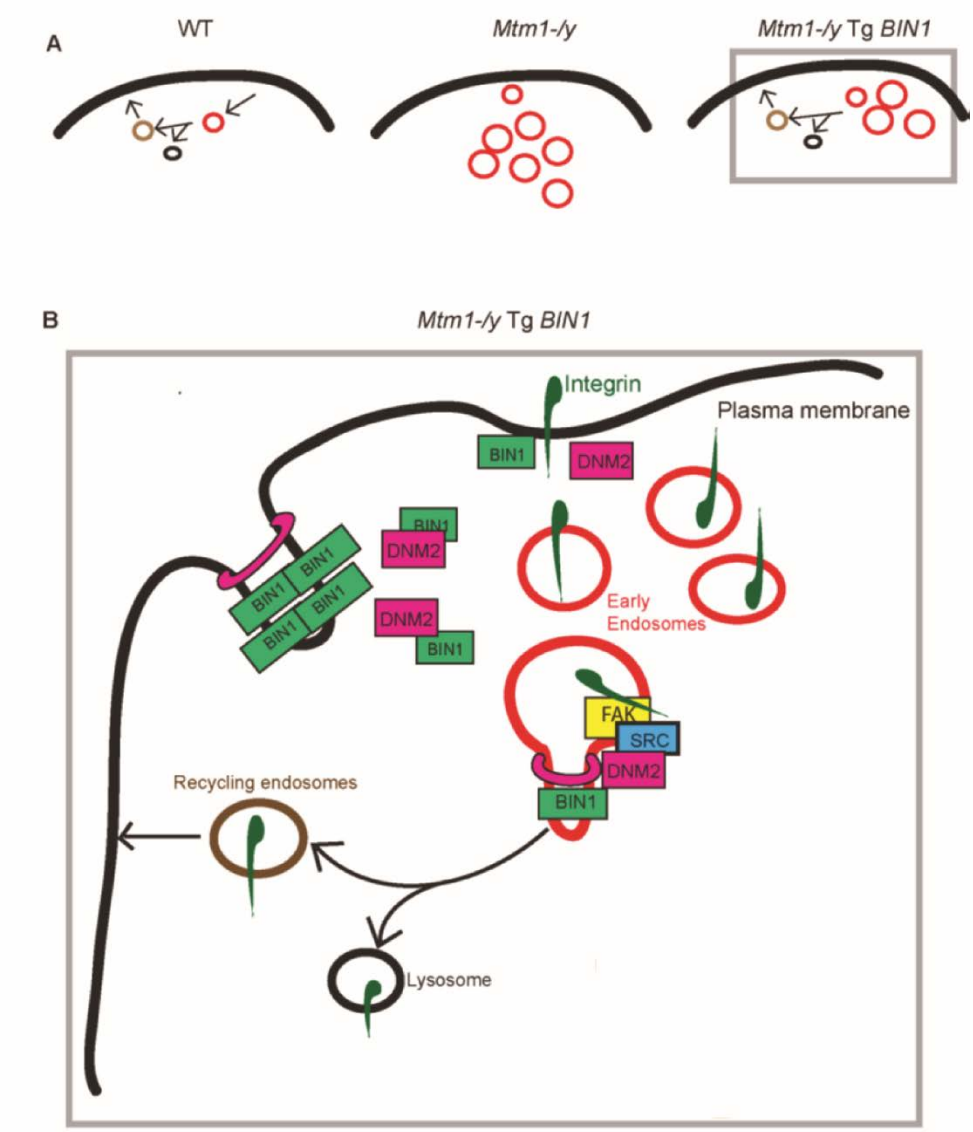

involved in the rescue of the life span of XLCNM.

Figure 35: Schematic representation of integrin recycling.

A, Recycling in WT, *Mtm1-/y* and *Mtm1-/y* Tg *BIN1 muscle fibers. Mtm1-*/y fibers have higher amount of early endosomes. **B,** The overexpression of BIN1 allows membrane tabulation of early endosomes facilitating recycling. In addition it binds free DNM2 in cells regulating its activity.

Bibliography

Abercrombie, M., Heaysman, J.E., and Pegrum, S.M. (1971). The locomotion of fibroblasts in culture. IV. Electron microscopy of the leading lamella. Exp Cell Res *67*, 359-367.

Adam, J., Basnet, N., and Mizuno, N. (2015). Structural insights into the cooperative remodeling of membranes by amphiphysin/BIN1. Sci Rep *5*, 15452.

Aghbolaghi, A.G., and Lechpammer, M. (2017). A rare case of centronuclear myopathy with DNM2 mutation: genotype-phenotype correlation. Autops Case Rep *7*, 43-48.

Agrawal, P.B., Pierson, C.R., Joshi, M., Liu, X., Ravenscroft, G., Moghadaszadeh, B., Talabere, T., Viola, M., Swanson, L.C., Haliloglu, G.*, et al.* (2014). SPEG Interacts with Myotubularin, and Its Deficiency Causes Centronuclear Myopathy with Dilated Cardiomyopathy. Am J Hum Genet *95*, 218-226.

Al-Qusairi, L., and Laporte, J. (2011). T-tubule biogenesis and triad formation in skeletal muscle and implication in human diseases. Skelet Muscle *1*, 26.

Al-Qusairi, L., Prokic, I., Amoasii, L., Kretz, C., Messaddeq, N., Mandel, J.L., and Laporte, J. (2013). Lack of myotubularin (MTM1) leads to muscle hypotrophy through unbalanced regulation of the autophagy and ubiquitin-proteasome pathways. FASEB J *27*, 3384-3394.

Al-Qusairi, L., Weiss, N., Toussaint, A., Berbey, C., Messaddeq, N., Kretz, C., Sanoudou, D., Beggs, A.H., Allard, B., Mandel, J.L.*, et al.* (2009). T-tubule disorganization and defective excitation-contraction coupling in muscle fibers lacking myotubularin lipid phosphatase. Proc Natl Acad Sci U S A *106*, 18763-18768.

Alanko, J., and Ivaska, J. (2016). Endosomes: Emerging Platforms for Integrin-Mediated FAK Signalling. Trends Cell Biol *26*, 391-398.

Amburgey, K., Tsuchiya, E., de Chastonay, S., Glueck, M., Alverez, R., Nguyen, C.T., Rutkowski, A., Hornyak, J., Beggs, A.H., and Dowling, J.J. (2017). A natural history study of X-linked myotubular myopathy. Neurology *89*, 1355-1364.

Amoasii, L., Hnia, K., Chicanne, G., Brech, A., Cowling, B.S., Muller, M.M., Schwab, Y., Koebel, P., Ferry, A., Payrastre, B.*, et al.* (2013). Myotubularin and PtdIns3P remodel the sarcoplasmic reticulum in muscle in vivo. J Cell Sci *126*, 1806-1819.

Anderson, L.R., Owens, T.W., and Naylor, M.J. (2014). Integrins in development and cancer. Biophys Rev *6*, 191-202.

Antonny, B., Burd, C., De Camilli, P., Chen, E., Daumke, O., Faelber, K., Ford, M., Frolov, V.A., Frost, A., Hinshaw, J.E.*, et al.* (2016). Membrane fission by dynamin: what we know and what we need to know. EMBO J *35*, 2270-2284.

Arjonen, A., Alanko, J., Veltel, S., and Ivaska, J. (2012). Distinct recycling of active and inactive beta1 integrins. Traffic *13*, 610-625.

Beggs, A.H., Bohm, J., Snead, E., Kozlowski, M., Maurer, M., Minor, K., Childers, M.K., Taylor, S.M., Hitte, C., Mickelson, J.R.*, et al.* (2010). MTM1 mutation associated with X-linked myotubular myopathy in Labrador Retrievers. Proc Natl Acad Sci U S A *107*, 14697-14702.

Biancalana, V., Caron, O., Gallati, S., Baas, F., Kress, W., Novelli, G., D'Apice, M.R., Lagier-Tourenne, C., Buj-Bello, A., Romero, N.B.*, et al.* (2003). Characterisation of mutations in 77 patients with X-linked myotubular myopathy, including a family with a very mild phenotype. Hum Genet *112*, 135-142.

Biancalana, V., Scheidecker, S., Miguet, M., Laquerriere, A., Romero, N.B., Stojkovic, T., Abath Neto, O., Mercier, S., Voermans, N., Tanner, L.*, et al.* (2017). Affected female carriers of MTM1 mutations display a wide spectrum of clinical and pathological involvement: delineating diagnostic clues. Acta Neuropathol *134*, 889-904.

Billcliff, P.G., and Lowe, M. (2014). Inositol lipid phosphatases in membrane trafficking and human disease. Biochem J *461*, 159-175.

Bitoun, M., Durieux, A.C., Prudhon, B., Bevilacqua, J.A., Herledan, A., Sakanyan, V., Urtizberea, A., Cartier, L., Romero, N.B., and Guicheney, P. (2009). Dynamin 2 mutations associated with human diseases impair clathrin-mediated receptor endocytosis. Hum Mutat *30*, 1419-1427.

Bitoun, M., Maugenre, S., Jeannet, P.Y., Lacene, E., Ferrer, X., Laforet, P., Martin, J.J., Laporte, J., Lochmuller, H., Beggs, A.H*., et al.* (2005). Mutations in dynamin 2 cause dominant centronuclear myopathy. Nat Genet *37*, 1207-1209.
Bloch, R.J., and Gonzalez-Serratos, H. (2003). Lateral force transmission across costameres in skeletal muscle. Exerc Sport Sci Rev *31*, 73-78.
Blondeau, F., Laporte, J., Bodin, S., Superti-Furga, G., Payrastre, B., and Mandel, J.L. (2000). Myotubularin, a phosphatase deficient in myotubular myopathy, acts on phosphatidylinositol 3-kinase and phosphatidylinositol 3-phosphate pathway. Hum Mol Genet *9*, 2223-2229.
Bohm, J., Biancalana, V., Malfatti, E., Dondaine, N., Koch, C., Vasli, N., Kress, W., Strittmatter, M., Taratuto, A.L., Gonorazky, H*., et al.* (2014). Adult-onset autosomal dominant centronuclear myopathy due to BIN1 mutations. Brain *137*, 3160-3170.
Bohm, J., Vasli, N., Maurer, M., Cowling, B., Shelton, G.D., Kress, W., Toussaint, A., Prokic, I., Schara, U., Anderson, T.J*., et al.* (2013). Altered Splicing of the BIN1 Muscle-Specific Exon in Humans and Dogs with Highly Progressive Centronuclear Myopathy. PLoS Genet *9*, e1003430.
Bottcher, R.T., Stremmel, C., Meves, A., Meyer, H., Widmaier, M., Tseng, H.Y., and Fassler, R. (2012). Sorting nexin 17 prevents lysosomal degradation of beta1 integrins by binding to the beta1-integrin tail. Nat Cell Biol *14*, 584-592.
Brinas, L., Vassilopoulos, S., Bonne, G., Guicheney, P., and Bitoun, M. (2013). Role of dynamin 2 in the disassembly of focal adhesions. J Mol Med (Berl) *91*, 803-809.
Buj-Bello, A., Biancalana, V., Moutou, C., Laporte, J., and Mandel, J.L. (1999). Identification of novel mutations in the MTM1 gene causing severe and mild forms of X-linked myotubular myopathy. Hum Mutat *14*, 320-325.
Buj-Bello, A., Fougerousse, F., Schwab, Y., Messaddeq, N., Spehner, D., Pierson, C.R., Durand, M., Kretz, C., Danos, O., Douar, A.M*., et al.* (2008). AAV-mediated intramuscular delivery of myotubularin corrects the myotubular myopathy phenotype in targeted murine muscle and suggests a function in plasma membrane homeostasis. Hum Mol Genet *17*, 2132-2143.
Buj-Bello, A., Furling, D., Tronchere, H., Laporte, J., Lerouge, T., Butler-Browne, G.S., and Mandel, J.L. (2002a). Muscle-specific alternative splicing of myotubularin-related 1 gene is impaired in DM1 muscle cells. Hum Mol Genet *11*, 2297-2307.
Buj-Bello, A., Laugel, V., Messaddeq, N., Zahreddine, H., Laporte, J., Pellissier, J.F., and Mandel, J.L. (2002b). The lipid phosphatase myotubularin is essential for skeletal muscle maintenance but not for myogenesis in mice. Proc Natl Acad Sci U S A *99*, 15060-15065.
Buono, S., Ross, J.A., Tasfaout, H., Levy, Y., Kretz, C., Tayefeh, L., Matson, J., Guo, S., Kessler, P., Monia, B.P*., et al.* (2018). Reducing dynamin 2 (DNM2) rescues DNM2-related dominant centronuclear myopathy. Proc Natl Acad Sci U S A *115*, 11066-11071.
Burridge, K. (2017). Focal adhesions: a personal perspective on a half century of progress. FEBS J *284*, 3355-3361.
Butler, M.H., David, C., Ochoa, G.C., Freyberg, Z., Daniell, L., Grabs, D., Cremona, O., and De Camilli, P. (1997). Amphiphysin II (SH3P9; BIN1), a member of the amphiphysin/Rvs family, is concentrated in the cortical cytomatrix of axon initial segments and nodes of Ranvier in brain and around T tubules in skeletal muscle. J Cell Biol *137*, 1355-1367.
Campbell, I.D., and Humphries, M.J. (2011). Integrin structure, activation, and interactions. Cold Spring Harb Perspect Biol *3*.
Cao, C., Backer, J.M., Laporte, J., Bedrick, E.J., and Wandinger-Ness, A. (2008). Sequential actions of myotubularin lipid phosphatases regulate endosomal PI(3)P and growth factor receptor trafficking. Mol Biol Cell *19*, 3334-3346.
Cao, C., Laporte, J., Backer, J.M., Wandinger-Ness, A., and Stein, M.P. (2007). Myotubularin lipid phosphatase binds the hVPS15/hVPS34 lipid kinase complex on endosomes. Traffic *8*, 1052-1067.
Cao, H., Garcia, F., and McNiven, M.A. (1998). Differential distribution of dynamin isoforms in mammalian cells. Mol Biol Cell *9*, 2595-2609.
Capes, E.M., Loaiza, R., and Valdivia, H.H. (2011). Ryanodine receptors. Skelet Muscle *1*, 18.

Carmignac, V., and Durbeej, M. (2012). Cell-matrix interactions in muscle disease. J Pathol *226*, 200-218.
Cassandrini, D., Trovato, R., Rubegni, A., Lenzi, S., Fiorillo, C., Baldacci, J., Minetti, C., Astrea, G., Bruno, C., Santorelli, F.M.*, et al.* (2017). Congenital myopathies: clinical phenotypes and new diagnostic tools. Ital J Pediatr *43*, 101.
Ceyhan-Birsoy, O., Agrawal, P.B., Hidalgo, C., Schmitz-Abe, K., DeChene, E.T., Swanson, L.C., Soemedi, R., Vasli, N., Iannaccone, S.T., Shieh, P.B.*, et al.* (2013). Recessive truncating titin gene, TTN, mutations presenting as centronuclear myopathy. Neurology *81*, 1205-1214.
Chappie, J.S., Acharya, S., Liu, Y.W., Leonard, M., Pucadyil, T.J., and Schmid, S.L. (2009). An intramolecular signaling element that modulates dynamin function in vitro and in vivo. Mol Biol Cell *20*, 3561-3571.
Chapuis, J., Hansmannel, F., Gistelinck, M., Mounier, A., Van Cauwenberghe, C., Kolen, K.V., Geller, F., Sottejeau, Y., Harold, D., Dourlen, P.*, et al.* (2013). Increased expression of BIN1 mediates Alzheimer genetic risk by modulating tau pathology. Mol Psychiatry *18*, 1225-1234.
Childers, M.K., Joubert, R., Poulard, K., Moal, C., Grange, R.W., Doering, J.A., Lawlor, M.W., Rider, B.E., Jamet, T., Daniele, N.*, et al.* (2014). Gene therapy prolongs survival and restores function in murine and canine models of myotubular myopathy. Sci Transl Med *6*, 220ra210.
Chin, Y.H., Lee, A., Kan, H.W., Laiman, J., Chuang, M.C., Hsieh, S.T., and Liu, Y.W. (2015). Dynamin-2 mutations associated with centronuclear myopathy are hypermorphic and lead to T-tubule fragmentation. Hum Mol Genet *24*, 5542-5554.
Claeys, K.G., Maisonobe, T., Bohm, J., Laporte, J., Hezode, M., Romero, N.B., Brochier, G., Bitoun, M., Carlier, R.Y., and Stojkovic, T. (2010). Phenotype of a patient with recessive centronuclear myopathy and a novel BIN1 mutation. Neurology *74*, 519-521.
Couchman, J.R., and Rees, D.A. (1979). The behaviour of fibroblasts migrating from chick heart explants: changes in adhesion, locomotion and growth, and in the distribution of actomyosin and fibronectin. J Cell Sci *39*, 149-165.
Cowling, B.S., Chevremont, T., Prokic, I., Kretz, C., Ferry, A., Coirault, C., Koutsopoulos, O., Laugel, V., Romero, N.B., and Laporte, J. (2014). Reducing dynamin 2 expression rescues X-linked centronuclear myopathy. J Clin Invest *124*, 1350-1363.
Cowling, B.S., Prokic, I., Tasfaout, H., Rabai, A., Humbert, F., Rinaldi, B., Nicot, A.S., Kretz, C., Friant, S., Roux, A.*, et al.* (2017). Amphiphysin (BIN1) negatively regulates dynamin 2 for normal muscle maturation. J Clin Invest.
Cowling, B.S., Toussaint, A., Amoasii, L., Koebel, P., Ferry, A., Davignon, L., Nishino, I., Mandel, J.L., and Laporte, J. (2011). Increased expression of wild-type or a centronuclear myopathy mutant of dynamin 2 in skeletal muscle of adult mice leads to structural defects and muscle weakness. Am J Pathol *178*, 2224-2235.
Cowling, B.S., Toussaint, A., Muller, J., and Laporte, J. (2012). Defective membrane remodeling in neuromuscular diseases: insights from animal models. PLoS Genet *8*, e1002595.
Cui, X., De Vivo, I., Slany, R., Miyamoto, A., Firestein, R., and Cleary, M.L. (1998). Association of SET domain and myotubularin-related proteins modulates growth control. Nat Genet *18*, 331-337.
D'Alessandro, M., Hnia, K., Gache, V., Koch, C., Gavriilidis, C., Rodriguez, D., Nicot, A.S., Romero, N.B., Schwab, Y., Gomes, E.*, et al.* (2015). Amphiphysin 2 Orchestrates Nucleus Positioning and Shape by Linking the Nuclear Envelope to the Actin and Microtubule Cytoskeleton. Dev Cell *35*, 186-198.
Daumke, O., Roux, A., and Haucke, V. (2014). BAR domain scaffolds in dynamin-mediated membrane fission. Cell *156*, 882-892.
de Gouyon, B.M., Zhao, W., Laporte, J., Mandel, J.L., Metzenberg, A., and Herman, G.E. (1997). Characterization of mutations in the myotubularin gene in twenty six patients with X-linked myotubular myopathy. Hum Mol Genet *6*, 1499-1504.
Dowling, J.J., Joubert, R., Low, S.E., Durban, A.N., Messaddeq, N., Li, X., Dulin-Smith, A.N., Snyder, A.D., Marshall, M.L., Marshall, J.T.*, et al.* (2012). Myotubular myopathy and the neuromuscular junction: a novel therapeutic approach from mouse models. Dis Model Mech *5*, 852-859.

Dowling, J.J., Vreede, A.P., Low, S.E., Gibbs, E.M., Kuwada, J.Y., Bonnemann, C.G., and Feldman, E.L. (2009). Loss of myotubularin function results in T-tubule disorganization in zebrafish and human myotubular myopathy. PLoS Genet *5*, e1000372.
Durieux, A.C., Vignaud, A., Prudhon, B., Viou, M.T., Beuvin, M., Vassilopoulos, S., Fraysse, B., Ferry, A., Laine, J., Romero, N.B.*, et al.* (2010). A centronuclear myopathy-dynamin 2 mutation impairs skeletal muscle structure and function in mice. Hum Mol Genet *19*, 4820-4836.
Ellis, J.D., Barrios-Rodiles, M., Colak, R., Irimia, M., Kim, T., Calarco, J.A., Wang, X., Pan, Q., O'Hanlon, D., Kim, P.M.*, et al.* (2012). Tissue-specific alternative splicing remodels protein-protein interaction networks. Mol Cell *46*, 884-892.
Faelber, K., Gao, S., Held, M., Posor, Y., Haucke, V., Noe, F., and Daumke, O. (2013). Oligomerization of dynamin superfamily proteins in health and disease. Prog Mol Biol Transl Sci *117*, 411-443.
Faelber, K., Posor, Y., Gao, S., Held, M., Roske, Y., Schulze, D., Haucke, V., Noe, F., and Daumke, O. (2011). Crystal structure of nucleotide-free dynamin. Nature *477*, 556-560.
Falcone, S., Roman, W., Hnia, K., Gache, V., Didier, N., Laine, J., Aurade, F., Marty, I., Nishino, I., Charlet-Berguerand, N.*, et al.* (2014). N-WASP is required for Amphiphysin-2/BIN1-dependent nuclear positioning and triad organization in skeletal muscle and is involved in the pathophysiology of centronuclear myopathy. EMBO Mol Med *6*, 1455-1475.
Fassler, R., and Meyer, M. (1995). Consequences of lack of beta 1 integrin gene expression in mice. Genes Dev *9*, 1896-1908.
Fetalvero, K.M., Yu, Y., Goetschkes, M., Liang, G., Valdez, R.A., Gould, T., Triantafellow, E., Bergling, S., Loureiro, J., Eash, J.*, et al.* (2013). Defective autophagy and mTORC1 signaling in myotubularin null mice. Mol Cell Biol *33*, 98-110.
Flucher, B.E. (1992). Structural analysis of muscle development: transverse tubules, sarcoplasmic reticulum, and the triad. Dev Biol *154*, 245-260.
Frontera, W.R., and Ochala, J. (2015). Skeletal muscle: a brief review of structure and function. Calcif Tissue Int *96*, 183-195.
Fugier, C., Klein, A.F., Hammer, C., Vassilopoulos, S., Ivarsson, Y., Toussaint, A., Tosch, V., Vignaud, A., Ferry, A., Messaddeq, N.*, et al.* (2011). Misregulated alternative splicing of BIN1 is associated with T tubule alterations and muscle weakness in myotonic dystrophy. Nat Med *17*, 720-725.
Gayi, E., Neff, L.A., Massana Munoz, X., Ismail, H.M., Sierra, M., Mercier, T., Decosterd, L.A., Laporte, J., Cowling, B.S., Dorchies, O.M.*, et al.* (2018). Tamoxifen prolongs survival and alleviates symptoms in mice with fatal X-linked myotubular myopathy. Nat Commun *9*, 4848.
Gibbs, E.M., Davidson, A.E., Telfer, W.R., Feldman, E.L., and Dowling, J.J. (2014). The myopathy-causing mutation DNM2-S619L leads to defective tubulation in vitro and in developing zebrafish. Dis Model Mech *7*, 157-161.
Graham, Z.A., Gallagher, P.M., and Cardozo, C.P. (2015). Focal adhesion kinase and its role in skeletal muscle. J Muscle Res Cell Motil *36*, 305-315.
Guimas Almeida, C., Sadat Mirfakhar, F., Perdigao, C., and Burrinha, T. (2018). Impact of late-onset Alzheimer's genetic risk factors on beta-amyloid endocytic production. Cell Mol Life Sci *75*, 2577-2589.
Hanson, J., and Huxley, H.E. (1953). Structural basis of the cross-striations in muscle. Nature *172*, 530-532.
Harburger, D.S., and Calderwood, D.A. (2009). Integrin signalling at a glance. J Cell Sci *122*, 159-163.
Hayashi, Y.K., Chou, F.L., Engvall, E., Ogawa, M., Matsuda, C., Hirabayashi, S., Yokochi, K., Ziober, B.L., Kramer, R.H., Kaufman, S.J.*, et al.* (1998). Mutations in the integrin alpha7 gene cause congenital myopathy. Nat Genet *19*, 94-97.
Hnia, K., Tronchere, H., Tomczak, K.K., Amoasii, L., Schultz, P., Beggs, A.H., Payrastre, B., Mandel, J.L., and Laporte, J. (2011). Myotubularin controls desmin intermediate filament architecture and mitochondrial dynamics in human and mouse skeletal muscle. J Clin Invest *121*, 70-85.
Hohendahl, A., Roux, A., and Galli, V. (2016). Structural insights into the centronuclear myopathy-associated functions of BIN1 and dynamin 2. J Struct Biol *196*, 37-47.

Hussain, N.K., Jenna, S., Glogauer, M., Quinn, C.C., Wasiak, S., Guipponi, M., Antonarakis, S.E., Kay, B.K., Stossel, T.P., Lamarche-Vane, N.*, et al.* (2001). Endocytic protein intersectin-l regulates actin assembly via Cdc42 and N-WASP. Nat Cell Biol *3*, 927-932.
Huttenlocher, A., and Horwitz, A.R. (2011). Integrins in cell migration. Cold Spring Harb Perspect Biol *3*, a005074.
Hynes, R.O. (2004). The emergence of integrins: a personal and historical perspective. Matrix Biol *23*, 333-340.
Jungbluth, H., Ochala, J., Treves, S., and Gautel, M. (2017). Current and future therapeutic approaches to the congenital myopathies. Semin Cell Dev Biol *64*, 191-200.
Jungbluth, H., and Voermans, N.C. (2016). Congenital myopathies: not only a paediatric topic. Curr Opin Neurol *29*, 642-650.
Jungbluth, H., Wallgren-Pettersson, C., and Laporte, J. (2008). Centronuclear (myotubular) myopathy. Orphanet J Rare Dis *3*, 26.
Kenniston, J.A., and Lemmon, M.A. (2010). Dynamin GTPase regulation is altered by PH domain mutations found in centronuclear myopathy patients. Embo J *29*, 3054-3067.
Ketel, K., Krauss, M., Nicot, A.S., Puchkov, D., Wieffer, M., Muller, R., Subramanian, D., Schultz, C., Laporte, J., and Haucke, V. (2016). A phosphoinositide conversion mechanism for exit from endosomes. Nature *529*, 408-412.
Kim, C., Ye, F., and Ginsberg, M.H. (2011). Regulation of integrin activation. Annu Rev Cell Dev Biol *27*, 321-345.
Kojima, C., Hashimoto, A., Yabuta, I., Hirose, M., Hashimoto, S., Kanaho, Y., Sumimoto, H., Ikegami, T., and Sabe, H. (2004). Regulation of Bin1 SH3 domain binding by phosphoinositides. Embo J *23*, 4413-4422.
Koutsopoulos, O.S., Koch, C., Tosch, V., Bohm, J., North, K.N., and Laporte, J. (2011). Mild functional differences of dynamin 2 mutations associated to centronuclear myopathy and charcot-marie-tooth peripheral neuropathy. PLoS One *6*, e27498.
Laporte, J., Bedez, F., Bolino, A., and Mandel, J.L. (2003). Myotubularins, a large disease-associated family of cooperating catalytically active and inactive phosphoinositides phosphatases. Hum Mol Genet *12 Spec No 2*, R285-292.
Laporte, J., Biancalana, V., Tanner, S.M., Kress, W., Schneider, V., Wallgren-Pettersson, C., Herger, F., Buj-Bello, A., Blondeau, F., Liechti-Gallati, S.*, et al.* (2000). MTM1 mutations in X-linked myotubular myopathy. Hum Mutat *15*, 393-409.
Laporte, J., Blondeau, F., Gansmuller, A., Lutz, Y., Vonesch, J.L., and Mandel, J.L. (2002). The PtdIns3P phosphatase myotubularin is a cytoplasmic protein that also localizes to Rac1-inducible plasma membrane ruffles. J Cell Sci *115*, 3105-3117.
Laporte, J., Guiraud-Chaumeil, C., Tanner, S.M., Blondeau, F., Hu, L.J., Vicaire, S., Liechti-Gallati, S., and Mandel, J.L. (1998). Genomic organization of the MTM1 gene implicated in X-linked myotubular myopathy. Eur J Hum Genet *6*, 325-330.
Laporte, J., Guiraud-Chaumeil, C., Vincent, M.C., Mandel, J.L., Tanner, S.M., Liechti-Gallati, S., Wallgren-Pettersson, C., Dahl, N., Kress, W., Bolhuis, P.A.*, et al.* (1997a). Mutations in the MTM1 gene implicated in X-linked myotubular myopathy. ENMC International Consortium on Myotubular Myopathy. European Neuro- Muscular Center. Hum Mol Genet *6*, 1505-1511.
Laporte, J., Hu, L.J., Kretz, C., Mandel, J.L., Kioschis, P., Coy, J.F., Klauck, S.M., Poustka, A., and Dahl, N. (1996). A gene mutated in X-linked myotubular myopathy defines a new putative tyrosine phosphatase family conserved in yeast. Nat Genet *13*, 175-182.
Laporte, J., Kioschis, P., Hu, L.J., Kretz, C., Carlsson, B., Poustka, A., Mandel, J.L., and Dahl, N. (1997b). Cloning and characterization of an alternatively spliced gene in proximal Xq28 deleted in two patients with intersexual genitalia and myotubular myopathy. Genomics *41*, 458-462.
Laury-Kleintop, L.D., Mulgrew, J.R., Heletz, I., Nedelcoviciu, R.A., Chang, M.Y., Harris, D.M., Koch, W.J., Schneider, M.D., Muller, A.J., and Prendergast, G.C. (2015). Cardiac-specific disruption of Bin1

in mice enables a model of stress- and age-associated dilated cardiomyopathy. J Cell Biochem *116*, 2541-2551.
Lawlor, M.W., Beggs, A.H., Buj-Bello, A., Childers, M.K., Dowling, J.J., James, E.S., Meng, H., Moore, S.A., Prasad, S., Schoser, B.*, et al.* (2016). Skeletal Muscle Pathology in X-Linked Myotubular Myopathy: Review With Cross-Species Comparisons. J Neuropathol Exp Neurol *75*, 102-110.
Lee, E., Marcucci, M., Daniell, L., Pypaert, M., Weisz, O.A., Ochoa, G.C., Farsad, K., Wenk, M.R., and De Camilli, P. (2002). Amphiphysin 2 (Bin1) and T-tubule biogenesis in muscle. Science *297*, 1193-1196.
Leprince, C., Le Scolan, E., Meunier, B., Fraisier, V., Brandon, N., De Gunzburg, J., and Camonis, J. (2003). Sorting nexin 4 and amphiphysin 2, a new partnership between endocytosis and intracellular trafficking. J Cell Sci *116*, 1937-1948.
Liu, Y.W., Lukiyanchuk, V., and Schmid, S.L. (2011). Common membrane trafficking defects of disease-associated dynamin 2 mutations. Traffic *12*, 1620-1633.
Long, C., Amoasii, L., Mireault, A.A., McAnally, J.R., Li, H., Sanchez-Ortiz, E., Bhattacharyya, S., Shelton, J.M., Bassel-Duby, R., and Olson, E.N. (2016). Postnatal genome editing partially restores dystrophin expression in a mouse model of muscular dystrophy. Science *351*, 400-403.
Lorenzo, O., Urbe, S., and Clague, M.J. (2006). Systematic analysis of myotubularins: heteromeric interactions, subcellular localisation and endosome related functions. J Cell Sci *119*, 2953-2959.
Luo, B.H., and Springer, T.A. (2006). Integrin structures and conformational signaling. Curr Opin Cell Biol *18*, 579-586.
Maani, N., Sabha, N., Rezai, K., Ramani, A., Groom, L., Eltayeb, N., Mavandadnejad, F., Pang, A., Russo, G., Brudno, M.*, et al.* (2018). Tamoxifen therapy in a murine model of myotubular myopathy. Nat Commun *9*, 4849.
Mack, D.L., Poulard, K., Goddard, M.A., Latournerie, V., Snyder, J.M., Grange, R.W., Elverman, M.R., Denard, J., Veron, P., Buscara, L.*, et al.* (2017). Systemic AAV8-Mediated Gene Therapy Drives Whole-Body Correction of Myotubular Myopathy in Dogs. Mol Ther *25*, 839-854.
Mao, N.C., Steingrimsson, E., DuHadaway, J., Wasserman, W., Ruiz, J.C., Copeland, N.G., Jenkins, N.A., and Prendergast, G.C. (1999). The murine Bin1 gene functions early in myogenesis and defines a new region of synteny between mouse chromosome 18 and human chromosome 2. Genomics *56*, 51-58.
Marat, A.L., and Haucke, V. (2016). Phosphatidylinositol 3-phosphates-at the interface between cell signalling and membrane traffic. EMBO J *35*, 561-579.
Mayer, U. (2003). Integrins: redundant or important players in skeletal muscle? J Biol Chem *278*, 14587-14590.
Mayer, U., Saher, G., Fassler, R., Bornemann, A., Echtermeyer, F., von der Mark, H., Miosge, N., Poschl, E., and von der Mark, K. (1997). Absence of integrin alpha 7 causes a novel form of muscular dystrophy. Nat Genet *17*, 318-323.
McMahon, H.T., Wigge, P., and Smith, C. (1997). Clathrin interacts specifically with amphiphysin and is displaced by dynamin. FEBS letters *413*, 319-322.
Messina, S., Onofri, F., Bongiorno-Borbone, L., Giovedi, S., Valtorta, F., Girault, J.A., and Benfenati, F. (2003). Specific interactions of neuronal focal adhesion kinase isoforms with Src kinases and amphiphysin. J Neurochem *84*, 253-265.
Muller, A.J., Baker, J.F., DuHadaway, J.B., Ge, K., Farmer, G., Donover, P.S., Meade, R., Reid, C., Grzanna, R., Roach, A.H.*, et al.* (2003). Targeted disruption of the murine Bin1/Amphiphysin II gene does not disable endocytosis but results in embryonic cardiomyopathy with aberrant myofibril formation. Mol Cell Biol *23*, 4295-4306.
Nakashima, H., Kibe, T., and Yokochi, K. (2009). 'Congenital muscular dystrophy caused by integrin alpha7 deficiency'. Dev Med Child Neurol *51*, 245.
Negorev, D., Riethman, H., Wechsler-Reya, R., Sakamuro, D., Prendergast, G.C., and Simon, D. (1996). The Bin1 gene localizes to human chromosome 2q14 by PCR analysis of somatic cell hybrids and fluorescence in situ hybridization. Genomics *33*, 329-331.

Nicot, A.S., Toussaint, A., Tosch, V., Kretz, C., Wallgren-Pettersson, C., Iwarsson, E., Kingston, H., Garnier, J.M., Biancalana, V., Oldfors, A.*, et al.* (2007). Mutations in amphiphysin 2 (BIN1) disrupt interaction with dynamin 2 and cause autosomal recessive centronuclear myopathy. Nat Genet *39*, 1134-1139.
Nishimura, T., Morone, N., and Suetsugu, S. (2018). Membrane re-modelling by BAR domain superfamily proteins via molecular and non-molecular factors. Biochem Soc Trans *46*, 379-389.
North, K.N., Wang, C.H., Clarke, N., Jungbluth, H., Vainzof, M., Dowling, J.J., Amburgey, K., Quijano-Roy, S., Beggs, A.H., Sewry, C.*, et al.* (2014). Approach to the diagnosis of congenital myopathies. Neuromuscul Disord *24*, 97-116.
Olsen, L.A., Nicoll, J.X., and Fry, A.C. (2019). The skeletal muscle fiber: a mechanically sensitive cell. Eur J Appl Physiol.
Pant, S., Sharma, M., Patel, K., Caplan, S., Carr, C.M., and Grant, B.D. (2009). AMPH-1/Amphiphysin/Bin1 functions with RME-1/Ehd1 in endocytic recycling. Nat Cell Biol *11*, 1399-1410.
Paul, N.R., Jacquemet, G., and Caswell, P.T. (2015). Endocytic Trafficking of Integrins in Cell Migration. Curr Biol *25*, R1092-1105.
Pegoraro, E., Cepollaro, F., Prandini, P., Marin, A., Fanin, M., Trevisan, C.P., El-Messlemani, A.H., Tarone, G., Engvall, E., Hoffman, E.P.*, et al.* (2002). Integrin alpha 7 beta 1 in muscular dystrophy/myopathy of unknown etiology. Am J Pathol *160*, 2135-2143.
Perkins, A.D., Ellis, S.J., Asghari, P., Shamsian, A., Moore, E.D., and Tanentzapf, G. (2010). Integrin-mediated adhesion maintains sarcomeric integrity. Dev Biol *338*, 15-27.
Peter, B.J., Kent, H.M., Mills, I.G., Vallis, Y., Butler, P.J., Evans, P.R., and McMahon, H.T. (2004). BAR domains as sensors of membrane curvature: the amphiphysin BAR structure. Science *303*, 495-499.
Posey, A.D., Jr., Swanson, K.E., Alvarez, M.G., Krishnan, S., Earley, J.U., Band, H., Pytel, P., McNally, E.M., and Demonbreun, A.R. (2014). EHD1 mediates vesicle trafficking required for normal muscle growth and transverse tubule development. Dev Biol *387*, 179-190.
Posterino, G.S., and Lamb, G.D. (2003). Effect of sarcoplasmic reticulum Ca2+ content on action potential-induced Ca2+ release in rat skeletal muscle fibres. J Physiol *551*, 219-237.
Powelka, A.M., Sun, J., Li, J., Gao, M., Shaw, L.M., Sonnenberg, A., and Hsu, V.W. (2004). Stimulation-dependent recycling of integrin beta1 regulated by ARF6 and Rab11. Traffic *5*, 20-36.
Prokic, I., Cowling, B.S., and Laporte, J. (2014). Amphiphysin 2 (BIN1) in physiology and diseases. J Mol Med (Berl) *92*, 453-463.
Raess, M.A., Friant, S., Cowling, B.S., and Laporte, J. (2017). WANTED - Dead or alive: Myotubularins, a large disease-associated protein family. Adv Biol Regul *63*, 49-58.
Ratcliffe, C.D., Sahgal, P., Parachoniak, C.A., Ivaska, J., and Park, M. (2016). Regulation of Cell Migration and beta1 Integrin Trafficking by the Endosomal Adaptor GGA3. Traffic *17*, 670-688.
Razzaq, A., Robinson, I.M., McMahon, H.T., Skepper, J.N., Su, Y., Zelhof, A.C., Jackson, A.P., Gay, N.J., and O'Kane, C.J. (2001). Amphiphysin is necessary for organization of the excitation-contraction coupling machinery of muscles, but not for synaptic vesicle endocytosis in Drosophila. Genes Dev *15*, 2967-2979.
Ribeiro, I., Yuan, L., Tanentzapf, G., Dowling, J.J., and Kiger, A. (2011). Phosphoinositide regulation of integrin trafficking required for muscle attachment and maintenance. PLoS Genet *7*, e1001295.
Robinson, F.L., and Dixon, J.E. (2006). Myotubularin phosphatases: policing 3-phosphoinositides. Trends Cell Biol *16*, 403-412.
Roman, W., Martins, J.P., and Gomes, E.R. (2018). Local Arrangement of Fibronectin by Myofibroblasts Governs Peripheral Nuclear Positioning in Muscle Cells. Dev Cell *46*, 102-111 e106.
Romero, N.B. (2010). Centronuclear myopathies: a widening concept. Neuromuscul Disord *20*, 223-228.
Romero, N.B., and Bitoun, M. (2011). Centronuclear myopathies. Semin Pediatr Neurol *18*, 250-256.
Romero, N.B., Herasse, M., Monnier, N., Leroy, J.P., Fischer, D., Ferreiro, A., Viollet, L., Eymard, B., Laforet, P., Monges, S.*, et al.* (2005). Clinical and histopathological aspects of central core disease associated and non-associated with RYR1 locus. Acta Myol *24*, 70-73.

Royer, B., Hnia, K., Gavriilidis, C., Tronchere, H., Tosch, V., and Laporte, J. (2013). The myotubularin-amphiphysin 2 complex in membrane tubulation and centronuclear myopathies. EMBO Rep *14*, 907-915.
Sakamuro, D., Elliott, K.J., Wechsler-Reya, R., and Prendergast, G.C. (1996). BIN1 is a novel MYC-interacting protein with features of a tumour suppressor. Nat Genet *14*, 69-77.
Sarnat, H.B., Roth, S.I., and Jimenez, J.F. (1981). Neonatal myotubular myopathy: neuropathy and failure of postnatal maturation of fetal muscle. CanJNeurolSci *8*, 313-320.
Schaletzky, J., Dove, S.K., Short, B., Lorenzo, O., Clague, M.J., and Barr, F.A. (2003). Phosphatidylinositol-5-phosphate activation and conserved substrate specificity of the myotubularin phosphatidylinositol 3-phosphatases. Curr Biol *13*, 504-509.
Schwander, M., Leu, M., Stumm, M., Dorchies, O.M., Ruegg, U.T., Schittny, J., and Muller, U. (2003). Beta1 integrins regulate myoblast fusion and sarcomere assembly. Dev Cell *4*, 673-685.
Shattil, S.J., Kim, C., and Ginsberg, M.H. (2010). The final steps of integrin activation: the end game. Nat Rev Mol Cell Biol *11*, 288-300.
Shichiji, M., Biancalana, V., Fardeau, M., Hogrel, J.Y., Osawa, M., Laporte, J., and Romero, N.B. (2013). Extensive morphological and immunohistochemical characterization in myotubular myopathy. Brain Behav *3*, 476-486.
Shpetner, H.S., and Vallee, R.B. (1989). Identification of dynamin, a novel mechanochemical enzyme that mediates interactions between microtubules. Cell *59*, 421-432.
Spiro, A.J., Shy, G.M., and Gonatas, N.K. (1966). Myotubular myopathy. Persistence of fetal muscle in an adolescent boy. Arch Neurol *14*, 1-14.
Squire, J.M. (1997). Architecture and function in the muscle sarcomere. Curr Opin Struc Biol *7*, 247-257.
Sun, Z., Guo, S.S., and Fassler, R. (2016). Integrin-mediated mechanotransduction. J Cell Biol *215*, 445-456.
Sweeney, H.L., and Hammers, D.W. (2018). Muscle Contraction. Cold Spring Harb Perspect Biol *10*.
Takeda, T., Kozai, T., Yang, H., Ishikuro, D., Seyama, K., Kumagai, Y., Abe, T., Yamada, H., Uchihashi, T., Ando, T*., et al.* (2018). Dynamic clustering of dynamin-amphiphysin helices regulates membrane constriction and fission coupled with GTP hydrolysis. Elife *7*.
Tanabe, K., and Takei, K. (2009). Dynamic instability of microtubules requires dynamin 2 and is impaired in a Charcot-Marie-Tooth mutant. J Cell Biol *185*, 939-948.
Tanner, S.M., Laporte, J., Guiraud-Chaumeil, C., and Liechti-Gallati, S. (1998). Confirmation of prenatal diagnosis results of X-linked recessive myotubular myopathy by mutational screening, and description of three new mutations in the MTM1 gene. Hum Mutat *11*, 62-68.
Tasfaout, H., Buono, S., Guo, S., Kretz, C., Messaddeq, N., Booten, S., Greenlee, S., Monia, B.P., Cowling, B.S., and Laporte, J. (2017). Antisense oligonucleotide-mediated Dnm2 knockdown prevents and reverts myotubular myopathy in mice. Nat Commun *8*, 15661.
Tasfaout, H., Cowling, B.S., and Laporte, J. (2018a). Centronuclear myopathies under attack: A plethora of therapeutic targets. J Neuromuscul Dis.
Tasfaout, H., Lionello, V.M., Kretz, C., Koebel, P., Messaddeq, N., Bitz, D., Laporte, J., and Cowling, B.S. (2018b). Single Intramuscular Injection of AAV-shRNA Reduces DNM2 and Prevents Myotubular Myopathy in Mice. Mol Ther *26*, 1082-1092.
Taverna, D., Disatnik, M.H., Rayburn, H., Bronson, R.T., Yang, J., Rando, T.A., and Hynes, R.O. (1998). Dystrophic muscle in mice chimeric for expression of alpha5 integrin. J Cell Biol *143*, 849-859.
Taylor, G.S., Maehama, T., and Dixon, J.E. (2000). Inaugural article: myotubularin, a protein tyrosine phosphatase mutated in myotubular myopathy, dephosphorylates the lipid second messenger, phosphatidylinositol 3-phosphate. Proc Natl Acad Sci U S A *97*, 8910-8915.
Tosch, V., Rohde, H.M., Tronchere, H., Zanoteli, E., Monroy, N., Kretz, C., Dondaine, N., Payrastre, B., Mandel, J.L., and Laporte, J. (2006). A novel PtdIns3P and PtdIns(3,5)P2 phosphatase with an inactivating variant in centronuclear myopathy. Hum Mol Genet *15*, 3098-3106.

Toussaint, A., Cowling, B.S., Hnia, K., Mohr, M., Oldfors, A., Schwab, Y., Yis, U., Maisonobe, T., Stojkovic, T., Wallgren-Pettersson, C.*, et al.* (2011). Defects in amphiphysin 2 (BIN1) and triads in several forms of centronuclear myopathies. Acta Neuropathol *121*, 253-266.
Trochet, D., Prudhon, B., Beuvin, M., Peccate, C., Lorain, S., Julien, L., Benkhelifa-Ziyyat, S., Rabai, A., Mamchaoui, K., Ferry, A.*, et al.* (2017). Allele-specific silencing therapy for Dynamin 2-related dominant centronuclear myopathy. EMBO Mol Med.
Tronchere, H., Laporte, J., Pendaries, C., Chaussade, C., Liaubet, L., Pirola, L., Mandel, J.L., and Payrastre, B. (2004). Production of phosphatidylinositol 5-phosphate by the phosphoinositide 3-phosphatase myotubularin in mammalian cells. J Biol Chem *279*, 7304-7312.
Tsujita, K., Itoh, T., Ijuin, T., Yamamoto, A., Shisheva, A., Laporte, J., and Takenawa, T. (2004). Myotubularin regulates the function of the late endosome through the gram domain-phosphatidylinositol 3,5-bisphosphate interaction. J Biol Chem *279*, 13817-13824.
van Dam, E.M., and Stoorvogel, W. (2002). Dynamin-dependent transferrin receptor recycling by endosome-derived clathrin-coated vesicles. Mol Biol Cell *13*, 169-182.
Van der Ven, P.F., Jap, P.H., Barth, P.G., Sengers, R.C., Ramaekers, F.C., and Stadhouders, A.M. (1995). Abnormal expression of intermediate filament proteins in X-linked myotubular myopathy is not reproduced in vitro. NeuromusculDisord *5*, 267-275.
Velichkova, M., Juan, J., Kadandale, P., Jean, S., Ribeiro, I., Raman, V., Stefan, C., and Kiger, A.A. (2010). Drosophila Mtm and class II PI3K coregulate a PI(3)P pool with cortical and endolysosomal functions. J Cell Biol *190*, 407-425.
Wallgren-Pettersson, C., Clarke, A., Samson, F., Fardeau, M., Dubowitz, V., Moser, H., Grimm, T., Barohn, R.J., and Barth, P.G. (1995). The myotubular myopathies: differential diagnosis of the X linked recessive, autosomal dominant, and autosomal recessive forms and present state of DNA studies. JMedGenet *32*, 673-679.
Wang, L., Barylko, B., Byers, C., Ross, J.A., Jameson, D.M., and Albanesi, J.P. (2010). Dynamin 2 mutants linked to centronuclear myopathies form abnormally stable polymers. J Biol Chem *285*, 22753-22757.
Wang, Y., Cao, H., Chen, J., and McNiven, M.A. (2011). A direct interaction between the large GTPase dynamin-2 and FAK regulates focal adhesion dynamics in response to active Src. Mol Biol Cell *22*, 1529-1538.
Wechsler-Reya, R., Sakamuro, D., Zhang, J., Duhadaway, J., and Prendergast, G.C. (1997). Structural analysis of the human BIN1 gene. Evidence for tissue-specific transcriptional regulation and alternate RNA splicing. J Biol Chem *272*, 31453-31458.
Wechsler-Reya, R.J., Elliott, K.J., and Prendergast, G.C. (1998). A role for the putative tumor suppressor Bin1 in muscle cell differentiation. Mol Cell Biol *18*, 566-575.
Whitley, P., Reaves, B.J., Hashimoto, M., Riley, A.M., Potter, B.V., and Holman, G.D. (2003). Identification of mammalian Vps24p as an effector of phosphatidylinositol 3,5-bisphosphate-dependent endosome compartmentalization. J Biol Chem *278*, 38786-38795.
Wigge, P., Kohler, K., Vallis, Y., Doyle, C.A., Owen, D., Hunt, S.P., and McMahon, H.T. (1997). Amphiphysin heterodimers: potential role in clathrin-mediated endocytosis. Mol Biol Cell *8*, 2003-2015.
Wilmshurst, J.M., Lillis, S., Zhou, H., Pillay, K., Henderson, H., Kress, W., Muller, C.R., Ndondo, A., Cloke, V., Cullup, T.*, et al.* (2010). RYR1 mutations are a common cause of congenital myopathies with central nuclei. Ann Neurol *68*, 717-726.
Wu, T., Shi, Z., and Baumgart, T. (2014). Mutations in BIN1 associated with centronuclear myopathy disrupt membrane remodeling by affecting protein density and oligomerization. PLoS One *9*, e93060.
Zelhof, A.C., Bao, H., Hardy, R.W., Razzaq, A., Zhang, B., and Doe, C.Q. (2001). Drosophila Amphiphysin is implicated in protein localization and membrane morphogenesis but not in synaptic vesicle endocytosis. Development *128*, 5005-5015.

RESUME

Les Myopathies Centronucléaires (Centronuclear Myopathies, CNM) sont des maladies congénitales graves caractérisées par une faiblesse musculaire, une atrophie des fibres et une localisation anormale des noyaux au centre des fibres du muscle squelettique. Ils n'existent pas encore à ce jour de traitements disponibles pour soigner les patients atteints par ces maladies. Les CNMs sont classifiées principalement en 3 groupes: les CNMs liées à l'X (XLCNM) provoqués par des mutations sur le gène *MTM1(Laporte et al., 2000)*, les CNMs autosomiques récessives (ARCNM) provoquées par des mutations du gène *BIN1* (Nicot et al., 2007) et les CNM autosomiques dominantes (ADCNM) causées par des mutations sur le gène *DNM2 (Wallgren-Pettersson et al., 1995).*

La forme de CNM liée à l'X est la forme la plus grave de la maladie. Cette dernière est due à des mutations sur le gène *MTM1* encodant pour la phosphoinositide phosphatase myotubularine (MTM1) (Blondeau et al., 2000; Laporte et al., 1997a). Ces mutations entraînent le plus souvent une perte de l'expression de MTM1. Cette protéine régule le niveau de phosphatidylinositol-5-phosphate (PtdIns5P), PtdIns(3,5)P_2 et PtdIns3P. Les patients atteints de XLCNM présentent une hypotonie profonde, une faiblesse à la naissance et une déficience respiratoire grave apparaissant peu de temps après la naissance (Romero et al., 2005).

La forme de CNM autosomique dominant est liée à des mutations sur le gène *DNM2*. *DNM2* encode pour la Dynamine 2 (DNM2), une grande protéine GTPase exprimée de manière ubiquitaire et impliquée dans l'endocytose et le trafic membranaire. Plusieurs mutations sur DNM2 sont à l'origine de l'ADCNM et sont associées à différents phénotypes cliniques. Les patients peuvent présenter des phénotypes légers apparaissant à l'âge adulte ou des phénotypes graves débutant dès l'enfance (Bitoun et al., 2005).

La forme de CNM autosomique récessif est provoquée par des mutations du gène *BIN1*. Le gène *BIN1* encode pour l'amphiphysine 2 (BIN1), une protéine exprimée de manière ubiquitaire, essentielle pour l'endocytose, le recyclage et le remodelage des membranes. Plusieurs isoformes de BIN1 ont été découverts avec des distributions spécifiques en fonction des différents tissus. L'isoforme 8, l'isoforme spécifique du muscle squelettique, contient un domaine de liaison aux phosphoinositides (PI)(Lee et al., 2002; Toussaint et al., 2011). La présence de ce domaine chez BIN1 est associée à un rôle fondamental dans l'organisation du système réticule sarcoplasmiques T-tubes (Al-Qusairi and Laporte, 2011).

La relation entre les trois protéines encodées par ces gènes dans le muscle squelettique reste en grande partie inconnue. Des études antérieures ont montré que MTM1, BIN1 et DNM2

étaient toutes impliquées dans le remodelage membranaire, car elles participent à la tubulation et au recyclage des membranes, des voies compromises pour chaque forme de CNM (Nicot et al., 2007; Royer et al., 2013). Les mutations sur les gènes *MTM1* et *BIN1* causant des XLCNM et ARCNM, entraînent une perte de fonction protéique ainsi que des anomalies dans le recyclage des endosomes et des défauts dans la tubulation membranaire. Des défauts de tubulation membranaire ont aussi été observés dans les cellules de muscle squelettique de souris modèle pour l'ADCNM. Les mutations responsables de l'ADCNM favorisent généralement la dimérisation de DNM2, rendant le complexe plus stable et probablement plus actif avec une capacité de fission de DNM2 plus importante (Buono et al., 2018; Cowling et al., 2011). Il a aussi été observé que MTM1 pouvait interagir avec BIN1 et que cette interaction était cruciale pour la régulation de la tubulation de la membrane. Enfin, BIN1 peut se lier à plusieurs autres protéines via son domaine SH3, dont DNM2 (Kojima et al., 2004). Notre laboratoire a montré que les mutations de *BIN1* causant une CNM induisaient une perte de fonction de la protéine et modifiaient la conformation de BIN1 et donc sa liaison avec MTM1, soulignant ainsi l'importance de l'interaction entre MTM1-BIN1 dans le muscle squelettique (Royer et al., 2013). L'analyse *in vivo* du muscle squelettique XLCNM a révélé une surexpression du la protéine DNM2 (Cowling et al., 2014). Il a été montré dans notre laboratoire que la surexpression exogène de DNM2 dans le muscle squelettique induisait de graves problèmes structuraux et des défauts de la force du muscle squelettique (Cowling et al., 2011). Suite à cette étude, le laboratoire a cherché à savoir si la réduction des niveaux de DNM2 pouvait améliorer les phénotypes de CNM. Un sauvetage positif a été obtenu pour le modèle murin de XLCNM et pour le modèle murin de ARCNM grâce à la réduction des niveaux de DNM2 (Cowling et al., 2014; Tasfaout et al., 2017; Tasfaout et al., 2018b). J'ai durant ma thèse participait à ces études. Ces résultats suggèrent que MTM1 et BIN1 régulent négativement DNM2. Cependant, la nature de la relation entre BIN1 et MTM1 dans cette voie hypothétique n'a pas encore été clairement caractérisée. L'hypothèse de mon doctorat est que MTM1 peut activer BIN1, ce qui régule négativement DNM2. Si cette hypothèse est vraie, la surexpression de BIN1 devrait sauver les phénotypes de CNM pour les modèles murins de XLCNM et d'ADCNM. L'objectif principal de ma thèse est de moduler l'expression de BIN1 dans le modèle murin de XLCNM et dans le modèle murins d'ADCNM, afin d'identifier une nouvelle voie thérapeutique menant à de nouvelles stratégies de traitements. Cette approche devrait aussi permettre de mieux comprendre le lien fonctionnel entre MTM1-BIN1-DNM2 dans le muscle squelettique *in vivo*.

Modulation de l'expression de BIN1 : une nouvelle cible pour la myopathie centronucléaire liée à l'X

Les souris *Mtm1-/y* développent une faiblesse musculaire progressive à partir de la troisième semaine avec des caractéristiques similaires à celle développé chez les patients (Buj-Bello et al., 2002b). Elles meurent généralement après seulement 7 semaines. Durant la progression de la maladie, elles développent une kyphosis ainsi que des difficultés respiratoires et locomotrices (Buj-Bello et al., 2002b). De manière frappante, à la suite du croisement avec des souris transgéniques sur-exprimant BIN1 (Tg *BIN1*), les souris *Mtm1*-/y / Tg *BIN1* ne développent pas de phénotype de type CNM. La durée de vie des souries *Mtm1*-/y / Tg *BIN1* est rétablie au même niveau que celle des souris sauvages, allant jusqu'à 2 ans. La croissance et la prise de poids chez ces souris sont comparables à celles des souris sauvages, et le phénotype atrophique ne se développe pas chez ces souris. Afin de mieux caractériser l'avancement de la myopathie, une étude plus poussée a été réalisée sur un muscle représentatif, le Tibialis Antérieur (TA) situé sur chaque patte arrière. Chez les souris *Mtm1* -/y de 7 semaines, le TA est atrophique et sans force, avec des fibres dont le noyau est en position centrale dans 30% des cas. Chez les souris *Mtm1-/y* / Tg *BIN1,* les mesures de force musculaire sur le TA ont permis de révéler une force similaire aux souris contrôles tout au long de leur vie. Enfin la caractérisation des muscles au niveau histologique a révélé une organisation des fibres hexagonales, avec des noyaux en positions périphériques similaire à celle des muscles des souris sauvages. À la suite de ces résultats prometteurs, je me suis focaliséesur le développement d'une approche plus translationnelle, qui pourrait être utilisée après la naissance des souris, afin de savoir s'il était possible d'empêcher le développement de la maladie grâce cette stratégie chez les patients. Afin de surexprimer BIN1 chez les souris, j'ai utilisé un virus adeno-associé (AAV) modifié exprimant le gène *BIN1* humain, qui ne s'intègre pas dans le génome et ne se réplique pas. Dans notre procédure, le virus AAV *BIN1* a été injecté dans un des deux muscles TA de souris *Mtm1* -/y et de souris contrôles à l'âge de 3 semaines. Nous avons ensuite réalisé une analyse de force sur les TA à 2 et 4 semaines post-injections. L'augmentation des niveaux de BIN1 après la naissance permet une augmentation significative de la force musculaire chez les souris *Mtm1* -/y. Suite à ces résultats, l'isoforme 8 de l'AAV-BIN1 a été injectée par voie intra-péritonéale à des souriceaux le premier jour après leur naissance. La surexpression systémique de BIN1 après la naissance a permis de complètement sauver le phénotype des souris *Mtm1*-/y. La force musculaire spécifique du TA a été sauvée chez les souris *Mtm1* KO ayant reçu une injection de AAV-*BIN1*. Cette approche a permis la mise au point d'outils qui pourraient être potentiellement rapidement utilisés chez les patients.

Dans un second temps, j'ai cherché à comprendre les mécanismes moléculaires liés au sauvetage du phénotype. Les principales caractéristiques musculaires des patients XLCNM sont la réduction de la taille des fibres, des fibres rondes et une augmentation de l'espace

interfibre, ce qui indique une probable dérégulation de l'attachement inter-fibre. Je me suis intéressée en particulier à la protéine intégrine β1, car cette protéine normalement localisée à la membrane plasmique est impliquée dans l'adhérence cellulaire, et est modifiée chez la *Drosophile* mutée pour le gène orthologue *mtm (Ribeiro et al., 2011)*. En outre, Ketel *et al*. ont montré que l'intégrine β1 s'accumulait dans les endosomes des fibroblastes de patients *MTM1* suggérant que son trafic était contrôlé par l'activité de MTM1 (Ketel et al., 2016). J'ai confirmé une mauvaise localisation de l'intégrine beta1 dans les fibres musculaires et une augmentation du niveau de l'intégrine beta1 chez les souris *Mtm1* -/y. J'ai ensuite identifié que l'intégrine beta1 co-localisait avec EEA1, un marqueur endosomal de recyclage précoce, dans le muscle squelettique de souris adulte *Mtm1*-/y. Cela prouve un défaut du recyclage à la membrane de l'intégrine β1 chez les souris atteintes de XLCNM dans les cellules musculaires. Pour mieux étudier le défaut de l'intégrine beta1, j'ai vérifié la localisation de l'intégrine beta1 dans les myoblastes primaires WT et *Mtm1* -/y. J'ai observé des vésicules plus grosses positive à l'intégrine β1 dans le myoblaste primaire *Mtm1-/y* par rapport au WT. Ce résultat confirme le défaut observé dans le muscle squelettique adulte. J'ai ensuite étudié si la mauvaise localisation de l'intégrine β1 pouvait affecter certains phénotypes cellulaires. Les myoblastes primaires *Mtm1-/y* présentent des défauts d'adhésion cellulaire, de migration cellulaire (Ratcliffe et al., 2016) et de fusion (Schwander et al., 2003). De manière importante, la surexpression de BIN1 prévient l'apparition d'agrégats d'intégrine β1 dans le muscle. Ces résultats suggèrent que le recyclage des intégrines β1 est régulé par une voie contrôlée à la fois par MTM1 et BIN1. Ils montrent que les myoblastes primaires *Mtm1*-/y présentent un défaut d'adhésion, de migration et d'indice de fusion cellulaire en raison d'un défaut de localisation et de turnover de l'intégrine β1.

En parallèle, j'ai évalué l'impact de la modulation de l'expression de BIN1 chez les souris

Dnm2$^{+/R465W}$ qui récapitule une ADCNM.

La modulation de l'expression de BIN 1 restaure la myopathie centronucléaire autosomique dominante.

La mutation ADCNM la plus fréquente pour *DNM2* est la mutation R465W où une arginine est échangée contre un tryptophane dans le domaine intermédiaire de DNM2 (Durieux et al., 2010). Durieux *et al.* Ont publié en 2010 le premier modèle knock-in exprimant cette mutation induisant un gain de fonction pour DNM2 (Bitoun et al., 2009). La plupart des souris homozygotes pour cette mutation meurent à la naissance et seules quelques souris survivent jusqu'à l'âge d'une semaine (Bitoun et al., 2009). Les souris hétérozygotes (*Dnm2*$^{R465W/+}$) sont viables mais développent une atrophie musculaire vers l'âge de 8 semaines et présentent une

légère réduction de la force musculaire *in situ*. L'histologie du muscle *Dnm2*$^{+/R465W}$ ne révèle pas de noyaux cellulaire en position centrale chez ces souris, mais les fibres ont une coloration anormale et réduite pour la dinucléotide-tétrazolium réductase (NADH). Afin de vérifier si la surexpression de BIN1 chez la souris sauve la durée de vie chez la souris homozygote et la faiblesse musculaire du muscle *Dnm2* **$^{R465W/+}$**, des souris transgéniques BIN1 ont été croisées avec la femelle *Dnm2* **$^{R465W/+}$** pour produire Tg*BIN1 Dnm2* **$^{R465W/+}$**. Des mâles Tg*BIN1 Dnm2* **$^{R465W/+}$** ont ensuite été croisés avec des femelle *Dnm2* **$^{R465W/+}$** afin d'obtenir des souris homozygotes Tg*BIN1 Dnm2* $^{R465W/R465W}$. La surexpression de BIN1 prolonge avec succès la durée de vie *Dnm2* $^{R465W /R465W}$. Aucune différence n'a été détectée entre Tg*BIN1 Dnm2* $^{R465W /R465W}$, WT et Tg*BIN1 Dnm2* **$^{R465W/+}$** au niveau de leur survie. Une légère différence de poids a été observée entre les souris Tg*BIN1 Dnm2* $^{R465W /R465W}$ et le témoin WT, alors qu'il n'existait aucune différence détectable entre le Tg*BIN1 Dnm2* **$^{R465W/+}$** et le WT. Nous avons ensuite testé la force musculaire TA. Malgré leur survie, les souris Tg*BIN1 Dnm2* $^{R465W /R465W}$ présentent encore une force significativement inférieure à celle du témoin WT à 2 mois. Enfin la caractérisation des muscles au niveau histologique a révélé une coloration NADH chez les souris Tg *BIN1 Dnm2* **$^{R465W/+}$** similaire à celle des muscles des souris sauvages pedant les souris Tg*BIN1 Dnm2* $^{R465W /R465W}$ présentent une coloration NADH anomale.

En résumé, la surexpression de BIN1 a permis de sauver la mortalité néonatale des souris *Dnm2* $^{R465W /R465W}$ et de améliorer les caractéristiques histologiques du muscle squelettique chez les souris *Dnm2* **$^{R465W/+}$** sur-exprimant BIN1.

En résumé, cette étude a permis d'identifier une nouvelle stratégie permettant de sauver à la fois la myopathie XLCNM et ADCNM sur des modèles murins. Ces résultats montrent un lien fonctionnel entre BIN1 et MTM1 nécessaire pour l'adhésion focale au niveaux musculaire. MTM1 régule positivement BIN1 et BIN1 régule négativement DNM2 dans le muscle squelettique. Notre étude montre que MTM1, BIN1 et DNM2 participe à une voie de signalisation commune. BIN1 et DNM2 représentent de nouvelles cibles thérapeutiques pour le traitement des différentes formes de CNMs.

Université de Strasbourg

Valentina Maria LIONELLO

École Doctorale des Sciences de la Vie et de la Santé STRASBOURG

Modulation of BIN1 expression rescues different forms of Centronuclear myopathies in murine models

Résumé

Les myopathies centro-nucléaires (CNM) sont un groupe de maladies musculaires sévères caractérisées par une faiblesse musculaire générale. La forme la plus sévère est la CNM liée à l'X (XLCNM), causée par des mutations de la Myotubularine (*MTM1*). D'autres formes autosomales existent et sont causées par des mutations de l'Amphiphysine 2 (*BIN1*) et de la Dynamine 2 (*DNM2*). Les mécanismes pathologiques menant aux CNMs restent à éclaircir et à ce jour aucune thérapie n'est disponible pour traiter les patients. Dans ce but, nous avons modulé l'expression de MTM1, BIN1 et DNM2 dans des modèles murins de CNMs. Nous avons mis en évidence que la sous-régulation de la protéine DNM2, ainsi que surexpression de la protéine BIN1 humaine restaurent le phénotype du modèle murin de XLCNM et la forme autosomale dominante de CNM. Nous avons aussi montré que MTM1 régulait l'adhésion cellulaire et le recyclage de l'intégrine dans le muscle. La surexpression de la protéine BIN1 restaure le recyclage de l'intégrine dans le modèle murin de XLCNM. Ceci suggère un lien fonctionnel entre BIN1 et MTM1 nécessaire pour l'adhésion focale des fibres musculaires. Notre étude montre que MTM1, BIN1 et DNM2 participent à une voie de signalisation commune et BIN1 et DNM2 représentent de nouvelles cibles thérapeutiques pour le traitement des différentes formes de CNMs.

Résumé en anglais

Centronuclear myopathies (CNM) are a group of severe muscle disorder characterized by general muscle weakness. The most severe form is the X-linked CNM (XLCNM), caused by mutations in Myotubularin (*MTM1*). Others autosomal forms are caused by mutations in Amphiphysin 2 (*BIN1*) and Dynamin 2 (*DNM2*). The CNM pathomechanisms are still unclear and to date there are no therapies available to the disease. To investigate the pathways dysregulated in CNM and to identify new therapeutic strategies, we modulated MTM1, BIN1 and DNM2 protein levels in the CNM mouse models. We discovered that DNM2 downregulation rescued the XLCNM mouse model and that the overexpression of human BIN1 rescued the XLCNM and the autosomal dominant CNM form due to DNM2 mutations. We have also showed that MTM1 controls cell adhesion and integrin recycling in mammalian skeletal muscle and BIN1 overexpression rescued the integrin recycling alteration in XLCNM mouse model suggesting that MTM1 and BIN1 are functionally linked and necessary for focal adhesions in muscle. Therefore, our studies highlight that MTM1, BIN1 and DNM2 are in a common pathway and, BIN1 and DNM2 could be new therapeutic targets to treat the different forms of CNM.